Mechanisms Linking Lipid Metabolism and Longevity in Yeast

Simon D. Bourque

A Thesis

in

The Department

of

Biology

Presented in Partial Fulfillment of the Requirements

For the Degree of Doctor of Philosophy at

Concordia University

Montreal, Quebec, Canada

April 2011

CONCORDIA UNIVERSITY

SCHOOL OF GRADUATE STUDIES

This is to certify that the thesis prepared

By: **Simon D. Bourque**

Entitled: **Mechanisms Linking Lipid Metabolism and Longevity in Yeast**

and submitted in partial fulfillment of the requirements for the degree of

DOCTOR OF PHILOSOPHY (Biology)

complies with the regulations of the University and meets the accepted standards with

respect to originality and quality.

Signed by the final examining committee:

Dr. William M. Bukiowski	Chair
Dr. Dusica Maysinger	External Examiner
Dr. Peter D. Pawelek	External to Program
Dr. Reginald K. Storms	Examiner
Dr. Ann M. English	Examiner
Dr. Vladimir I. Titorenki	Thesis Supervisor

Approved by   _____

Chair of Department or Graduate Program Director

_____ 2011   _____

Dean of Faculty

ABSTRACT

Mechanisms Linking Lipid Metabolism and Longevity in Yeast

Simon D. Bourque, Ph.D.

Concordia University 2011

Proper control of lipid metabolism in the endoplasmic reticulum, lipid bodies, peroxisomes and mitochondria is essential for longevity regulation. However, the molecular mechanisms linking longevity and lipid metabolism in these organelles have not been defined prior to studies described here. The establishment of such mechanisms operating in chronologically aging yeast was the objective of my thesis.

To develop a tool for quantitative monitoring of the age-related dynamics of changes in the cellular and organellar lipidomes of chronologically aging yeast, I was able to solve the inherent limitations of the currently used methods for lipidomic analysis (including the limitations characteristic of mass spectrometry-based techniques) by devising a survey-scan electrospray ionization mass spectrometry method for quantitative lipidomics. This novel method enables within a very limited period of time and using a very low number of cells to resolve, unequivocally identify and accurately quantitate all molecular forms of lipid species composing yeast lipidome and the majority of molecular forms of lipid species composing the lipidome of cultured human cells.

Using a combination of the functional genetic, cell biological, electron and fluorescence microscopical, proteomic, lipidomic, and metabolomic analyses, I established three molecular mechanisms linking longevity and lipid metabolism confined to the endoplasmic reticulum, lipid bodies, peroxisomes and mitochondria. One of these mechanisms underlies the ability of a caloric restriction diet to extend longevity of

chronologically aging yeast by specifically remodeling the metabolism of neutral lipids in the endoplasmic reticulum, lipid bodies and peroxisomes. The other mechanism underlies the ability of lithocholic acid, a novel anti-aging compound that my research enabled to identify, to extend yeast chronological life span by targeting the longevity-defining aspects of lipid metabolism confined to the endoplasmic reticulum, lipid bodies and peroxisomes. The third mechanism underlies the ability of lithocholic acid to extend yeast chronological life span under caloric restriction conditions by remodeling lipid metabolism in the mitochondrial membrane, thereby altering the repertoire of membrane lipids in mitochondria and influencing several longevity-defining processes confined to these organelles.

Acknowledgements

Table of Contents

List of Figures

List of Tables

List of Equations

List of Abbreviations

ACO, aconitase; AMPK/TOR, AMP-activated protein kinase/target of rapamycin; cAMP/PKA, cAMP/protein kinase A; C/EBPα, CCAAT/enhancer-binding protein; CCO, cytochrome c oxidase; CFU, colony forming units; CL, cardiolipin; CLS, chronological life span; CR, caloric restriction; DAG, diacylglycerols; DHAP, dihydroxyacetone phosphate; DHR, dihydrorhodamine 123; DR, dietary restriction; EE, ergosteryl esters; ESI/MS, electrospray ionization mass spectrometry; ER, endoplasmic reticulum; ERG, ergosterol; FA-CoA, CoA esters of fatty acids; FFA, free fatty acids; FoxO, Forkhead box type O; GC/MS, gas chromatography followed by mass spectrometry; HPLC, high performance liquid chromatography; IGF-1, insulin/insulin-like growth factor 1; LBs, lipid bodies; LOD, limit of detection; LOQ, limit of quantitation; LPA, lysophosphatidic acid; MCA, metabolic control analysis; PA, phosphatidic acid; PC, phosphatidylcholine; PE, phosphatidylethanolamine; PI, phosphatidylinositol; PI3K, phosphatidylinositol-3-kinase; PKC, protein kinase C; PMBC, peripheral blood mononuclear cells; rDNA, ribosomal DNA; ROS, reactive oxygen species; RLS, replicative life span; SD, standard deviation; SDH, succinate dehydrogenase; TAG, triacylglycerols; TLC, thin-layer chromatography; TORC1, TOR complex 1; WAT, white adipose tissue.

1. Introduction

1.1. A complexity of biological aging

Aging is a highly complex biological phenomenon, which at the organismal level manifests itself as the progressive decline in the ability of an organism to resist stress, damage and disease [1 - 4]. At the demographic level, aging can be defined as an exponential increase in the mortality rate with the age of the cohort [1, 4, 5]. Aging of multicellular eukaryotic organisms affects numerous processes within cells [2 - 4, 6 - 10]. Some of these processes damage cellular macromolecules and organelles, while the others prevent the collapse of cellular homeostasis by repairing the damage [1, 3 - 5]. A lifelong accumulation of unrepaired cellular damage increases a risk of disease and death [1, 4, 6, 11]. A challenge is to understand how the spatiotemporal organization of damage-producing and damage-repairing processes influences longevity and how cells integrate and control these processes. The most important unanswered question is whether aging is the final step of a developmental program governed by a certain signaling network [12 - 18] or merely a result of the lifelong accumulation of unrepaired cellular and molecular damage [1, 5, 19].

1.2. An evolutionarily conserved signaling network regulates longevity

Growing evidence supports the view that the fundamental mechanisms of aging are conserved across phyla [1, 3, 5, 20 - 23]. The identification of single-gene mutations that extend life span in yeast, worms, flies and mice revealed numerous proteins that regulate longevity. These proteins have been implicated in a wide array of cellular processes including cell cycle, cell growth, stress response, protein folding, apoptosis, autophagy,

1

proteasomal protein degradation, actin organization, signal transduction, nuclear DNA replication, chromatin assembly and maintenance, ribosome biogenesis and translation, lipid and carbohydrate metabolism, oxidative metabolism in mitochondria, NAD^+ homeostasis, amino acid biosynthesis and degradation, and ammonium and amino acid uptake [2-4, 7, 22 - 25]. The spatiotemporal organization of all these numerous cellular processes and their functional states are governed by a limited number of nutrient- and energy-sensing signaling pathways that are conserved across phyla and include the insulin/IGF-1, AMPK/TOR and cAMP/PKA pathways (Figure 1.1) [7, 26, 27].

In response to an endocrine signal that monitors the nutritional status of the whole organism, the insulin/insulin-like growth factor 1 (IGF-1) pathway regulates longevity in worms, fruit flies and mice (Figure 1.1) [28]. If activated by an insulin-like ligand, this pathway operates through a phosphatidylinositol-3-kinase (PI3K) and a cascade of protein kinases to ultimately cause phosphorylation of a Forkhead box type O (FoxO) family transcription factor, thereby sequestering it in the cytosol [29, 30]. Reduced signaling through the insulin/IGF-1 pathway increases the life spans of worms, fruit flies and mice by inhibiting phosphorylation of their FoxO transcription factors (DAF-16, dFOXO and FoxO1, respectively), thus allowing their translocation into the nucleus [31]. Within the nucleus, FoxO orchestrates a pro-longevity transcriptional program by activating or repressing transcription of a number of genes involved in signaling, development, transcription, translation, metabolism, detoxification, stress response and apoptosis [32, 33].

Unlike the insulin/IGF-1 signaling pathway regulating longevity in response to the nutritional status of the whole organism, the AMP-activated protein kinase/target of

rapamycin (AMPK/TOR) pathway functions as an intracellular sensor for the nutrient and energy status (Figure 1.1) [34, 35]. This pathway regulates longevity in yeast, worms, fruit flies and mammals [27, 36 - 38]. Activated under low nutrient or energy conditions, AMPK responds to the high AMP:ATP ratio by inhibiting TOR protein kinase that associates with several other proteins into the TOR complex 1 (TORC1) [34, 35]. The resulting inhibition of TORC1 slows down the energy-consuming processes of cellular growth, ribosome biogenesis and protein translation, orchestrates a pro-longevity translational program by causing a switch from cap-dependent to cap-independent translation, promotes nutrient- and energy-producing autophagy aimed at the removal of damaged macromolecules and organelles, activates mitochondrial translation of oxidative phosphorylation subunits, and alters mitochondrial gene expression [34, 39 - 41]. Noteworthy, under low levels of amino acids, the life-extending inhibition of TORC1 can be also achieved in an AMPK-independent manner [42 - 45]. Moreover, under low nutrient or energy conditions, the phosphorylation of AMPK by the LKB1 protein kinase increases the life span of worms in a TORC1-independent fashion by decelerating hydrolysis of the neutral lipids triacylglycerols (TAG) [46].

The cAMP/protein kinase A (cAMP/PKA) pathway regulates longevity in yeast and mice. In yeast, glucose deprivation reduces cAMP/PKA signaling by attenuating several activators of adenylate cyclase Cyr1p, including the G protein-coupled receptor Gpr1p, Gα protein Gpa2p and two small GTP-binding proteins, Ras1p and Ras2p (Figure 1.1) [47, 48]. Reduced signaling through the cAMP/PKA pathway inhibits phosphorylation of the protein kinase Rim15p and stress response transcription factors Msn2p and Msn4p by PKA in the cytosol, thereby restoring the kinase activity of

Rim15p and allowing the translocation of Msn2p and Msn4p into the nucleus [49 - 51]. Upon entering the nucleus, Msn2p and Msn4p orchestrate - in a Rim15p-dependent fashion - a pro-longevity transcriptional program by activating transcription of a number of genes involved in stress protection, reactive oxygen species (ROS) detoxification, proteolysis, the tricarboxylic acid cycle, carbohydrate metabolism, trehalose biosynthesis and cell growth regulation [52 - 55]. The resulting establishment of a pro-longevity transcriptional pattern increases yeast chronological life span (CLS), which is measured by the length of time a yeast cells remains viable in a nondividing state and reminiscent of the life span of a postmitotic cell in a multicellular organism [56]. One of the longevity genes whose transcription in the nucleus is activated by Msn2p and Msn4p encodes the nicotinamidase Pnc1p [49]. The Pnc1p-dependent degradation of nicotinamide, an inhibitor of the sirtuins Sir2p and Hst2p, enhances their ability to stabilize arrayed repeats of the ribosomal DNA (rDNA) locus in the nucleus [57]. The resulting attenuation of the formation of toxic extrachromosomal circular forms of rDNA increases yeast replicative life span (RLS), which is defined by the maximum number of daughter cells that a mother cell can produce before senescence and reminiscent of the life span of a mitotically active cell in a multicellular organism [8]. In mice, the cAMP/PKA signaling pathway regulates longevity in response to cAMP produced by the AC5 isoform of adenylate cyclase, which is highly abundant in the heart and brain [58]. Reduced cAMP/PKA signaling in mice lacking AC5 attenuates the inhibitory effect of PKA on the Raf/MEK/ERK protein kinase cascade [58]. The resulting activation of the protein kinase ERK enhances the susceptibility of mice to oxidative stress (perhaps, due to the observed increase in the abundance of the ROS scavenging enzyme manganese superoxide

dismutase) and apoptosis, ultimately extending longevity and delaying age-related degenerative processes in the heart and bone [58]. Of note, the Ste11p/Ste7p/Kss1p protein kinase cascade in yeast - which is homologous to the Raf/MEK/ERK cascade in mammals - may also regulate yeast chronological life span in response to cAMP/PKA signaling [58], thereby modulating yeast longevity synergistically with the other downstream effectors of PKA (*i.e.*, Rim15p, Msn2p and Msn4p). A recently reported life span extension in mice lacking a regulatory subunit of PKA and the observed in these mice - and in mice lacking its catalytic subunit – significant attenuation of age-related pathologies [59 - 60] further support the essential role for cAMP/PKA in regulating longevity and modulating physiological processes underlying healthy aging.

By sharing a compendium of protein kinases and adaptor proteins, the insulin/IGF-1, AMPK/TOR and cAMP/PKA pathways in yeast, worms, fruit flies and mammals converge into a complex network regulating longevity [7, 26, 27, 34, 35]. It is conceivable that this network may also include several protein components that currently are not viewed as being in any of these three pathways (Rtg2p in yeast; CLK-1, ISP-1, JNK, MST-1, PHA-4, Rictor/TORC2/SGK-1, SIR-2.1, SKN-1 and SMK-1 in worms; dSir2 and JNK in fruit flies; and MCLK, P66^{Shc}, SIRT1, SIRT6, and SIRT7 in mammals) [7, 27, 61 - 63]. Moreover, this network responds to the age-related partial mitochondrial dysfunction and is modulated by mitochondrially produced ROS [27, 34, 62, 64]. By sensing the nutritional status of the whole organism as well as the intracellular nutrient and energy status, functional state of mitochondria, and concentration of ROS produced in mitochondria, the longevity network regulates life span across species by coordinating information flow along its convergent, divergent and multiply branched signaling

pathways. These pathways function as biochemical logic circuits that process information via positive and negative feedback and feed-forward regulatory loops, dual-control switches, and protein scaffolds.
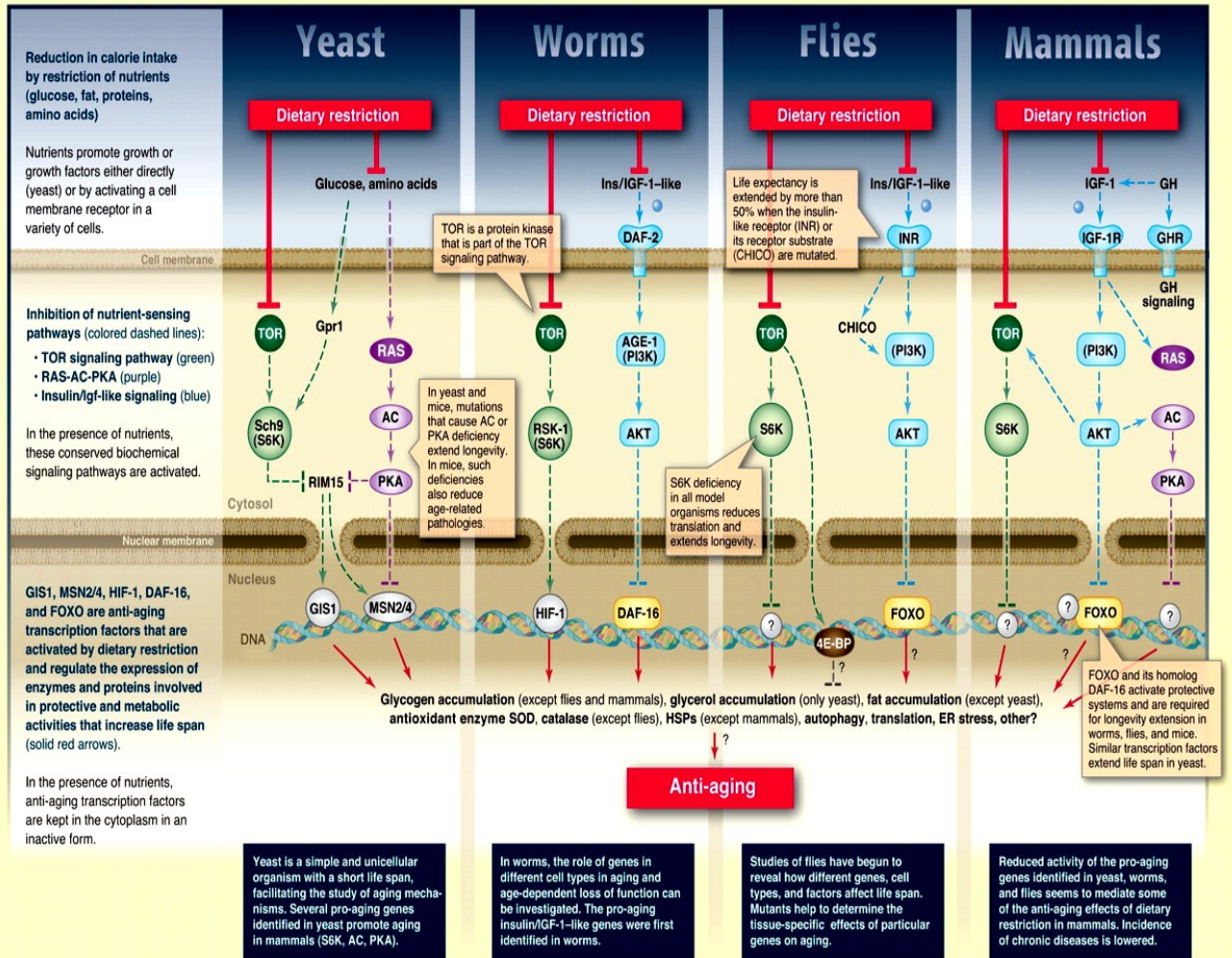
Figure 1.1. The spatiotemporal organization of numerous longevity-related cellular processes and their functional states are governed by a limited number of nutrient- and energy-sensing signaling pathways that are conserved across phyla and include the insulin/IGF-1, AMPK/TOR and cAMP/PKA pathways (see text in section 1.2 for details). Reproduced from Fontana, L., Partridge, L. and Longo, V.D. (2010). Extending healthy life span - from yeast to humans. *Science* 328:321-326.

1.3. Certain diets and pharmacological interventions can extend longevity

By defining the organismal and intracellular nutrient and energy status, nutrient intake plays an important role in modulating life span and influences a wide spectrum of age-related pathologies [9, 65 – 67]. Two dietary regimens are known to have the most profound life-extending effects across species and, in some cases, to improve overall health by delaying the onset of age-related diseases. These dietary interventions extend life span in evolutionarily distant organisms ranging from yeast to rhesus monkeys and include: 1) caloric restriction (CR), a diet in which only calorie intake is reduced but the supply of amino acids, vitamins and other nutrients is not compromised [66 - 69]; and 2) dietary restriction (DR), in which the intake of nutrients (but not necessarily of calories) is reduced by limiting food supply without causing malnutrition (Figure 1.2) [65, 70 - 72].

In a "TOR-centric" view of longevity regulation, TORC1 alone governs the life-extending and health-improving effects of CR/DR by: 1) integrating the flow of information on the organismal and intracellular nutrient and energy status from the protein kinases AMPK, PKA, PKB/AKT (the insulin/IGF-1 pathway) and ERK1/2 (the Raf/MEK/ERK cascade) as well as from the mitochondrial redox protein P66^{Shc}; 2) sensing the intracellular levels of amino acids in an AMPK-independent manner; and 3) operating as a control center which, based on the information it has gathered and processed, modulates a plethora of longevity-related processes in a sirtuin-independent fashion [73 – 75]. The inability of CR to increase the replicative life spans of yeast mutants lacking components of the TOR signaling pathway [76] and the lack of the beneficial effect of DR on life span in worms with reduced TOR signaling [77, 78]

support the proposed central role for TOR in orchestrating the life-extending effect of CR/DR in these two longevity paradigms. Moreover, although the postulated by the TOR-centric model dispensability of sirtuins for the longevity benefit associated with DR has been confirmed in worms [78], the importance of the sirtuin Sir2p in mediating the life-extending effect of CR in replicatively aging yeast is controversial [79, 80]. Some data imply that Sir2p is not required for such effect under severe CR conditions [76, 81]. In contrast, other data demonstrate that Sir2p plays an essential role in the extension of yeast replicative life span under moderate CR [82, 83], perhaps by being a downstream effector of the nutrient- and energy-sensing cAMP/PKA signaling pathway acting parallel to TOR [49].

It should be stressed that, while TOR is a central regulator of the life-extending effect of CR in replicatively aging yeast, the longevity benefit associated with CR in chronologically aging yeast is mediated by a signaling network that includes: 1) the TOR and cAMP/PKA pathways converged on the protein kinase Rim15p, which therefore acts as a nutritional integrator; and 2) some other, currently unknown signaling pathways that are not centered on Rim15p [26]. Considering the well-established convergence of the insulin/IGF-1, AMPK/TOR and cAMP/PKA signaling pathways into a complex network regulating longevity in worms, fruit flies and mammals [7, 9, 27, 34, 35], it is conceivable that – akin to TOR – the insulin/IGF-1 and cAMP/PKA pathways may contribute to the beneficial effect of CR/DR on their longevity. Although some data supports the involvement of the insulin/IGF-1 pathway in the longevity benefit associated with CR/DR [7, 84 - 87], other data imply that such benefit is independent of insulin/IGF-1 signaling in worms, fruit flies and mammals [88 - 93]. The role of

cAMP/PKA signaling in the life-extending effect of CR/DR in these multicellular eukaryotes remains to be tested. It should be stressed that a recently reported in worms involvement of both independent and overlapping pathways in life span extension by different DR regimens [94] supports the notion that the longevity benefit associated with nutrient limitation is mediated by a signaling network that regulates longevity by coordinating information flow along its convergent, divergent and multiply branched signaling pathways.

Akin to CR and DR regimens, certain pharmacological interventions can extend life span across phyla and, in some cases, improve overall health by beneficially influencing age-related pathologies (Figure 1.2). Many of the currently known anti-aging compounds increase life span and, some of them, promote healthy aging by targeting the AMPK/TOR signaling pathway responsive to the intracellular nutrient and energy status. By activating AMPK and thereby reducing TORC1 signaling, the type 2 diabetes therapeutics metformin extends longevity in worms [95] and mice [96]. The glutamine synthetase inhibitor methionine sulfoximine decreases the intracellular level of glutamine, an activator of TORC1, thus attenuating TORC1 signaling and extending the chronological life span of yeast [97, 98]. By inhibiting upstream TORC1 activators PI3K and MEK, LY294002 and U0126 (respectively) increase the replicative life span of cultured human fibrosarcoma cells by lowering TORC1 signaling [99]. Through its FKBP12-mediated inhibition of TORC1, the potent life-extending compound rapamycin extends 1) the replicative and chronological life spans of yeast [49, 98, 100]; 2) the replicative life spans of cultured rodent fibroblasts, human epithelium cells and human fibrosarcoma cells [101]; and 3) longevity in fruit flies and mice [36, 38]. The xanthine

alkaloid caffeine increases yeast chronological life span by decreasing the catalytic activity of Tor1p [102].
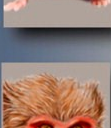
Mianserin, a serotonin receptor antagonist used as an antidepressant in humans, increases life span in worms by modulating an upstream step in the insulin/IGF-1 signaling pathway responsive to the organismal nutrient status, perhaps by mimicking a DR-like physiological state through the inhibition of neurotransmission related to food sensing [103]. In contrast, valproic acid, a mood stabilizer and an anticonvulsant in humans, targets a downstream step in this pathway by promoting the translocation of the FoxO transcriptional factor DAF-16 into the nucleus [104].

Several anti-aging compounds increase life span and, some of them, promote healthy aging by targeting a compendium of longevity-related processes that currently are not assigned to the insulin/IGF-1, AMPK/TOR and/or cAMP/PKA pathways. Being specifically modulated by such life-extending compounds, these processes extend longevity due to their integration into a longevity signaling network that coordinates information flow along its convergent, divergent and multiply branched signaling pathways. One of these compounds is resveratrol. By activating the protein deacetylase activities of the sirtuins Sir2p (yeast), SIR-2.1 (worms), dSir2 (fruit flies) and SIRT1 (mammals) [79, 105] (the ability of resveratrol to activate sirtuins *in vivo* is disputed [106, 107]) and/or by interacting with and modulating activities of its many other protein targets [108, 109], resveratrol extends 1) the replicative, but not chronological, life span of yeast [110]; 2) the replicative life span of cultured human fibroblasts [111]; and 3) longevity in worms, fruit flies, fishes and mice [112 - 115]. The life-extending and health-improving effects of resveratrol across species are due to its ability to modulate a

plethora of longevity-related processes [110, 113, 115 - 119]. Longevity can also be extended by a pharmacological intervention that raises the intracellular level of a sirtuin. In fact, the ability of sodium nitroprusside to increase the replicative life span of cultured human peripheral blood mononuclear cells (PMBC) correlates with its ability to activate expression of the sirtuin SIRT1; the resulting enhancement of SIRT1-dependent histone H4 lysine 16 deacetylation may induce an anti-aging pattern of transcription [120]. Another anti-aging compound that increases life span by reducing the extent of histone acetylation is spermidine. This natural polyamine extends 1) the chronological life span of yeast; 2) the replicative life span of cultured human PMBC; and 3) longevity in worms and fruit flies [121]. The life-extending effect of spermidine is due to its ability to inhibit histone acetyltransferases and promote histone H3 deacetylation; the resulting activation of transcription of numerous autophagy-related genes suppresses age-related necrotic cell death [105, 121]. Moreover, histone modification is also modulated by Li^+, an anti-aging compound in worms and a mood stabilizer in humans, that influences the age-related chromatin reorganization by altering transcription of genes involved in histone methylation, nucleosome composition and chromatin structure [122].

The plastoquinone derivate SkQ1 extends longevity in fungi, daphnias and fruit flies as well as increases life span and promotes healthy aging in mice by influencing longevity-related processes confined to mitochondria [123], organelles whose functional state modulates a complex signaling network governing longevity regulation [27, 62, 64, 124]. Following its specific targeting to mitochondria, SkQ1 acts as an antioxidant that prevents oxidative damage to mitochondrial proteins and lipids, alters mitochondrial morphology, and reduces hydrogen peroxide-induced apoptosis and necrosis controlled

by mitochondria [123]. Moreover, the thermal stress mimetics lipoic acid, propyl gallate, trolox and taxifolin function as antioxidants that increase life span in worms (all of them) and fruit flies (lipoic acid), perhaps by detoxifying free radicals and/or enhancing resistance to age-related oxidative stress [125, 126].

	Life-span increase		Beneficial health effects	
	Dietary restriction	**Mutations/ drugs**	**Dietary restriction**	**Mutations/ drugs**
Yeast	**3-fold**	**10-fold** (with starvation/ DR)	Extended reproductive period	Extended reproductive period, decreased DNA damage/mutations
Worms	**2- to 3-fold**	**10-fold**	Resistance to misexpressed toxic proteins	Extended motility Resistance to mis-expressed toxic proteins and germ-line cancer
Flies	**2-fold**	**60–70%**	None reported	Resistance to bacterial infection, extended ability to fly
Mice	**30–50%**	**30–50%** (~100% in combination with DR)	Protection against cancer, diabetes, atherosclerosis, cardio-myopathy, autoimmune, kidney, and respiratory diseases; reduced neurodegeneration	Reduced tumor incidence; protection against age-dependent cognitive decline, cardio-myopathy, fatty liver and renal lesions. Extended insulin sensitivity
Monkeys	**Trend noted**	**Not tested**	Prevention of obesity; protection against diabetes, cancer, and cardiovascular disease	**Not tested**
Humans	**Not determined**	**Not determined** (GHR-deficient subjects reach old age)	Prevention of obesity, diabetes, hypertension Reduced risk factors for cancer and cardiovascular disease	Possible reduction in cancer and diabetes

Figure 1.2. Certain diets and pharmacological interventions can extend longevity and improve overall health by delaying the onset of age-related diseases in evolutionarily distant organisms (see text in section 1.3 for details). Reproduced from Fontana, L., Partridge, L. and Longo, V.D. (2010). Extending healthy life span - from yeast to humans. *Science* 328:321-326.

All of the currently known anti-aging compounds increase life span under non-CR or non-DR conditions. Under such conditions, many of these molecules have been shown to 1) provide the longevity and health benefits associated with CR and DR, but without restricting caloric and nutrient intake; and 2) mimic numerous life-extending effects of CR and DR on gene expression pattern, metabolic and physiological processes, and stress response pathways. Therefore, the names "CR mimetics" and "DR mimetics" have been coined for such life-extending compounds [127 - 129]. Importantly, nearly all CR mimetics and DR mimetics are known to target the signaling pathways that modulate longevity in response to the organismal and intracellular nutrient and energy status, including the insulin/IGF-1 and AMPK/TOR pathways as well as the sirtuin-governed protein deacetylation module of the longevity signaling network integrating these pathways. Furthermore, such compounds as resveratrol, metformin and mianserin increase life span only under non-CR or non-DR conditions, but are unable to do so if the supply of calories or nutrients is limited [95, 103, 110, 112, 113]. Hence, one could envision that most, if not all, of the existing longevity pathways - currently known and those that, perhaps, remain to be discovered – are "adaptable" by nature, *i.e.*, that they modulate longevity only in response to certain changes in the extracellular and intracellular nutrient and energy status of an organism. However, Li$^+$ in worms and rapamycin in fruits flies have been recently shown to extend life span even under DR conditions [38, 122]. It is conceivable therefore that certain longevity pathways could be "constitutive" or "housekeeping" by nature, that is, that they 1) modulate longevity irrespective of the organismal and intracellular nutrient and energy status; and 2) do not overlap (or only partially overlap) with the longevity pathways that are under the

stringent control of calorie and/or nutrient availability. The challenge is to identify such housekeeping longevity pathway(s), perhaps by using a chemical screen for anti-aging compounds that can extend longevity even under CR/DR conditions. Because under such conditions the adaptable pro-aging pathways would be fully suppressed and the adaptable anti-aging pathways would be fully activated, a compound that can further increase life span is expected to target the housekeeping longevity pathway(s). It seems conceivable that such a compound can also increase life span under non-CR or non-DR conditions, although perhaps to a lesser extent than it does if the supply of calories or nutrients is limited.

1.4. Yeast is a valuable model organism for studying the basic biology of aging and revealing longevity regulation mechanisms in multicellular eukaryotes

The budding yeast *Saccharomyces cerevisiae*, a genetically and biochemically manipulable unicellular eukaryote with annotated genome, is a valuable model for unveiling mechanisms of cellular aging in multicellular eukaryotes [130 - 132]. Yeast aging can be measured in two different ways. Replicative aging is defined by the maximum number of daughter cells that a mother cell can produce before senescence and models aging of a mitotically active cell in a multicellular organism (Figure 1.3) [131, 133]. In contrast, chronological aging is measured by the length of time a yeast cell remains viable in a nondividing state and models aging of postmitotic mammalian cells (*e.g.*, neurons) (Figure 1.3) [56, 131, 132]. In a simple clonogenic assay for measuring

14
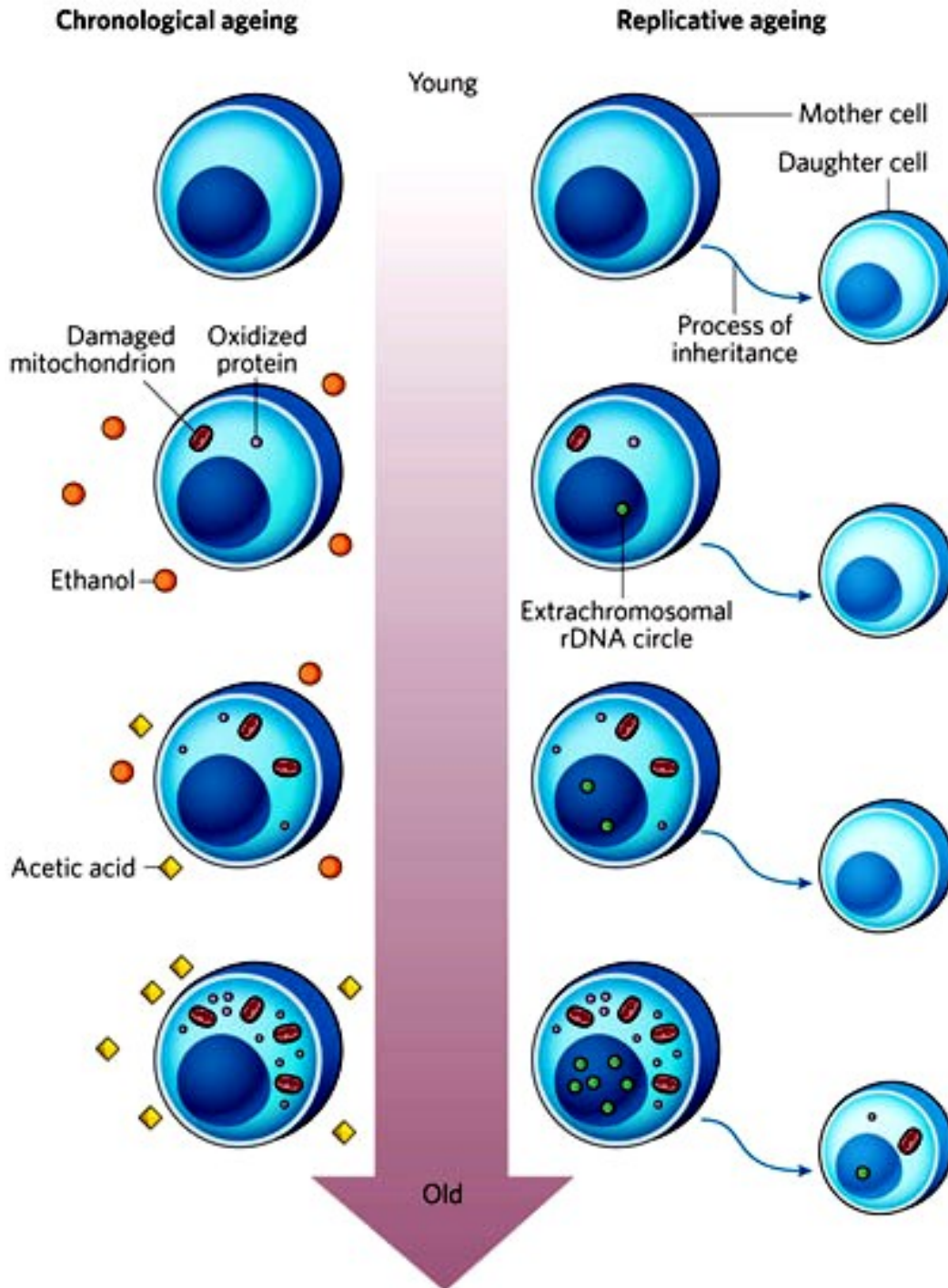
Figure 1.3. Two different ways to monitor yeast aging and age-related macromolecular damage to yeast cells. Yeast replicative aging is measured by the maximum number of daughter cells that a mother cell can produce before senescence, thereby modeling aging of a mitotically active cell in a multicellular eukaryotic organism. Yeast chronological aging is measured by the length of time a yeast cell remains viable in a nondividing state, thereby modeling aging of postmitotic mammalian cells (*e.g.*, neurons). (See text in section 1.4 for details). Reproduced from Kaeberlein, M. (2010). Lessons on longevity from budding yeast. Nature 464:513-519.

yeast chronological aging, the percentage of viable yeast cells in their aging population is monitored at different time points before and after this population enters the non-proliferative stationary phase [56]. Both replicative and chronological aging of yeast can be decelerated by caloric restriction (CR), a low-calorie dietary regimen that extends life span in various multicellular eukaryotic organisms and delays the onset or reduces the incidence of many age-related diseases in mice and primates [66 - 69, 131, 134 - 136]. Because the fundamental mechanisms of aging are conserved across phyla [1, 3, 5, 20 - 23], the relatively short and easily measured life span of yeast - in combination with their amenability to comprehensive biochemical, genetic, cell biological, chemical biological and system biological analyses - enabled for the first time to identify numerous longevity genes later shown to govern aging process in multicellular eukaryotes, define the nature of the molecular damage to biological macromolecules that contributes to aging and age-related disorders in higher eukaryotic organisms, and reveal potent anti-aging compounds later demonstrated to extend longevity in a wide range of eukaryotic organisms [130 - 137].

1.5. The deposition and lipolytic degradation of neutral lipids contribute to longevity regulation and age-related pathologies

Proper control of the deposition and mobilization of neutral lipids is mandatory for maintaining energy homeostasis and, thus, may play an important role in longevity regulation [138 - 141]. The molecular and cellular mechanisms linking metabolism of neutral lipids and longevity are yet to be defined. The establishment of such mechanisms operating in chronologically aging yeast was one of the major objectives of my thesis.

Triacylglycerols (TAG) and ergosteryl esters (EE) are the two major species of neutral lipids that in yeast cells are deposited in so-called lipid bodies (LBs) [142 - 144]. TAG and EE serve as the main storage molecules for free fatty acids (FFA), diacylglycerols (DAG) and ergosterol (ERG). Lipolysis of TAG generates FFA, which can be either incorporated into newly synthesized phospholipids and cardiolipins or degraded through β-oxidation in the peroxisome of yeast [143, 144]. Lipolysis of TAG also produces various DAG species, which not only serve as building blocks for synthesis of the phospholipids phosphatidylethanolamine (PE) and phosphatidylcholine (PC) but also operate as potent signaling molecules modulating a protein kinase C (PKC)-dependent signal transduction network governing multiple stress response- and longevity-related processes [145, 146]. Lipolysis of EE in yeast results in the formation of FFA and ERG, a sterol lipid known to play an important role in numerous essential functions of cellular membranes [142 - 144, 147, 148]. Thus, the ability of yeast to modulate the biosynthesis and degradation of neutral lipids is crucial for regulating 1) energy homeostasis; 2) phospholipid and cardiolipin biosynthesis; 3) neutralization of excessive amounts of membrane-perturbing species of FFA, ERG and TAG; 4) the FFA- and DAG-induced lipoapoptotic and necrotic forms of cell death; and 5) a DAG-modulated, PKC-dependent signal transduction network that governs multiple stress response- and longevity-related processes [142 - 148]. All these processes are currently viewed as vital for modulating the aging process in evolutionarily distant organisms [138 - 141, 145, 146, 149 - 151].

Neutral lipid synthesis in yeast cells takes place in the endoplasmic reticulum (ER) [143, 144, 147, 152]. TAG is formed through several acylation and dephosphorylation

steps from lysophosphatidic acid (LPA), which itself can be formed in one of the following two ways: 1) acylation of glycerol-3-phosphate by either Gpt2p or Sct1p protein or 2) acylation of dihydroxyacetone phosphate (DHAP), also by Gpt2p or Sct1p, followed by reduction of 1-acyl-DHAP in an Ayr1p-catalyzed reaction [143, 144, 147, 152]. Another acyl group is transferred to the *sn*-2 position of LPA to form phosphatidic acid (PA). PA is then dephosphorylated by one of three dephosphorylases, Pah1p, Dpp1p or Lpp1p, to form DAG; DAG can also be formed from glycerophospholipids by removal of the head group-phosphate. TAG is formed from DAG by acylation of the *sn*-3 position either with acyl-CoA (catalyzed by Dga1p, Are1p or Are2p) or with acyl groups transferred from glycerophospholipids (catalyzed by Lro1p). EE synthesis in the ER is driven by Are1p or Are2p, which catalyze the transfer of an acyl group from acyl-CoA to ERG [143, 144, 147, 152].

TAG degradation in yeast cells takes place in LBs and is driven by the Tgl2p, Tgl3p, Tgl4p and Tgl5p lipases, whereas EE hydrolysis occurs either within the plasma membrane in a Yeh2p-catalyzed reaction or within LBs in a reaction that is catalyzed by the Tgl1p lipase [143, 144, 147, 152].

Growing evidence supports the view that the deposition and lipolytic degradation of neutral lipids in LBs of fat storage tissues define longevity of multicellular eukaryotic organisms [153]. Found in most eukaryotic and some prokaryotic cells, LBs have been also referred to as lipid droplets, lipid particles, oil bodies and by many other different names that reflect their cellular and biochemical context in various biological systems [154, 155]. LBs have long been viewed as relatively inert organellar compartments [156, 157]. They were believed to function only as a site for storing excess energy and

stockpiling FFA and sterols in the form of neutral lipids, mainly TAG and steryl esters [154, 160, 161]. Surrounded by a monolayer of phospholipids and associated proteins, the neutral lipid core of LBs can be hydrolyzed in a regulated fashion by lipases [160, 161]. The resulting retrieval of stored FFA, phospholipids and sterols provides energy via fatty acid oxidation during times of nutrient scarcity, maintains the homeostasis of membrane lipids during cell growth and division, and modulates the levels of free sterols inside and outside of the cell [154 - 161].

An important recent advance in our understanding of the cell biology of LBs is that they constitute highly dynamic organellar compartments whose protein and lipid composition, *de novo* formation from the ER template, growth, fragmentation, shrinkage due to lipolysis, movement, and association with other organelles is regulated by a complex network of protein machines [157 - 159, 161 - 172]. It has also become clear that LBs are dynamically integrated into several vital processes and can serve both as an intracellular signaling compartment and as an organizing platform orchestrating these processes. In yeast, the phosphorylation and activation of the LBs-associated lipase Tgl4p by cyclin-dependent kinase 1 controls cell-cycle progression by mobilizing triacylglycerols, thereby providing fatty acids and phospholipids for the secretory vesicle-dependent bud formation and ultimately enabling the G1/S phase transition [173]. Furthermore, it appears that LBs in white adipose tissue (WAT) of mice function as a hub in a regulatory network that, by modulating the synthesis and secretion of adipokines and the lipokine C16:1n7-palmitoleate, is central to the multiple defects in metabolic homeostasis associated with obesity, insulin resistance, type 2 diabetes, atherosclerosis and inflammatory disorders [165, 167, 174 - 178]. Moreover, by recruiting certain

proteins from other cellular locations, temporally housing them, managing their availability and modulating their activities, LBs have been proposed to play important roles in the regulation of various cellular processes [157, 167, 171]. It has been suggested that, by sequestering proteins, LBs function as an organizing platform that 1) removes excess proteins from other organellar compartments, inactivates them and/or stores them for later use; 2) promotes the refolding of unfolded proteins targeted to LBs by recruiting molecular chaperones from the cytosol; 3) provides a surface for the ordered degradation of partially unfolded and misfolded LBs-bound proteins that otherwise can form toxic aggregates in the cytosol; and 4) delivers some LBs-associated proteins to their target organellar compartments via permanent or transient contact sites [157, 167, 171, 179 - 181].

One of the recently discovered new and unexpected functions of LBs is the essential role they play in longevity regulation. It appears that various interventions that inhibit the deposition of neutral lipids in LBs or activate their lipolytic degradation in fat storage tissues of the nematode *Caenorhabditis elegans*, the fruit fly *Drosophila melanogaster* or laboratory mice also extend the life spans of these organisms. In fact, presently unknown humoral signals produced and secreted by somatic cells in the gonad of *C. elegans* promote the nuclear localization of the forkhead transcription factor DAF-16 in intestinal cells, the principal site of neutral lipid storage in this organism [182]. DAF-16 then induces the expression of a gene encoding a specific lipase, thereby promoting the lipolysis of neutral lipids stored in LBs of intestinal cells and extending longevity by a yet-to-be established mechanism [182]. Furthermore, the elimination of LBs-associated lipases Brummer or ATGL (adipose triacylglycerol lipase) in the fat body

20

of flies or WAT of mice, respectively, shortens life span [183, 184]. Moreover, by greatly diminishing the levels of stored neutral lipids in WAT, both the elimination of WAT-specific insulin receptor and the replacement of the C/EBPα (CCAAT/enhancer-binding protein) protein with its paralogue C/EBPβ extend longevity in mice [185 - 187]. Importantly, a low-calorie dietary regimen known as caloric restriction (CR) extends life span in a wide spectrum of organisms and delays the onset of age-related diseases in rodent models [174]. The life-extending effect of CR in worms and flies is mediated by so-called sirtuins, a family of NAD^+-dependent protein deacetylases and ADP ribosylases [174, 186]. In mice, CR diet increases the abundance of the sirtuin SIRT1, which has been shown to repress transcription of genes that are required for the LBs-confined accumulation of neutral lipids in WAT [174, 188]. It has been therefore proposed that SIRT1 delays aging of CR mice by shifting a balance between the opposing processes of LBs' formation and degradation in WAT towards lipolytic degradation of neutral lipids in this fat storage tissue [174, 188].

Altogether, these findings imply that the LBs-confined deposition and lipolytic degradation of neutral lipids in fat storage tissues define longevity of multicellular eukaryotic organisms. A key challenge for the future will be to establish the molecular mechanisms by which a delicate balance between the opposing processes of neutral lipids accumulation and their lipolytic degradation regulates longevity in these organisms. Recent studies suggested three such mechanisms (Figures 1.4, 1.5 and 1.6). First, the size of LBs in WAT of mice modulates the ability of the ER in this tissue to synthesize and send for secretion various anti-hyperglycaemic and pro-hyperglycaemic protein hormones that control metabolic homeostasis in other tissues [174, 175, 189, 190]. In

intestine of worms, LBs that accumulate in this fat storage tissue contribute sterols for the biosynthesis in the ER and the subsequent secretion of the lipophilic hormones dafachronic acids and pregnenolone, both of which delay cellular aging in other tissues [190]. Thus, it is conceivable that the dynamics of LBs-confined deposition and lipolytic degradation of neutral lipids in fat storage tissues modulates their ability to synthesize in the ER and then secrete humoral signals that control longevity-related processes in other tissues (Figure 1.4).
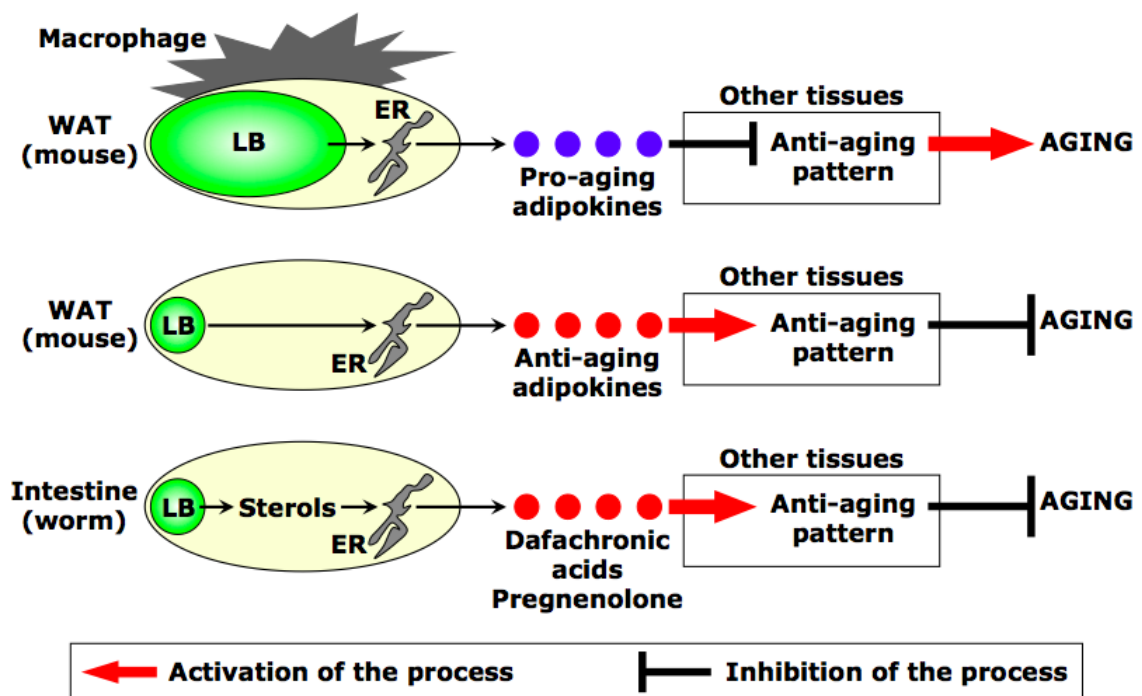
Figure 1.4. The first possible mechanism by which the deposition and lipolytic degradation of neutral lipids in lipid bodies (LBs) of fat storage tissues define longevity of multicellular eukaryotic organisms. The size of LBs in white adipose tissue (WAT) of mice modulates the ability of the endoplasmic reticulum (ER) in this tissue to synthesize and send for secretion various pro- and anti-aging adipokines that control longevity-related processes in other tissues. Overloading LBs in WAT with neutral lipids results in the recruitment of macrophages to this fat storage tissue. Macrophages that infiltrate WAT secrete some of the pro-aging adipokines, whereas adipocytes of WAT secrete others. In intestine of worms, LBs that accumulate in this fat storage tissue contribute sterols for the biosynthesis in the ER and the subsequent secretion of the lipophilic hormones dafachronic acids and pregnenolone, both of which delay cellular aging in other tissues.

Second, the lipolysis of LB-deposited neutral lipids results in the release of the lipokine C16:1n7-palmitoleate, an unsaturated FFA, from WAT of mice [177]. This recently discovered lipid hormone regulates systemic carbohydrate and lipid homeostasis in muscle and liver by promoting muscle insulin sensitivity and attenuating hepatic steatosis [177]. Hence, the LBs-derived C16:1n7-palmitoleate produced in and then secreted by WAT of mice could function as a signaling molecule that plays an important role in longevity regulation (Figure 1.5).
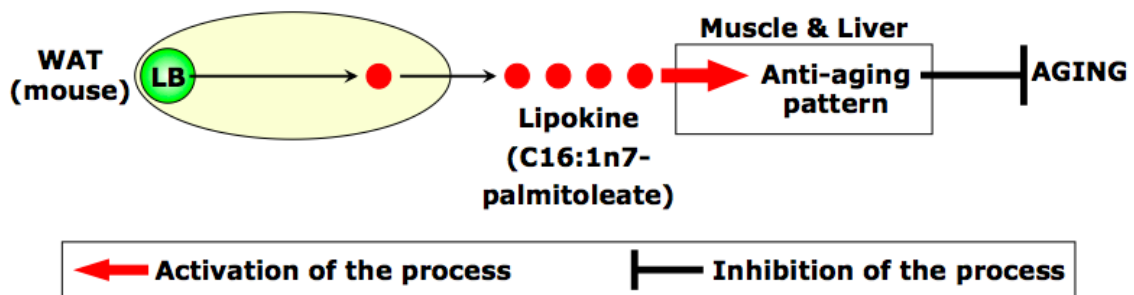
Figure 1.5. The second possible mechanism by which the deposition and lipolytic degradation of neutral lipids in lipid bodies (LBs) of fat storage tissues define longevity of multicellular eukaryotic organisms. The lipolysis of LB-deposited neutral lipids results in the release of the lipokine C16:1n7-palmitoleate, an unsaturated fatty acid, from WAT of mice. This LB-derived lipid hormone regulates longevity-related processes in muscle and liver.

Third, in response to enhanced lipolysis of LB-deposited neutral lipids, WAT of mice and the fat body of flies activate certain regulatory networks that stimulate mitochondrial biogenesis and β-oxidation of FFA in mitochondria [178, 187, 191]. This, in turn, decreases the levels of saturated FFA secreted by these fat storage tissues, thereby reducing the risk of lipotoxicity in other tissues and preventing muscle insulin resistance and hepatic steatosis [176 - 178, 192]. Importantly, such stimulation of mitochondrial biogenesis and β-oxidation of FFA in WAT of mice expressing the β paralogue of C/EBP

increases their life span [187]. Therefore, it is likely that this third mechanism, which is confined to fat storage tissues, plays an important role in delaying cellular aging in peripheral tissues and increasing longevity of the entire organism (Figure 1.6).
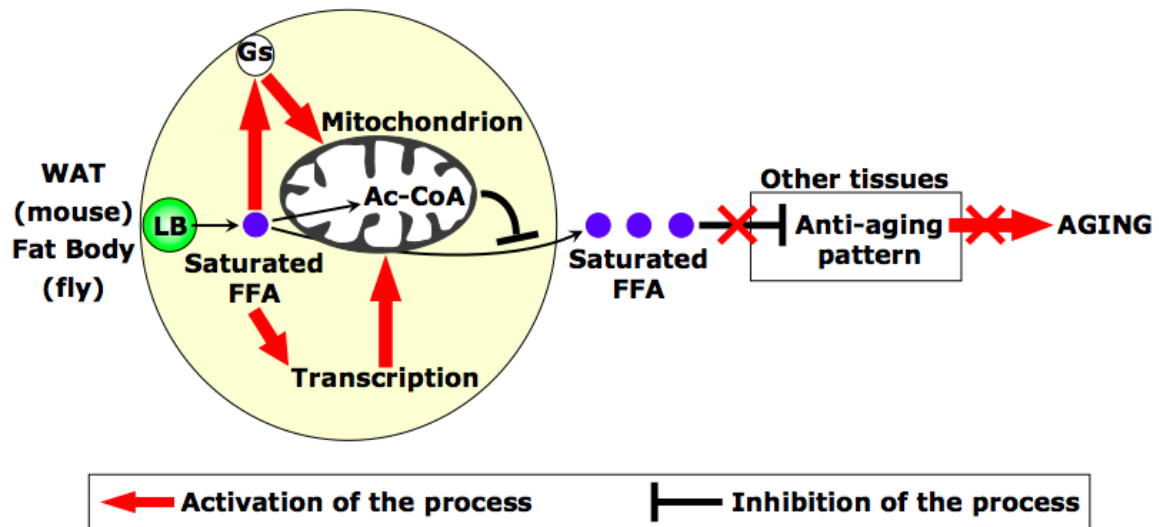
Figure 1.6. The third possible mechanism by which the deposition and lipolytic degradation of neutral lipids in lipid bodies (LBs) of fat storage tissues define longevity of multicellular eukaryotic organisms. In response to enhanced lipolysis of LB-deposited neutral lipids, adipocytes in WAT of mice increase the level of the G protein α stimulatory subunit (Gs), whereas cells in the fat body of flies activate transcription of numerous genes positively regulated by the hepatocyte nuclear factor 4. This, in turn, stimulates mitochondrial biogenesis and β-oxidation of free fatty acids (FFA) in mitochondria, thereby decreasing the levels of saturated FFA secreted by these fat storage tissues. Saturated FFA are lipotoxic in peripheral tissues and cause muscle insulin resistance and hepatic steatosis. Thus, the stimulation of mitochondrial biogenesis and FFA β-oxidation in fat storage tissues displaying enhanced lipolysis of neutral lipids plays an important role in delaying cellular aging in peripheral tissues. Other abbreviations: Ac-CoA, acetyl-CoA.

1.6. Cardiolipin lipid species in the mitochondrial membrane modulate mitochondria-governed processes whose dysfunction underlies aging and age-related pathologies

Cardiolipin (CL) is the mitochondria-specific dimeric glycerophospholipid, which contains three glycerol backbones and four acyl chains and almost exclusively localized in the mitochondrial inner membrane [193 - 200]. Various molecular species of this signature lipid of the mitochondrial inner membrane have been shown to 1) associate with and modulate activities of all five complexes of the mitochondrial respiratory chain, also promoting their organization into supramolecular assemblies; 2) bind to and modulate the activity of cytochrome c, a heme-containing mobile component of the mitochondrial respiratory chain also known for its essential role in mitochondria-controlled apoptosis; 3) associate with and regulate the activity of the adenine nucleotide translocator; 4) play an essential role in maintaining the electrochemical gradient across the mitochondrial inner membrane; 5) confer fluidity and stability to the inner membrane of mitochondria; 6) be primary targets of an ROS-inflicted damage because of their highly unsaturated acyl chains; 7) regulate the protein import into mitochondria [193 - 200]. Due to its ability to interact by non-covalent bonds with a number of unrelated proteins in the mitochondrial inner membrane, CL operates as a molecular chaperone that governs the assembly of a number of protein assemblies involved in a plethora of biological processes [194 - 200]. Moreover, the conversion of CL to phosphatidic acid (PA) is essential for mitochondrial fission and fusion [201 - 203].

Because of the involvement of CL in all these basic biological processes, specific alterations in its content and/or composition have been reported in pathological states characteristic of various disorders. A distinct set of mutations in the tafazzin gene, which in humans encodes an enzyme involved in the remodeling of CL acyl chains, causes so-called Barth Syndrome by reducing total CL levels, elevating monolysocardiolipin

concentrations and decreasing the levels of unsaturated fatty acyl species of CL [193, 195, 198]. The clinical manifestations of this X-linked recessive disorder include cardioskeletal myopathy, neutropenia and abnormal growth [193, 195]. Furthermore, reduced levels of CL and the resulting accumulation of dysfunctional mitochondria are characteristic of the early stages of aging in rodents and humans [194, 195, 198]. It should be stressed that CL is particularly susceptible to the age-related accumulation of mitochondrially produced ROS – due to its high content of oxidative damage-vulnerable unsaturated fatty acids and its proximity to the sites of ROS generation in mitochondria [194, 196 - 199]. Moreover, alterations in CL content and/or composition have been linked to several other disorders, including Tangier disease, diabetic cardiomyopathy, dilated cardiomyopathy with ataxia and non-alcoholic fatty liver disease [195, 198].

Little is known about the molecular mechanisms underlying the essential role of CL in regulating various mitochondria-governed processes whose dysfunction underlies aging and age-related pathologies. It has been proposed that CL modulates the ability of prohibitins Phb1p and Phb2p - two evolutionarily conserved proteins that form large complexes with each other in the mitochondrial inner membrane - to maintain the organization and functional integrity of this membrane [197, 200, 204 - 207]. The multimeric, high-molecular weight complexes of prohibitins function as protein scaffolds that control the integrity and functionality of the mitochondrial inner membrane [197, 200, 204 - 207]. Such scaffolding function of prohibitins relies on their ability to coordinate activities of numerous protein components of the mitochondrial inner and outer membranes. These physically and/or functionally interacting protein partners of prohibitins include: 1) proteins that function in the assembly of the respiratory chain; 2)

proteins that are essential for both the maintenance of mitochondrial morphology and the assembly of β-barrel proteins in the outer membrane; 3) the *m*-AAA protease, an ATP-dependent protease with a critical role in protein quality control within the inner mitochondrial membrane; and 4) proteins that regulate, in a highly coordinated fashion, the levels of CL and the glycerophospholipid phosphatidylethanolamine (PE) [197, 200, 204 - 207]. One of the major objectives of my thesis was therefore to define the molecular mechanisms underlying the essential role of CL in regulating longevity of chronologically aging yeast.

1.7. Thesis outline and contributions of colleagues

Chapter 2 describes my successful attempt to solve the inherent limitations of the currently used methods for lipidomic analysis (including the limitations characteristic of the mass spectrometry-based analysis) by developing a survey-scan method for quantitative assessment of the entire complement of lipids in yeast cells using electrospray ionization mass spectroscopy (ESI/MS). The survey-scan ESI/MS method of lipidomic analysis that I developed demonstrated that: 1) yeast has a relatively simple lipidome with 7 major lipid classes; 2) the majority of individual molecular forms within each of these different lipid classes have chain length of 16 or 18 carbon atoms; and 3) the fatty acyl moieties of all of lipid species composing yeast lipidome are either mono-unsaturated or saturated, perhaps due to the presence of a single acyl desaturase enzyme in yeast. Furthermore, the method that I developed is highly sensitive as it is: 1) sensitive to the low μM range (0.6 to 2 μM depending on lipid class) for all lipid species tested; and 2) linear to the hundreds of μM range, with the concentration linearity spreading over

2 to 3 orders of magnitude. Moreover, the method that I developed enables very accurate quantitation of different lipid species within a wide range of lipid concentrations. Importantly, if compared to the currently used ESI/MS-MS-based method of lipidomic analysis, my method has the following important advantages: 1) unlike the ESI/MS-MS-based method, it can be carried out within a very limited period of time; 2) unlike the ESI/MS-MS-based method, it does not require to maintain stable spray conditions at the ESI source for long periods of time; 3) unlike the ESI/MS-MS-based method, it does not have a bias towards certain lipid species, thereby being sufficiently sensitive to unexpected changes in lipid spectra of analyzed cells; 4) it is more sensitive than the ESI/MS-MS-based method and, thus, does not require abundant quantities of cells for lipid extraction and analysis; and 5) it has lower than the ESI/MS-MS-based method limits of detection and quantitation for all yeast lipid species. I have successfully applied this method to quantitatively assess not only the lipidomes of whole yeast cells and their highly purified organelles, but also the entire complement of lipids in cultured human microglial cells. My findings presented in Chapter 2 support the notion that the survey-scan ESI/MS method of lipidomic analysis that I developed enables within a very limited period of time and using a very low number of cells to resolve, unequivocally identify and accurately quantitate all molecular forms of lipid species composing yeast lipidome and the majority of molecular forms of lipid species composing the lipidome of cultured human microglial cells.

Chapter 3 describes how I used a combination of functional genetic, cell biological, electron and fluorescence microscopical, proteomic, lipidomic, and metabolomic analyses to establish the molecular mechanism underlying the ability of CR to extend

longevity of chronologically aging yeast by specifically remodelling lipid metabolism in the ER, LBs and peroxisomes. In this mechanism, LBs in yeast cells function as a hub in a regulatory network that modulates neutral lipids synthesis in the ER and fatty acid oxidation in peroxisomes. Ethanol accumulated in yeast placed on a calorie-rich diet represses the synthesis of Fox1p, Fox2p and Fox3p, thereby suppressing peroxisomal oxidation of FFA that originate from TAG synthesized in the ER and deposited within LBs. The resulting build-up of arrays of FFA (called gnarls) within LBs of non-CR yeast initiates several negative feedback loops regulating the metabolism of TAG. Due to the action of these negative feedback loops, chronologically aging non-CR yeast not only amass TAG in LBs but also accumulate FFA and DAG in the ER. FFA and DAG regulate longevity by two different mechanisms that operate at two different stages of the aging process. One mechanism involves sensing the concentration of DAG maintained by cells (in a diet- and genotype-dependent fashion) during diauxic (D) and post-diauxic (PD) growth phases. DAG concentration during D and PD phases programs cell viability during the non-proliferative stationary (ST) growth phase by modulating the FFA- and DAG-induced necrotic cell death pathway, but not by influencing the mitochondria-controlled apoptotic pathway of cell death. Another mechanism involves sensing the concentrations of FFA and DAG during ST phase. Any diet or genetic manipulation that causes the build-up of these two lipids during ST phase shortens the chronological life span of yeast in part by promoting rapid mitochondria-controlled apoptotic cell death, but not by activating FFA- and DAG-induced necrotic cell death pathway.

Chapter 4 describes how I used a combination of functional genetic, cell biological, electron and fluorescence microscopical, proteomic, lipidomic, and metabolomic

analyses to find a short-lived mutant strain most suitable for conducting a high-throughput screen of novel anti-aging compounds that can extend longevity by altering lipid metabolism under CR conditions. Based on my findings, I proposed to use *pex5Δ* as such mutant strain. As described in Chapter 4, I found that in yeast placed on a CR diet this mutation leads to: 1) increase in FFA, DAG, TAG and EE and their build-up in the ER and LBs; 2) excessive accumulation of the ER membranes and ER-originated LBs; and 3) enhanced susceptibility to necrotic cell death caused to a short-term exposure to exogenously added FFA and DAG. Using the short-lived *pex5Δ* mutant strain, Alexander Goldberg in Dr. Titorenko's laboratory conducted a high-throughput screen of novel anti-aging compounds that can extend the chronological life span (CLS) of yeast by targeting these longevity-defining aspects of lipid metabolism under CR conditions. One of the life-extending compounds identified in such screen was lithocholic acid (LCA), a bile acid. LCA greatly extends the CLS of wild-type (WT) strain of yeast placed on a CR diet. As described in Chapter 4, by elucidating how LCA influences the metabolism of lipids as well as age-related forms of necrotic and apoptotic death in chronologically aging yeast and how it alters yeast proteome, I established the molecular mechanism underlying the ability of LCA to extend yeast CLS by targeting these longevity-defining aspects of lipid metabolism confined to the ER, LBs and peroxisomes. In such mechanism, under CR conditions LCA accelerates the biosynthesis of TAG from FFA and DAG in the ER as well as decelerates the FFA- and DAG-generating lipolysis of TAG in LBs. The resulting reduction of the ER- and LB-confined levels of FFA and DAG during diauxic (D), post-diauxic (PD) and stationary (ST) growth phases affects both mechanisms by which these two lipid species regulate longevity. First, by lowering the intracellular

concentration of DAG during D and PD phases, LCA attenuates the FFA- and DAG-induced necrotic cell death pathway – thereby impairing the age-related form of necrotic cell death and ultimately extending longevity of chronologically aging yeast placed on a CR diet. Second, by reducing the intracellular concentrations of FFA and DAG during ST phase, LCA attenuates the mitochondria-controlled apoptotic cell death pathway – thereby impairing the age-related form of apoptotic cell death and ultimately extending longevity of chronologically aging yeast under CR conditions.

Chapter 5 describes how I used a combination of functional genetic, cell biological, electron and fluorescence microscopical, and lipidomic analyses to establish the molecular mechanism underlying the ability of LCA to extend yeast life span by targeting the metabolism of membrane lipids in mitochondria. My findings imply that under CR conditions LCA extends yeast longevity by remodeling the composition of mitochondrial membrane lipids and thereby modulating longevity-defining processes confined to and/or governed by mitochondria. I concluded that LCA extends the CLS of WT yeast by: 1) increasing the level of phosphatidylserine (PS) in the mitochondrial membrane, thereby enhancing its positive effect on longevity-defining processes in this membrane; 2) decreasing the level of phosphatidylethanolamine (PE) in the mitochondrial membrane, thereby weakening its negative effect on longevity-defining processes in this membrane; and 3) proportionally decreasing the levels of PE and cardiolipin (CL) in the mitochondrial membrane, thereby increasing PS/CL and PS/PE ratios but maintaining PE/CL ratio of mitochondrial membrane lipids and causing some longevity-extending changes in this membrane. My analysis of the biological implications of these LCA-driven specific changes in mitochondrial membrane lipids revealed that, by altering the

levels of PS, CL and PE, LCA: 1) changes the curvature of the inner mitochondrial membrane; and 2) enhances the positive effect of PS and weakens the negative effect of PE on membrane proteins whose activity depends on these two lipid species - thereby enhancing the ability of the inner mitochondrial membrane to form cristae and activating protein machines involved in mitochondrial respiration, the maintenance of mitochondrial membrane potential and ROS production in mitochondria.

Some of the findings described in Chapter 2 have been published in *The Journal of Visualized Experiments* [Bourque, S.D. and Titorenko, V.I. (2009). A quantitative assessment of the yeast lipidome using electrospray ionization mass spectrometry. *J. Vis. Exp.* 30:1-3]. I carried out all experiments described in this publication and prepared the first draft of the manuscript. Dr. V. Titorenko provided intellectual leadership of this project and edited the manuscript. Furthermore, my presented in Chapter 2 data on characteristic changes in the lipidome of human microglia exposed to various pro-inflammatory and anti-inflammatory interventions constitute an integral part of a soon-to-be submitted to *FASEB Journal* manuscript [Khatchadourian, A., Bourque, S.D., Richard, V.R., Titorenko, V.I. and Maysinger, D.[*]corresponding author (2011). LPS induces lipid droplet accumulation and perilipin-2 expression in microglia. *FASEB Journal*]. I carried out and supervised about 50% of the work on lipidomic analysis of human microglia described in this publication and prepared the first draft of sections relevant to my work. Dr. Maysinger and Dr. V. Titorenko provided intellectual leadership of this project and edited the manuscript. Moreover, most of the findings described in Chapter 2 are presented in the manuscript of a paper [Bourque, S.D., Richard, V.R., Beach, A. and Titorenko, V.I. Analysis of the *Saccharomyces cerevisiae* lipidome using survey-scan

electrospray-ionization mass spectroscopy] that is currently in preparation for submission to *The Journal of Lipid Research*. I expect this manuscript to be submitted for publication in late April or early May 2011.

Some of the findings described in Chapter 3 have been published in *The Biochemical Society Transactions* [Goldberg, A.A., Bourque, S.D., Kyryakov, P., Boukh-Viner, T., Gregg, C., Beach, A., Burstein, M.T., Machkalyan, G., Richard, V., Rampersad, S. and Titorenko, V.I. (2009). A novel function of lipid droplets in regulating longevity. *Biochem. Soc. Trans.* 37:1050-1055] and *Experimental Gerontology* [Goldberg, A.A., Bourque, S.D., Kyryakov, P., Gregg, C., Boukh-Viner, T., Beach, A., Burstein, M.T., Machkalyan, G., Richard, V., Rampersad, S., Cyr, D., Milijevic, S. and Titorenko, V.I. (2009). Effect of calorie restriction on the metabolic history of chronologically aging yeast. *Exp. Gerontol*. 44:555-571]. I carried out and supervised more than 30% of all of the work described in each of these publications and prepared the first draft of sections relevant to my work. I am an equally contributed first co-author on both these publications. Dr. V. Titorenko provided intellectual leadership of these projects and edited both manuscripts. Moreover, most of the findings described in Chapter 3 are presented in the manuscript of a paper [Bourque, S.D., Richard, V.R., Beach, A., Burstein, M.T., Goldberg, A.A., Kyryakov, P. and Titorenko, V.I. A mechanism linking lipid metabolism and longevity in chronologically aging yeast] that is currently in preparation for submission to *Cell Metabolism*. I expect this manuscript to be submitted for publication in late July or early August 2011.

Some of the findings described in Chapter 4 have been published in *Aging* [Goldberg, A.A., Richard, V.R., Kyryakov, P., Bourque, S.D., Beach, A., Burstein, M.T.,

Glebov, A., Koupaki, O., Boukh-Viner, T., Gregg, C., Juneau, M., English, A.M., Thomas, D.Y. and Titorenko, V.I. (2010). Chemical genetic screen identifies lithocholic acid as an anti-aging compound that extends yeast chronological life span in a TOR-independent manner, by modulating housekeeping longevity assurance processes. *Aging* 2:393-414]. I carried out and supervised approximately 25% of the work described in this publication and prepared the first draft of sections relevant to my work. I am an equally contributed first co-author on this publication. Dr. V. Titorenko provided intellectual leadership of this project and edited the manuscript. Moreover, most of the findings described in Chapter 4 are presented in the manuscript of a paper [Bourque, S.D., Richard, V.R., Beach, A., Burstein, M.T., Goldberg, A.A., Kyryakov, P. and Titorenko, V.I. Lithocholic acid extends yeast longevity in part by targeting the longevity-defining aspects of lipid metabolism confined to the endoplasmic reticulum, lipid bodies and peroxisomes] that is currently in preparation for submission to *Developmental Cell*. I expect this manuscript to be submitted for publication in late September or early October 2011.

Findings described in Chapter 5 are presented in the manuscript of a paper [Bourque, S.D., Richard, V.R., Beach, A., Burstein, M.T., Koupaki, O., Goldberg, A.A., Kyryakov, P. and Titorenko, V.I. Lithocholic acid extends yeast longevity in part by altering the composition of mitochondrial membrane lipids] that is currently in preparation for submission to *The Journal of Cell Biology*. I expect this manuscript to be submitted for publication in late October or early November 2011. I am the first author on this manuscript. I carried out and supervised approximately 40% of the work described in it and prepared the first draft of sections relevant to my work. Dr. V.

Titorenko provided intellectual leadership of this project and is currently editing the manuscript.

All abbreviations, citations, and the numbering of figures and tables that have been used in the published paper and in the manuscripts in preparation have been changed to the format of this thesis.

2. Development of a method for quantitative assessment of the lipidomes of yeast and cultured human cells using survey-scan electrospray ionization mass spectrometry (ESI/MS)

2.1. Abstract

Existing methods for lipid identification and quantification - such as fluorescence microscopy, high performance liquid chromatography (HPLC), thin-layer chromatography (TLC) and gas chromatography followed by mass spectrometry (GC/MS) - are well established but suffer from low sensitivity, are time consuming, insufficiently separate various molecular forms of lipids and require lipid derivatization prior to analysis. In order to overcome these inherent limitations of the currently used methods for lipidomic analysis, I have devised a method for quantitative assessment of the the entire complement of lipids in yeast cells using survey-scan ESI/MS. This method exceeds currently available methods for lipid identification and quantification in the ability to resolve various molecular forms of lipids, sensitivity, and speed. I have successfully applied this method to quantitatively assess not only the lipidomes of whole yeast cells and their highly purified organelles, but also the entire complement of lipids in cultured human microglial cells.

2.2. Introduction

Lipids are one of the major classes of biomolecules and play important roles in membrane dynamics, energy storage and signaling [208 - 211]. The budding yeast *Saccharomyces cerevisiae*, a genetically and biochemically manipulable unicellular eukaryote with annotated genome and very simple lipidome, is a valuable model for

studying biological functions of various lipid species in multicellular eukaryotes [208, 211, 212]. *S. cerevisiae* has a relatively simple lipidome, with the normal compliment of glycerophospholipids, neutral lipids and ceramides [213, 214]. Due to the presence of only one acyl desaturase enzyme in yeast, the fatty acyl moieties of all of its lipid species are either mono-unsaturated or saturated [212 - 215]. Furthermore, about 95% of the glycerophospholipid and neutral lipid species found in yeast cells have chain length of 16 or 18 carbon atoms [212 - 215]. Of note, the lipid makeups of yeast and mammalian cells have some differences. Specifically, yeast has ergosterol and ergosteryl esters instead of cholesterol and cholesteryl esters found in mammalian cells [212 - 215]. In addition, unlike glucosyl-based sphingolipids in mammalian cells, sphingolipids in yeast cells carry mannosyl residues [213 - 215]. Despite these differences, the pathways of lipid synthesis and degradation are among the most evolutionarily conserved metabolic pathways known [212 - 216].

Existing methods for lipid identification and quantification - such as fluorescence microscopy, HPLC, TLC and GC/MS - are well established but have low sensitivity, insufficiently separate various molecular forms of lipids, require lipid derivatization prior to analysis and are quite time consuming. Electrospray ionization mass spectroscopy (ESI/MS) is particularly suited to lipid analysis due to its high sensitivity, ability to distinguish between different lipid species, ease of sample preparation and speed [213, 214]. This method is advantageous for quantitative lipidomics because 1) the decomposition spectra of the major lipid classes are well established [217]; and 2) although the head groups of different molecular forms of the same lipid species and the degrees of unsaturation and/or lengths of their acyl chains lengths vary and thus can

complicate the acquisition of quantitative data, these pitfalls are easily to overcome by using specific and well established protocols for sample preparation and lipid standards selection [213, 214, 217 - 219]. However, it should be stressed that the ESI/MS-MS-based quantitative assessment of lipidomes has the following limitations and disadvantages as a method relying on the use of tandem MS: 1) it is time consuming; 2) it requires to maintain stable spray conditions at the ESI source for long periods of time; 3) because it relies on lipid decomposition, it has a bias towards some lipid species – thereby being insufficiently sensitive to unexpected changes in lipid spectra of analyzed cells; 4) it has a limit of sensitivity and hence requires abundant quantities of cells for lipid extraction and analysis; and 5) it has fairly high limits of detection and quantitation for some lipid species [213 - 220]. I decided to solve these inherent limitations of the currently used methods for lipidomic analysis (including the limitations characteristic of the ESI/MS-MS-based analysis) by developing a survey-scan method for quantitative assessment of the the entire complement of lipids in yeast and cultured human cells using ESI/MS.

2.3. Materials and Methods

Reagents

Various molecular forms of the glycerophospholipids phosphatidylcholine (PC), phosphatidylethanolamine (PE), phosphatidylinositol (PI), phosphatidylserine (PS) and phosphatidic acid (PA), as well as of cardiolipin (CL), were from Avanti Polar Lipid (Alabaster, AL, USA). Different species of free fatty acids (FFA) and triacylglycerols

(TAG) were from Larodan (Malmo, Sweden). Biotech grade chloroform and methanol were form Sigma-Aldrich (St. Louis, MO, USA).

Yeast strains and growth conditions

The wild-type strain BY4742 (*MATα his3Δ1 leu2Δ0 lys2Δ0 ura3Δ0*) and single-gene-deletion mutant strains in the BY4742 genetic background (all from Open Biosystems; Huntsville, AL, USA) were grown in rich YEPD medium (1% yeast extract, 2% peptone, 2% glucose). Cells were cultured at 30°C with rotational shaking at 200 rpm in Erlenmeyer flasks at a "flask volume/medium volume" ratio of 5:1.

Collection and storage of yeast cells for lipid extraction

A 50-ml culture of yeast cells was harvested by centrifugation at 3000 ×x g for 5 min and then washed twice with 25 ml of ice-cold water. The cell pellet was resuspended in 1.5 ml of ice-cold water, and the resulting cell suspension was transferred to Eppendorf tube. Cells were harvested by centrifugation at 16, 000 × g for 2 min, the supernatant was discarded, and the cell pellet was frozen at -80°C until use. For freezing cells quickly, a beaker of isopropyl alcohol kept in the -80°C freezer was used.

Lipid extraction from yeast cells

Lipids were extracted using a modification of the protocol described by Bligh and Dyer [221]. All manipulations with extracted lipids were performed using glass pipettes or syringes because a contact of plastics with chloroform resulted in a large background signal. The exact volumes of chloroform and MeOH used for lipid extraction were not

critical as long as the ratios of 1:2:0.8 and 2:2:1.8 for chloroform - MeOH - H_2O at the described below steps 3 and 7 (respectively) of lipid extraction were conserved.

Lipid extraction was performed as follows:

1. Resuspend frozen cells in 1.6 ml of ice-cold distilled H_2O.

2. Transfer 1.6 ml of the cell suspension to high-speed glass centrifuge tubes.

3. Add 6 ml of chloroform and MeOH (1:2) mix and 0.8 ml of glass beads to the cell suspension.

4. Vortex the cell suspension with glass beads two times for 1 min.

5. Add 2 ml of chloroform and mix gently.

6. Incubate for 5 min at room temperature with occasional mixing.

7. Add 2 ml of distilled H_2O and mix gently.

8. Incubate for 5 min at room temperature with occasional mixing.

9. Centrifuge for 5 min at 3000 × g at room temperature.

10. Collect the entire liquid phase into a new high-speed glass centrifuge tube.

11. Add 3.2 ml of chloroform to the cell pellets from step 9.

12. Vortex two times for 1 min.

13. Centrifuge for 5 min at 3000 × g at room temperature.

14. Add the supernatant to the liquid phase from step 10.

15. Centrifuge for 5 min at 3000 × g at room temperature.

16. Discard the upper (aqueous) phase and transfer the lower (organic) phase into a new high-speed glass centrifuge tube.

17. Centrifuge for 5 min at 3000 × g at room temperature.

18. Transfer the entire supernatant into a glass vial and dry under nitrogen.

19. Dissolve the lipid film in 50-200 µl of fresh chloroform, place in a glass vial and store at -20ºC for a maximum of two weeks.

Analysis of lipids by ESI/MS

A stock mix of lipid standards in chloroform was prepared beforehand as per Table 2.1, as well as a stock solution of MeOH - chloroform (1:1) with 0.1% (v/v) ammonium hydroxide, all in glass vials.

The ESI/MS analysis was performed as follows:

1. Prior to injection, combine 10 µl of a sample with 10 µl of the standard mix of lipids in 200 µl of MeOH - chloroform (1:1) with 0.1% ammonium hydroxide. The standard to sample ratio can be changed as needed.

2. Resolve lipids using a Micromass Q-TOF 2 mass spectrometer equipped with a nano-electrospray source operating at a flow rate of 1 µl/min. Although we have taken advantage of the high resolution of a Q-TOF type of mass spectrometer, it is not a mandatory requirement. Exact instrument parameters will vary from instrument to instrument. See Table 2.2 for the settings for a Micromass Q-ToF 2 (Waters, Milford, MA, USA) equipped with a nano-electrospray source. To analyze PC and TAG, the cone voltage was set to 28 v and the capillary voltage to 3.0 kv in positive mode. For the analysis of FFA, CL, PE, PS, PA and PI, the cone voltage was set to 30 v and the capillary voltage to 3.2 kv in negative mode. In both modes, the collision gas was set to 10 (arbitrary units). Survey MS data were acquired for up to 3 minutes or until the ion count of the standards was above 2×10^3.

Post-processing of MS data

After acquisition, the mass spectra were smoothed and background subtracted and centred using the MassLynx software package (Waters, Milford, MA, USA). The peak list was then imported into Microsoft Excel for deconvolution and deisotoping. The list was first searched using equation 2.1 to determine the peaks of interest. The resulting peak list was then deconvoluted and deisotoped using a lookup table, which represented the relative intensities of the isotope peaks (see Table 2.2). The peak list was first scanned specifically for CL species and, using the I_1 isotope, the contribution of these lipid species to isobaric peaks was determined and subtracted. The peak list was then scanned for other lipid classes from low to high mass, the peaks deisotoped and the contribution to isobaric isotope peaks subtracted. Peak intensities were then normalized to the internal standard of the appropriate lipid class. The molecular forms of various lipid classes detected following lipid extraction from whole yeast cells are listed in Table 2.3.

Table 2.1. Internal lipid standards, their concentrations in the standard mix and the MS mode for their analysis.

Lipid class	Standard chain composition	Mass of standard	Concentration (µg/ml)	MS mode
Phosphatidic acid	14:0/14:0	591.40	100	Negative
Phosphatidylethanolamine	14:0/14:0	634.45	200	Negative
Phosphatidylinositol	N/A	N/A	N/A	Negative
Phosphatidylserine	14:0/14:0	622.37	40	Negative
Cardiolipin	4x14:0	619.92	100	Negative
Free fatty acids	19:0	297.28	100	Negative
Phosphatidylcholine	14:0/14:0	650.48	100	Positive
Triacylglycerols	13:0/13:0/13:0	698.63	200	Positive

Table 2.2. Instrument settings for a Micromass Q-ToF 2 (Waters, Milford, MA, USA) equipped with a nano-electrospray source.

	Flow rate	Cone voltage	Capillary voltage	Collision gas
Positive mode	1µl/min	-28 v	3.0 kv	10
Negative mode	1µl/min	30 v	-32 kv	10

Equation 2.1. The following Excel function was used to search the column LookUpVector and return the corresponding value in the column ResultsVector, which are within the range LookUpValue +/- Error:

=IF(ISNA(LOOKUP(1,1/(ABS(LookUpVector-LookUpValue)

<=Error),ResultsVector)),0,LOOKUP(1,1/(ABS(LookUpVector-LookUpValue)

<=Error),ResultsVector))

Table 2.3. The molecular forms of various lipid classes detected following lipid extaction from whole yeast cells and their exact masses.

Lipid Class	Chain Composition	Mass
	38:0	731.55
	38:1	729.54
	38:2	727.52
	38:4	723.49
	36:0	703.52
	36:1	701.51
	36:2	699.49
	34:0	675.49
	34:1	673.48
PA	34:2	671.46
	32:0	647.46
	32:1	645.44
	32:2	643.43
	30:0	619.43
	30:1	617.42
	30:2	615.40
	28:0	591.40
	28:1	589.39
	28:2	587.37
PE	38:0	774.60
	38:1	772.59

	38:2	770.57
	38:4	766.54
	36:0	746.57
	36:1	744.55
	36:2	742.53
	34:0	718.53
	34:1	716.52
	34:2	714.51
	32:0	690.51
	32:1	688.49
	32:2	686.48
	30:0	662.48
	30:1	660.46
	30:2	658.45
	28:0	634.45
	28:1	632.43
	28:2	630.41
	38:0	893.61
	38:1	891.60
	38:2	889.58
	38:4	885.55
	36:0	865.58
	36:1	863.56
	36:2	861.55
	34:0	837.55
	34:1	835.53
PI	34:2	833.52
	32:0	809.52
	32:1	807.50
	32:2	805.49
	30:0	781.49
	30:1	779.47
	30:2	777.46
	28:0	753.46
	28:1	751.44
	28:2	749.42
	38:0	790.56
	38:1	788.54
	38:2	786.53
	36:0	762.53
PS	36:1	760.51
	36:2	758.50
	34:0	734.50
	34:1	732.48
	34:2	730.47
	32:0	706.47

	32:1	704.45
	32:2	702.43
	30:0	678.43
	30:1	676.42
	30:2	674.40
	28:0	650.40
	28:1	648.39
	28:2	646.37
	26:0	622.37
	C10:0	171.13
	C10:1	169.12
	C12:0	199.17
	C12:1	197.15
	C14:0	227.20
	C14:1	225.19
FFA	C16:0	255.23
	C16:1	253.22
	C18:0	283.26
	C18:1	281.25
	C20:0	311.29
	C20:1	309.28
	C22:0	339.33
	C22:1	337.31
	56:0	619.92
	64:4	671.95
	64:3	672.96
	64:2	673.96
	64:1	674.97
	64:0	675.98
	66:4	685.96
	66:3	686.97
	66:2	687.98
	66:1	688.99
	66:0	689.99
CL	68:4	699.99
	68:3	700.99
	68:2	701.99
	68:1	703.00
	68:0	704.01
	70:4	713.99
	70:3	715.00
	70:2	716.01
	70:1	717.01
	70:0	718.02
	72:4	728.01
	72:3	729.02

	72:2	730.03
	72:1	731.0335
	72:0	732.0413
	38:0	818.6637
	38:1	816.6481
	38:2	814.6325
	36:0	790.6325
	36:1	788.6169
	36:2	786.6013
	34:0	762.6013
	34:1	760.5857
	34:2	758.5701
PC	32:0	734.5701
	32:1	732.5545
	32:2	730.5389
	30:0	706.5389
	30:1	704.5233
	30:2	702.5077
	28:0	678.5077
	28:1	676.4921
	28:2	674.4765
	26:0	650.4765
	39:0	698.6298
	42:0	740.6765
	48:0	824.7706
	48:1	822.755
	48:2	820.7394
	48:3	818.7238
	50:0	852.8018
	50:1	850.7862
	50:2	848.7706
	50:3	846.755
	52:0	880.833
	52:1	878.8174
TAG	52:2	876.8018
	52:3	874.7862
	54:0	908.8642
	54:1	906.8486
	54:2	904.833
	54:3	902.8174
	56:0	936.8954
	56:1	934.8798
	56:2	932.8642
	56:3	930.8486
	58:0	964.9266
	58:1	962.911

58:2	960.8954
58:3	958.8798
60:0	992.9578
60:1	990.9422
60:2	988.9266
60:3	986.911

2.4. Results

2.4.1. Survey-scan ESI/MS enables to resolve and unequivocally identify all molecular forms of lipid species extracted from whole yeast cells

Figure 2.1 shows the typical negative (A) and positive (B) mass spectra of lipid species extracted from whole yeast cells and identified using survey-scan ESI/MS; the positions of various molecular forms of these lipids are indicated. Confirming previously published data [212 - 219], the survey-scan ESI/MS method of lipidomic analysis that I developed demonstrated that the yeast *S. cerevisiae* has a relatively simple lipidome with 7 major lipid classes, namely PA, PE, PS, PI, CL, PC and TAG (Figure 2.1). Furthermore, my survey-scan ESI/MS method of lipidomic analysis revealed that the majority of individual molecular forms within each of these different lipid classes have chain length of 16 or 18 carbon atoms (Figure 2.1). Moreover, my survey-scan ESI/MS lipidomic analysis showed that the fatty acyl moieties of all of lipid species composing yeast lipidome are either mono-unsaturated or saturated (Figure 2.1), perhaps due to the presence of a single acyl desaturase enzyme in yeast [212 - 215]. In sum, the survey-scan ESI/MS method of lipidomic analysis that I developed enables within a very limited period of time and using a very low number of yeast cells to resolve and unequivocally identify all molecular forms of lipid species composing the lipidome of yeast. Of note,
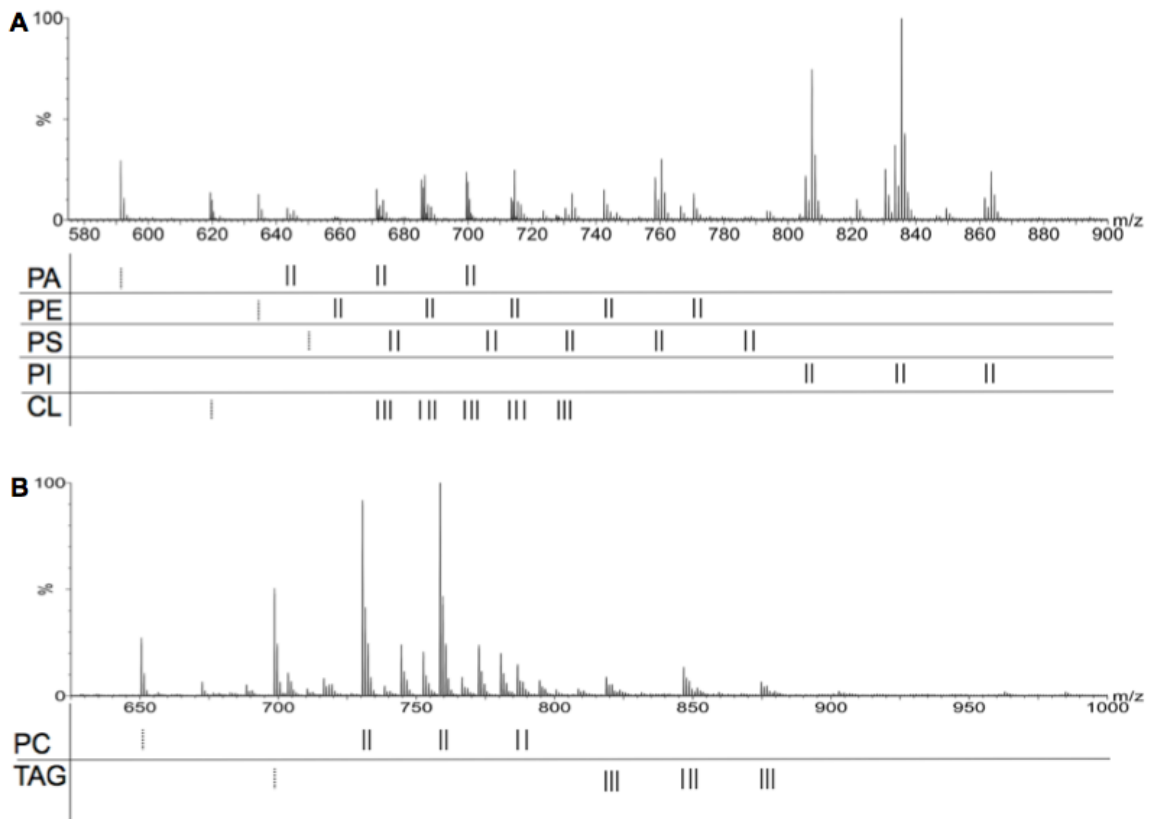
Figure 2.1. The typical negative (A) and positive (B) mass spectra of lipid species extracted from whole yeast cells and identified using survey-scan ESI/MS. The positions of various molecular forms of phosphatidic acid (PA), phosphatidylethanolamine (PE), phosphatidylserine (PS), phosphatidylinositol (PI), cardiolipin (CL), phosphatidylcholine (PC) and triacylglycerols (TAG) are indicated.

this method allows the unequivocal identification of all molecular forms of yeast lipid species despite the following two theoretically possible cases of isobaric peak overlap within the *S. cerevisiae* lipidome: 1) an overlap between PS and PE species - due to the fact that the difference in mass between their head groups is equivalent to 3 carbon atoms; the observed lack of overlap between yeast species of PS and PE (Figure 2.1) can be attributed to the fact that fatty acyl chain moieties with odd numbers of carbon atoms are not naturally present in eukaryotes [212 - 215]; and 2) an overlap between doubly charged CL species and some species of PA, PE and PS; to by-pass this overlap, the

survey-scan ESI/MS method of lipidomic analysis that I developed uses the I_1 isotope of CL for deconvolution.

2.4.2. The survey-scan ESI/MS method of lipidomic analysis is highly sensitive

To determine the limit of sensitivity for the survey-scan ESI/MS method of lipidomic analysis, I used it to determine concentrations of commercially available standard lipids within a very wide concentration range. The commercially available standard lipids, each belonging to a different major class of yeast lipids, were added to a whole-cell yeast lipid extract in known concentrations spreading over 2 to 3 orders of magnitude. For each standard lipid, the limit of detection (LOD) was determined as 3 SD (standard deviation) of the background and the limit of quantitation (LOQ) as 10 SD of the background (Table 2.4). I found that the survey-scan ESI/MS method of lipidomic analysis that I developed is 1) sensitive to the low μM range (0.6 to 2 μM depending on lipid class) for all lipid species tested; and 2) linear to the hundreds of μM range, with the concentration linearity spreading over 2 to 3 orders of magnitude; of note, the useful quantitative range for each lipid species tested was different (Figures 2.2 and 2.3).

2.4.3. The survey-scan ESI/MS method of lipidomic analysis enables very accurate lipid quantitation within a wide range of lipid concentrations

To determine the accuracy and precision of the survey-scan ESI/MS method of lipidomic analysis, the experimentally determined concentrations of the standard lipids (which were added to a whole-cell yeast lipid extract as described in section 2.4.2) were plotted

against the known concentrations (Figures 2.2 and 2.3). For all lipid species tested, I observed 1) linearity through a wide range of the lipid concentrations used; and 2) a very good fit to the linear regression curve ($R^2 > 0.98$) and, thus, an excellent precision throughout (Figures 2.2 and 2.3). Importantly, the glycerophospholipid species PE, PS, PA and PC all displayed similar ionization efficiencies regardless of the head group, with a slope of 1 +/- 0.05 (Figures 2.2 and 2.3). In contrast, some (but not all) molecular forms of CL and TAG had variable slopes, thereby making the quantitation of these forms a challenging task. However, it should be stressed that the experimental to known concentrations ratio was constant for all molecular species of CL and TAG, thereby enabling the quantitative comparison of their concentrations in different biological samples (Figures 2.2 and 2.3). Of note, because appropriate PI standards are not commercially available, the quantitative analysis of this lipid class cannot be performed. However, I found that the PI species present in whole-cell extracts of yeast lipids displayed linearity through a range of the extract dilutions used and, thus, that the relative concentrations of these lipid species in different biological samples can be determined semi-quantitatively.

2.4.4. Survey-scan ESI/MS enables high-throughput quantitative analysis of the lipidome of cultured human microglial cells

Within a framework of Dr. Titorenko's ongoing collaboration with Dr. Dusica Maysinger in the Department of Pharmacology and Therapeutics at McGill University, I am successfully using the survey-scan ESI/MS method of lipidomic analysis that I developed to resolve, unequivocally identify and accurately quantitate - within a very limited period

of time and using a very low number of cells - the majority of molecular forms of lipid species composing the lipidome of cultured human microglial cells. My data on characteristic changes in the lipidome of human microglia exposed to various pro-inflammatory and anti-inflammatory interventions constitute an integral part of: 1) a soon-to-be submitted to *FASEB Journal* manuscript (Khatchadourian, A., Bourque, S.D., Richard, V.R., Titorenko, V.I. and Maysinger, D.[*]corresponding author (2011). LPS induces lipid droplet accumulation and perilipin-2 expression in microglia. *FASEB Journal*); and 2) an ongoing collaborative project with Dr. Dusica Maysinger's laboratory on opposite and opposing effects that lipopolysaccharide (a pro-inflammatory endotoxin produced by gram-negative bacteria) and docosahexaenoic acid (an anti-inflammatory omega-3 fatty acid) have in cultured human microglial cells.

2.5. Discussion

To solve the inherent limitations of the currently used methods for lipidomic analysis (including the limitations characteristic of the ESI/MS-MS-based analysis; see section 2.2), I have developed a survey-scan method for quantitative assessment of the the entire complement of lipids in yeast cells using ESI/MS. The survey-scan ESI/MS method of lipidomic analysis that I developed demonstrated that: 1) yeast has a relatively simple lipidome with 7 major lipid classes, namely PA, PE, PS, PI, CL, PC and TAG; 2) the majority of individual molecular forms within each of these different lipid classes have chain length of 16 or 18 carbon atoms; and 3) the fatty acyl moieties of all of lipid

Table 2.4. The limits of detection (LOD) and quantitation (LOQ) for different lipid classes. The LOD is 3 SD (standard deviation) of the background signal, whereas the LOQ is 10 SD of the background. N/A, not

applicable (because appropriate PI standards are not commercially available, the quantitative analysis of this lipid class cannot be performed).

Lipid class	LOD (μM)	LOQ (μM)
Phosphatidic acid (PA)	0.2	0.6
Phosphatidylethanolamine (PE)	0.2	0.6
Phosphatidylinositol (PI)	N/A	N/A
Phosphatidylserine (PS)	0.3	1.1
Cardiolipin (CL)	0.3	0.9
Free fatty acids (FFA)	0.6	2.0
Phosphatidylcholine (PC)	0.4	1.2
Triacylglycerols (TAG)	0.6	2.0

species composing yeast lipidome are either mono-unsaturated or saturated, perhaps due to the presence of a single acyl desaturase enzyme in yeast [212 - 215]. Furthermore, the method that I developed is highly sensitive as it is: 1) sensitive to the low μM range (0.6 to 2 μM depending on lipid class) for all lipid species tested; and 2) linear to the hundreds of μM range, with the concentration linearity spreading over 2 to 3 orders of magnitude. Moreover, the method that I developed enables very accurate quantitation of different lipid species within a wide range of lipid concentrations. Importantly, if compared to the currently used ESI/MS-MS-based method of lipidomic analysis [213 - 220], my method has the following important advantages: 1) unlike the ESI/MS-MS-based method, it can be carried out within a very limited period of time; 2) unlike the ESI/MS-MS-based

Figure 2.2. Calibration curves for PA, PC, PE and PS. Peak areas of individual lipid spikes were normalized to an internal standard of the same lipid class (see Table 2.1). For a 36:2 species of PA spike, slope = 0.92 and R2 = 1.00. For a 30:0 species of PC spike, slope = 1.04 and R2 = 1.00. For a 34:0 species of PE, slope = 1.03 and R2 = 1.00. For a 32:0 species of PS spike, slope = 1.00 and R2 = 1.00. Experimentally determined concentrations (in μM) are on the ordinate axis and known concentrations (in μM) on the abscissa. Error bars represent standard deviations.
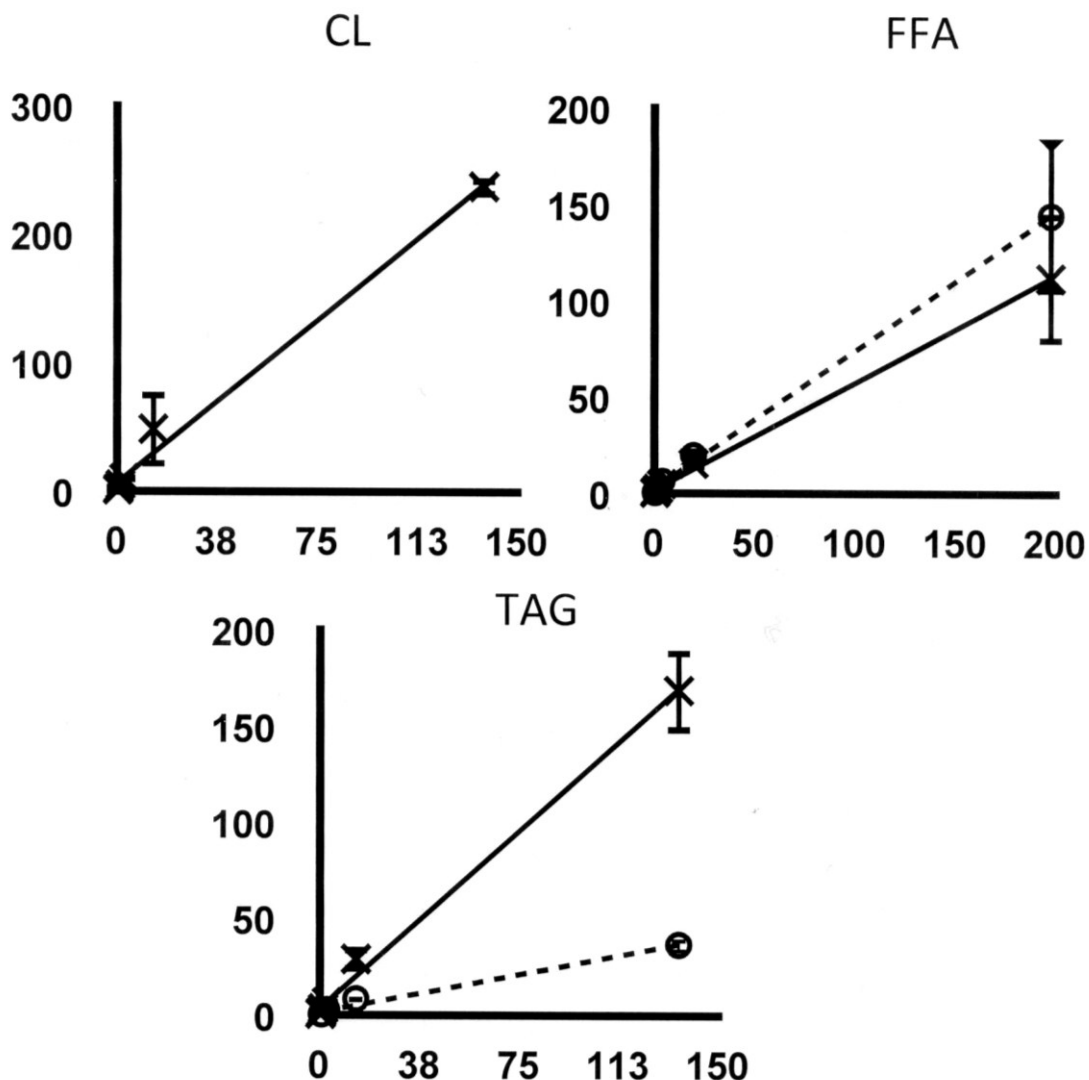
Figure 2.3. Calibration curves for CL, FFA and TAG. Peak areas of individual lipid spikes were normalized to an internal standard of the same lipid class (see Table 2.1). For a 72:4 species of CL spike, slope = 1.70 and R2 = 1.00. For an 18:1 species of FFA spike (dashed line), slope = 0.72 and R2 = 1.00; for a 16:1 species of FFA spike (solid line), slope = 0.56, R2= 1.00. For a 36:0 species of TAG spike (dashed line), slope = 1.23 and R2 = 1.00. For a 42:0 species of TAG spike (solid line), slope = 0.26 and R2 = 1.0. Experimentally determined concentrations (in μM) are on the ordinate axis and known concentrations (in μM) on the abscissa. Error bars represent standard deviations.

method, it does not require to maintain stable spray conditions at the ESI source for long periods of time; 3) unlike the ESI/MS-MS-based method, it does not have a bias towards certain lipid species, thereby being sufficiently sensitive to unexpected changes in lipid

spectra of analyzed cells; 4) it is more sensitive than the ESI/MS-MS-based method and, thus, does not require abundant quantities of cells for lipid extraction and analysis; and 5) it has lower than the ESI/MS-MS-based method limits of detection and quantitation for all yeast lipid species.

2.6. Conclusions

My findings support the notion that the survey-scan ESI/MS method of lipidomic analysis that I developed enables within a very limited period of time and using a very low number of cells to resolve, unequivocally identify and accurately quantitate all molecular forms of lipid species composing yeast lipidome and the majority of molecular forms of lipid species composing the lipidome of cultured human microglial cells.

3. A mechanism underlying the ability of caloric restriction to extend yeast longevity by remodeling lipid metabolism

3.1. Abstract

Growing evidence supports the view that the deposition and lipolytic degradation of neutral lipids play an important role in longevity regulation across phyla [18, 138 - 141, 153, 177, 182 - 192, 222, 223]. In yeast, longevity can be extended by caloric restriction (CR), a low-calorie dietary regimen that extends life span in a wide spectrum of organisms and delays the onset or reduces the incidence of many age-related diseases in rodents and primates [65 - 72, 131, 134 - 136]. A CR diet can be imposed in yeast by reducing the glucose concentration from 2% to 0.5% [8]. The molecular and cellular mechanisms linking longevity-defining changes in lipid metabolism and longevity-extending effect of CR are yet to be characterized. The establishment of such mechanisms operating in chronologically aging yeast was the objective of my experiments described in this Chapter.

I first elucidated the effect of CR on the metabolic history of chronologically aging yeast. My comparison of the metabolic histories of long-lived CR yeast and short-lived non-CR yeast suggests that, by designing a diet-specific pattern of lipid metabolism in the endoplasmic reticulum (ER), lipid bodies (LBs) and peroxisomes prior to entry into a non-proliferative state, yeast define their long-term viability. I therefore proposed that longevity in chronologically aging yeast is programmed by the level of metabolic capacity and organelle organization they developed, in a diet-specific fashion, prior to reproductive maturation.

Using a combination of functional genetic, cell biological, electron and fluorescence microscopical, proteomic, lipidomic, and metabolomic experimental approaches, I deciphered the molecular mechanism underlying the essential role of lipid metabolism in modulating programmed by calorie availability chronological aging in yeast. In this mechanism, LBs in yeast cells function as a hub in a regulatory network that modulates neutral lipids synthesis in the ER and fatty acid oxidation in peroxisomes. Ethanol accumulated in yeast placed on a calorie-rich diet represses the synthesis of Fox1p, Fox2p and Fox3p, thereby suppressing peroxisomal oxidation of FFA that originate from triacylglycerols (TAG) synthesized in the ER and deposited within LBs. The resulting build-up of arrays of free fatty acids (gnarls) within LBs of non-CR yeast initiates several negative feedback loops regulating the metabolism of TAG. Due to the action of these negative feedback loops, chronologically aging non-CR yeast not only amass TAG in LBs but also accumulate FFA and diacylglycerol (DAG) in the ER. FFA and DAG regulate longevity by two different mechanisms that operate at two different stages of the aging process. One mechanism involves sensing the concentration of DAG maintained by cells (in a diet- and genotype-dependent fashion) during diauxic (D) and post-diauxic (PD) growth phases. DAG concentration during D and PD phases programs cell viability during stationary (ST) growth phase by modulating the FFA- and DAG-induced necrotic cell death pathway, but not by influencing the mitochondria-controlled apoptotic pathway of cell death. Another mechanism involves sensing the concentrations of FFA and DAG during ST phase. Any diet or genetic manipulation that causes the build-up of these two lipids during ST phase shortens the chronological life span of yeast

in part by promoting rapid mitochondria-controlled apoptotic cell death, but not by activating FFA- and DAG-induced necrotic cell death pathway.

3.2. Introduction

Aging is a highly complex biological phenomenon, which affects numerous processes within cells [1 - 10]. These cellular processes include cell cycle, cell growth, stress response, protein folding, apoptosis, autophagy, proteasomal protein degradation, actin organization, signal transduction, nuclear DNA replication, chromatin assembly and maintenance, ribosome biogenesis and translation, lipid and carbohydrate metabolism, oxidative metabolism in mitochondria, NAD^+ homeostasis, amino acid biosynthesis and degradation, and ammonium and amino acid uptake [2-4, 7, 22 - 25]. Some of these processes damage cellular macromolecules and organelles, while the others prevent the collapse of cellular homeostasis by repairing the damage [1, 3 - 5]. A lifelong accumulation of unrepaired cellular damage increases a risk of disease and death [1, 4, 6, 11]. A challenge is to understand how the spatiotemporal organization of damage-producing and damage-repairing processes influences longevity and how cells integrate and control these processes. The most important unanswered question is whether aging is the final step of a developmental program governed by a certain signaling network [12 - 18] or merely a result of the lifelong accumulation of unrepaired cellular and molecular damage [1, 5, 19]. To identify the cellular processes that play a critical role in longevity regulation and to rank their relative contributions to aging, the concepts and methodologies of so-called metabolic control analysis (MCA) can be useful [224 - 225]. It has been envisioned that the application of these concepts and methodologies to the analysis of empirical data on the cell metabolic histories of model organisms will enable

to 1) infer the relative contributions of various cellular processes to aging; and 2) define how interventions such as dietary restriction delay aging by modulating these processes [224 - 225].

The budding yeast *Saccharomyces cerevisiae*, a genetically and biochemically manipulable unicellular eukaryote with annotated genome, is a valuable model for unveiling mechanisms of cellular aging in multicellular eukaryotes [130 - 132]. Yeast aging can be measured in two different ways. Replicative aging is defined by the maximum number of daughter cells that a mother cell can produce before senescence and models aging of a mitotically active cell in a multicellular organism [131, 133]. In contrast, chronological aging is measured by the length of time a yeast cell remains viable in a nondividing state and models aging of postmitotic mammalian cells (*e.g.*, neurons) [56, 131, 132]. In a simple clonogenic assay for measuring yeast chronological aging, the percentage of viable yeast cells in their aging population is monitored at different time points before and after this population enters the non-proliferative stationary phase [56]. Both replicative and chronological aging of yeast can be decelerated by CR, a low-calorie dietary regimen that extends life span in various multicellular eukaryotic organisms and delays the onset or reduces the incidence of many age-related diseases in mice and primates [66 - 69, 131, 134 - 136].

In studies described in this chapter, I made a first step towards the use of MCA for defining the molecular causes of cellular aging by elucidating the effect of CR on the metabolic history of chronologically aging yeast. My comparison of the metabolic histories of long-lived CR yeast and short-lived non-CR yeast led me to the conclusion that longevity in chronologically aging yeast is programmed by the level of metabolic

capacity and organelle organization they developed, in a diet-specific fashion, prior to reproductive maturation. I found that the developmental program of chronological aging in yeast is governed, in part, by a specific pattern of lipid metabolism in the ER, LBs and peroxisomes that yeast design in a diet-dependent fashion prior to entry into a non-proliferative state. I therefore focused my study on establishing the molecular mechanism underlying the essential role of lipid metabolism in modulating programmed by calorie availability chronological aging in yeast.

3.3. Materials and Methods

Strains and media

The wild-type strain *Saccharomyces cerevisiae* BY4742 (*MATα his3Δ1 leu2Δ0 lys2Δ0 ura3Δ0*) and mutant strains *pex1Δ* (*MATα his3Δ1 leu2Δ0 lys2Δ0 ura3Δ0 pex1Δ::kanMX4*), *pex5Δ* (*MATα his3Δ1 leu2Δ0 lys2Δ0 ura3Δ0 pex5Δ::kanMX4*), *pex6Δ* (*MATα his3Δ1 leu2Δ0 lys2Δ0 ura3Δ0 pex6Δ::kanMX4*), *pex7Δ* (*MATα his3Δ1 leu2Δ0 lys2Δ0 ura3Δ0 pex7Δ::kanMX4*), *fox1Δ* (*MATα his3Δ1 leu2Δ0 lys2Δ0 ura3Δ0 fox1Δ::kanMX4*), *cta1Δ* (*MATα his3Δ1 leu2Δ0 lys2Δ0 ura3Δ0 cta1Δ::kanMX4*), *fox2Δ* (*MATα his3Δ1 leu2Δ0 lys2Δ0 ura3Δ0 fox2Δ::kanMX4*), *fox3Δ* (*MATα his3Δ1 leu2Δ0 lys2Δ0 ura3Δ0 fox3Δ::kanMX4*), *adh1Δ* (*MATα his3Δ1 leu2Δ0 lys2Δ0 ura3Δ0 adh1Δ::kanMX4*), *adh2Δ* (*MATα his3Δ1 leu2Δ0 lys2Δ0 ura3Δ0 adh2Δ::kanMX4*), *gpt2Δ* (*MATα his3Δ1 leu2Δ0 lys2Δ0 ura3Δ0 gpt2Δ::kanMX4*), *sct1Δ* (*MATα his3Δ1 leu2Δ0 lys2Δ0 ura3Δ0 sct1Δ::kanMX4*), *ayr1Δ* (*MATα his3Δ1 leu2Δ0 lys2Δ0 ura3Δ0 ayr1Δ::kanMX4*), *slc1Δ* (*MATα his3Δ1 leu2Δ0 lys2Δ0 ura3Δ0 slc1Δ::kanMX4*), *lpp1Δ* (*MATα his3Δ1 leu2Δ0 lys2Δ0 ura3Δ0 lpp1Δ::kanMX4*), *dpp1Δ* (*MATα his3Δ1 leu2Δ0

lys2Δ0 ura3Δ0 mdh3Δ::kanMX4), *fox3Δ (MATα his3Δ1 leu2Δ0 lys2Δ0 ura3Δ0 dpp1Δ::kanMX4)*

dga1Δ (MATα his3Δ1 leu2Δ0 lys2Δ0 ura3Δ0 dga1Δ::kanMX4), *are1Δ (MATα his3Δ1 leu2Δ0 lys2Δ0 ura3Δ0 are1Δ::kanMX4)*, *are2Δ (MATα his3Δ1 leu2Δ0 lys2Δ0 ura3Δ0 are2Δ::kanMX4)*, *lro1Δ (MATα his3Δ1 leu2Δ0 lys2Δ0 ura3Δ0 lro1Δ::kanMX4)*, *tgl1Δ (MATα his3Δ1 leu2Δ0 lys2Δ0 ura3Δ0 tgl1Δ::kanMX4)*, *tgl2Δ (MATα his3Δ1 leu2Δ0 lys2Δ0 ura3Δ0 tgl2Δ::kanMX4)*, *tgl3Δ (MATα his3Δ1 leu2Δ0 lys2Δ0 ura3Δ0 rgl3Δ::kanMX4)*, *tgl4Δ (MATα his3Δ1 leu2Δ0 lys2Δ0 ura3Δ0 tgl4Δ::kanMX4)*, and *tgl5Δ (MATα his3Δ1 leu2Δ0 lys2Δ0 ura3Δ0 tgl5Δ::kanMX4)* were used in this study. Media components were as follows: 1) YEPD (0.2% Glucose), 1% yeast extract, 2% peptone, 0.2% glucose; and 2) YEPD (2% Glucose), 1% yeast extract, 2% peptone, 2% glucose.

A plating assay for the analysis of chronological life span

Cells were grown in YEPD (0.2% Glucose) medium at 30°C with rotational shaking at 200 rpm in Erlenmeyer flasks at a flask volume/medium volume ratio of 5:1. A sample of cells was removed from each culture at various time points. A fraction of the cell sample was diluted in order to determine the total number of cells per ml of culture using a hemacytometer. 10 μl of serial dilutions (1:10 to $1:10^{3}$) of cells were applied to the hemacytometer, where each large square is calibrated to hold 0.1 μl. The number of cells in 4 large squares was then counted and an average was taken in order to ensure greater accuracy. The concentration of cells was calculated as follows: number of cells per large

square x dilution factor $\times$ 10 $\times$ 1,000 = total number of cells per ml of culture. A second fraction of the cell sample was diluted and serial dilutions ($1:10^2$ to $1:10^5$) of cells were plated onto YEPD (2% Glucose) plates in triplicate in order to count the number of viable cells per ml of each culture. 100 μl of diluted culture was plated onto each plate. After a 48-h incubation at 30^oC, the number of colonies per plate was counted. The number of colony forming units (CFU) equals to the number of viable cells in a sample. Therefore, the number of viable cells was calculated as follows: number of colonies $\times$ dilution factor $\times$ 10 = number of viable cells per ml. For each culture assayed, % viability of the cells was calculated as follows: number of viable cells per ml / total number of cells per ml $\times$ 100%. The % viability of cells in mid-logarithmic phase was set at 100% viability for that particular culture.

Plating assays for the analysis of resistance to various stresses

For the analysis of hydrogen peroxide resistance, serial dilutions ($1:10^0$ to $1:10^5$) of wild-type and mutant cells removed from mid-logarithmic phase (day 1) and from diauxic phase (days 2 and 3) in YEPD (0.2% Glucose) were spotted onto two sets of plates. One set of plates contained YEPD (2% Glucose) medium alone, whereas the other set contained YEPD (2% Glucose) medium supplemented with 5 mM hydrogen peroxide. Pictures were taken after a 3-day incubation at 30^oC.

For the analysis of oxidative stress resistance, serial dilutions ($1:10^0$ to $1:10^5$) of wild-type and mutant cells removed from mid-logarithmic phase (day 1) and from diauxic phase (days 2 and 3) in YEPD (0.2% Glucose) were spotted onto two sets of plates. One set of plates contained YEPD (2% Glucose) medium alone, whereas the other

set contained YEPD (2% Glucose) medium supplemented with 2.5 mM of the superoxide/hydrogen peroxide-generating agent paraquat. Pictures were taken after a 3-day incubation at 30°C.

For the analysis of heat-shock resistance, serial dilutions (1:10^{0} to 1:10^{5}) of wild-type and mutant cells removed from mid-logarithmic phase (day 1) and from diauxic phase (days 2 and 3) in YEPD (0.2% Glucose) were spotted onto two sets of YEPD (2% Glucose) plates. One set of plates was incubated at 30oC. The other set of plates was initially incubated at 55°C for 30 min, and was then transferred to 30°C. Pictures were taken after a 3-day incubation at 30°C.

For the analysis of salt stress resistance, serial dilutions (1:10^{0} to 1:10^{5}) of wild-type and mutant cells removed from mid-logarithmic phase (day 1) and from diauxic phase (days 2 and 3) in YEPD (0.2% Glucose) were spotted onto two sets of plates. One set of plates contained YEPD (2% Glucose) medium alone, whereas the other set contained YEPD (2% Glucose) medium supplemented with 0.5 M NaCl. Pictures were taken after a 3-day incubation at 30°C.

For the analysis of osmotic stress resistance, serial dilutions (1:10^{0} to 1:10^{5}) of wild-type and mutant cells removed from mid-logarithmic phase (day 1) and from diauxic phase (days 2 and 3) in YEPD (0.2% Glucose) were spotted onto two sets of plates. One set of plates contained YEPD (2% Glucose) medium alone, whereas the other set contained YEPD (2% Glucose) medium supplemented with 1 M sorbitol. Pictures were taken after a 3-day incubation at 30°C.

Monitoring the formation of ROS

Wild-type and mutant cells grown in YEPD (0.2% Glucose) were tested microscopically for the production of ROS by incubation with dihydrorhodamine 123 (DHR). In the cell, this nonfluorescent compound can be oxidized to the fluorescent chromophore rhodamine 123 by ROS. Cells were also probed with a fluorescent counterstain Calcofluor White M2R (CW), which stains the yeast cell walls fluorescent blue. CW was added to each sample in order to label all cells for their proper visualization. DHR was stored in the dark at –20$^\text{o}$C as 50 μl aliquots of a 1 mg/ml solution in ethanol. CW was stored in the dark at –20$^\text{o}$C as the 5 mM stock solution in anhydrous DMSO (dimethylsulfoxide).

The concurrent staining of cells with DHR and CW was carried out as follows. The required amounts of the 50 μl DHR aliquots (1 mg/ml) and of the 5 mM stock solution of CW were taken out of the freezer and warmed to room temperature. The solutions of DHR and CW were then centrifuged at 21,000 × g for 5 min in order to clear them of any aggregates of fluorophores. For cell cultures with a titre of ~ 10^7 cells/ml, 100 μl was taken out of the culture to be treated. If the cell titre was lower, proportionally larger volumes were used. 6 μl of the 1 mg/ml DHR and 1 μl of the 5 mM CW solutions were added to each 100 μl aliquot of culture. After a 2-h incubation in the dark at room temperature, the samples were centrifuged at 21,000 × g for 5 min. Pellets were resuspended in 10 μl of PBS buffer (20 mM KH$_2$PO$_4$/KOH, pH 7.5, and 150 mM NaCl). Each sample was then supplemented with 5 μl of mounting medium, added to a microscope slide, covered with a coverslip, and sealed using nail polish. Once the slides were prepared, they were visualized under the Zeiss Axioplan fluorescence microscope mounted with a SPOT Insight 2 megapixel color mosaic digital camera. Several pictures of the cells on each slide were taken, with two pictures taken of each frame. One of the

two pictures was of the cells seen through a rhodamine filter in order to detect cells dyed with DHR. The second picture was of the cells seen through a DAPI filter in order to visualize CW, and therefore all the cells present in the frame.

For evaluating the percentage of DHR-positive cells, the UTHSCSA Image Tool (Version 3.0) software was used to calculate both the total number of cells and the number of stained cells. Fluorescence of individual DHR-positive cells in arbitrary units was determined by using the UTHSCSA Image Tool software (Version 3.0). In each of 3-5 independent experiments, the value of median fluorescence was calculated by analyzing at least 800-1000 cells that were collected at each time point. The median fluorescence values were plotted as a function of the number of days cells were cultured.

Visualization of intracellular lipid bodies (LBs)

Wild-type and mutant cells grown in YEPD (0.2% Glucose) were tested microscopically for the presence of intracellular LBs by incubation with BODIPY 493/503. Cells were also probed with a fluorescent counterstain CW in order to visualize all cells in the population. BODIPY 493/503 was stored in the dark at -20°C as 100 µl aliquots of a 1 mM solution in ethanol. CW was stored in the dark at -20°C as the 5 mM stock solution in anhydrous DMSO.

The concurrent staining of cells with BODIPY 493/503 and CW was carried out as follows. The required amounts of the 100 µl BODIPY 493/503 aliquots (1 mM) and of the 5 mM stock solution of CW were taken out of the freezer and warmed to room temperature. The solutions of DHR and CW were then centrifuged at 21,000 × g for 5 min in order to clear them of any aggregates of fluorophores. For cell cultures with a titre

of $\sim 10^7$ cells/ml, 100 μl was taken out of the culture to be treated. If the cell titre was lower, proportionally larger volumes were used. The samples were then centrifuged at $21,000 \times g$ for 1 min, and pelleted cells were resuspended in 100 μl of TNT buffer (25 mM Tris/HCl (pH 7.5), 150 mM NaCl and 0.2 % Triton X-100). After a 10-min incubation at room temperature, the samples were centrifuged at $21,000 \times g$ for 1 min. Pellets were then resuspended in 100 μl of TN buffer (25 mM Tris/HCl (pH 7.5), 150 mM NaCl), and the samples were subjected to centrifugation at $21,000 \times g$ for 1 min. Pelleted cells were finally resuspended in 100 μl of TN buffer. Each 100 μl aliquot of cells was then supplemented with 1 μl of the 1 mM BODIPY 493/503 and 1 μl of the 5 mM CW solutions. After a 15-min incubation in the dark at room temperature, the samples were centrifuged at $21,000 \times g$ for 5 min. Pellets were resuspended in 100 μl of TN buffer. The samples were centrifuged again at $21,000 \times g$ for 5 min, and pellets were resuspended in 100 μl of TN buffer. 10 μl of the BODIPY 493/503- and CW-treated cell suspension was then added to a microscope slide and covered with a coverslip. The slides were then sealed using nail polish. Once the slides were prepared, they were visualized under the Zeiss Axioplan fluorescence microscope mounted with a SPOT Insight 2 megapixel color mosaic digital camera. Several pictures of the cells on each slide were taken, with two pictures taken of each frame. One of the two pictures was of the cells seen through a fluorescein filter in order to detect cells dyed with BODIPY 493/503. The second picture was of the cells seen through a DAPI filter in order to visualize CW, and therefore all the cells present in the frame. For evaluating the percentage of BODIPY 493/503-positive cells, the UTHSCSA Image Tool (Version 3.0) software was used to calculate both the total number of cells and the number of stained cells.

Immunofluorescence microscopy

Cell cultures were fixed in 3.7% formaldehyde for 45 min at room temperature. The cells were washed in solution B (100 mM KH$_2$PO4/KOH pH 7.5, 1.2 M sorbitol), treated with Zymolyase 100T (MP Biomedicals, 1 μg Zymolyase 100T/1 mg cells) for 30 min at 30°C and then processed as previously described [66]. Monoclonal antibody raised against porin (Invitrogen, 0.25 μg/μl in TBSB buffer [20 mM Tris/HCl pH 7.5, 150 mM NaCl, 1mg/ml BSA]) was used as a primary antibody. Alexa Fluor 568 goat anti-mouse IgG (Invitrogen, 2 μg/μl in TBSB buffer) was used as a secondary antibody. The labeled samples were mounted in mounting solution (16.7 mM Tris/HCl pH 9.0, 1.7 mg/ml *p*-phenylenediamine, 83% glycerol). Images were collected with a Zeiss Axioplan fluorescence microscope (Zeiss) mounted with a SPOT Insight 2 megapixel color mosaic digital camera (Spot Diagnostic Instruments).

Oxygen consumption assay

The rate of oxygen consumption by yeast cells recovered at various time points was measured continuously in a 2-ml stirred chamber using a custom-designed biological oxygen monitor (Science Technical Center of Concordia University) equipped with a Clark-type oxygen electrode. 1 ml of YEPD medium supplemented with 0.2% glucose was added to the electrode for approximately 5 minutes to obtain a baseline. Cultured cells of a known titre were spun down at 3,000 × g for 5 minutes. The resulting pellet was resuspended in YEPD medium supplemented with 0.2% glucose and then added to the electrode with the medium that was used to obtain a baseline. The resulting slope was used to calculate the rate of oxygen consumption in O$_2$% x min^{-1} × 10^9 cells.

Electron microscopy and morphometric analysis

Cells were fixed in 1.5% $KMnO_4$ for 20 min at room temperature, dehydrated by successive incubations in increasing concentrations of ethanol, and embedded in Poly/Bed 812 epoxy resin (Polysciences). Ultrathin sections were cut using an Ultra-Cut E Microtome (Reichert-Jung). Silver/gold thin sections from the embedded blocks were examined in a JEOL JEM-2000FX transmission electron microscope. For morphometric analysis of random electron microscopic sections of cells, digitized images were analyzed using the UTHSCSA Image Tool (Version 3.0) software. In each of 2 independent experiments, the percentage of cells that contain pexopodia and/or accumulate gnarled LBs was calculated by analyzing at least 300 cells that were collected at each time point. The values of the percentage of cells containing pexopodia and/or accumulating gnarled LBs were plotted as a function of the number of days cells were cultured.

Preparation of total cell lysates

An aliquot containing 1×10^9 cells was centrifuged for 7 min at 3,000 rpm at room temperature. Pelleted cells were washed twice with distilled water and further centrifuged for 3 min at 16,000 × g at room temperature. The recovered cell pellet was then resuspended in 500 μl of 4% CHAPS in 25 mM Tris/HCl buffer (pH 8.5) and centrifuged for 15 sec at 16,000 × g at room temperature. The cells were then washed again, first by resuspending them in 500 μl of 4% CHAPS in 25 mM Tris/HCl buffer (pH 8.5) and then by centrifuging for 15 sec at 16,000 × g at room temperature. The pellet of washed cells was then resuspended in 1 ml of ice-cold 4% CHAPS in 25 mM Tris/HCl buffer (pH 8.5), divided into 5 equal aliquots of 200 μl each and placed in Eppendorf tubes kept on ice.

Each 200 μl aliquot was supplemented with ~100 μl of glass beads and vortexed three times for 1 minute. Apart from the vortexing steps, the samples were kept on ice at all times. Glass beads and cell debris were then pelleted by 5 min centrifugation at 16,000 × g at 4°C. The resulting supernatant of the glass bead lysate was immediately transferred into a pre-chilled Eppendorf tube and stored at -20°C for further analysis.

Isolation of the crude mitochondrial fraction

Yeast cells were pelleted at 3,000 × g for 5 min at room temperature, washed twice with distilled water, resuspended in DTT buffer (100 mM Tris-H$_2$SO$_4$, pH 9.4, 10 mM dithiothreitol [DTT]), and incubated for 20 min at 30°C to weaken the cell wall. The cells were then washed with Zymolyase buffer (1.2 M sorbitol, 20 mM potassium phosphate, pH 7.4), centrifuged at 3,000 × g for 5 min at room temperature, and incubated with 3 mg/g (wet wt) of Zymolyase-100T in 7 ml/g (wet wt) Zymolyase buffer for 45 min at 30°C. Following an 8-min centrifugation at 2,200 × g at 4°C, the isolated spheroplasts were washed in ice-cold homogenization buffer (5 ml/g) (0.6 M sorbitol, 10 mM Tris-HCl, pH7.4, 1 mM EDTA, 0.2% (w/v) BSA) and then centrifuged at 2,200 × g for 8 min at 4°C. Washed spheroplasts were homogenized in ice-cold homogenization buffer using 15 strokes. The cell debris was removed by centrifuging the resulting homogenates at 1,500 × g for 5 min at 4°C. The supernatant was further centrifuged at 3,000 × g for 5 min at 4°C to remove residual cell debris. The resulting supernatant was then centrifuged at 12,000 × g for 15 min at 4°C to pellet mitochondria. The remnant cell debris was removed by centrifuging the mitochondrial fraction at 3,000 × g for 5 min at 4°C. The resulting supernatant was then centrifuged at 12,000 × g for 15 min at 4°C to obtain the

crude mitochondrial pellet, which was then resuspended in 3 ml of SEM Buffer (250 mM sucrose, 1 mM EDTA, 10 mM MOPS, pH 7.2) and used for the purification of mitochondria as described below.

Purification of mitochondria devoid of microsomal and cytosolic contaminations

A sucrose gradient was made by carefully overlaying 1.5 ml of 60% sucrose with 4 ml of 32% sucrose, 1.5 ml of 23% sucrose, and then 1.5 ml of 15% sucrose (all in EM buffer; 1 mM EDTA, 10 mM MOPS, pH 7.2). Finally, a 3-ml aliquot of the crude mitochondrial fraction in SEM buffer was applied to the gradient and centrifuged at 134,000 × g (33,000 rpm) overnight at 2°C in vacuum (Rotor SW50Ti, Beckman). The purified mitochondria found at the 60%/32% sucrose interface were carefully removed and stored at - 80°C.

Purification of the ER

Reagents and solutions

1. TSD reduction buffer: 0.1 M Tris/Sulfate (pH 9.4), 10 mM DTT

2. HEPES lysis buffer: 20 mM HEPES/KOH, pH 6.8, 50 mM KCl, 200 mM sorbitol, 2 mM EDTA, 1 mM DTT

3. Spheroplast medium A (pH 7.5): 0.67% yeast nitrogen base (w/o) amino acids, 2 % (w/v) glucose, 1 M sorbitol, 20 mM Tris/HCl (pH 7.5)

4. Spheroplast medium B: 0.67% yeast nitrogen base (w/o) amino acids, 2 % (w/v) glucose, 1 M sorbitol

5. 1.2 M sucrose/ HEPES, 36% (w/w): 7.2 g sucrose + 12.8 ml HEPES lysis buffer

6. 1.5 M sucrose/ HEPES, 43% (w/w): 8.6 g sucrose + 11.4 ml HEPES lysis buffer

7. MES buffer 1 (MES breaking buffer): 10 mM MES/Tris (pH 6.9), 12 % (w/w) Ficoll 400, 0.2 mM EDTA

8. MES buffer 2: 10 mM MES/Tris (pH 6.9), 8 % (w/w) Ficoll 400, 0.2 mM EDTA

9. MES buffer 3: 10 mM MES/Tris (pH 6.9), 0.6 M sorbitol, 8 % (w/w) Ficoll 400, 0.2 mM EDTA

10. MES buffer 4: 10 mM MES/Tris (pH 6.9), 0.25 M sorbitol, 0.2 mM EDTA

11. KPi buffer (pH 7.4): 20 mM KH_2PO_4/KOH (pH 7.4), 1.2 M sorbitol

Procedure

Wild-type and mutant cells were grown in YEPD (0.2% glucose) medium. Cultures were harvested at mid-exponential and diauxic phases, checked for contamination by bright-field microscopy and used to measure cell density at OD_{600}. The non-contaminated wild-type and mutant cells were pelleted at 4,000 × g for 5 min at room temperature. Cells were then resuspended at 10 OD_{600} units/ml in TSD reduction buffer, incubated for 10 min at room temperature and centrifuged for 5 min at 4,000 × g at room temperature. Pelleted cells were then resuspended at 20 OD_{600} units/ml in Spheroplast medium A and supplemented with Zymolyase 100T at a concentration of 7.5 µg per OD_{600} units of cells. 10 µl of each cell suspension was then removed, diluted in 990 µl of H_2O and used to measure the OD_{600}. The remaining cell suspensions were incubated at 30°C for 30 min and the efficiency of cell wall removal was monitored by measuring the OD_{600}. Cell wall digestion was allowed to proceed until the OD_{600} measurement of the diluted cell suspension became 5% of the original value, with the total digestion time not exceeding 1

hour. Spheroplasts were then harvested by centrifugation at 1,500 × g for 5 min at room temperature, followed by resuspending at 1 to 5 OD$_{600}$ units/ml in Spheroplast medium B by gentle swirling of the tube or gentle stirring with a glass rod. Spheroplasts were then harvested by centrifugation at 1,500 × g for 5 min at 4°C and then resuspended at a concentration of 1,000 OD$_{600}$ units/ml of ice-cold HEPES lysis buffer with freshly-added DTT. Spheroplasts were then homogenized using 20 strokes and resulting lysates were centrifuged at 1, 000 × g for 10 min at 4°C. The supernatants (S$_{1000}$) were subjected to another round of centrifugation at 1, 000 × g for 10 min at 4°C, and resulting supernatants were further centrifuged at 27,000 × g for 10 min at 4°C. The pelleted membranes (P$_{27,000}$) were resuspended in 1.0 ml of HEPES lysis buffer (5,000 OD$_{600}$ equivalents per ml) using a trimmed 1-ml pipette tip and carefully layered on top of a sucrose gradient prepared in advance (2.1 ml of 1.5 M sucrose/HEPES solution was deposited to the bottom of a Beckman Ultra-Clear centrifuge tube for the Beckman MLS-50 rotor, and then overlaid with 2.1 ml of 1.2 M sucrose/HEPES solution). The gradient tubes were then placed in the pre-chilled swinging bucket Beckman MLS-50 rotor and centrifuged at 100,000 × g (36,000 rpm) for 1 hr at 4°C using the slow acceleration and deceleration setting to minimize disruption of gradients. 18 gradient fractions of 227 μl each were then collected starting from the top of the sucrose gradient and stored at -20°C for further analyses.

Purification of LBs

Reagents and solutions

1. TSD reduction buffer: 0.1 M Tris/Sulfate (pH 9.4), 10 mM DTT

2. HEPES lysis buffer: 20 mM HEPES/KOH, pH 6.8, 50 mM KCl, 200 mM sorbitol, 2 mM EDTA, 1 mM DTT

3. Spheroplast medium A (pH 7.5): 0.67% yeast nitrogen base (w/o) amino acids, 2 % (w/v) glucose, 1 M sorbitol, 20 mM Tris/HCl (pH 7.5)

4. Spheroplast medium B: 0.67% yeast nitrogen base (w/o) amino acids, 2 % (w/v) glucose, 1 M sorbitol

5. 1.2 M sucrose/ HEPES, 36% (w/w): 7.2 g sucrose + 12.8 ml HEPES lysis buffer

6. 1.5 M sucrose/ HEPES, 43% (w/w): 8.6 g sucrose + 11.4 ml HEPES lysis buffer

7. MES buffer 1 (MES breaking buffer): 10 mM MES/Tris (pH 6.9), 12 % (w/w) Ficoll 400, 0.2 mM EDTA

8. MES buffer 2: 10 mM MES/Tris (pH 6.9), 8 % (w/w) Ficoll 400, 0.2 mM EDTA

9. MES buffer 3: 10 mM MES/Tris (pH 6.9), 0.6 M sorbitol, 8 % (w/w) Ficoll 400, 0.2 mM EDTA

10. MES buffer 4: 10 mM MES/Tris (pH 6.9), 0.25 M sorbitol, 0.2 mM EDTA

11. KPi buffer (pH 7.4): 20 mM KH_2PO_4/KOH (pH 7.4), 1.2 M sorbitol

Procedure

Wild-type and mutant cells were grown in YEPD (0.2% glucose) medium. Cultures were harvested at mid-exponential and diauxic phases, checked for contamination by bright-field microscopy and used to measure cell density at OD_{600}. The non-contaminated wild-type and mutant cells were pelleted at 4,000 × g for 5 min at room temperature. The cells were then washed once with distilled water and resuspended in the TSD reduction buffer at 10 x OD_{600} units/ml. Following a 10-min incubation at room temperature, the cells

were pelleted by centrifugation at 4,000 × g for 5min at room temperature and then washed once in Spheroplasts medium A. The cells were then resuspended in Spheroplasts medium A at 20 × OD$_{600}$ units/ml, supplemented with Zymolyase 100T at a concentration of 2.5 μg per OD$_{600}$ units of cells, and incubated at 30°C for 45 min on a shaker set at 75 rpm. Spheroplasts were then pelleted by 5min centrifugation at 1,500 × g at room temperature, resuspended in the ice-cold Spheroplasts medium B at 5 × OD$_{600}$ units/ml using pipettes with cut tips, and centrifuged for 5 min at 1,500 × g at 4°C. Spheroplasts were then washed twice by resuspending the pellets in ice-cold KPi buffer at a concentration of 5 OD$_{600}$ units/ml followed by centrifugation for 5 min at 1,500 × g at 4°C. After the second wash and centrifugation step, clean spheroplasts were resuspended in ice-cold MES Buffer 1 at a concentration of 1,000 OD$_{600}$ units/ml using pipettes with non-cut tips. Spheroplasts were then lysed in a homogenizer using 20 strokes at 4°C. Lysates were centrifuged for 5 min at 5,000 × g at 4°C and the resulting supernatants (S$_{5,000}$) were transferred to pre-chilled centrifuge tubes kept on ice. LBs were then purified by subjecting the spheroplast lysates to a series of flotation gradient centrifugations using a MLS 50 swinging bucket rotor (Beckman). The first flotation gradient was prepared by placing 2.5 ml of the S$_{5,000}$ fraction to the bottom of a centrifuge tube (Ultra-Clear Beckman tubes for MLS 50 rotor) and overlaying it with 2.5 ml of ice-cold MES Buffer 1. Following 1 hour centrifugation at 100,000 × g (36,000 rpm) at 4°C, the floating layer from the top portions of the gradients was collected with a cut tip and transferred to the bottom of a new centrifuge tube, which was then supplemented with MES buffer 2 to a total volume of 2.5 ml and gently mixed by pipetting. Resulting suspension was overlaid with 2.5 ml of ice-cold MES buffer 2 and then centrifuged for 1

hr at 100,000 × g (36,000 rpm) at 4°C. The floating layer from the top portions of the gradients was again collected with a cut tip and transferred to the bottom of a new centrifuge tube, which was then supplemented with MES buffer 3 to a total volume of 2.5 ml and gently mixed by pipetting. Resulting suspension was overlaid with 2.5 ml of ice-cold MES buffer 4 and then centrifuged for 1 hr at 100,000 × g (36,000 rpm) at 4°C. The floating layer from the top portions of the gradients was collected with a cut tip and purified lipid bodies were stored -20°C for further analyses.

Protein precipitation, SDS-PAGE and silver staining of gels

Protein concentration was determined using the RC DC protein assay kit (Bio-Rad) according to the manufacturer's instructions. Proteins were precipitated by adding trichloroacetic acid (TCA) to the final concentration of 10%, incubated on ice for 30 min, pelleted by centrifugation, and then washed with ice-cold 80% acetone. Dried protein pellets were then resuspended in the SDS-PAGE sample buffer and the pH was adjusted to neutral using 2 M Tris/HCl (pH 8.8). The samples were boiled for 5 min at 63°C, centrifuged for 30 sec at 16,000 x g, loaded onto a 7.5%, 10%, 12.5% or 16% gel and resolved by SDS-PAGE. Following an overnight incubation of the gels in 50% methanol, proteins were visualized by silver staining using the mass spectrometry-compatible silver staining kit (Bio-Rad Silver Staining Plus) according to the manufacturer's instructions. The Bio-Rad unstained molecular marker and a 0.1 mg/ml solution of BSA in the SDS-PAGE sample buffer were also subjected to SDS-PAGE. The proteins were then visualized by silver staining.

Analysis of proteins by mass spectrometry

Proteins were resolved by SDS-PAGE and visualized by silver staining [226]. Protein bands were excised from the gel, reduced, alkylated and in-gel digested with trypsin [226]. The proteins were identified by matrix-assisted laser desorption/ionization mass spectrometric (MALDI MS) peptide mapping [227], using a Micromass M@LDI time-of-flight (TOF) mass spectrometer (Waters). Database searching using peptide masses was performed with the Mascot web-based search engine. For evaluating relative levels of individual proteins recovered in total cell lysates or purified mitochondria, a selected protein band was excised from the silver-stained gel and placed into an Eppendorf tube. A band of BSA containing 2 μg of this protein, which was also excised from the silver-stained gel, was added to each of the protein bands to be analyzed. Protein bands were reduced, alkylated and in-gel digested with trypsin [226]. The desalted peptide mixture was added to the surface of a MALDI target plate and allowed to air dry. The sample spot was then overlaid with MALDI matrix solution containing the Angiotensin I peptide standard (1:1 ratio). The presence of Angiotensin I in the sample carrying the analyzed mixture of peptides provided an additional estimate of the mass measurement accuracy after calibration, giving an opportunity to calculate the value of peptide mass tolerance for each individual mass spectrum. After the desalted peptide mixture was analyzed by MALDI-TOF, the monoisotopic masses of recovered BSA peptides and the intensities of their monoisotopic peaks were grouped separately from the masses and intensities of peptides originated from the protein of interest. These data provided an additional estimate of the mass measurement accuracy and were used for the quantitation of relative levels of the same protein recovered in different samples. For evaluating relative levels of

the protein of interest found in the samples to be compared, a ratio "the intensity of the monoisotopic peak of a peptide originated from the protein of interest/the intensity of the monoisotopic peak of a BSA peptide with the monoisotopic mass closest to the mass of the peptide of interest" was calculated for each peptide originated from the protein of interest. Based on these data, the average value for relative levels of the protein of interest found in the two compared samples was calculated. The method for evaluating relative levels of the protein of interest recovered in different samples was validated by calculating relative levels of several standard proteins in the samples supplemented with different quantities of each of these proteins.

Analysis of lipids by mass spectrometry

1×10^{10} cells were harvested by centrifugation and washed three times with cold water. The lipids were extracted by resuspending the cells in 3.8 ml of chloroform - methanol - water (1:2:0.8) and by vortexing the cell suspension with glass beads two times for 1 min. 1 ml of chloroform was then added, and the extract was incubated for 5 min with occasional mixing. 1 ml of water was then added, and the extract was incubated for 5 min with occasional mixing. The extract was centrifuged and the entire supernatant was collected. The pellet was resuspended in 1.6 ml of chloroform, and the lipids were extracted by vortexing the suspension with glass beads two times for 1 min. The extract was then centrifuged and the entire supernatant was collected. The pooled supernatants were centrifuged and the organic phase was collected. The lipid extract was dried under nitrogen. The lipid film was dissolved in 400 µl of chloroform - methanol (1:1) containing either 3 mM ammonium hydroxide for positive-ion analyses or no additive for

negative-ion measurements. Mass spectrometric analyses were performed with a Micromass Q-TOF 2 mass spectrometer equipped with a nano-electrospray source operating at a flow rate of 1 μl/min. The instrument was used in the single-stage mass spectrometry mode for positive- or negative-ion analyses as described in Chapter 2 of this thesis. For quantification of individual lipid molecular species, the commercially available lipids (Avanti Polar Lipids, Larodan AB and Sigma) with non-natural fatty acid compositions were used as internal standards that do not occur in a significant amount in the sample to be analyzed. Lipid quantification was performed as described in Chapter 2 of this thesis.

Miscellaneous procedures

SDS-PAGE and immunoblotting using a Trans-Blot SD semi-dry electrophoretic transfer system (Bio-Rad) were performed as previously described [228]. Blots were decorated with monoclonal antibodies raised against actin (Abcam) or porin (Invitrogen) or polyclonal antisera raised against Aco1p (kind gift of Dr. Ronald A. Butow, University of Texas Southwestern Medical Center) or cytochrome c (kind gift of Dr. Roland Lill, Philipps Universität Marburg). Antigen-antibody complexes were detected by enhanced chemiluminescence using an Amersham ECL Western blotting detection reagents (GE Healthcare). Enzymatic activities of cytochrome c oxidase [229], succinate dehydrogenase [230] and aconitase [231] were determined by established methods. For measuring ethanol and acetic acid concentrations, 1-ml aliquots of yeast cultures were centrifuged and supernatants frozen at -80°C. The supernatants were subjected to gas chromatography using an Agilent 6890 Networked GC system equipped with a Supelco

Equity-1 (0.32 mm × 30 cm) column and FID detector. Ethanol and acetic acid concentrations were calculated using the Chemstation 3 software (Agilent). Protocols for lipid extraction, separation by TLC, visualization by 5% phosphomolybdic acid in ethanol, and quantitation by densitometric analysis of TLC plates have been described elsewhere [232]. Preparation of cellular extracts and microanalytic biochemical assays for measuring ATP, glucose, trehalose and glycogen concentrations was performed as previously described [233].

3.4. Results

3.4.1. CR extends the chronological life span of yeast

To study the effect of CR on the chronological life span, I incubated the wild-type (WT) strain BY4742 in rich YP medium initially containing 0.2%, 0.5%, 1% or 2% glucose. The full growth cycle of WT culture in each of these four media began with logarithmic (L) phase and progressed through diauxic (D) and post-diauxic (PD) phases to stationary (ST) phase (Figure 3.1A). Notably, the rates of growth (Figure 3.1A) and glucose consumption (Figure 3.1B) in L phase were similar for WT cells cultured in any of the four media, whereas the maximum cell density in ST-phase cultures varied within a 28-% range and correlated with the initial glucose concentration (Figure 3.1A). CR cells of WT grown on 0.2% or 0.5% glucose lived significantly longer than WT cells grown under non-CR conditions on 1% or 2% glucose (Figure 3.1C). The mean chronological life span of cells grown on 0.2% glucose was extended by more than 60% and that of cells grown on 0.5% glucose was extended by almost 2-fold, as compared to the mean chronological life span of cells grown on 2% glucose (Figure 3.1D). Of note, CR yeast grown on 0.5%
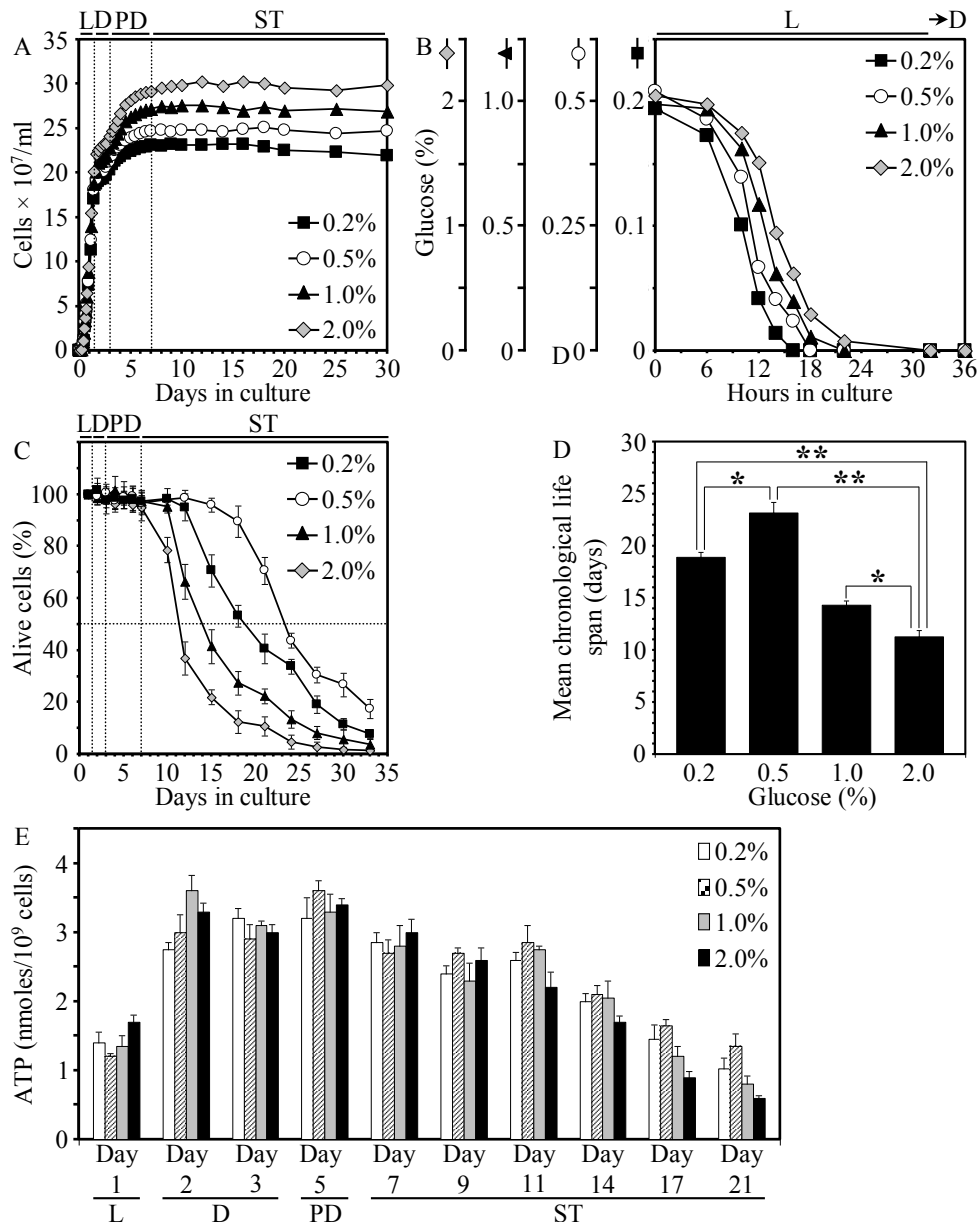
Figure 3.1. CR extends the chronological life span of yeast. (A and B) Kinetics of growth (A) and glucose consumption (B) for the WT strain BY4742. Each plot shows a representative experiment repeated 4-6 times in triplicate with similar results. (C) Survival of chronologically aging WT cells. Data are presented as mean ± SEM (n = 16-28). p < 0.001 at days 10 to 33 for cells grown on 0.2% or 0.5% glucose vs. cells grown on 2% glucose. (D) The mean chronological life spans of WT cells. Data are presented as mean ± SEM (n = 16-28); *p < 0.01, **p < 0.001. (E) ATP levels in chronologically aging WT cells. Data are presented as mean ± SEM (n = 3-5). (A-E) Cells were cultured in YP medium containing 0.2%, 0.5%, 1% or 2% glucose. Abbreviations: Diauxic (D), logarithmic (L), post-diauxic (PD) or stationary (ST) phase.

glucose lived longer than CR yeast grown on 0.2% glucose (Figure 3.1D).

Noteworthy, unlike yeast cells grown in the nutrient-limited SC medium [234, 235], cells cultured in the nutrient-rich YP medium with 0.5% glucose lived longer than cells cultured in YP medium containing 0.05% glucose (Figure 3.2). Thus, the largest increase in the chronological life span of yeast grown under CR conditions in YP medium occurs at 0.5% glucose. The observed difference in the lowest concentration of glucose that is optimal for life-span extension under CR conditions between yeast grown in SC or YP medium could be due to at least two factors. First, YP medium is enriched, as compared to SC medium, in amino acids, nucleotides, vitamins and other essential nutrients. It is conceivable that at least some of these nutrients could modulate the effect of different glucose concentrations on chronological life span by influencing certain metabolic and/or nutrient-sensing signaling pathways operating in CR yeast. Second, the initial pH in yeast cultures grown in SC medium was 3.9-4.0 [236], whereas in yeast cultures grown in YP medium it was 6.9 (Figure 3.3). Furthermore, both the dynamics of age-related changes in the pH of culture medium and the final medium pH reached after several days of growth in SC with 0.5% or 0.05% glucose [236] differ from those observed for yeast that aged chronologically in YP medium containing either of these two glucose concentrations (Figure 3.3). It is feasible that such differences between SC and YP in the initial pH and/or its age-related homeostasis could contribute to the observed difference between these two media in the lowest concentration of glucose at which the highest beneficial effect of CR on chronological life span can be achieved.

Importantly, ATP levels and the dynamics of their change during chronological aging were very similar for CR and non-CR yeast (Figure 3.1E). Thus, CR yeast are not
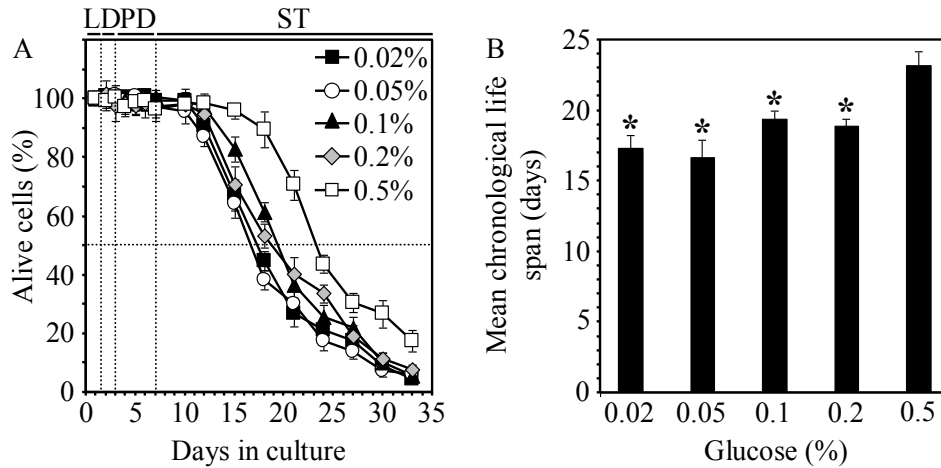
Figure 3.2. Survival of the chronologically aging wild-type strain BY4742 (A) and the mean chronological life spans of different cultures of BY4742 (B) grown in YP medium initially containing 0.02%, 0.05%, 0.1%, 0.2% or 0.5% glucose. Data are presented as mean ± SEM (n = 3 for cells grown on 0.02%, 0.05% or 0.1% glucose; n = 35 for cells grown on 0.2% glucose; n = 24 for cells grown on 0.5% glucose). *p < 0.01 (for cells grown on 0.02%, 0.05%, 0.1% or 0.2% glucose vs. cells grown on 0.5% glucose). Abbreviations: Diauxic (D), logarithmic (L), post-diauxic (PD) or stationary (ST) phase.
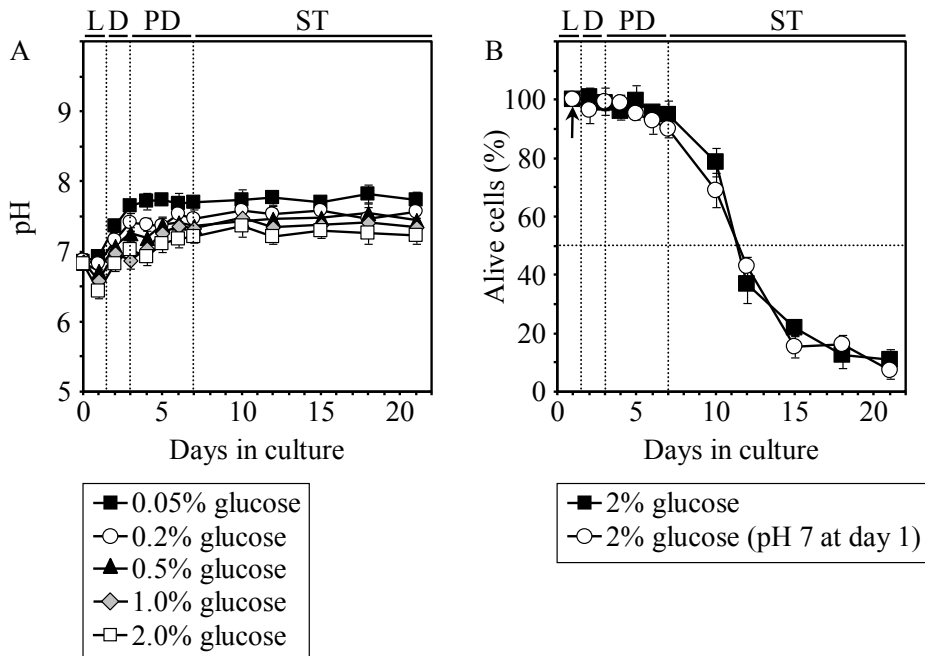
Figure 3.3. (A) The dynamics of age-related changes in the pH of culture medium for the wild-type strain BY4742 grown in YP medium initially containing 0.05%, 0.2%, 0.5%, 1.0% or 2.0% glucose. Data are presented as mean ± SEM (n = 3). (B) Survival of chronologically aging BY4742 grown either in YP

medium initially containing 2% glucose or in YP medium with 2% glucose to which HEPES-KOH buffer (pH 7.0) was added at day 1 to the final concentration of 25 mM. Data are presented as mean ± SEM (n = 22 for cells grown on 2% glucose; n = 3 for cells grown on 2% glucose and supplemented with a pH 7 HEPES buffer at day 1). Abbreviations: Diauxic (D), logarithmic (L), post-diauxic (PD) or stationary (ST) phase.

starving. Based on this important conclusion, I hypothesized that: 1) CR yeast remodel their metabolism in order to match the level of ATP produced in non-CR yeast; and 2) such specific remodeling of metabolism in CR yeast prolongs their life span.

3.4.2.   CR promotes the consumption of neutral lipids deposited in LBs

I sought to define a specific pattern of metabolism that is responsible for the anti-aging effect of CR. In laboratory mice, the biosynthesis and degradation of TAG in white adipose tissue and mitochondrial fatty acid oxidation in skeletal muscle may play a role in longevity regulation [138 -141, 185 - 187]. I therefore assessed the dynamics of age-dependent changes in levels of TAG and ergosteryl esters (EE), the two major neutral lipids that in yeast are synthesized in the ER and then deposited in LBs [212]. TAG and EE serve as the main storage molecules for FFA, DAG and ergosterol (ERG). Hence, the ability of yeast to modulate the biosynthesis and degradation of neutral lipids is crucial for regulating 1) energy homeostasis; 2) phospholipid and cardiolipin biosynthesis; 3) neutralization of excessive amounts of membrane-perturbing species of FFA and ERG; 4) FFA- and DAG-induced lipoapoptosis or necrosis; and 5) DAG-dependent signal transduction networks [148, 212, 222].

Using TLC for measuring total cell lipids, I found that the concentrations of neutral lipids in WT cells increased gradually in logarithmic (L) and diauxic (D) phases, reaching
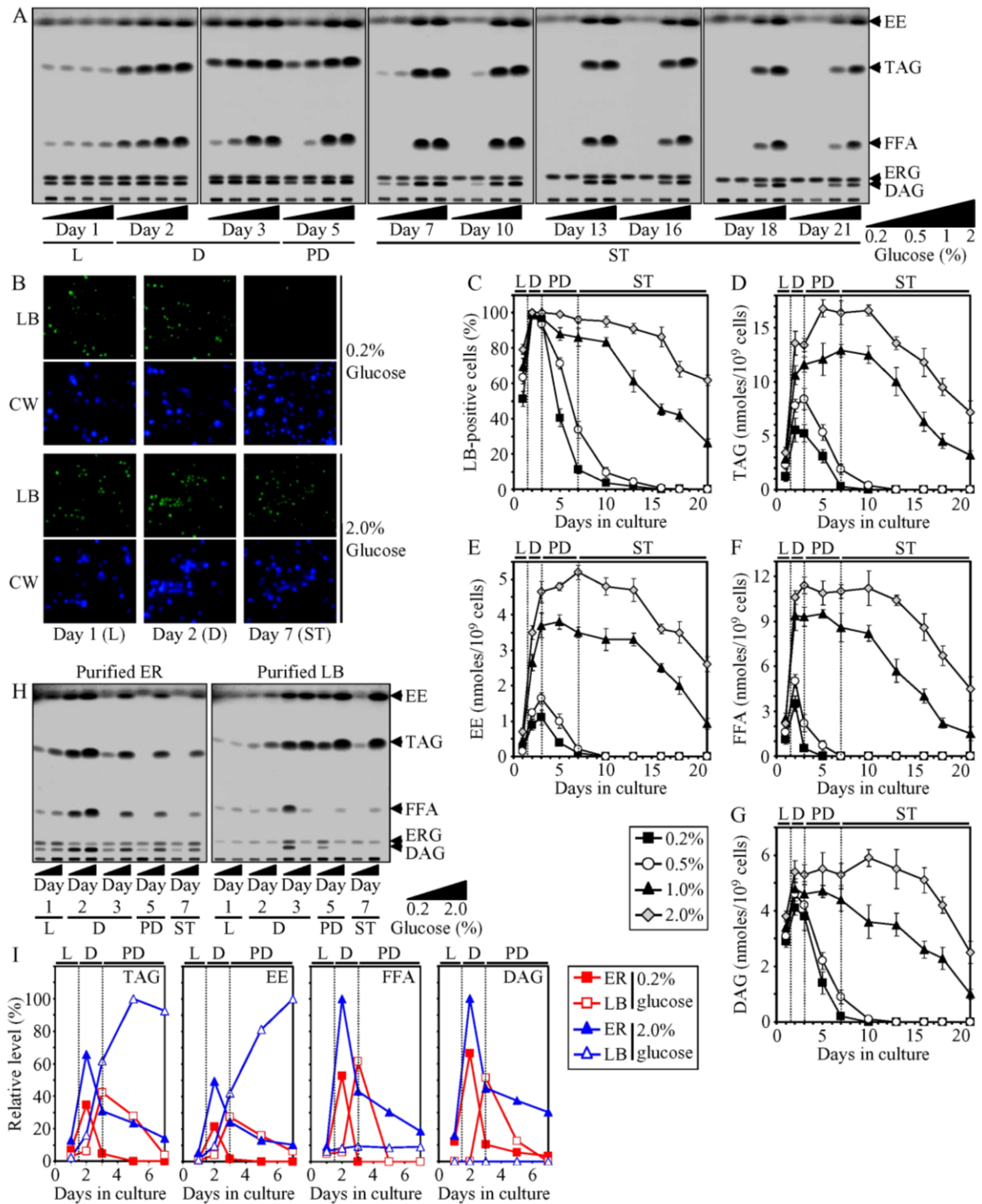
Figure 3.4. CR promotes the consumption of neutral lipids deposited in LBs. A) Spectra of lipids extracted from equal numbers of WT cells and analyzed by TLC. A representative of 4 independent experiments is shown. (B) WT cells were visualized using Calcofluor White M2R (CW) and stained with BODIPY 493/503 to detect neutral lipids of lipid bodies (LB). (C) Percent of cells that contain lipid bodies. Images similar to the representative images shown in (B) were quantitated. Data are presented as mean ±

SEM (n = 5). p < 0.001 at days 5 to 21 for cells grown on 0.2% or 0.5% glucose vs. cells grown on 2% glucose. (D-G) Lipid species shown in (A) were quantitated by densitometric analysis of TLC plates. Data are presented as mean ± SEM (n = 4). p < 0.001 at days 2 to 21 (for TAG, EE and FFA) or at days 5 to 21 (for DAG) for cells grown on 0.2% or 0.5% glucose vs. cells grown on 2% glucose. (H and I) Spectra of lipids (H) that were extracted from purified ER and lipid bodies of WT cells. The equivalent of 200 μg of ER proteins and 20 μg of lipid body proteins was used for lipid extraction at each time point. Lipids were analyzed by TLC and quantitated by densitometric analysis of TLC plates (I). Each plot shows a representative experiment repeated 3 times with similar results. (A, C-G) Cells were cultured in YP medium containing 0.2%, 0.5%, 1% or 2% glucose. (B, H and I) Cells were cultured in YP medium containing 0.2% or 2% glucose. Abbreviations: DAG, diacylglycerols; EE, ergosteryl esters; ERG, ergosterol; FFA, free fatty acids; TAG, triacylglycerols.

higher levels in non-CR yeast than in CR yeast (Figures 3.4A, 3.4D and 3.4E). During the subsequent post-diauxic (PD) phase, CR yeast completely consumed neutral lipids, whereas non-CR yeast continued to accumulate them. In contrast to yeast under CR, non-CR yeast began to consume their deposited neutral lipids only after they have entered stationary (ST) phase (Figures 3.4A, 3.4D and 3.4E). The data of TLC analysis were supported by a quantitative assessment of the age-dependent changes in levels of 55 different species of TAG, predominantly present as the 16:1/16:1/16:1, 16:1/16:1/18:1 and 16:1/18:1/18:1 molecular forms, with the help of electrospray ionization mass spectrometry (ESI/MS; Figure 3.5). Live-cell fluorescence microscopy further supported the notion that CR accelerates the consumption of neutral lipids deposited in lipid bodies (Figures 3.4B and 3.4C).

I then examined the spatial dynamics of lipids in aging yeast. Consistent with the ER origin of LBs [160], neutral lipids were synthesized in the ER during L and D phases, prior to being relocated to and accumulated in LBs (Figures 3.4H and 3.4I). CR yeast completely consumed neutral lipids during the following PD phase, whereas non-CR

yeast continued to deposit them in LBs. The age-dependent buildup of neutral lipids in

LBs of non-CR yeast coincided with the deceleration of their exit from the ER *en route* to
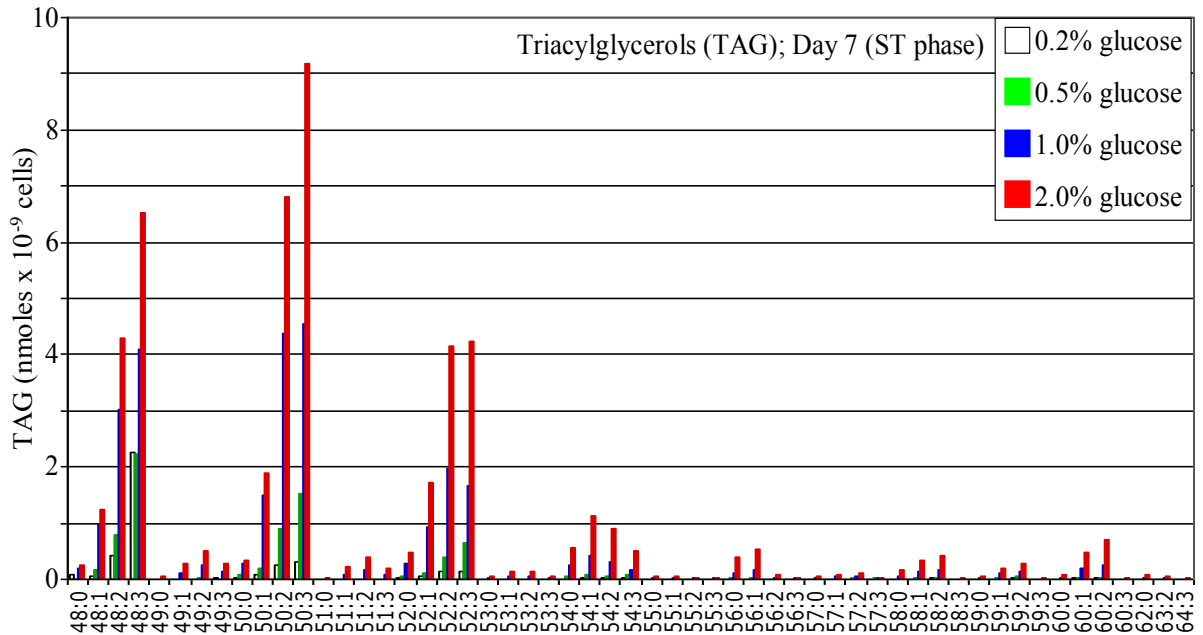
Figure 3.5. CR decreases the levels of various molecular species of triacylglycerols (TAG) in chronologically aging WT cells. Different molecular forms of TAG were identified and quantitated using electrospray ionization mass spectrometry. The plot shows a representative experiment repeated 3 times with similar results. Cells were cultured in rich YP medium initially containing 0.2%, 0.5%, 1% or 2% glucose.

LBs (Figures 3.4H and 3.4I).

The biosynthesis of FFA and DAG during early D phase was followed by their

incorporation into TAG within the ER during late D phase (Figures 3.4F-3.4I). Soon after

their relocation from the ER to LBs, TAG in CR yeast were hydrolyzed to yield FFA and

DAG, both of which were rapidly degraded during PD phase (Figures 3.4F-3.4I).

Alternatively, non-CR yeast accumulated both FFA and DAG within the ER (Figures

3.4F-3.4I). The data of TLC analysis were supported by the ESI/MS-assisted quantitative

assessment of the age-dependent changes in concentrations of 25 different forms of FFA, with 16:0, 16:1, 18:0 and 18:1 being the most abundant molecular species (Figure 3.6).
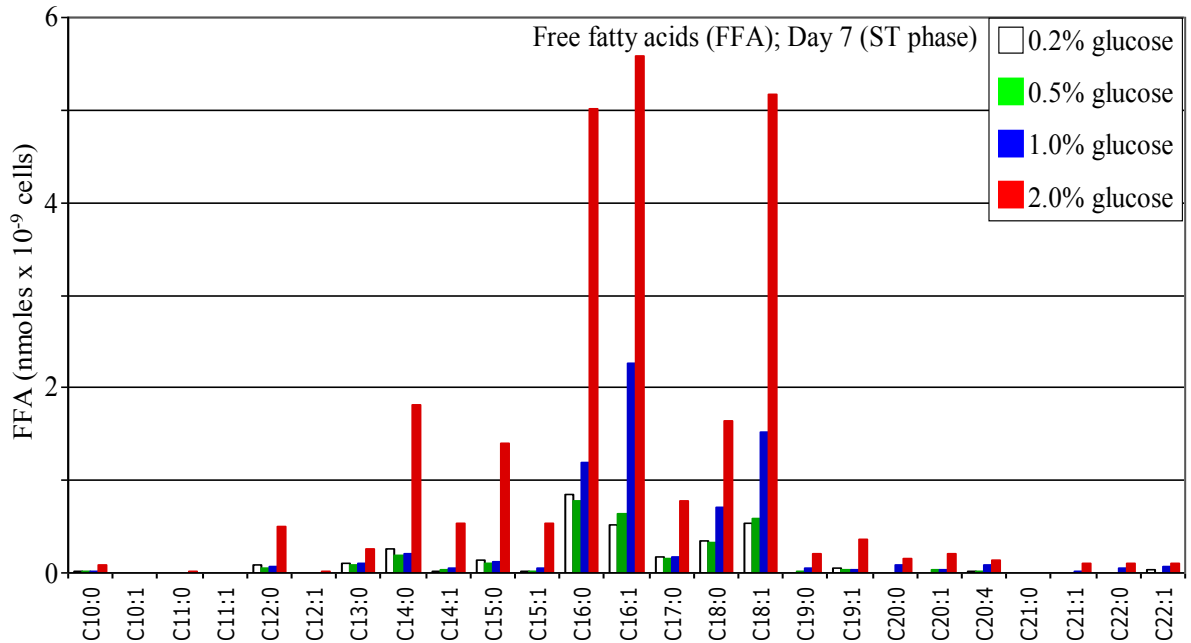
Figure 3.6. CR decreases the levels of various molecular species of free fatty acids (FFA) in chronologically aging WT cells. Different molecular forms of FFA were identified and quantitated using electrospray ionization mass spectrometry. The plot shows a representative experiment repeated 3 times with similar results. Cells were cultured in rich YP medium initially containing 0.2%, 0.5%, 1% or 2% glucose.

My findings suggest that, due to the deceleration of the exit of TAG from and their resulting buildup within the ER, significant quantities of both FFA and DAG in non-CR yeast were unable to be used for the biosynthesis of TAG, perhaps because of a feedback inhibition of this process.

3.4.3. CR alters the levels of proteins that function in carbohydrate and lipid metabolism

The described in section 3.4.2 measurement of lipids revealed that CR yeast undergo specific remodeling of lipid metabolism prior to entry into the non-proliferative ST phase. My MS-based quantitative proteomics of aging CR and non-CR yeast further supported this notion (Figure 3.7; Tables 3.1 and 3.2). In fact, as one can expect judging from the age-dependent dynamics of neutral lipids, I found that CR elevates the levels of enzymes that function in the degradation of these lipid species within LBs, concomitantly lowering the levels of ER- and LB-confined enzymes involved in their biosynthesis (Figure 3.7B). Moreover, the fact that CR elevated the levels of enzymes functioning in the formation of CoA esters of fatty acids (FA-CoA) and in their uptake and oxidation by peroxisomes (Figure 3B) can satisfactorily explain our observation that CR promoted fatty acids consumption during D and PD phases (Figures 2A and 2F). My proteomic analysis also implies that aging CR yeast re-design carbohydrate metabolism. Specifically, I found that the CR diet increases the levels of key enzymes that function in the biosynthesis of trehalose and glycogen, concurrently decreasing the levels of key enzymes catalyzing their degradation (Figure 3.7B). My data on the age-dependent dynamics of trehalose and glycogen (Figures 3.8B and 3.8C) support the notion that CR promotes the accumulation of these two major glucose stores in aging yeast. Furthermore, by decreasing the level of Adh1p, an enzyme that is required for ethanol synthesis, and by increasing the level of Adh2p, an enzyme that catalyzes ethanol degradation (Figure 3.7B), CR greatly accelerated the depletion of ethanol from yeast cells (Figure 3.8D). Moreover, I found that CR elevates the levels of the three key enzymes of gluconeogenesis, a reverse to glycolysis process of synthesizing glucose from pyruvate (Figure 3.7B). The resulting shift of CR yeast toward glucose formation, away from its
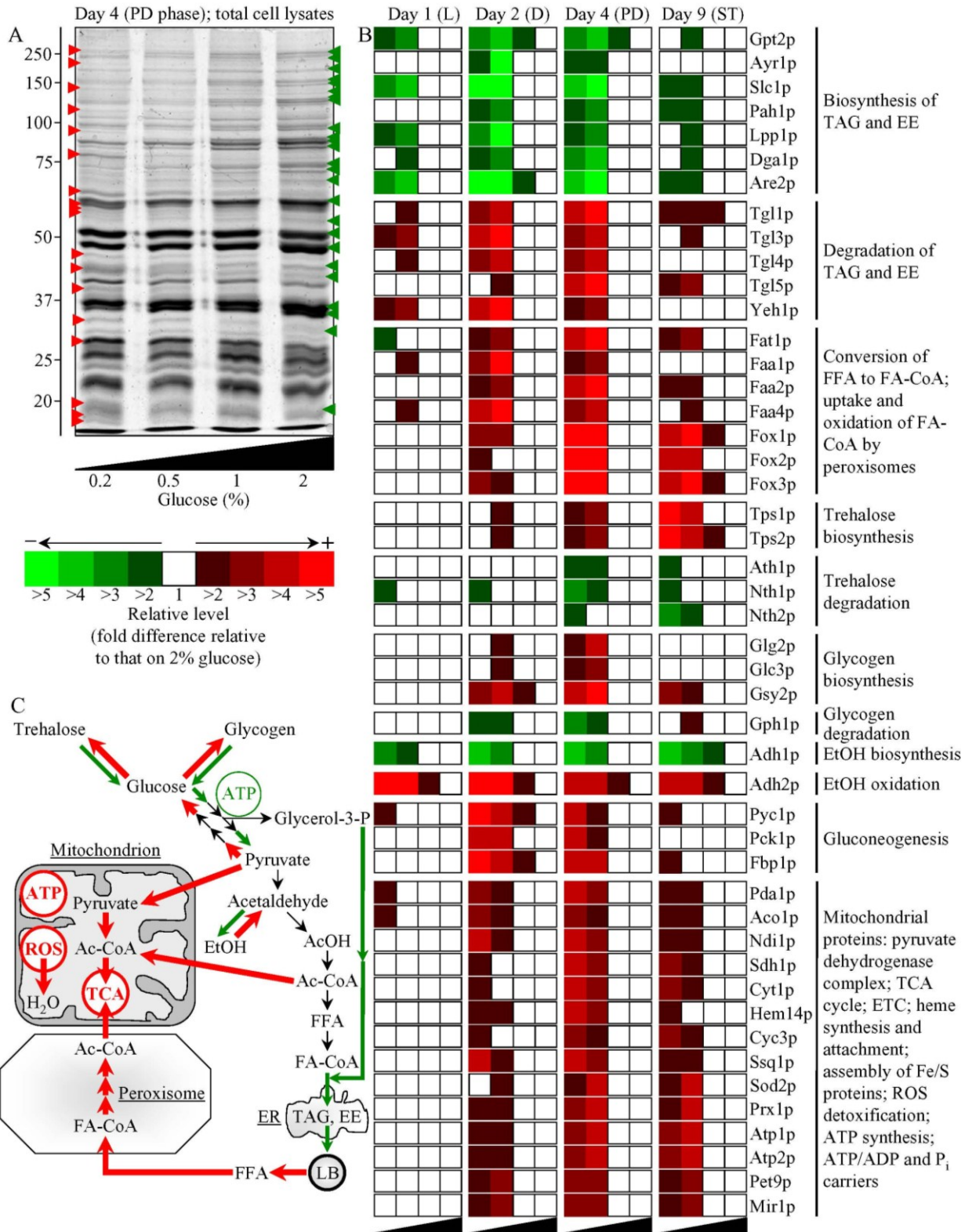
Figure 3.7. CR yeast undergo remodeling of carbohydrate and lipid metabolism prior to entry into the non-proliferative ST phase. (A) The spectra of proteins recovered in total lysates of WT cells. Cells were

cultured in YP medium containing 0.2%, 0.5%, 1% or 2% glucose. A representative of 2 independent experiments is shown. (B) Relative levels (fold difference relative to that on 2% glucose) of proteins recovered in total lysates of WT cells. Proteins were identified and quantitated using mass spectrometry. The complete list of proteins and their relative levels are provided in Tables 3.1 and 3.2, respectively. (C) Outline of metabolic pathways and interorganellar communications that were accelerated (red arrows) or decelerated (green arrows) by CR prior to entry into the non-proliferative ST phase. Abbreviations: AcOH, acetic acid; Ac-CoA, acetyl-CoA; DAG, diacylglycerols; EE, ergosteryl esters; ERG, ergosterol; EtOH, ethanol; FA-CoA, CoA esters of fatty acids; FFA, free fatty acids; LB, lipid bodies; ROS, reactive oxygen species; TAG, triacylglycerols.

Table 3.1. List of proteins recovered in total lysates of WT cells cultured in YP medium initially containing 0.2%, 0.5%, 1% or 2% glucose. For making total lysates, cells were collected at day 1 (L phase), day 2 (D phase), day 4 (PD phase) and day 9 (ST phase). Proteins were identified using matrix-assisted laser desorption/ionization mass spectrometric (MALDI MS) peptide mapping.

Protein	NCBI accession no.	Function	Number of identified peptides	Sequence coverage (%)	Mowse score[1]	Expectation value[2]
YP + 0.2% glucose; Day 1 (L phase)						
Tps1p	NP_009684	Trehalose biosynthesis	7	18	114	6e-08
Tps2p	NP_010359	Trehalose biosynthesis	9	9	115	1.7e-05
Ath1p	NP_015351	Trehalose degradation	10	8	122	9.5e-09
Nth1p	NP_010284	Trehalose degradation	8	11	108	2.4e-07
Nth2p	NP_009555	Trehalose degradation	9	13	127	3e-09
Glg2p	NP_012398	Glycogen biosynthesis	7	18	120	1.5e-08
Glc3p	NP_010905	Glycogen biosynthesis	10	15	143	2.7e-08
Gsy2p	NP_013359	Glycogen biosynthesis	9	14	131	1.2e-09
Gph1p	NP_015486	Glycogen degradation	12	15	164	6e-13
Gpt2p	NP_012993	Biosynthesis of TAG	10	14	135	4.8e-10
Ayr1p	NP_012142	Biosynthesis of TAG	6	28	112	9.5e-08
Slc1p	NP_010231	Biosynthesis of TAG	8	32	138	2.4e-10
Pah1p	NP_013888	Biosynthesis of TAG	7	9	97	2.9e-06
Lpp1p	NP_010791	Biosynthesis of TAG	5	19	93	8.3e-06
Dga1p	NP_014888	Biosynthesis of TAG	6	17	102	9.5e-07
Are2p	NP_014416	Biosynthesis of TAG and EE	7	10	106	3.8e-07
Tgl1p	NP_012782	Degradation of EE	6	15	103	7.6e-07
Tgl3p	NP_014044	Degradation of TAG	7	12	105	4.8e-07
Tgl4p	NP_013015	Degradation of TAG	9	12	128	2.4e-09
Tgl5p	NP_014724	Degradation of TAG	7	10	96	3.4e-06
Yeh1p	NP_013089	Degradation of EE	6	13	94	5.7e-06
Fat1p	NP_009597	Conversion of FFA to FA-CoA	5	10	74	0.00057
Faa1p	NP_014962	Conversion of FFA to FA-CoA	6	10	89	1.9e-05
Faa2p	NP_010931	Conversion of FFA to FA-CoA	7	12	102	9.5e-07

Faa4p	NP_013974	Conversion of FFA to FA-CoA	10	15	147	3e-11
Fox1p	NP_011310	Peroxisomal oxidation of FA-CoA	7	11	93	7.6e-06
Fox2p	NP_012934	Peroxisomal oxidation of FA-CoA	8	12	115	4.8e-08
Fox3p	NP_012106	Peroxisomal oxidation of FA-CoA	6	21	105	4.8e-07
Adh1p	NP_014555	Ethanol biosynthesis	8	27	145	4.8e-11
Adh2p	NP_014032	Ethanol oxidation	9	29	142	9.5e-11
Pyc1p	NP_011453	Gluconeogenesis	8	9	98	2.3e-06
Pck1p	NP_013023	Gluconeogenesis	7	17	115	4.8e-08
Fbp1p	NP_013481	Gluconeogenesis	6	22	107	3e-07
Pda1p	NP_011105	Mitochondrial PDH complex	7	17	109	1.9e-07
Aco1p	NP_013407	Mitochondrial TCA cycle	11	17	160	1.5e-12
Ndi1p	NP_013586	Mitochondrial ETC	8	18	128	2.4e-09
Sdh1p	NP_012774	Mitochondrial TCA cycle and ETC	7	12	105	4.8e-07
Cyt1p	NP_014708	Mitochondrial ETC	6	26	113	7.6e-08
Hem14p	NP_010930	Heme synthesis in mitochondria	9	20	140	1.5e-10
Cyc3p	NP_009361	Heme attachment to apo-cytochrome c	6	22	113	7.6e-08
Ssq1p	NP_013473	Assembly of Fe/S clusters into proteins	7	12	102	9.5e-07
Sod2p	NP_011872	Detoxification of ROS in mitochondria	6	30	119	1.9e-08
Prx1p	NP_009489	Detoxification of ROS in mitochondria	5	21	93	6.9e-06
Atp1p	NP_009453	Mitochondrial ATP synthase	8	19	132	9.5e-10
Atp2p	NP_012655	Mitochondrial ATP synthase	7	17	116	3.8e-08
Pet9p	NP_009523	Mitochondrial ADP/ATP carrier	6	20	102	9.5e-07
Mir1p	NP_012611	Mitochondrial phosphate carrier	5	20	93	7.2e-06
YP + 0.5% glucose; Day 1 (L phase)						
Tps1p	NP_009684	Trehalose biosynthesis	8	18	133	7.6e-10
Tps2p	NP_010359	Trehalose biosynthesis	7	8	90	1.4e-05
Ath1p	NP_015351	Trehalose degradation	9	7	113	7.6e-08
Nth1p	NP_010284	Trehalose degradation	10	13	137	3e-10
Nth2p	NP_009555	Trehalose degradation	8	12	117	3e-08
Glg2p	NP_012398	Glycogen biosynthesis	8	22	140	1.5e-10
Glc3p	NP_010905	Glycogen biosynthesis	9	13	133	7.6e-10
Gsy2p	NP_013359	Glycogen biosynthesis	10	16	149	1.9e-11
Gph1p	NP_015486	Glycogen degradation	9	12	127	3e-09
Gpt2p	NP_012993	Biosynthesis of TAG	8	11	110	1.5e-07
Ayr1p	NP_012142	Biosynthesis of TAG	5	25	97	3.2e-06
Slc1p	NP_010231	Biosynthesis of TAG	7	28	126	3.8e-09
Pah1p	NP_013888	Biosynthesis of TAG	6	8	86	3.5e-05
Lpp1p	NP_010791	Biosynthesis of TAG	4	16	76	0.0004
Dga1p	NP_014888	Biosynthesis of TAG	7	19	121	1.2e-08
Are2p	NP_014416	Biosynthesis of TAG and EE	5	7	76	0.00041
Tgl1p	NP_012782	Degradation of EE	5	12	83	8.1e-05
Tgl3p	NP_014044	Degradation of TAG	6	10	92	8.9e-06

Tgl4p	NP_013015	Degradation of TAG	11	14	154	6e-12
Tgl5p	NP_014724	Degradation of TAG	6	9	84	6.7e-05
Yeh1p	NP_013089	Degradation of EE	5	11	81	0.00012
Fat1p	NP_009597	Conversion of FFA to FA-CoA	7	13	108	2.4e-07
Faa1p	NP_014962	Conversion of FFA to FA-CoA	5	9	76	0.00035
Faa2p	NP_010931	Conversion of FFA to FA-CoA	6	10	90	1.3e-05
Faa4p	NP_013974	Conversion of FFA to FA-CoA	8	13	121	1.2e-08
Fox1p	NP_011310	Peroxisomal oxidation of FA-CoA	6	9	85	4.7e-05
Fox2p	NP_012934	Peroxisomal oxidation of FA-CoA	7	11	102	9.5e-07
Fox3p	NP_012106	Peroxisomal oxidation of FA-CoA	7	23	125	4.8e-09
Adh1p	NP_014555	Ethanol biosynthesis	6	21	110	1.5e-07
Adh2p	NP_014032	Ethanol oxidation	8	27	145	4.8e-11
Pyc1p	NP_011453	Gluconeogenesis	7	8	90	1.6e-05
Pck1p	NP_013023	Gluconeogenesis	9	20	146	3.8e-11
Fbp1p	NP_013481	Gluconeogenesis	5	20	92	8.9e-06
Pda1p	NP_011105	Mitochondrial PDH complex	6	15	91	1.2e-05
Aco1p	NP_013407	Mitochondrial TCA cycle	9	14	134	6e-10
Ndi1p	NP_013586	Mitochondrial ETC	6	15	98	2.7e-06
Sdh1p	NP_012774	Mitochondrial TCA cycle and ETC	9	15	134	6e-10
Cyt1p	NP_014708	Mitochondrial ETC	5	28	99	1.8e-06
Hem14p	NP_010930	Heme synthesis in mitochondria	8	18	125	4.8e-09
Cyc3p	NP_009361	Heme attachment to apo-cytochrome c	5	19	95	5.2e-06
Ssq1p	NP_013473	Assembly of Fe/S clusters into proteins	9	14	128	2.4e-09
Sod2p	NP_011872	Detoxification of ROS in mitochondria	5	26	100	1.7e-06
Prx1p	NP_009489	Detoxification of ROS in mitochondria	4	18	75	0.00046
Atp1p	NP_009453	Mitochondrial ATP synthase	7	17	116	3.8e-08
Atp2p	NP_012655	Mitochondrial ATP synthase	6	15	100	1.6e-06
Pet9p	NP_009523	Mitochondrial ADP/ATP carrier	5	17	85	5.2e-05
Mir1p	NP_012611	Mitochondrial phosphate carrier	7	26	129	1.9e-09
YP + 1% glucose; Day 1 (L phase)						
Tps1p	NP_009684	Trehalose biosynthesis	6	15	100	1.6e-06
Tps2p	NP_010359	Trehalose biosynthesis	8	8	107	3e-07
Ath1p	NP_015351	Trehalose degradation	9	7	110	1.5e-07
Nth1p	NP_010284	Trehalose degradation	6	9	84	5.9e-05
Nth2p	NP_009555	Trehalose degradation	10	14	145	4.8e-11
Glg2p	NP_012398	Glycogen biosynthesis	6	17	105	4.8e-07
Glc3p	NP_010905	Glycogen biosynthesis	8	12	115	4.8e-08
Gsy2p	NP_013359	Glycogen biosynthesis	7	12	106	3.8e-07
Gph1p	NP_015486	Glycogen degradation	10	13	141	1.2e-10

Gpt2p	NP_012993	Biosynthesis of TAG	8	11	116	3.8e-08
Ayr1p	NP_012142	Biosynthesis of TAG	7	34	135	4.8e-10
Slc1p	NP_010231	Biosynthesis of TAG	6	26	107	3e-07
Pah1p	NP_013888	Biosynthesis of TAG	8	11	114	6e-08
Lpp1p	NP_010791	Biosynthesis of TAG	4	16	76	0.00041
Dga1p	NP_014888	Biosynthesis of TAG	7	19	121	1.2e-08
Are2p	NP_014416	Biosynthesis of TAG and EE	6	9	91	1.2e-05
Tgl1p	NP_012782	Degradation of EE	5	13	83	7.6e-05
Tgl3p	NP_014044	Degradation of TAG	6	10	92	8.9e-06
Tgl4p	NP_013015	Degradation of TAG	10	14	141	1.2e-10
Tgl5p	NP_014724	Degradation of TAG	5	7	69	0.0017
Yeh1p	NP_013089	Degradation of EE	8	17	129	1.9e-09
Fat1p	NP_009597	Conversion of FFA to FA-CoA	7	14	109	1.9e-07
Faa1p	NP_014962	Conversion of FFA to FA-CoA	5	9	77	0.00032
Faa2p	NP_010931	Conversion of FFA to FA-CoA	6	11	92	1.1e-05
Faa4p	NP_013974	Conversion of FFA to FA-CoA	9	14	135	4.8e-10
Fox1p	NP_011310	Peroxisomal oxidation of FA-CoA	9	14	124	6e-09
Fox2p	NP_012934	Peroxisomal oxidation of FA-CoA	7	11	102	9.5e-07
Fox3p	NP_012106	Peroxisomal oxidation of FA-CoA	4	16	74	0.00064
Adh1p	NP_014555	Ethanol biosynthesis	6	22	110	1.5e-07
Adh2p	NP_014032	Ethanol oxidation	8	27	145	4.8e-11
Pyc1p	NP_011453	Gluconeogenesis	10	10	127	3e-09
Pck1p	NP_013023	Gluconeogenesis	6	14	99	1.9e-06
Fbp1p	NP_013481	Gluconeogenesis	5	18	92	1.1e-05
Pda1p	NP_011105	Mitochondrial PDH complex	7	17	109	1.9e-07
Aco1p	NP_013407	Mitochondrial TCA cycle	10	15	143	7.6e-11
Ndi1p	NP_013586	Mitochondrial ETC	6	14	97	3.2e-06
Sdh1p	NP_012774	Mitochondrial TCA cycle and ETC	9	15	134	6e-10
Cyt1p	NP_014708	Mitochondrial ETC	5	23	95	4.8e-06
Hem14p	NP_010930	Heme synthesis in mitochondria	11	23	169	1.9e-13
Cyc3p	NP_009361	Heme attachment to apo-cytochrome c	5	18	94	5.6e-06
Ssq1p	NP_013473	Assembly of Fe/S clusters into proteins	9	15	129	1.9e-09
Sod2p	NP_011872	Detoxification of ROS in mitochondria	5	26	99	1.7e-06
Prx1p	NP_009489	Detoxification of ROS in mitochondria	8	31	148	2.4e-11
Atp1p	NP_009453	Mitochondrial ATP synthase	7	17	116	3.8e-08
Atp2p	NP_012655	Mitochondrial ATP synthase	9	20	148	2.4e-11
Pet9p	NP_009523	Mitochondrial ADP/ATP carrier	5	17	85	5.2e-05
Mir1p	NP_012611	Mitochondrial phosphate carrier	7	27	130	1.5e-09
YP + 2% glucose; Day 1 (L phase)						

Tps1p	NP_009684	Trehalose biosynthesis	7	18	117	3e-08
Tps2p	NP_010359	Trehalose biosynthesis	8	8	107	3e-07
Ath1p	NP_015351	Trehalose degradation	9	7	113	7.6e-08
Nth1p	NP_010284	Trehalose degradation	8	11	111	1.2e-07
Nth2p	NP_009555	Trehalose degradation	7	11	101	1.2e-06
Glg2p	NP_012398	Glycogen biosynthesis	9	21	139	1.9e-10
Glc3p	NP_010905	Glycogen biosynthesis	10	15	146	3.8e-11
Gsy2p	NP_013359	Glycogen biosynthesis	7	12	106	3.8e-07
Gph1p	NP_015486	Glycogen degradation	10	13	141	1.2e-10
Gpt2p	NP_012993	Biosynthesis of TAG	8	11	110	1.5e-07
Ayr1p	NP_012142	Biosynthesis of TAG	7	34	135	4.8e-10
Slc1p	NP_010231	Biosynthesis of TAG	8	32	142	9.5e-11
Pah1p	NP_013888	Biosynthesis of TAG	6	8	86	3.6e-05
Lpp1p	NP_010791	Biosynthesis of TAG	5	19	94	5.7e-06
Dga1p	NP_014888	Biosynthesis of TAG	8	20	136	3.8e-10
Are2p	NP_014416	Biosynthesis of TAG and EE	6	9	91	1.2e-05
Tgl1p	NP_012782	Degradation of EE	5	12	83	8.1e-05
Tgl3p	NP_014044	Degradation of TAG	5	8	76	0.00041
Tgl4p	NP_013015	Degradation of TAG	8	11	114	6e-08
Tgl5p	NP_014724	Degradation of TAG	6	9	84	6.7e-05
Yeh1p	NP_013089	Degradation of EE	8	16	128	2.4e-09
Fat1p	NP_009597	Conversion of FFA to FA-CoA	5	10	77	0.0003
Faa1p	NP_014962	Conversion of FFA to FA-CoA	8	12	120	1.5e-08
Faa2p	NP_010931	Conversion of FFA to FA-CoA	7	12	106	3.8e-07
Faa4p	NP_013974	Conversion of FFA to FA-CoA	9	14	135	4.8e-10
Fox1p	NP_011310	Peroxisomal oxidation of FA-CoA	9	13	125	4.8e-09
Fox2p	NP_012934	Peroxisomal oxidation of FA-CoA	7	11	102	9.5e-07
Fox3p	NP_012106	Peroxisomal oxidation of FA-CoA	6	21	108	2.4e-07
Adh1p	NP_014555	Ethanol biosynthesis	7	24	127	3e-09
Adh2p	NP_014032	Ethanol oxidation	11	37	199	1.9e-16
Pyc1p	NP_011453	Gluconeogenesis	10	10	126	3.8e-09
Pck1p	NP_013023	Gluconeogenesis	6	15	99	1.7e-06
Fbp1p	NP_013481	Gluconeogenesis	8	27	145	4.8e-11
Pda1p	NP_011105	Mitochondrial PDH complex	6	14	96	4.2e-06
Aco1p	NP_013407	Mitochondrial TCA cycle	10	15	145	4.8e-11
Ndi1p	NP_013586	Mitochondrial ETC	7	16	113	7.6e-08
Sdh1p	NP_012774	Mitochondrial TCA cycle and ETC	10	17	147	3e-11
Cyt1p	NP_014708	Mitochondrial ETC	5	22	94	5.5e-06
Hem14p	NP_010930	Heme synthesis in mitochondria	8	18	124	6e-09
Cyc3p	NP_009361	Heme attachment to apo-cytochrome c	5	19	95	5.2e-06
Ssq1p	NP_013473	Assembly of Fe/S clusters into proteins	10	16	145	4.8e-11
Sod2p	NP_011872	Detoxification of ROS in mitochondria	5	29	102	9.5e-07

Prx1p	NP_009489	Detoxification of ROS in mitochondria	8	30	147	3e-11
Atp1p	NP_009453	Mitochondrial ATP synthase	10	22	164	6e-13
Atp2p	NP_012655	Mitochondrial ATP synthase	6	15	100	1.6e-06
Pet9p	NP_009523	Mitochondrial ADP/ATP carrier	8	27	136	8.1e-08
Mir1p	NP_012611	Mitochondrial phosphate carrier	7	26	129	1.9e-09
YP + 0.2% glucose; Day 2 (D phase)						
Tps1p	NP_009684	Trehalose biosynthesis	7	18	117	3e-08
Tps2p	NP_010359	Trehalose biosynthesis	7	8	90	1.4e-05
Ath1p	NP_015351	Trehalose degradation	9	7	110	1.5e-07
Nth1p	NP_010284	Trehalose degradation	8	11	109	2e-07
Nth2p	NP_009555	Trehalose degradation	9	13	122	1.2e-09
Glg2p	NP_012398	Glycogen biosynthesis	8	22	141	1.1e-10
Glc3p	NP_010905	Glycogen biosynthesis	10	15	143	2.7e-08
Gsy2p	NP_013359	Glycogen biosynthesis	7	12	106	3.8e-07
Gph1p	NP_015486	Glycogen degradation	10	13	142	1.5e-10
Gpt2p	NP_012993	Biosynthesis of TAG	10	14	136	5.4e-10
Ayr1p	NP_012142	Biosynthesis of TAG	5	25	99	4.1e-06
Slc1p	NP_010231	Biosynthesis of TAG	8	32	140	4.8e-10
Pah1p	NP_013888	Biosynthesis of TAG	7	9	99	3.9e-06
Lpp1p	NP_010791	Biosynthesis of TAG	5	19	94	5.7e-06
Dga1p	NP_014888	Biosynthesis of TAG	8	20	129	1.4e-09
Are2p	NP_014416	Biosynthesis of TAG and EE	5	7	76	0.00041
Tgl1p	NP_012782	Degradation of EE	5	12	83	8.1e-05
Tgl3p	NP_014044	Degradation of TAG	6	10	92	8.9e-06
Tgl4p	NP_013015	Degradation of TAG	11	14	154	6e-12
Tgl5p	NP_014724	Degradation of TAG	5	7	69	0.0017
Yeh1p	NP_013089	Degradation of EE	8	17	129	2.1e-09
Fat1p	NP_009597	Conversion of FFA to FA-CoA	7	13	108	2.4e-07
Faa1p	NP_014962	Conversion of FFA to FA-CoA	5	9	77	0.00032
Faa2p	NP_010931	Conversion of FFA to FA-CoA	6	11	91	1.2e-05
Faa4p	NP_013974	Conversion of FFA to FA-CoA	10	15	147	3e-11
Fox1p	NP_011310	Peroxisomal oxidation of FA-CoA	9	14	125	5.4e-09
Fox2p	NP_012934	Peroxisomal oxidation of FA-CoA	7	11	102	9.5e-07
Fox3p	NP_012106	Peroxisomal oxidation of FA-CoA	7	22	110	4.8e-08
Adh1p	NP_014555	Ethanol biosynthesis	7	23	119	2.5e-08
Adh2p	NP_014032	Ethanol oxidation	9	29	142	9.5e-11
Pyc1p	NP_011453	Gluconeogenesis	10	10	126	3.8e-09
Pck1p	NP_013023	Gluconeogenesis	9	20	146	3.8e-11
Fbp1p	NP_013481	Gluconeogenesis	5	20	92	8.9e-06
Pda1p	NP_011105	Mitochondrial PDH complex	6	15	91	1.2e-05
Aco1p	NP_013407	Mitochondrial TCA cycle	10	15	144	2.6e-11
Ndi1p	NP_013586	Mitochondrial ETC	8	18	128	2.4e-09
Sdh1p	NP_012774	Mitochondrial TCA cycle and ETC	9	15	134	6e-10

Cyt1p	NP_014708	Mitochondrial ETC	5	23	95	4.8e-06
Hem14p	NP_010930	Heme synthesis in mitochondria	8	18	125	5.4e-09
Cyc3p	NP_009361	Heme attachment to apo-cytochrome c	6	22	113	7.6e-08
Ssq1p	NP_013473	Assembly of Fe/S clusters into proteins	9	15	129	1.9e-09
Prx1p	NP_009489	Detoxification of ROS in mitochondria	4	18	75	0.00046
Atp1p	NP_009453	Mitochondrial ATP synthase	7	17	116	3.8e-08
Atp2p	NP_012655	Mitochondrial ATP synthase	9	20	148	2.4e-11
Pet9p	NP_009523	Mitochondrial ADP/ATP carrier	5	17	85	5.2e-05
Mir1p	NP_012611	Mitochondrial phosphate carrier	5	20	93	7.2e-06
YP + 0.5% glucose; Day 2 (D phase)						
Tps1p	NP_009684	Trehalose biosynthesis	7	18	115	4.6e-08
Tps2p	NP_010359	Trehalose biosynthesis	7	8	90	1.4e-05
Ath1p	NP_015351	Trehalose degradation	9	7	110	1.5e-07
Nth1p	NP_010284	Trehalose degradation	8	11	109	1.8e-07
Nth2p	NP_009555	Trehalose degradation	8	12	117	3e-08
Glg2p	NP_012398	Glycogen biosynthesis	7	18	120	1.5e-08
Glc3p	NP_010905	Glycogen biosynthesis	10	15	146	3.8e-11
Gsy2p	NP_013359	Glycogen biosynthesis	10	16	149	1.9e-11
Gph1p	NP_015486	Glycogen degradation	12	15	164	6e-13
Gpt2p	NP_012993	Biosynthesis of TAG	10	14	135	4.8e-10
Ayr1p	NP_012142	Biosynthesis of TAG	5	25	97	3.2e-06
Slc1p	NP_010231	Biosynthesis of TAG	8	32	138	2.4e-10
Pah1p	NP_013888	Biosynthesis of TAG	6	8	86	3.5e-05
Lpp1p	NP_010791	Biosynthesis of TAG	5	19	94	5.7e-06
Dga1p	NP_014888	Biosynthesis of TAG	7	19	121	1.2e-08
Are2p	NP_014416	Biosynthesis of TAG and EE	7	10	106	3.8e-07
Tgl1p	NP_012782	Degradation of EE	5	12	83	8.1e-05
Tgl3p	NP_014044	Degradation of TAG	5	8	76	0.00041
Tgl4p	NP_013015	Degradation of TAG	9	12	128	2.4e-09
Tgl5p	NP_014724	Degradation of TAG	6	9	84	6.7e-05
Yeh1p	NP_013089	Degradation of EE	8	17	129	1.9e-09
Fat1p	NP_009597	Conversion of FFA to FA-CoA	7	14	109	1.9e-07
Faa1p	NP_014962	Conversion of FFA to FA-CoA	6	10	89	1.9e-05
Faa2p	NP_010931	Conversion of FFA to FA-CoA	7	12	106	3.8e-07
Faa4p	NP_013974	Conversion of FFA to FA-CoA	8	13	121	1.2e-08
Fox1p	NP_011310	Peroxisomal oxidation of FA-CoA	9	13	125	4.8e-09
Fox2p	NP_012934	Peroxisomal oxidation of FA-CoA	8	12	115	4.8e-08
Fox3p	NP_012106	Peroxisomal oxidation of FA-CoA	6	21	108	2.4e-07
Adh1p	NP_014555	Ethanol biosynthesis	6	22	110	1.5e-07
Adh2p	NP_014032	Ethanol oxidation	11	37	199	1.9e-16
Pyc1p	NP_011453	Gluconeogenesis	10	10	126	3.8e-09

Pck1p	NP_013023	Gluconeogenesis	7	17	115	4.8e-08
Fbp1p	NP_013481	Gluconeogenesis	5	20	92	8.9e-06
Pda1p	NP_011105	Mitochondrial PDH complex	6	14	96	4.2e-06
Aco1p	NP_013407	Mitochondrial TCA cycle	11	17	160	1.5e-12
Ndi1p	NP_013586	Mitochondrial ETC	6	15	98	2.7e-06
Sdh1p	NP_012774	Mitochondrial TCA cycle and ETC	9	15	134	6e-10
Cyt1p	NP_014708	Mitochondrial ETC	5	22	94	5.5e-06
Hem14p	NP_010930	Heme synthesis in mitochondria	9	20	140	1.5e-10
Cyc3p	NP_009361	Heme attachment to apo-cytochrome c	5	18	94	5.6e-06
Ssq1p	NP_013473	Assembly of Fe/S clusters into proteins	9	14	128	2.4e-09
Sod2p	NP_011872	Detoxification of ROS in mitochondria	5	29	102	9.5e-07
Prx1p	NP_009489	Detoxification of ROS in mitochondria	5	21	93	6.9e-06
Atp1p	NP_009453	Mitochondrial ATP synthase	7	17	116	3.8e-08
Atp2p	NP_012655	Mitochondrial ATP synthase	6	15	100	1.6e-06
Pet9p	NP_009523	Mitochondrial ADP/ATP carrier	8	27	136	8.1e-08
Mir1p	NP_012611	Mitochondrial phosphate carrier	7	27	130	1.5e-09
YP + 1% glucose; Day 2 (D phase)						
Tps1p	NP_009684	Trehalose biosynthesis	6	15	100	1.6e-06
Tps2p	NP_010359	Trehalose biosynthesis	7	8	90	1.4e-05
Ath1p	NP_015351	Trehalose degradation	9	7	110	1.5e-07
Nth1p	NP_010284	Trehalose degradation	8	11	111	1.2e-07
Nth2p	NP_009555	Trehalose degradation	8	12	117	3e-08
Glg2p	NP_012398	Glycogen biosynthesis	7	18	120	1.5e-08
Glc3p	NP_010905	Glycogen biosynthesis	10	15	146	3.8e-11
Gsy2p	NP_013359	Glycogen biosynthesis	10	16	149	1.9e-11
Gph1p	NP_015486	Glycogen degradation	12	15	164	6e-13
Gpt2p	NP_012993	Biosynthesis of TAG	8	11	110	1.5e-07
Ayr1p	NP_012142	Biosynthesis of TAG	6	28	112	9.5e-08
Slc1p	NP_010231	Biosynthesis of TAG	7	28	126	3.8e-09
Pah1p	NP_013888	Biosynthesis of TAG	7	9	97	2.9e-06
Lpp1p	NP_010791	Biosynthesis of TAG	5	19	94	5.7e-06
Dga1p	NP_014888	Biosynthesis of TAG	8	20	136	3.8e-10
Are2p	NP_014416	Biosynthesis of TAG and EE	5	7	76	0.00041
Tgl1p	NP_012782	Degradation of EE	6	15	103	7.6e-07
Tgl3p	NP_014044	Degradation of TAG	5	8	76	0.00041
Tgl4p	NP_013015	Degradation of TAG	10	14	141	1.2e-10
Tgl5p	NP_014724	Degradation of TAG	6	9	84	6.7e-05
Yeh1p	NP_013089	Degradation of EE	6	13	94	5.7e-06
Fat1p	NP_009597	Conversion of FFA to FA-CoA	5	10	77	0.0003
Faa1p	NP_014962	Conversion of FFA to FA-CoA	6	10	89	1.9e-05
Faa2p	NP_010931	Conversion of FFA to FA-CoA	7	12	106	3.8e-07
Faa4p	NP_013974	Conversion of FFA to FA-CoA	8	13	121	1.2e-08

Fox1p	NP_011310	Peroxisomal oxidation of FA-CoA	9	14	124	6e-09
Fox2p	NP_012934	Peroxisomal oxidation of FA-CoA	7	11	102	9.5e-07
Fox3p	NP_012106	Peroxisomal oxidation of FA-CoA	7	23	125	4.8e-09
Adh1p	NP_014555	Ethanol biosynthesis	8	27	145	4.8e-11
Adh2p	NP_014032	Ethanol oxidation	11	37	199	1.9e-16
Pyc1p	NP_011453	Gluconeogenesis	8	9	98	2.3e-06
Pck1p	NP_013023	Gluconeogenesis	6	14	99	1.9e-06
Fbp1p	NP_013481	Gluconeogenesis	5	20	92	8.9e-06
Pda1p	NP_011105	Mitochondrial PDH complex	6	15	91	1.2e-05
Aco1p	NP_013407	Mitochondrial TCA cycle	10	15	145	4.8e-11
Ndi1p	NP_013586	Mitochondrial ETC	6	15	98	2.7e-06
Sdh1p	NP_012774	Mitochondrial TCA cycle and ETC	7	12	105	4.8e-07
Cyt1p	NP_014708	Mitochondrial ETC	5	22	94	5.5e-06
Hem14p	NP_010930	Heme synthesis in mitochondria	8	18	125	4.8e-09
Cyc3p	NP_009361	Heme attachment to apo-cytochrome c	5	19	95	5.2e-06
Ssq1p	NP_013473	Assembly of Fe/S clusters into proteins	9	14	128	2.4e-09
Sod2p	NP_011872	Detoxification of ROS in mitochondria	5	26	99	1.7e-06
Prx1p	NP_009489	Detoxification of ROS in mitochondria	5	21	93	6.9e-06
Atp1p	NP_009453	Mitochondrial ATP synthase	10	22	164	6e-13
Atp2p	NP_012655	Mitochondrial ATP synthase	7	17	116	3.8e-08
Pet9p	NP_009523	Mitochondrial ADP/ATP carrier	5	17	85	5.2e-05
Mir1p	NP_012611	Mitochondrial phosphate carrier	7	26	129	1.9e-09
YP + 2% glucose; Day 2 (D phase)						
Tps1p	NP_009684	Trehalose biosynthesis	7	18	117	3e-08
Tps2p	NP_010359	Trehalose biosynthesis	9	9	115	1.7e-05
Ath1p	NP_015351	Trehalose degradation	9	7	113	7.6e-08
Nth1p	NP_010284	Trehalose degradation	8	11	108	2.4e-07
Nth2p	NP_009555	Trehalose degradation	7	11	101	1.2e-06
Glg2p	NP_012398	Glycogen biosynthesis	8	22	140	1.5e-10
Glc3p	NP_010905	Glycogen biosynthesis	9	13	133	7.6e-10
Gsy2p	NP_013359	Glycogen biosynthesis	9	14	131	1.2e-09
Gph1p	NP_015486	Glycogen degradation	10	13	141	1.2e-10
Gpt2p	NP_012993	Biosynthesis of TAG	8	11	110	1.5e-07
Ayr1p	NP_012142	Biosynthesis of TAG	6	28	112	9.5e-08
Slc1p	NP_010231	Biosynthesis of TAG	8	32	142	9.5e-11
Pah1p	NP_013888	Biosynthesis of TAG	6	8	86	3.5e-05
Lpp1p	NP_010791	Biosynthesis of TAG	5	19	93	8.3e-06
Dga1p	NP_014888	Biosynthesis of TAG	8	20	136	3.8e-10
Are2p	NP_014416	Biosynthesis of TAG and EE	5	7	76	0.00041
Tgl1p	NP_012782	Degradation of EE	6	15	103	7.6e-07
Tgl3p	NP_014044	Degradation of TAG	6	10	92	8.9e-06
Tgl4p	NP_013015	Degradation of TAG	9	12	128	2.4e-09
Tgl5p	NP_014724	Degradation of TAG	6	9	84	6.7e-05

Yeh1p	NP_013089	Degradation of EE	8	17	129	1.9e-09
Fat1p	NP_009597	Conversion of FFA to FA-CoA	7	13	108	2.4e-07
Faa1p	NP_014962	Conversion of FFA to FA-CoA	8	12	120	1.5e-08
Faa2p	NP_010931	Conversion of FFA to FA-CoA	7	12	102	9.5e-07
Faa4p	NP_013974	Conversion of FFA to FA-CoA	8	13	121	1.2e-08
Fox1p	NP_011310	Peroxisomal oxidation of FA-CoA	6	9	85	4.7e-05
Fox2p	NP_012934	Peroxisomal oxidation of FA-CoA	8	12	115	4.8e-08
Fox3p	NP_012106	Peroxisomal oxidation of FA-CoA	7	23	125	4.8e-09
Adh1p	NP_014555	Ethanol biosynthesis	8	27	145	4.8e-11
Adh2p	NP_014032	Ethanol oxidation	11	37	199	1.9e-16
Pyc1p	NP_011453	Gluconeogenesis	7	8	90	1.6e-05
Pck1p	NP_013023	Gluconeogenesis	9	20	146	3.8e-11
Fbp1p	NP_013481	Gluconeogenesis	6	22	107	3e-07
Pda1p	NP_011105	Mitochondrial PDH complex	6	14	96	4.2e-06
Aco1p	NP_013407	Mitochondrial TCA cycle	11	17	160	1.5e-12
Ndi1p	NP_013586	Mitochondrial ETC	7	16	113	7.6e-08
Sdh1p	NP_012774	Mitochondrial TCA cycle and ETC	7	12	105	4.8e-07
Cyt1p	NP_014708	Mitochondrial ETC	5	22	94	5.5e-06
Hem14p	NP_010930	Heme synthesis in mitochondria	11	23	169	1.9e-13
Cyc3p	NP_009361	Heme attachment to apo-cytochrome c	6	22	113	7.6e-08
Ssq1p	NP_013473	Assembly of Fe/S clusters into proteins	10	16	145	4.8e-11
Sod2p	NP_011872	Detoxification of ROS in mitochondria	5	26	99	1.7e-06
Prx1p	NP_009489	Detoxification of ROS in mitochondria	8	31	148	2.4e-11
Atp1p	NP_009453	Mitochondrial ATP synthase	7	17	116	3.8e-08
Atp2p	NP_012655	Mitochondrial ATP synthase	6	15	100	1.6e-06
Pet9p	NP_009523	Mitochondrial ADP/ATP carrier	6	20	102	9.5e-07
Mir1p	NP_012611	Mitochondrial phosphate carrier	5	20	93	7.2e-06
YP + 0.2% glucose; Day 4 (PD phase)						
Tps1p	NP_009684	Trehalose biosynthesis	7	18	117	3e-08
Tps2p	NP_010359	Trehalose biosynthesis	9	9	115	1.7e-05
Ath1p	NP_015351	Trehalose degradation	10	8	122	9.5e-09
Nth1p	NP_010284	Trehalose degradation	8	11	111	1.2e-07
Nth2p	NP_009555	Trehalose degradation	8	12	117	3e-08
Glg2p	NP_012398	Glycogen biosynthesis	9	21	139	1.9e-10
Glc3p	NP_010905	Glycogen biosynthesis	10	15	143	2.7e-08
Gsy2p	NP_013359	Glycogen biosynthesis	10	16	149	1.9e-11
Gph1p	NP_015486	Glycogen degradation	10	13	141	1.2e-10
Gpt2p	NP_012993	Biosynthesis of TAG	10	14	135	4.8e-10
Ayr1p	NP_012142	Biosynthesis of TAG	7	34	135	4.8e-10

Slc1p	NP_010231	Biosynthesis of TAG	8	32	138	2.4e-10
Pah1p	NP_013888	Biosynthesis of TAG	6	8	86	3.5e-05
Lpp1p	NP_010791	Biosynthesis of TAG	4	16	76	0.00041
Dga1p	NP_014888	Biosynthesis of TAG	6	17	102	9.5e-07
Are2p	NP_014416	Biosynthesis of TAG and EE	5	7	76	0.00041
Tgl1p	NP_012782	Degradation of EE	6	15	103	7.6e-07
Tgl3p	NP_014044	Degradation of TAG	7	12	105	4.8e-07
Tgl4p	NP_013015	Degradation of TAG	11	14	154	6e-12
Tgl5p	NP_014724	Degradation of TAG	6	9	84	6.7e-05
Yeh1p	NP_013089	Degradation of EE	6	13	94	5.7e-06
Fat1p	NP_009597	Conversion of FFA to FA-CoA	7	13	108	2.4e-07
Faa1p	NP_014962	Conversion of FFA to FA-CoA	6	10	89	1.9e-05
Faa2p	NP_010931	Conversion of FFA to FA-CoA	7	12	106	3.8e-07
Faa4p	NP_013974	Conversion of FFA to FA-CoA	9	14	135	4.8e-10
Fox1p	NP_011310	Peroxisomal oxidation of FA-CoA	6	9	85	4.7e-05
Fox2p	NP_012934	Peroxisomal oxidation of FA-CoA	8	12	115	4.8e-08
Fox3p	NP_012106	Peroxisomal oxidation of FA-CoA	6	21	108	2.4e-07
Adh1p	NP_014555	Ethanol biosynthesis	7	24	127	3e-09
Adh2p	NP_014032	Ethanol oxidation	9	29	142	9.5e-11
Pyc1p	NP_011453	Gluconeogenesis	8	9	98	2.3e-06
Pck1p	NP_013023	Gluconeogenesis	6	14	99	1.9e-06
Fbp1p	NP_013481	Gluconeogenesis	5	20	92	8.9e-06
Pda1p	NP_011105	Mitochondrial PDH complex	6	14	96	4.2e-06
Aco1p	NP_013407	Mitochondrial TCA cycle	11	17	160	1.5e-12
Ndi1p	NP_013586	Mitochondrial ETC	6	14	97	3.2e-06
Sdh1p	NP_012774	Mitochondrial TCA cycle and ETC	7	12	105	4.8e-07
Cyt1p	NP_014708	Mitochondrial ETC	5	28	99	1.8e-06
Hem14p	NP_010930	Heme synthesis in mitochondria	8	18	125	4.8e-09
Cyc3p	NP_009361	Heme attachment to apo-cytochrome c	5	18	94	5.6e-06
Ssq1p	NP_013473	Assembly of Fe/S clusters into proteins	7	12	102	9.5e-07
Sod2p	NP_011872	Detoxification of ROS in mitochondria	5	29	102	9.5e-07
Prx1p	NP_009489	Detoxification of ROS in mitochondria	8	31	148	2.4e-11
Atp1p	NP_009453	Mitochondrial ATP synthase	8	19	132	9.5e-10
Atp2p	NP_012655	Mitochondrial ATP synthase	9	20	148	2.4e-11
Pet9p	NP_009523	Mitochondrial ADP/ATP carrier	5	17	85	5.2e-05
Mir1p	NP_012611	Mitochondrial phosphate carrier	7	26	129	1.9e-09
YP + 0.5% glucose; Day 4 (PD phase)						
Tps1p	NP_009684	Trehalose biosynthesis	7	18	115	5.2e-08
Tps2p	NP_010359	Trehalose biosynthesis	7	8	90	1.4e-05

Ath1p	NP_015351	Trehalose degradation	9	7	111	1.2e-07
Nth1p	NP_010284	Trehalose degradation	6	9	84	5.9e-05
Nth2p	NP_009555	Trehalose degradation	7	11	101	1.2e-06
Glg2p	NP_012398	Glycogen biosynthesis	8	22	140	1.5e-10
Glc3p	NP_010905	Glycogen biosynthesis	10	15	146	3.8e-11
Gsy2p	NP_013359	Glycogen biosynthesis	10	16	149	1.9e-11
Gph1p	NP_015486	Glycogen degradation	9	12	127	3e-09
Gpt2p	NP_012993	Biosynthesis of TAG	8	11	110	1.5e-07
Ayr1p	NP_012142	Biosynthesis of TAG	6	28	112	9.5e-08
Slc1p	NP_010231	Biosynthesis of TAG	6	26	107	3e-07
Pah1p	NP_013888	Biosynthesis of TAG	6	8	86	3.5e-05
Lpp1p	NP_010791	Biosynthesis of TAG	5	19	93	8.3e-06
Dga1p	NP_014888	Biosynthesis of TAG	6	17	102	9.5e-07
Are2p	NP_014416	Biosynthesis of TAG and EE	6	9	91	1.2e-05
Tgl1p	NP_012782	Degradation of EE	5	13	83	7.6e-05
Tgl3p	NP_014044	Degradation of TAG	7	12	105	4.8e-07
Tgl4p	NP_013015	Degradation of TAG	11	14	154	6e-12
Tgl5p	NP_014724	Degradation of TAG	5	7	69	0.0017
Yeh1p	NP_013089	Degradation of EE	8	16	128	2.4e-09
Fat1p	NP_009597	Conversion of FFA to FA-CoA	7	13	108	2.4e-07
Faa1p	NP_014962	Conversion of FFA to FA-CoA	6	10	89	1.9e-05
Faa2p	NP_010931	Conversion of FFA to FA-CoA	7	12	106	3.8e-07
Faa4p	NP_013974	Conversion of FFA to FA-CoA	10	15	147	3e-11
Fox1p	NP_011310	Peroxisomal oxidation of FA-CoA	9	13	125	4.8e-09
Fox2p	NP_012934	Peroxisomal oxidation of FA-CoA	8	12	115	4.8e-08
Fox3p	NP_012106	Peroxisomal oxidation of FA-CoA	7	23	125	4.8e-09
Adh1p	NP_014555	Ethanol biosynthesis	8	27	145	4.8e-11
Adh2p	NP_014032	Ethanol oxidation	11	37	199	1.9e-16
Pyc1p	NP_011453	Gluconeogenesis	7	8	90	1.6e-05
Pck1p	NP_013023	Gluconeogenesis	6	14	99	1.9e-06
Fbp1p	NP_013481	Gluconeogenesis	6	22	107	3e-07
Pda1p	NP_011105	Mitochondrial PDH complex	6	15	91	1.2e-05
Aco1p	NP_013407	Mitochondrial TCA cycle	10	15	145	4.8e-11
Ndi1p	NP_013586	Mitochondrial ETC	6	15	98	2.7e-06
Sdh1p	NP_012774	Mitochondrial TCA cycle and ETC	7	12	105	4.8e-07
Cyt1p	NP_014708	Mitochondrial ETC	5	22	94	5.5e-06
Hem14p	NP_010930	Heme synthesis in mitochondria	9	20	140	1.5e-10
Cyc3p	NP_009361	Heme attachment to apo-cytochrome c	5	18	94	5.6e-06
Ssq1p	NP_013473	Assembly of Fe/S clusters into proteins	10	16	145	4.8e-11
Sod2p	NP_011872	Detoxification of ROS in mitochondria	6	30	119	1.9e-08
Prx1p	NP_009489	Detoxification of ROS in mitochondria	4	18	75	0.00046

Atp1p	NP_009453	Mitochondrial ATP synthase	7	17	116	3.8e-08
Atp2p	NP_012655	Mitochondrial ATP synthase	7	17	116	3.8e-08
Pet9p	NP_009523	Mitochondrial ADP/ATP carrier	5	17	85	5.2e-05
Mir1p	NP_012611	Mitochondrial phosphate carrier	7	27	130	1.5e-09
YP + 1% glucose; Day 4 (PD phase)						
Tps1p	NP_009684	Trehalose biosynthesis	6	15	100	1.6e-06
Tps2p	NP_010359	Trehalose biosynthesis	8	8	107	3e-07
Ath1p	NP_015351	Trehalose degradation	10	8	122	9.5e-09
Nth1p	NP_010284	Trehalose degradation	6	9	84	5.9e-05
Nth2p	NP_009555	Trehalose degradation	10	14	145	4.8e-11
Glg2p	NP_012398	Glycogen biosynthesis	7	18	120	1.5e-08
Glc3p	NP_010905	Glycogen biosynthesis	8	12	115	4.8e-08
Gsy2p	NP_013359	Glycogen biosynthesis	7	12	106	3.8e-07
Gph1p	NP_015486	Glycogen degradation	9	12	127	3e-09
Gpt2p	NP_012993	Biosynthesis of TAG	8	11	110	1.5e-07
Ayr1p	NP_012142	Biosynthesis of TAG	6	28	112	9.5e-08
Slc1p	NP_010231	Biosynthesis of TAG	6	26	107	3e-07
Pah1p	NP_013888	Biosynthesis of TAG	8	11	114	6e-08
Lpp1p	NP_010791	Biosynthesis of TAG	5	19	93	8.3e-06
Dga1p	NP_014888	Biosynthesis of TAG	6	17	102	9.5e-07
Are2p	NP_014416	Biosynthesis of TAG and EE	5	7	76	0.00041
Tgl1p	NP_012782	Degradation of EE	6	15	103	7.6e-07
Tgl3p	NP_014044	Degradation of TAG	6	10	92	8.9e-06
Tgl4p	NP_013015	Degradation of TAG	9	12	128	2.4e-09
Tgl5p	NP_014724	Degradation of TAG	6	9	84	6.7e-05
Yeh1p	NP_013089	Degradation of EE	5	11	81	0.00012
Fat1p	NP_009597	Conversion of FFA to FA-CoA	7	13	108	2.4e-07
Faa1p	NP_014962	Conversion of FFA to FA-CoA	8	12	120	1.5e-08
Faa2p	NP_010931	Conversion of FFA to FA-CoA	7	12	102	9.5e-07
Faa4p	NP_013974	Conversion of FFA to FA-CoA	8	13	121	1.2e-08
Fox1p	NP_011310	Peroxisomal oxidation of FA-CoA	7	11	93	7.6e-06
Fox2p	NP_012934	Peroxisomal oxidation of FA-CoA	7	11	102	9.5e-07
Fox3p	NP_012106	Peroxisomal oxidation of FA-CoA	6	21	105	4.8e-07
Adh1p	NP_014555	Ethanol biosynthesis	6	22	110	1.5e-07
Adh2p	NP_014032	Ethanol oxidation	9	29	142	9.5e-11
Pyc1p	NP_011453	Gluconeogenesis	7	8	90	1.6e-05
Pck1p	NP_013023	Gluconeogenesis	9	20	146	3.8e-11
Fbp1p	NP_013481	Gluconeogenesis	8	27	145	4.8e-11
Pda1p	NP_011105	Mitochondrial PDH complex	6	15	91	1.2e-05
Aco1p	NP_013407	Mitochondrial TCA cycle	10	15	145	4.8e-11
Ndi1p	NP_013586	Mitochondrial ETC	8	18	128	2.4e-09
Sdh1p	NP_012774	Mitochondrial TCA cycle and ETC	9	15	134	6e-10
Cyt1p	NP_014708	Mitochondrial ETC	5	22	94	5.5e-06
Hem14p	NP_010930	Heme synthesis in	9	20	140	1.5e-10

		mitochondria				
Cyc3p	NP_009361	Heme attachment to apo-cytochrome c	5	18	94	5.6e-06
Ssq1p	NP_013473	Assembly of Fe/S clusters into proteins	7	12	102	9.5e-07
Sod2p	NP_011872	Detoxification of ROS in mitochondria	6	30	119	1.9e-08
Prx1p	NP_009489	Detoxification of ROS in mitochondria	8	31	148	2.4e-11
Atp1p	NP_009453	Mitochondrial ATP synthase	7	17	116	3.8e-08
Atp2p	NP_012655	Mitochondrial ATP synthase	7	17	116	3.8e-08
Pet9p	NP_009523	Mitochondrial ADP/ATP carrier	5	17	85	5.2e-05
Mir1p	NP_012611	Mitochondrial phosphate carrier	5	20	93	7.2e-06
YP + 2% glucose; Day 4 (PD phase)						
Tps1p	NP_009684	Trehalose biosynthesis	7	18	114	6e-08
Tps2p	NP_010359	Trehalose biosynthesis	9	9	115	1.7e-05
Ath1p	NP_015351	Trehalose degradation	9	7	113	7.6e-08
Nth1p	NP_010284	Trehalose degradation	8	11	108	2.4e-07
Nth2p	NP_009555	Trehalose degradation	7	11	101	1.2e-06
Glg2p	NP_012398	Glycogen biosynthesis	8	22	140	1.5e-10
Glc3p	NP_010905	Glycogen biosynthesis	10	15	146	3.8e-11
Gsy2p	NP_013359	Glycogen biosynthesis	9	14	131	1.2e-09
Gph1p	NP_015486	Glycogen degradation	9	12	127	3e-09
Gpt2p	NP_012993	Biosynthesis of TAG	10	14	135	4.8e-10
Ayr1p	NP_012142	Biosynthesis of TAG	7	34	135	4.8e-10
Slc1p	NP_010231	Biosynthesis of TAG	6	26	107	3e-07
Pah1p	NP_013888	Biosynthesis of TAG	6	8	86	3.5e-05
Lpp1p	NP_010791	Biosynthesis of TAG	5	19	94	5.7e-06
Dga1p	NP_014888	Biosynthesis of TAG	6	17	102	9.5e-07
Are2p	NP_014416	Biosynthesis of TAG and EE	5	7	76	0.00041
Tgl1p	NP_012782	Degradation of EE	6	15	103	7.6e-07
Tgl3p	NP_014044	Degradation of TAG	6	10	92	8.9e-06
Tgl4p	NP_013015	Degradation of TAG	8	11	114	6e-08
Tgl5p	NP_014724	Degradation of TAG	7	10	96	3.4e-06
Yeh1p	NP_013089	Degradation of EE	6	13	94	5.7e-06
Fat1p	NP_009597	Conversion of FFA to FA-CoA	7	13	108	2.4e-07
Faa1p	NP_014962	Conversion of FFA to FA-CoA	6	10	89	1.9e-05
Faa2p	NP_010931	Conversion of FFA to FA-CoA	7	12	106	3.8e-07
Faa4p	NP_013974	Conversion of FFA to FA-CoA	10	15	147	3e-11
Fox1p	NP_011310	Peroxisomal oxidation of FA-CoA	6	9	85	4.7e-05
Fox2p	NP_012934	Peroxisomal oxidation of FA-CoA	7	11	102	9.5e-07
Fox3p	NP_012106	Peroxisomal oxidation of FA-CoA	6	21	108	2.4e-07
Adh1p	NP_014555	Ethanol biosynthesis	8	27	145	4.8e-11
Adh2p	NP_014032	Ethanol oxidation	8	27	145	4.8e-11
Pyc1p	NP_011453	Gluconeogenesis	8	9	98	2.3e-06

Pck1p	NP_013023	Gluconeogenesis	6	14	99	1.9e-06
Fbp1p	NP_013481	Gluconeogenesis	6	22	107	3e-07
Pda1p	NP_011105	Mitochondrial PDH complex	6	14	96	4.2e-06
Aco1p	NP_013407	Mitochondrial TCA cycle	11	17	160	1.5e-12
Ndi1p	NP_013586	Mitochondrial ETC	7	16	113	7.6e-08
Sdh1p	NP_012774	Mitochondrial TCA cycle and ETC	7	12	105	4.8e-07
Cyt1p	NP_014708	Mitochondrial ETC	5	28	99	1.8e-06
Hem14p	NP_010930	Heme synthesis in mitochondria	8	18	124	6e-09
Cyc3p	NP_009361	Heme attachment to apo-cytochrome c	6	22	113	7.6e-08
Ssq1p	NP_013473	Assembly of Fe/S clusters into proteins	7	12	102	9.5e-07
Sod2p	NP_011872	Detoxification of ROS in mitochondria	5	29	102	9.5e-07
Prx1p	NP_009489	Detoxification of ROS in mitochondria	4	18	75	0.00046
Atp1p	NP_009453	Mitochondrial ATP synthase	8	19	132	9.5e-10
Atp2p	NP_012655	Mitochondrial ATP synthase	9	20	148	2.4e-11
Pet9p	NP_009523	Mitochondrial ADP/ATP carrier	5	17	85	5.2e-05
Mir1p	NP_012611	Mitochondrial phosphate carrier	7	27	130	1.5e-09
YP + 0.2% glucose; Day 9 (ST phase)						
Tps1p	NP_009684	Trehalose biosynthesis	7	18	114	6e-08
Tps2p	NP_010359	Trehalose biosynthesis	9	9	115	1.7e-05
Ath1p	NP_015351	Trehalose degradation	9	7	110	1.5e-07
Nth1p	NP_010284	Trehalose degradation	6	9	84	5.9e-05
Nth2p	NP_009555	Trehalose degradation	7	11	101	1.2e-06
Glg2p	NP_012398	Glycogen biosynthesis	7	18	120	1.5e-08
Glc3p	NP_010905	Glycogen biosynthesis	9	13	133	7.6e-10
Gsy2p	NP_013359	Glycogen biosynthesis	9	14	131	1.2e-09
Gph1p	NP_015486	Glycogen degradation	10	13	141	1.2e-10
Gpt2p	NP_012993	Biosynthesis of TAG	8	11	116	3.8e-08
Ayr1p	NP_012142	Biosynthesis of TAG	6	28	112	9.5e-08
Slc1p	NP_010231	Biosynthesis of TAG	6	26	107	3e-07
Pah1p	NP_013888	Biosynthesis of TAG	7	9	97	2.9e-06
Lpp1p	NP_010791	Biosynthesis of TAG	5	19	94	5.7e-06
Dga1p	NP_014888	Biosynthesis of TAG	6	17	102	9.5e-07
Are2p	NP_014416	Biosynthesis of TAG and EE	5	7	76	0.00041
Tgl1p	NP_012782	Degradation of EE	6	15	103	7.6e-07
Tgl3p	NP_014044	Degradation of TAG	5	8	76	0.00041
Tgl4p	NP_013015	Degradation of TAG	11	14	154	6e-12
Tgl5p	NP_014724	Degradation of TAG	6	9	84	6.7e-05
Yeh1p	NP_013089	Degradation of EE	6	13	94	5.7e-06
Fat1p	NP_009597	Conversion of FFA to FA-CoA	5	10	77	0.0003
Faa1p	NP_014962	Conversion of FFA to FA-CoA	5	9	76	0.00035
Faa2p	NP_010931	Conversion of FFA to FA-CoA	7	12	106	3.8e-07
Faa4p	NP_013974	Conversion of FFA to FA-CoA	10	15	147	3e-11

Fox1p	NP_011310	Peroxisomal oxidation of FA-CoA	6	9	85	4.7e-05
Fox2p	NP_012934	Peroxisomal oxidation of FA-CoA	8	12	115	4.8e-08
Fox3p	NP_012106	Peroxisomal oxidation of FA-CoA	6	21	105	4.8e-07
Adh1p	NP_014555	Ethanol biosynthesis	8	27	145	4.8e-11
Adh2p	NP_014032	Ethanol oxidation	11	37	199	1.9e-16
Pyc1p	NP_011453	Gluconeogenesis	7	8	90	1.6e-05
Pck1p	NP_013023	Gluconeogenesis	9	20	146	3.8e-11
Fbp1p	NP_013481	Gluconeogenesis	6	22	107	3e-07
Pda1p	NP_011105	Mitochondrial PDH complex	6	14	96	4.2e-06
Aco1p	NP_013407	Mitochondrial TCA cycle	10	15	143	7.6e-11
Ndi1p	NP_013586	Mitochondrial ETC	8	18	128	2.4e-09
Sdh1p	NP_012774	Mitochondrial TCA cycle and ETC	10	17	147	3e-11
Cyt1p	NP_014708	Mitochondrial ETC	6	26	113	7.6e-08
Hem14p	NP_010930	Heme synthesis in mitochondria	8	18	125	4.8e-09
Cyc3p	NP_009361	Heme attachment to apo-cytochrome c	5	19	95	5.2e-06
Ssq1p	NP_013473	Assembly of Fe/S clusters into proteins	7	12	102	9.5e-07
Sod2p	NP_011872	Detoxification of ROS in mitochondria	5	29	102	9.5e-07
Prx1p	NP_009489	Detoxification of ROS in mitochondria	5	21	93	6.9e-06
Atp1p	NP_009453	Mitochondrial ATP synthase	7	17	116	3.8e-08
Atp2p	NP_012655	Mitochondrial ATP synthase	6	15	100	1.6e-06
Pet9p	NP_009523	Mitochondrial ADP/ATP carrier	8	27	136	8.1e-08
Mir1p	NP_012611	Mitochondrial phosphate carrier	5	20	93	7.2e-06
YP + 0.5% glucose; Day 9 (ST phase)						
Tps1p	NP_009684	Trehalose biosynthesis	6	15	100	1.6e-06
Tps2p	NP_010359	Trehalose biosynthesis	7	8	90	1.4e-05
Ath1p	NP_015351	Trehalose degradation	10	8	122	9.5e-09
Nth1p	NP_010284	Trehalose degradation	6	9	84	5.9e-05
Nth2p	NP_009555	Trehalose degradation	8	12	117	3e-08
Glg2p	NP_012398	Glycogen biosynthesis	6	17	105	4.8e-07
Glc3p	NP_010905	Glycogen biosynthesis	10	15	143	2.7e-08
Gsy2p	NP_013359	Glycogen biosynthesis	7	12	106	3.8e-07
Gph1p	NP_015486	Glycogen degradation	9	12	127	3e-09
Gpt2p	NP_012993	Biosynthesis of TAG	8	11	116	3.8e-08
Ayr1p	NP_012142	Biosynthesis of TAG	6	28	112	9.5e-08
Slc1p	NP_010231	Biosynthesis of TAG	8	32	142	9.5e-11
Pah1p	NP_013888	Biosynthesis of TAG	6	8	86	3.5e-05
Lpp1p	NP_010791	Biosynthesis of TAG	5	19	94	5.7e-06
Dga1p	NP_014888	Biosynthesis of TAG	6	17	102	9.5e-07
Are2p	NP_014416	Biosynthesis of TAG and EE	6	9	91	1.2e-05
Tgl1p	NP_012782	Degradation of EE	6	15	103	7.6e-07
Tgl3p	NP_014044	Degradation of TAG	6	10	92	8.9e-06
Tgl4p	NP_013015	Degradation of TAG	10	14	141	1.2e-10
Tgl5p	NP_014724	Degradation of TAG	7	10	96	3.4e-06

Yeh1p	NP_013089	Degradation of EE	8	16	128	2.4e-09
Fat1p	NP_009597	Conversion of FFA to FA-CoA	7	14	109	1.9e-07
Faa1p	NP_014962	Conversion of FFA to FA-CoA	6	10	89	1.9e-05
Faa2p	NP_010931	Conversion of FFA to FA-CoA	7	12	106	3.8e-07
Faa4p	NP_013974	Conversion of FFA to FA-CoA	8	13	121	1.2e-08
Fox1p	NP_011310	Peroxisomal oxidation of FA-CoA	7	11	93	7.6e-06
Fox2p	NP_012934	Peroxisomal oxidation of FA-CoA	7	11	102	9.5e-07
Fox3p	NP_012106	Peroxisomal oxidation of FA-CoA	4	16	74	0.00064
Adh1p	NP_014555	Ethanol biosynthesis	8	27	145	4.8e-11
Adh2p	NP_014032	Ethanol oxidation	11	37	199	1.9e-16
Pyc1p	NP_011453	Gluconeogenesis	8	9	98	2.3e-06
Pck1p	NP_013023	Gluconeogenesis	9	20	146	3.8e-11
Fbp1p	NP_013481	Gluconeogenesis	6	22	107	3e-07
Pda1p	NP_011105	Mitochondrial PDH complex	6	14	96	4.2e-06
Aco1p	NP_013407	Mitochondrial TCA cycle	10	15	143	7.6e-11
Ndi1p	NP_013586	Mitochondrial ETC	7	16	113	7.6e-08
Sdh1p	NP_012774	Mitochondrial TCA cycle and ETC	7	12	105	4.8e-07
Cyt1p	NP_014708	Mitochondrial ETC	5	28	99	1.8e-06
Hem14p	NP_010930	Heme synthesis in mitochondria	8	18	124	6e-09
Cyc3p	NP_009361	Heme attachment to apo-cytochrome c	5	18	94	5.6e-06
Ssq1p	NP_013473	Assembly of Fe/S clusters into proteins	7	12	102	9.5e-07
Sod2p	NP_011872	Detoxification of ROS in mitochondria	5	29	102	9.5e-07
Prx1p	NP_009489	Detoxification of ROS in mitochondria	8	31	148	2.4e-11
Atp1p	NP_009453	Mitochondrial ATP synthase	10	22	164	6e-13
Atp2p	NP_012655	Mitochondrial ATP synthase	7	17	116	3.8e-08
Pet9p	NP_009523	Mitochondrial ADP/ATP carrier	5	17	85	5.2e-05
Mir1p	NP_012611	Mitochondrial phosphate carrier	7	26	129	1.9e-09
YP + 1% glucose; Day 9 (ST phase)						
Tps1p	NP_009684	Trehalose biosynthesis	7	18	117	3e-08
Tps2p	NP_010359	Trehalose biosynthesis	9	9	115	1.7e-05
Ath1p	NP_015351	Trehalose degradation	9	7	113	7.6e-08
Nth1p	NP_010284	Trehalose degradation	6	9	84	5.9e-05
Nth2p	NP_009555	Trehalose degradation	7	11	101	1.2e-06
Glg2p	NP_012398	Glycogen biosynthesis	7	18	120	1.5e-08
Glc3p	NP_010905	Glycogen biosynthesis	8	12	115	4.8e-08
Gsy2p	NP_013359	Glycogen biosynthesis	9	14	131	1.2e-09
Gph1p	NP_015486	Glycogen degradation	10	13	141	1.2e-10
Gpt2p	NP_012993	Biosynthesis of TAG	8	11	116	3.8e-08
Ayr1p	NP_012142	Biosynthesis of TAG	6	28	112	9.5e-08

Slc1p	NP_010231	Biosynthesis of TAG	8	32	142	9.5e-11
Pah1p	NP_013888	Biosynthesis of TAG	6	8	86	3.5e-05
Lpp1p	NP_010791	Biosynthesis of TAG	5	19	94	5.7e-06
Dga1p	NP_014888	Biosynthesis of TAG	6	17	102	9.5e-07
Are2p	NP_014416	Biosynthesis of TAG and EE	5	7	76	0.00041
Tgl1p	NP_012782	Degradation of EE	6	15	103	7.6e-07
Tgl3p	NP_014044	Degradation of TAG	5	8	76	0.00041
Tgl4p	NP_013015	Degradation of TAG	10	14	141	1.2e-10
Tgl5p	NP_014724	Degradation of TAG	5	7	69	0.0017
Yeh1p	NP_013089	Degradation of EE	8	17	129	1.9e-09
Fat1p	NP_009597	Conversion of FFA to FA-CoA	7	13	108	2.4e-07
Faa1p	NP_014962	Conversion of FFA to FA-CoA	6	10	89	1.9e-05
Faa2p	NP_010931	Conversion of FFA to FA-CoA	7	12	106	3.8e-07
Faa4p	NP_013974	Conversion of FFA to FA-CoA	8	13	121	1.2e-08
Fox1p	NP_011310	Peroxisomal oxidation of FA-CoA	7	11	93	7.6e-06
Fox2p	NP_012934	Peroxisomal oxidation of FA-CoA	7	11	102	9.5e-07
Fox3p	NP_012106	Peroxisomal oxidation of FA-CoA	4	16	74	0.00064
Adh1p	NP_014555	Ethanol biosynthesis	8	27	145	4.8e-11
Adh2p	NP_014032	Ethanol oxidation	11	37	199	1.9e-16
Pyc1p	NP_011453	Gluconeogenesis	8	9	98	2.3e-06
Pck1p	NP_013023	Gluconeogenesis	9	20	146	3.8e-11
Fbp1p	NP_013481	Gluconeogenesis	6	22	107	3e-07
Pda1p	NP_011105	Mitochondrial PDH complex	7	17	109	1.9e-07
Aco1p	NP_013407	Mitochondrial TCA cycle	10	15	145	4.8e-11
Ndi1p	NP_013586	Mitochondrial ETC	6	15	98	2.7e-06
Sdh1p	NP_012774	Mitochondrial TCA cycle and ETC	10	17	147	3e-11
Cyt1p	NP_014708	Mitochondrial ETC	6	26	113	7.6e-08
Hem14p	NP_010930	Heme synthesis in mitochondria	11	23	169	1.9e-13
Cyc3p	NP_009361	Heme attachment to apo-cytochrome c	6	22	113	7.6e-08
Ssq1p	NP_013473	Assembly of Fe/S clusters into proteins	10	16	145	4.8e-11
Sod2p	NP_011872	Detoxification of ROS in mitochondria	5	26	99	1.7e-06
Prx1p	NP_009489	Detoxification of ROS in mitochondria	8	31	148	2.4e-11
Atp1p	NP_009453	Mitochondrial ATP synthase	8	19	132	9.5e-10
Atp2p	NP_012655	Mitochondrial ATP synthase	9	20	148	2.4e-11
Pet9p	NP_009523	Mitochondrial ADP/ATP carrier	6	20	102	9.5e-07
Mir1p	NP_012611	Mitochondrial phosphate carrier	7	27	130	1.5e-09
YP + 2% glucose; Day 9 (ST phase)						
Tps1p	NP_009684	Trehalose biosynthesis	6	15	100	1.6e-06
Tps2p	NP_010359	Trehalose biosynthesis	8	8	107	3e-07

Ath1p	NP_015351	Trehalose degradation	10	8	122	9.5e-09
Nth1p	NP_010284	Trehalose degradation	8	11	108	2.4e-07
Nth2p	NP_009555	Trehalose degradation	10	14	145	4.8e-11
Glg2p	NP_012398	Glycogen biosynthesis	6	17	105	4.8e-07
Glc3p	NP_010905	Glycogen biosynthesis	8	12	115	4.8e-08
Gsy2p	NP_013359	Glycogen biosynthesis	9	14	131	1.2e-09
Gph1p	NP_015486	Glycogen degradation	12	15	164	6e-13
Gpt2p	NP_012993	Biosynthesis of TAG	8	11	110	1.5e-07
Ayr1p	NP_012142	Biosynthesis of TAG	7	34	135	4.8e-10
Slc1p	NP_010231	Biosynthesis of TAG	8	32	138	2.4e-10
Pah1p	NP_013888	Biosynthesis of TAG	8	11	114	6e-08
Lpp1p	NP_010791	Biosynthesis of TAG	4	16	76	0.00041
Dga1p	NP_014888	Biosynthesis of TAG	7	19	121	1.2e-08
Are2p	NP_014416	Biosynthesis of TAG and EE	5	7	76	0.00041
Tgl1p	NP_012782	Degradation of EE	5	12	83	8.1e-05
Tgl3p	NP_014044	Degradation of TAG	5	8	76	0.00041
Tgl4p	NP_013015	Degradation of TAG	8	11	114	6e-08
Tgl5p	NP_014724	Degradation of TAG	7	10	96	3.4e-06
Yeh1p	NP_013089	Degradation of EE	6	13	94	5.7e-06
Fat1p	NP_009597	Conversion of FFA to FA-CoA	5	10	74	0.00057
Faa1p	NP_014962	Conversion of FFA to FA-CoA	8	12	120	1.5e-08
Faa2p	NP_010931	Conversion of FFA to FA-CoA	6	10	90	1.3e-05
Faa4p	NP_013974	Conversion of FFA to FA-CoA	8	13	121	1.2e-08
Fox1p	NP_011310	Peroxisomal oxidation of FA-CoA	9	13	125	4.8e-09
Fox2p	NP_012934	Peroxisomal oxidation of FA-CoA	8	12	115	4.8e-08
Fox3p	NP_012106	Peroxisomal oxidation of FA-CoA	6	21	108	2.4e-07
Adh1p	NP_014555	Ethanol biosynthesis	7	24	127	3e-09
Adh2p	NP_014032	Ethanol oxidation	11	37	199	1.9e-16
Pyc1p	NP_011453	Gluconeogenesis	8	9	98	2.3e-06
Pck1p	NP_013023	Gluconeogenesis	7	17	115	4.8e-08
Fbp1p	NP_013481	Gluconeogenesis	5	18	92	1.1e-05
Pda1p	NP_011105	Mitochondrial PDH complex	7	17	109	1.9e-07
Aco1p	NP_013407	Mitochondrial TCA cycle	10	15	143	7.6e-11
Ndi1p	NP_013586	Mitochondrial ETC	6	14	97	3.2e-06
Sdh1p	NP_012774	Mitochondrial TCA cycle and ETC	9	15	134	6e-10
Cyt1p	NP_014708	Mitochondrial ETC	5	28	99	1.8e-06
Hem14p	NP_010930	Heme synthesis in mitochondria	8	18	124	6e-09
Cyc3p	NP_009361	Heme attachment to apo-cytochrome c	5	19	95	5.2e-06
Ssq1p	NP_013473	Assembly of Fe/S clusters into proteins	7	12	102	9.5e-07
Sod2p	NP_011872	Detoxification of ROS in mitochondria	6	30	119	1.9e-08
Prx1p	NP_009489	Detoxification of ROS in mitochondria	8	30	147	3e-11

Atp1p	NP_009453	Mitochondrial ATP synthase	8	19	132	9.5e-10
Atp2p	NP_012655	Mitochondrial ATP synthase	9	20	148	2.4e-11
Pet9p	NP_009523	Mitochondrial ADP/ATP carrier	5	17	85	5.2e-05
Mir1p	NP_012611	Mitochondrial phosphate carrier	7	26	129	1.9e-09

[1]The probability based Mowse score for comparing the calculated peptide masses for each entry in the sequence database with the set of experimental mass spectrometry data; Mowse scores greater than 54 are significant ($p < 0.05$).

[2]The expectation value for the matching peptides, which provides the number of matches with equal or better Mowse scores that are expected to occur by chance alone.

Table 3.2. Relative levels of proteins recovered in total lysates of WT cells cultured in YP medium initially containing 0.2%, 0.5%, 1% or 2% glucose. For making total lysates, cells were collected at day 1 (L phase), day 2 (D phase), day 4 (PD phase) and day 9 (ST phase). Proteins were identified and quantified using MALDI MS peptide mapping. Relative protein levels are presented as fold difference relative to that on 2% glucose.

Protein	NCBI accession no.	Function	Protein level			
			Glucose concentration (%)			
			0.2	0.5	1	2
Day 1 (L phase)						
Tps1p	NP_009684	Trehalose biosynthesis	1.22 ± 0.31	1.42 ± 0.13	1.14 ± 0.43	1
Tps2p	NP_010359	Trehalose biosynthesis	0.92 ± 0.13	1.34 ± 0.32	1.21 ± 0.24	1
Ath1p	NP_015351	Trehalose degradation	0.80 ± 0.22	1.12 ± 0.43	1.36 ± 0.12	1
Nth1p	NP_010284	Trehalose degradation	0.37 ± 0.04	0.68 ± 0.11	0.91 ± 0.15	1
Nth2p	NP_009555	Trehalose degradation	1.14 ± 0.29	0.86 ± 0.18	0.88 ± 0.11	1
Glg2p	NP_012398	Glycogen biosynthesis	1.25 ± 0.21	1.37 ± 0.30	1.18 ± 0.24	1
Glc3p	NP_010905	Glycogen biosynthesis	0.89 ± 0.14	1.18 ± 0.27	0.93 ± 0.17	1
Gsy2p	NP_013359	Glycogen biosynthesis	1.26 ± 0.33	1.19 ± 0.46	0.88 ± 0.28	1
Gph1p	NP_015486	Glycogen degradation	0.79 ± 0.17	0.93 ± 0.28	1.28 ± 0.24	1
Gpt2p	NP_012993	Biosynthesis of TAG	0.41 ± 0.07	0.28 ± 0.09	0.87 ± 0.13	1
Ayr1p	NP_012142	Biosynthesis of TAG	0.92 ± 0.18	0.88 ± 0.29	1.19 ± 0.33	1
Slc1p	NP_010231	Biosynthesis of TAG	0.30 ± 0.08	0.22 ± 0.06	0.92 ± 0.21	1
Pah1p	NP_013888	Biosynthesis of TAG	1.08 ± 0.26	0.82 ± 0.22	1.21 ± 0.15	1
Lpp1p	NP_010791	Biosynthesis of TAG	0.44 ± 0.07	0.26 ± 0.09	0.83 ± 0.21	1
Dga1p	NP_014888	Biosynthesis of TAG	0.71 ± 0.24	0.35 ± 0.04	1.32 ± 0.41	1
Are2p	NP_014416	Biosynthesis of TAG and EE	0.26 ± 0.11	0.21 ± 0.05	0.81 ± 0.22	1
Tgl1p	NP_012782	Degradation of EE	1.31 ± 0.33	2.51 ± 0.23	1.19 ± 0.13	1
Tgl3p	NP_014044	Degradation of TAG	2.73 ± 0.15	3.46 ± 0.32	1.42 ± 0.25	1
Tgl4p	NP_013015	Degradation of TAG	1.69 ± 0.27	2.78 ± 0.41	1.29 ± 0.23	1
Tgl5p	NP_014724	Degradation of TAG	1.48 ± 0.34	1.72 ± 0.23	1.07 ± 0.41	1
Yeh1p	NP_013089	Degradation of EE	2.81 ± 0.42	3.69 ± 0.31	1.46 ± 0.33	1
Fat1p	NP_009597	Conversion of FFA to FA-CoA	0.44 ± 0.12	0.88 ± 0.20	1.14 ± 0.27	1
Faa1p	NP_014962	Conversion of FFA to FA-CoA	1.72 ± 0.33	2.49 ± 0.28	0.91 ± 0.29	1
Faa2p	NP_010931	Conversion of FFA to FA-CoA	1.43 ± 0.28	1.67 ± 0.41	1.22 ± 0.32	1
Faa4p	NP_013974	Conversion of FFA to FA-CoA	1.59 ± 0.33	2.83 ± 0.19	1.30 ± 0.41	1

Fox1p	NP_011310	Peroxisomal oxidation of FA-CoA	1.77 ± 0.21	1.59 ± 0.32	1.17 ± 0.19	1
Fox2p	NP_012934	Peroxisomal oxidation of FA-CoA	1.19 ± 0.13	1.31 ± 0.42	0.79 ± 0.18	1
Fox3p	NP_012106	Peroxisomal oxidation of FA-CoA	1.62 ± 0.31	1.47 ± 0.19	1.31 ± 0.42	1
Adh1p	NP_014555	Ethanol biosynthesis	0.29 ± 0.08	0.37 ± 0.11	0.88 ± 0.13	1
Adh2p	NP_014032	Ethanol oxidation	5.21 ± 0.53	5.73 ± 0.39	2.28 ± 0.21	1
Pyc1p	NP_011453	Gluconeogenesis	2.39 ± 0.31	1.76 ± 0.17	1.27 ± 0.32	1
Pck1p	NP_013023	Gluconeogenesis	1.33 ± 0.15	1.47 ± 0.29	0.84 ± 0.12	1
Fbp1p	NP_013481	Gluconeogenesis	1.79 ± 0.27	1.56 ± 0.18	1.31 ± 0.37	1
Pda1p	NP_011105	Mitochondrial PDH complex	2.49 ± 0.31	1.72 ± 0.31	1.19 ± 0.25	1
Aco1p	NP_013407	Mitochondrial TCA cycle	2.73 ± 0.23	1.59 ± 0.16	1.24 ± 0.13	1
Ndi1p	NP_013586	Mitochondrial ETC	1.89 ± 0.29	1.28 ± 0.31	0.89 ± 0.16	1
Sdh1p	NP_012774	Mitochondrial TCA cycle and ETC	1.43 ± 0.13	1.22 ± 0.22	1.17 ± 0.33	1
Cyt1p	NP_014708	Mitochondrial ETC	1.58 ± 0.24	1.39 ± 0.18	1.28 ± 0.29	1
Hem14p	NP_010930	Heme synthesis in mitochondria	1.65 ± 0.19	1.43 ± 0.28	1.41 ± 0.21	1
Cyc3p	NP_009361	Heme attachment to apo-cytochrome c	0.89 ± 0.13	1.21 ± 0.24	0.91 ± 0.17	1
Ssq1p	NP_013473	Assembly of Fe/S clusters into proteins	1.33 ± 0.32	1.19 ± 0.21	1.41 ± 0.31	1
Sod2p	NP_011872	Detoxification of ROS in mitochondria	0.79 ± 0.08	0.83 ± 0.19	1.22 ± 0.24	1
Prx1p	NP_009489	Detoxification of ROS in mitochondria	1.42 ± 0.32	1.76 ± 0.23	0.81 ± 0.17	1
Atp1p	NP_009453	Mitochondrial ATP synthase	1.17 ± 0.16	1.53 ± 0.29	1.33 ± 0.32	1
Atp2p	NP_012655	Mitochondrial ATP synthase	1.34 ± 0.27	1.47 ± 0.33	0.79 ± 0.09	1
Pet9p	NP_009523	Mitochondrial ADP/ATP carrier	1.39 ± 0.12	1.45 ± 0.31	1.08 ± 0.21	1
Mir1p	NP_012611	Mitochondrial phosphate carrier	1.59 ± 0.21	1.32 ± 0.28	0.86 ± 0.16	1
Day 2 (D phase)						
Tps1p	NP_009684	Trehalose biosynthesis	1.79 ± 0.33	2.67 ± 0.29	1.28 ± 0.18	1
Tps2p	NP_010359	Trehalose biosynthesis	1.34 ± 0.22	2.82 ± 0.34	0.91 ± 0.21	1
Ath1p	NP_015351	Trehalose degradation	0.87 ± 0.13	0.76 ± 0.26	1.23 ± 0.17	1
Nth1p	NP_010284	Trehalose degradation	0.38 ± 0.08	0.81 ± 0.21	1.34 ± 0.32	1
Nth2p	NP_009555	Trehalose degradation	0.69 ± 0.13	1.23 ± 0.30	0.93 ± 0.14	1
Glg2p	NP_012398	Glycogen biosynthesis	1.71 ± 0.21	2.56 ± 0.15	1.44 ± 0.33	1
Glc3p	NP_010905	Glycogen biosynthesis	1.85 ± 0.13	2.78 ± 0.31	1.19 ± 0.19	1
Gsy2p	NP_013359	Glycogen biosynthesis	3.59 ± 0.61	4.72 ± 0.52	2.24 ± 0.21	1
Gph1p	NP_015486	Glycogen degradation	0.38 ± 0.11	0.43 ± 0.34	0.82 ± 0.17	1
Gpt2p	NP_012993	Biosynthesis of TAG	0.28 ± 0.08	0.21 ± 0.06	0.45 ± 0.07	1
Ayr1p	NP_012142	Biosynthesis of TAG	0.34 ± 0.05	0.22 ± 0.03	0.76 ± 0.18	1
Slc1p	NP_010231	Biosynthesis of TAG	0.21 ± 0.06	0.25 ± 0.09	0.85 ± 0.21	1
Pah1p	NP_013888	Biosynthesis of TAG	0.44 ± 0.09	0.29 ± 0.05	1.21 ± 0.33	1
Lpp1p	NP_010791	Biosynthesis of TAG	0.26 ± 0.03	0.22 ± 0.07	0.87 ± 0.20	1
Dga1p	NP_014888	Biosynthesis of TAG	0.47 ± 0.13	0.31 ± 0.08	0.93 ± 0.32	1
Are2p	NP_014416	Biosynthesis of TAG and EE	0.20 ± 0.05	0.24 ± 0.07	0.46 ± 0.12	1
Tgl1p	NP_012782	Degradation of EE	3.63 ± 0.51	4.59 ± 0.44	1.28 ± 0.26	1
Tgl3p	NP_014044	Degradation of TAG	4.84 ± 0.32	5.66 ± 0.58	1.17 ± 0.15	1
Tgl4p	NP_013015	Degradation of TAG	3.47 ± 0.42	4.79 ± 0.31	0.89 ± 0.11	1
Tgl5p	NP_014724	Degradation of TAG	1.67 ± 0.23	2.33 ± 0.31	1.28 ± 0.19	1
Yeh1p	NP_013089	Degradation of EE	4.78 ± 0.43	5.29 ± 0.67	1.67 ± 0.32	1
Fat1p	NP_009597	Conversion of FFA to FA-CoA	2.87 ± 0.33	3.45 ± 0.49	1.34 ± 0.21	1
Faa1p	NP_014962	Conversion of FFA to FA-CoA	3.59 ± 0.54	5.84 ± 0.66	1.74 ± 0.19	1
Faa2p	NP_010931	Conversion of FFA to FA-CoA	2.77 ± 0.34	3.83 ± 0.49	1.36 ± 0.31	1
Faa4p	NP_013974	Conversion of FFA to FA-CoA	4.39 ± 0.53	5.67 ± 0.71	1.73 ± 0.49	1
Fox1p	NP_011310	Peroxisomal oxidation of FA-CoA	3.87 ± 0.45	3.39 ± 0.53	1.19 ± 0.32	1
Fox2p	NP_012934	Peroxisomal oxidation of FA-CoA	2.78 ± 0.33	1.81 ± 0.16	1.34 ± 0.43	1
Fox3p	NP_012106	Peroxisomal oxidation of FA-CoA	3.45 ± 0.56	2.73 ± 0.44	1.44 ± 0.17	1
Adh1p	NP_014555	Ethanol biosynthesis	0.22 ± 0.04	0.29 ± 0.09	0.87 ± 0.11	1
Adh2p	NP_014032	Ethanol oxidation	5.87 ± 0.56	5.95 ± 0.33	2.31 ± 0.47	1

Pyc1p	NP_011453	Gluconeogenesis	5.69 ± 0.49	4.37 ± 0.52	2.23 ± 0.31	1
Pck1p	NP_013023	Gluconeogenesis	4.49 ± 0.32	4.25 ± 0.56	1.36 ± 0.23	1
Fbp1p	NP_013481	Gluconeogenesis	5.69 ± 0.67	4.48 ± 0.52	2.23 ± 0.37	1
Pda1p	NP_011105	Mitochondrial PDH complex	3.34 ± 0.42	2.59 ± 0.30	1.23 ± 0.13	1
Aco1p	NP_013407	Mitochondrial TCA cycle	3.69 ± 0.39	2.78 ± 0.41	1.36 ± 0.20	1
Ndi1p	NP_013586	Mitochondrial ETC	4.49 ± 0.13	2.34 ± 0.32	1.25 ± 0.17	1
Sdh1p	NP_012774	Mitochondrial TCA cycle and ETC	2.54 ± 0.33	1.49 ± 0.21	0.87 ± 0.15	1
Cyt1p	NP_014708	Mitochondrial ETC	2.76 ± 0.39	1.39 ± 0.44	0.74 ± 0.19	1
Hem14p	NP_010930	Heme synthesis in mitochondria	2.87 ± 0.37	2.56 ± 0.43	1.33 ± 0.21	1
Cyc3p	NP_009361	Heme attachment to apo-cytochrome c	2.91 ± 0.18	1.67 ± 0.32	1.18 ± 0.21	1
Ssq1p	NP_013473	Assembly of Fe/S clusters into proteins	4.45 ± 0.80	2.67 ± 0.28	0.81 ± 0.19	1
Sod2p	NP_011872	Detoxification of ROS in mitochondria	1.76 ± 0.45	2.80 ± 0.39	1.19 ± 0.16	1
Prx1p	NP_009489	Detoxification of ROS in mitochondria	2.34 ± 0.34	2.67 ± 0.48	0.76 ± 0.15	1
Atp1p	NP_009453	Mitochondrial ATP synthase	2.59 ± 0.41	2.73 ± 0.54	1.43 ± 0.23	1
Atp2p	NP_012655	Mitochondrial ATP synthase	2.76 ± 0.53	2.59 ± 0.33	1.14 ± 0.19	1
Pet9p	NP_009523	Mitochondrial ADP/ATP carrier	2.69 ± 0.34	3.76 ± 0.45	0.87 ± 0.11	1
Mir1p	NP_012611	Mitochondrial phosphate carrier	2.83 ± 0.44	3.59 ± 0.56	1.34 ± 0.17	1
Day 4 (PD phase)						
Tps1p	NP_009684	Trehalose biosynthesis	2.78 ± 0.33	3.56 ± 0.41	1.29 ± 0.23	1
Tps2p	NP_010359	Trehalose biosynthesis	2.89 ± 0.44	3.77 ± 0.23	1.17 ± 0.19	1
Ath1p	NP_015351	Trehalose degradation	0.35 ± 0.09	0.41 ± 0.05	1.25 ± 0.11	1
Nth1p	NP_010284	Trehalose degradation	0.27 ± 0.06	0.38 ± 0.04	0.87 ± 0.09	1
Nth2p	NP_009555	Trehalose degradation	0.39 ± 0.09	0.81 ± 0.11	1.23 ± 0.12	1
Glg2p	NP_012398	Glycogen biosynthesis	2.65 ± 0.22	4.19 ± 0.15	0.78 ± 0.23	1
Glc3p	NP_010905	Glycogen biosynthesis	2.78 ± 0.31	3.65 ± 0.22	1.34 ± 0.17	1
Gsy2p	NP_013359	Glycogen biosynthesis	4.78 ± 0.61	5.64 ± 0.43	1.45 ± 0.24	1
Gph1p	NP_015486	Glycogen degradation	0.30 ± 0.10	0.41 ± 0.08	0.88 ± 0.12	1
Gpt2p	NP_012993	Biosynthesis of TAG	0.27 ± 0.06	0.22 ± 0.04	0.45 ± 0.13	1
Ayr1p	NP_012142	Biosynthesis of TAG	0.35 ± 0.08	0.41 ± 0.09	0.86 ± 0.16	1
Slc1p	NP_010231	Biosynthesis of TAG	0.21 ± 0.04	0.17 ± 0.05	0.91 ± 0.21	1
Pah1p	NP_013888	Biosynthesis of TAG	0.38 ± 0.09	0.26 ± 0.07	1.23 ± 0.13	1
Lpp1p	NP_010791	Biosynthesis of TAG	0.34 ± 0.06	0.29 ± 0.04	0.88 ± 0.17	1
Dga1p	NP_014888	Biosynthesis of TAG	0.28 ± 0.03	0.22 ± 0.09	0.91 ± 0.28	1
Are2p	NP_014416	Biosynthesis of TAG and EE	0.21 ± 0.04	0.14 ± 0.02	0.77 ± 0.31	1
Tgl1p	NP_012782	Degradation of EE	4.67 ± 0.61	5.91 ± 0.52	1.34 ± 0.26	1
Tgl3p	NP_014044	Degradation of TAG	3.77 ± 0.43	4.29 ± 0.31	1.29 ± 0.13	1
Tgl4p	NP_013015	Degradation of TAG	3.56 ± 0.21	4.77 ± 0.49	1.59 ± 0.19	1
Tgl5p	NP_014724	Degradation of TAG	4.49 ± 0.60	5.73 ± 0.53	1.12 ± 0.21	1
Yeh1p	NP_013089	Degradation of EE	2.76 ± 0.32	3.34 ± 0.41	0.83 ± 0.27	1
Fat1p	NP_009597	Conversion of FFA to FA-CoA	4.81 ± 0.56	5.76 ± 0.38	1.53 ± 0.33	1
Faa1p	NP_014962	Conversion of FFA to FA-CoA	2.72 ± 0.34	3.49 ± 0.43	1.71 ± 0.41	1
Faa2p	NP_010931	Conversion of FFA to FA-CoA	4.34 ± 0.52	5.67 ± 0.35	1.19 ± 0.23	1
Faa4p	NP_013974	Conversion of FFA to FA-CoA	3.56 ± 0.41	4.49 ± 0.22	0.84 ± 0.11	1
Fox1p	NP_011310	Peroxisomal oxidation of FA-CoA	5.59 ± 0.53	5.87 ± 0.41	1.37 ± 0.23	1
Fox2p	NP_012934	Peroxisomal oxidation of FA-CoA	5.83 ± 0.61	5.61 ± 0.22	1.71 ± 0.41	1
Fox3p	NP_012106	Peroxisomal oxidation of FA-CoA	5.19 ± 0.33	5.49 ± 0.28	1.29 ± 0.12	1
Adh1p	NP_014555	Ethanol biosynthesis	0.22 ± 0.07	0.29 ± 0.04	0.78 ± 0.17	1
Adh2p	NP_014032	Ethanol oxidation	4.78 ± 0.49	4.56 ± 0.37	2.23 ± 0.22	1
Pyc1p	NP_011453	Gluconeogenesis	4.49 ± 0.51	2.77 ± 0.24	1.34 ± 0.19	1
Pck1p	NP_013023	Gluconeogenesis	4.83 ± 0.25	2.44 ± 0.19	0.86 ± 0.22	1
Fbp1p	NP_013481	Gluconeogenesis	4.78 ± 0.61	4.81 ± 0.52	1.39 ± 0.21	1
Pda1p	NP_011105	Mitochondrial PDH complex	4.63 ± 0.57	3.72 ± 0.33	1.17 ± 0.23	1
Aco1p	NP_013407	Mitochondrial TCA cycle	3.48 ± 0.35	2.71 ± 0.22	0.76 ± 0.23	1

Ndi1p	NP_013586	Mitochondrial ETC	4.45 ± 0.52	3.59 ± 0.18	1.18 ± 0.17	1
Sdh1p	NP_012774	Mitochondrial TCA cycle and ETC	4.88 ± 0.38	3.32 ± 0.42	0.84 ± 0.24	1
Cyt1p	NP_014708	Mitochondrial ETC	4.56 ± 0.51	3.83 ± 0.23	1.32 ± 0.19	1
Hem14p	NP_010930	Heme synthesis in mitochondria	4.28 ± 0.33	3.49 ± 0.37	0.87 ± 0.28	1
Cyc3p	NP_009361	Heme attachment to apo-cytochrome c	3.77 ± 0.44	2.85 ± 0.20	0.79 ± 0.34	1
Ssq1p	NP_013473	Assembly of Fe/S clusters into proteins	4.55 ± 0.26	3.74 ± 0.42	0.92 ± 0.33	1
Sod2p	NP_011872	Detoxification of ROS in mitochondria	2.89 ± 0.32	4.53 ± 0.56	1.42 ± 0.29	1
Prx1p	NP_009489	Detoxification of ROS in mitochondria	3.65 ± 0.41	4.79 ± 0.39	1.23 ± 0.17	1
Atp1p	NP_009453	Mitochondrial ATP synthase	3.56 ± 0.24	4.45 ± 0.50	1.38 ± 0.21	1
Atp2p	NP_012655	Mitochondrial ATP synthase	3.79 ± 0.38	4.93 ± 0.27	1.67 ± 0.34	1
Pet9p	NP_009523	Mitochondrial ADP/ATP carrier	3.88 ± 0.23	3.57 ± 0.36	0.85 ± 0.19	1
Mir1p	NP_012611	Mitochondrial phosphate carrier	3.56 ± 0.38	3.74 ± 0.41	0.92 ± 0.23	1
Day 9 (ST phase)						
Tps1p	NP_009684	Trehalose biosynthesis	5.48 ± 0.34	4.72 ± 0.23	1.87 ± 0.28	1
Tps2p	NP_010359	Trehalose biosynthesis	5.54 ± 0.21	4.41 ± 0.42	2.29 ± 0.33	1
Ath1p	NP_015351	Trehalose degradation	0.36 ± 0.06	0.86 ± 0.18	1.16 ± 0.34	1
Nth1p	NP_010284	Trehalose degradation	0.42 ± 0.08	0.79 ± 0.26	1.29 ± 0.46	1
Nth2p	NP_009555	Trehalose degradation	0.27 ± 0.05	0.42 ± 0.08	0.83 ± 0.20	1
Glg2p	NP_012398	Glycogen biosynthesis	1.67 ± 0.45	1.89 ± 0.22	1.24 ± 0.17	1
Glc3p	NP_010905	Glycogen biosynthesis	1.78 ± 0.33	1.65 ± 0.16	1.15 ± 0.22	1
Gsy2p	NP_013359	Glycogen biosynthesis	3.67 ± 0.41	2.78 ± 0.23	1.45 ± 0.11	1
Gph1p	NP_015486	Glycogen degradation	1.34 ± 0.25	2.89 ± 0.16	1.31 ± 0.24	1
Gpt2p	NP_012993	Biosynthesis of TAG	0.75 ± 0.12	0.36 ± 0.28	1.29 ± 0.37	1
Ayr1p	NP_012142	Biosynthesis of TAG	0.83 ± 0.11	0.76 ± 0.23	1.37 ± 0.29	1
Slc1p	NP_010231	Biosynthesis of TAG	0.34 ± 0.04	0.42 ± 0.09	0.85 ± 0.12	1
Pah1p	NP_013888	Biosynthesis of TAG	0.43 ± 0.06	0.35 ± 0.04	1.24 ± 0.09	1
Lpp1p	NP_010791	Biosynthesis of TAG	0.77 ± 0.16	0.42 ± 0.07	0.92 ± 0.22	1
Dga1p	NP_014888	Biosynthesis of TAG	0.89 ± 0.12	0.35 ± 0.05	1.56 ± 0.17	1
Are2p	NP_014416	Biosynthesis of TAG and EE	0.34 ± 0.07	0.46 ± 0.09	0.83 ± 0.22	1
Tgl1p	NP_012782	Degradation of EE	2.87 ± 0.18	2.95 ± 0.34	2.28 ± 0.13	1
Tgl3p	NP_014044	Degradation of TAG	1.82 ± 0.27	2.73 ± 0.42	1.57 ± 0.38	1
Tgl4p	NP_013015	Degradation of TAG	1.78 ± 0.31	1.86 ± 0.23	0.76 ± 0.12	1
Tgl5p	NP_014724	Degradation of TAG	2.87 ± 0.42	3.79 ± 0.54	1.59 ± 0.33	1
Yeh1p	NP_013089	Degradation of EE	1.43 ± 0.21	1.84 ± 0.36	1.17 ± 0.21	1
Fat1p	NP_009597	Conversion of FFA to FA-CoA	2.69 ± 0.37	3.77 ± 0.45	1.56 ± 0.30	1
Faa1p	NP_014962	Conversion of FFA to FA-CoA	1.56 ± 0.22	1.87 ± 0.34	1.29 ± 0.18	1
Faa2p	NP_010931	Conversion of FFA to FA-CoA	2.86 ± 0.41	2.73 ± 0.42	1.18 ± 0.16	1
Faa4p	NP_013974	Conversion of FFA to FA-CoA	1.39 ± 0.23	2.92 ± 0.37	0.67 ± 0.11	1
Fox1p	NP_011310	Peroxisomal oxidation of FA-CoA	4.45 ± 0.67	5.76 ± 0.73	2.23 ± 0.52	1
Fox2p	NP_012934	Peroxisomal oxidation of FA-CoA	4.69 ± 0.43	4.73 ± 0.55	1.72 ± 0.23	1
Fox3p	NP_012106	Peroxisomal oxidation of FA-CoA	4.46 ± 0.61	5.57 ± 0.38	2.34 ± 0.32	1
Adh1p	NP_014555	Ethanol biosynthesis	0.21 ± 0.06	0.29 ± 0.09	0.42 ± 0.13	1
Adh2p	NP_014032	Ethanol oxidation	4.67 ± 0.62	4.85 ± 0.54	2.48 ± 0.29	1
Pyc1p	NP_011453	Gluconeogenesis	2.68 ± 0.35	1.73 ± 0.27	0.82 ± 0.18	1
Pck1p	NP_013023	Gluconeogenesis	1.77 ± 0.23	1.59 ± 0.31	0.67 ± 0.13	1
Fbp1p	NP_013481	Gluconeogenesis	2.74 ± 0.35	1.86 ± 0.25	0.79 ± 0.26	1
Pda1p	NP_011105	Mitochondrial PDH complex	2.75 ± 0.44	2.37 ± 0.39	1.12 ± 0.19	1
Aco1p	NP_013407	Mitochondrial TCA cycle	2.63 ± 0.37	2.42 ± 0.42	0.73 ± 0.15	1
Ndi1p	NP_013586	Mitochondrial ETC	2.77 ± 0.54	2.84 ± 0.28	1.23 ± 0.26	1
Sdh1p	NP_012774	Mitochondrial TCA cycle and ETC	3.86 ± 0.61	2.73 ± 0.39	1.35 ± 0.22	1
Cyt1p	NP_014708	Mitochondrial ETC	3.65 ± 0.27	2.49 ± 0.16	1.19 ± 0.34	1
Hem14p	NP_010930	Heme synthesis in mitochondria	2.84 ± 0.34	1.59 ± 0.23	0.73 ± 0.16	1
Cyc3p	NP_009361	Heme attachment to apo-cytochrome c	3.67 ± 0.45	2.85 ± 0.42	1.35 ± 0.27	1

Ssq1p	NP_013473	Assembly of Fe/S clusters into proteins	2.76 ± 0.37	2.43 ± 0.18	1.28 ± 0.32	1
Sod2p	NP_011872	Detoxification of ROS in mitochondria	2.89 ± 0.21	4.45 ± 0.33	1.64 ± 0.19	1
Prx1p	NP_009489	Detoxification of ROS in mitochondria	2.57 ± 0.36	4.87 ± 0.52	1.57 ± 0.13	1
Atp1p	NP_009453	Mitochondrial ATP synthase	3.76 ± 0.44	4.59 ± 0.60	1.72 ± 0.21	1
Atp2p	NP_012655	Mitochondrial ATP synthase	3.68 ± 0.51	4.74 ± 0.43	1.34 ± 0.32	1
Pet9p	NP_009523	Mitochondrial ADP/ATP carrier	2.45 ± 0.37	3.87 ± 0.49	1.29 ± 0.17	1
Mir1p	NP_012611	Mitochondrial phosphate carrier	2.87 ± 0.43	3.71 ± 0.22	1.66 ± 0.24	1
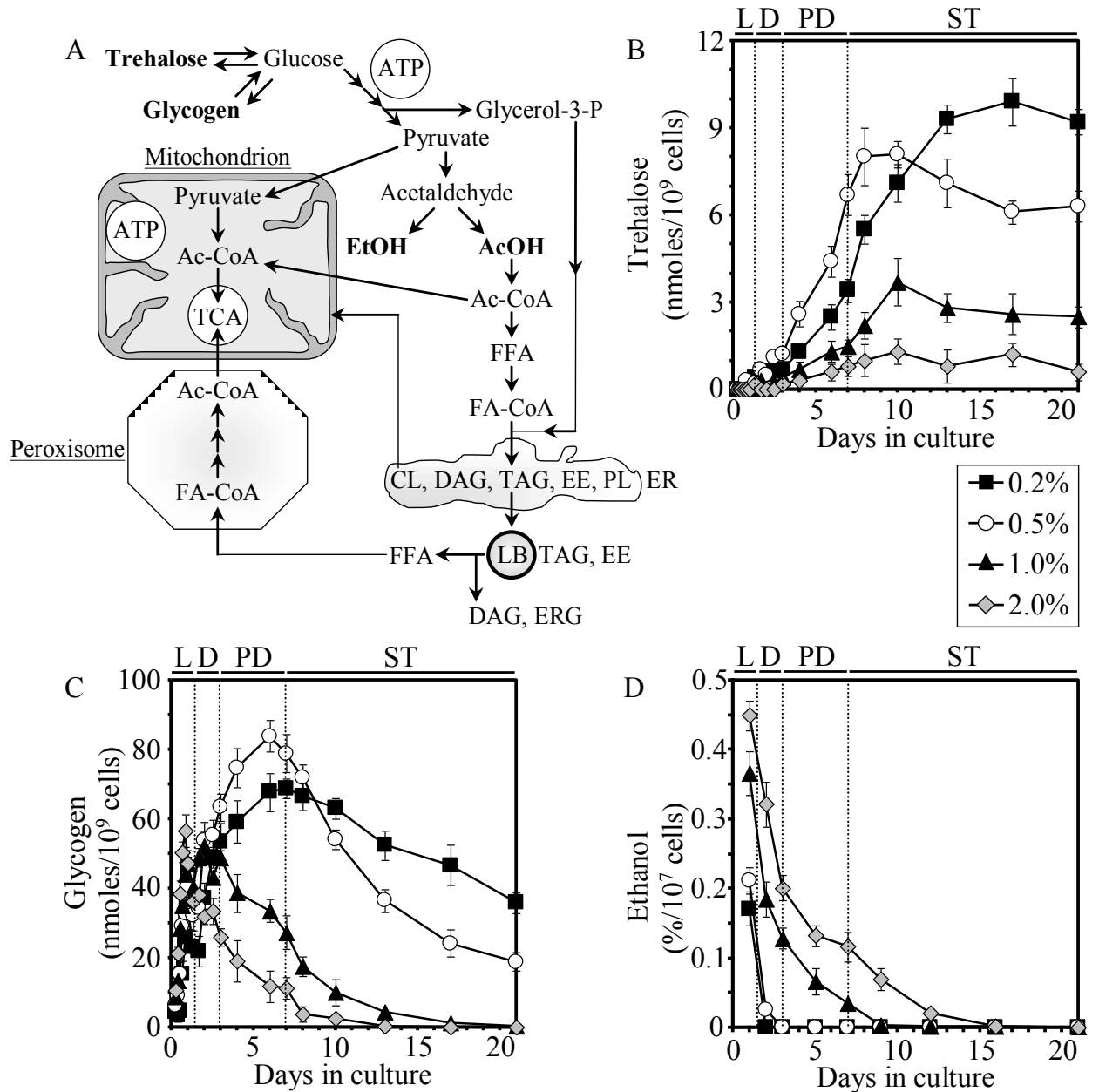
Figure 3.8. CR remodels trehalose and glycogen metabolism and accelerates ethanol catabolism. (A) Outline of metabolic pathways and interorganellar communications operating in chronologically aging yeast. (B-D) The dynamics of age-dependent changes in the intracellular levels of trehalose (B) and glycogen (C) and in the extracellular concentrations of ethanol (D) during chronological aging of WT cells. Cells were cultured in rich YP medium initially containing 0.2%, 0.5%, 1% or 2% glucose. Data are presented as mean ± SEM (n = 3-5). For trehalose and glycogen levels, $p < 0.001$ at days 3 to 21 for cells grown on 0.2% or 0.5% glucose versus cells grown on 2% glucose. For ethanol levels, $p < 0.001$ at days 1 to 9 for cells grown on 0.2% or 0.5% glucose versus cells grown on 2% glucose. Abbreviations: Ac-CoA, acetyl-CoA; AcOH, acetic acid; CL, cardiolipins; DAG, diacylglycerols; EE, ethyl esters; ER, endoplasmic reticulum; EtOH, ethanol; FA-CoA, CoA esters of fatty acids; FFA, free fatty acids; LB, lipid bodies; PL, phospholipids; TAG, triacylglycerols.

glycolytic oxidation, can adequately explain the observed dynamics of age-dependent changes in levels of trehalose and glycogen (Figures 3.8B and 3.8C). Finally, I also found that CR increases the levels of mitochondrial proteins serving the formation of acetyl-CoA and its subsequent oxidation via the tricarboxylic acid (TCA) cycle, electron transport and oxidative phosphorylation coupled to ATP synthesis, as well as the detoxification of mitochondrially formed reactive oxygen species (ROS) (Figure 3.7B).

Taken together, my lipidomic, proteomic and metabolomic analyses suggest the following scenario for the CR-promoted remodeling of carbohydrate and lipid metabolism that yeast undergo prior to entry into the non-proliferative ST phase (Figure 3.7C). Chronologically aging CR yeast shift carbohydrate metabolism toward glucose formation via gluconeogenesis. By activating the synthesis of enzymes catalyzing the biosynthesis of trehalose and glycogen and by suppressing the synthesis of enzymes required for their degradation, CR promotes the accumulation of these two major glucose stores. In contrast, the deposited in LBs neutral lipids TAG and EE, the two major lipid stores, are rapidly hydrolyzed by CR yeast prior to entry into the non-proliferative ST phase. The rapid lipolysis of neutral lipids in CR yeast produces substantial amounts of

FFA. FFA are rapidly converted to FA-CoA that are then oxidized to acetyl-CoA via a peroxisome-confined pathway greatly accelerated by CR. The subsequent oxidation of the peroxisome-derived acetyl-CoA in mitochondria generates the bulk of ATP in CR yeast. This process also generates considerable quantities of mitochondrial ROS (see data presented further in this Chapter of the thesis). Within the mitochondrion, ROS are decomposed in CR-promoted antioxidant scavenger reactions catalyzed by superoxide dismutase Sod2p and peroxiredoxin Prx1p, both of which are induced by CR (Figure 3.7B). In contrast to CR yeast, chronologically aging non-CR yeast generate the bulk of ATP via glycolytic oxidation of glycogen-derived glucose. The glycolytic oxidation of glucose to pyruvate in non-CR yeast is followed by its conversion to ethanol, which accumulates in non-CR yeast. On the contrary, CR yeast avoid ethanol accumulation by modulating the quantities of Adh1p and Adh2p, the two alcohol dehydrogenase isozymes that catalyze ethanol synthesis and degradation, respectively. The importance of this effect of CR on ethanol concentration for longevity is discussed further in this Chapter of the thesis.

3.4.4. Concentration of ethanol is one of the key factors influencing chronological aging

I found that the steady-state level of ethanol depends on a balance of enzymatic activities of the Adh1p and Adh2p isozymes of alcohol dehydrogenase (Figure 3.9A). Both isozymes are under the control of CR. In fact, by decreasing the level of Adh1p and by increasing the level of Adh2p (Figure 3.7B), CR greatly accelerated the depletion of
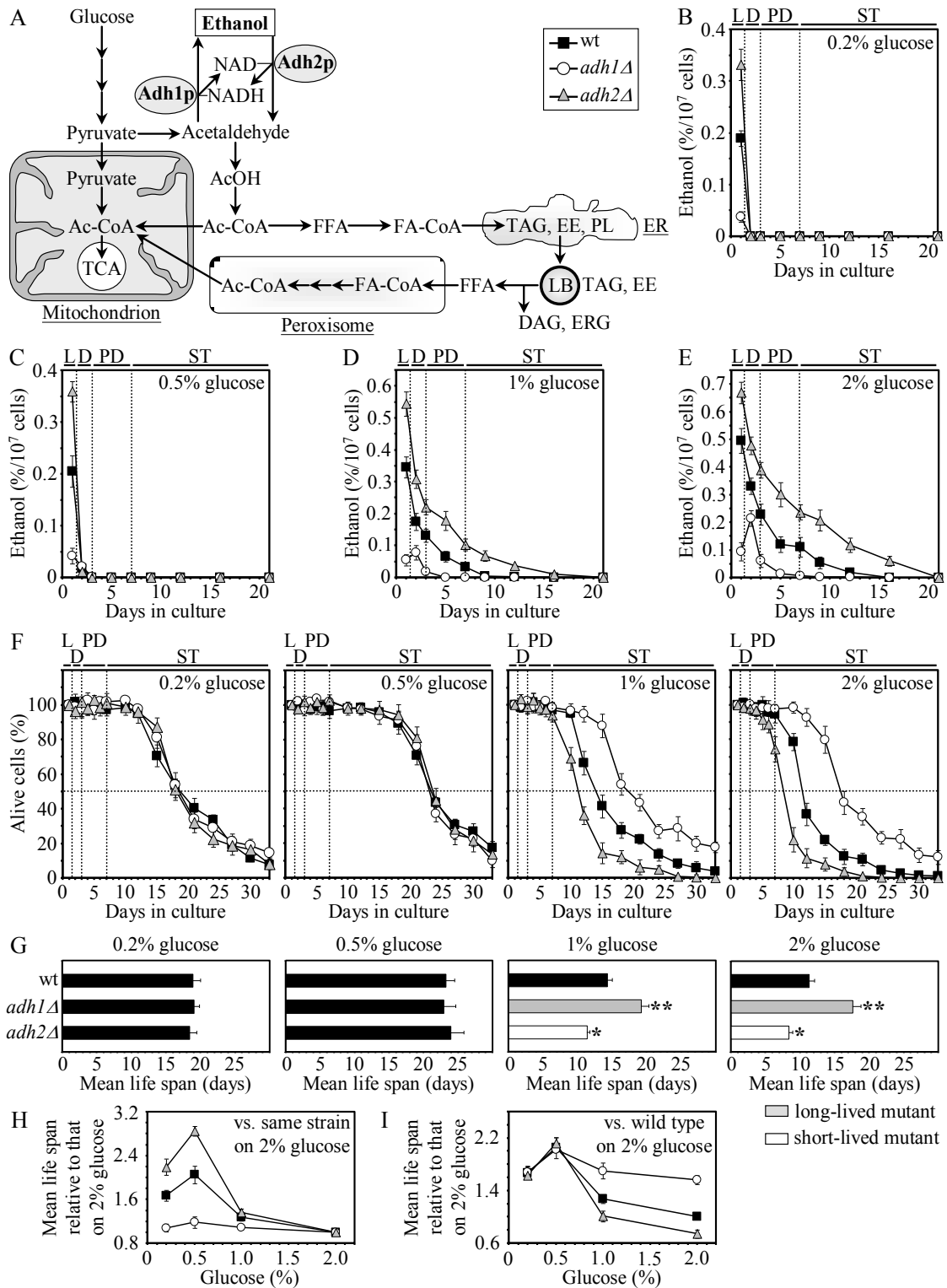
Figure 3.9. Ethanol is one of the key factors regulating longevity. (A) Outline of metabolic pathways and interorganellar communications operating in chronologically aging yeast cells. (B-E) The dynamics of age-dependent changes in the extracellular concentration of ethanol for WT, *adh1Δ* and *adh2Δ*. Data are

presented as mean ± SEM (n = 3-5). (F and G) Survival (F) and the mean chronological life spans (G) of WT, *adh1Δ* and *adh2Δ*. Data are presented as mean ± SEM (n = 3-5); *p < 0.05, **p < 0.005. (H and I) A dose-response relationship between the mean chronological life span and the degree of CR for WT, *adh1Δ* and *adh2Δ*. Data are presented as mean ± SEM (n = 3-5). (B-I) Cells were cultured in YP medium initially containing 0.2%, 0.5%, 1% or 2% glucose.

ethanol from yeast grown on 0.2% or 0.5% glucose (Figure 3.8D). To evaluate the effect of endogenously produced ethanol on longevity, I incubated WT, *adh1Δ* and *adh2Δ* strains in media containing different glucose concentrations. I monitored the chronological life spans of these strains and assessed the dynamics of changes in ethanol concentration during their aging. When yeast were placed on the CR diet by incubating them on 0.2% or 0.5% glucose, lack of Adh1p or Adh2p did not affect ethanol concentration (Figures 3.9B and 3.9C) or chronological life span (Figures 3.9F and 3.9G). Conversely, lack of Adh1p substantially decreased ethanol concentration when yeast were grown on 1% or 2% glucose (Figures 3.9D and 3.94E), prolonging their life span (Figures 3.9F and 3.9G). Furthermore, lack of Adh2p led to a considerable rise of ethanol concentration in non-CR yeast grown on 1% or 2% glucose (Figures 3.9D and 3.9E), shortening their life span (Figures 3.9F and 3.9G). By extending life span of non-CR yeast, *adh1Δ* to a great extent abolished the positive effect of CR on longevity (Figures 3.9H and 3.9I). Alternatively, by shortening life span of non-CR yeast, *adh2Δ* enhanced the benefit of CR for longevity (Figures 3.9H and 3.9I).

My data also strongly suggest that ethanol modulates the dynamics of trehalose, glycogen, neutral lipids, FFA and DAG in chronologically aging yeast. In fact, by decreasing ethanol concentration in non-CR yeast, *adh1Δ* remodelled the metabolism of these key for longevity compounds in non-CR yeast by making it similar to the metabolic
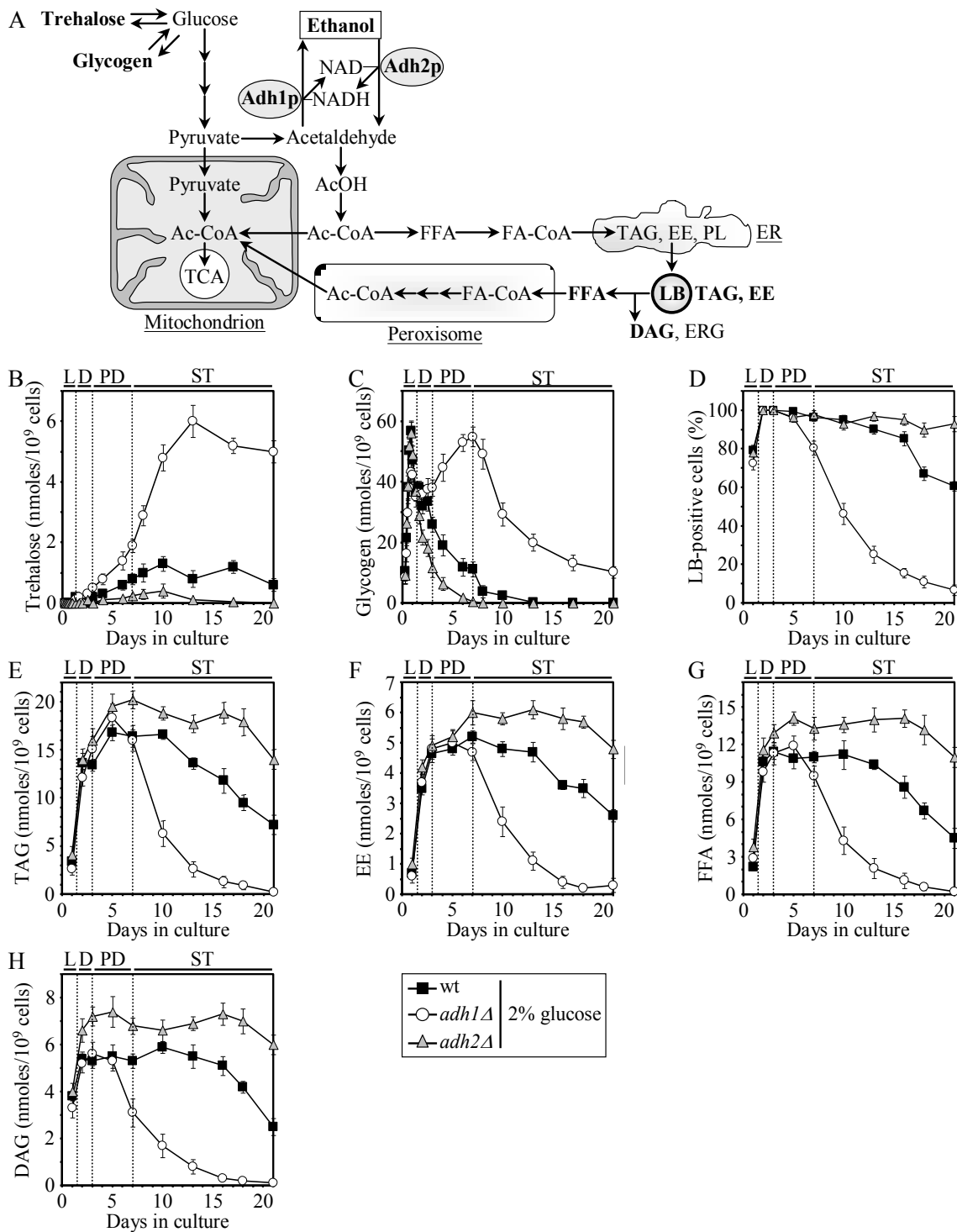
Figure 3.10. In chronologically aging yeast, ethanol modulates the dynamics of trehalose, glycogen, neutral lipids, FFA and DAG. (A) Outline of metabolic pathways and interorganellar communications operating in chronologically aging yeast. (B, C, E-H) The dynamics of age-dependent changes in the levels of trehalose

(B), glycogen (C), TAG (E), EE (F), FFA (G) and DAG (H) during chronological aging of WT, *adh1Δ* and *adh2Δ*. Data are presented as mean ± SEM (n = 3-4). (D) Percent of WT, *adh1Δ* and *adh2Δ* cells that contain lipid bodies. Data are presented as mean ± SEM (n = 4). (B-H) Cells were cultured in rich YP medium initially containing 2% glucose. Abbreviations: Ac-CoA, acetyl-CoA; AcOH, acetic acid; DAG, diacylglycerols; EE, ethyl esters; ER, endoplasmic reticulum; FA-CoA, CoA esters of fatty acids; FFA, free fatty acids; LB, lipid bodies; PL, phospholipids; TAG, triacylglycerols.

design of CR yeast. Specifically, the *adh1Δ* mutation 1) increased the level of trehalose (Figure 3.10B); 2) redesigned glycogen metabolism by promoting glycogen accumulation in PD phase and delaying its consumption until ST phase (Figure 3.10C); 3) accelerated the lipolytic consumption of lipid bodies-deposited neutral lipids (Figures 3.10D-3.10F); 4) accelerated the consumption of FFA and DAG during late PD and early ST phases (Figures 3.10G and 3.10H). In contrast, by elevating ethanol level in non-CR yeast, *adh2Δ* enhanced the negative effect of a calorie-rich diet on longevity by further decreasing trehalose concentration, accelerating glycogen consumption, slowing down neutral lipids lipolysis, and decelerating FFA and DAG consumption (Figure 3.10).

In sum, based on the findings presented in Chapter 3.4.4, I concluded that ethanol is one of the key factors regulating longevity by specifically modulating the metabolism of trehalose, glycogen, neutral lipids, FFA and DAG in chronologically aging yeast.

3.4.5. Ethanol decelerates the consumption of neutral lipids deposited in lipid bodies (LBs) by slowing down fatty acid oxidation in peroxisomes that are associated with LBs

I sought to define a mechanism by which ethanol modulates the dynamics of neutral lipids, FFA and DAG in chronologically aging yeast. Importantly, I found that the

observed rapid depletion of ethanol seen in CR yeast (Figure 3.8D) coincides with 1) elevated levels of Fox1p, Fox2p and Fox3p (Figure 3.7B), all of which are the core enzymes of peroxisomal fatty acid β-oxidation [237]; and 2) rapid consumption of FFA during PD phase (Figure 3.4F). Of note, it has been previously shown that in the yeast species that need peroxisomes to utilize methanol as a sole carbon source for growth, ethanol suppresses the synthesis of peroxisomal enzymes catalyzing methanol oxidation [238]. Based on these findings, I hypothesized that the accumulation of ethanol in non-CR yeast cultures (Figure 3.8D) suppresses peroxisomal oxidation of FFA by repressing the synthesis of Fox1p, Fox2p and Fox3p, thereby causing the accumulation of FFA during PD phase (Figure 3.4F). This hypothesis was confirmed by my finding that a premature depletion of ethanol from non-CR cells of *adh1Δ* (Figures 3.9D and 3.9E) led to an early synthesis of Fox1p, Fox2p and Fox3p in PD phase (Figure 3.11B) and promoted FFA consumption (Figure 3.10G). In addition, I found that a postponed depletion of ethanol from non-CR cells of *adh2Δ* (Figures 3.9D and 3.9E) delays the synthesis of Fox1p, Fox2p and Fox3p (Figure 3.11B) and slows down FFA consumption (Figure 3.10G).

How exactly ethanol modulates the dynamics of neutral lipids in chronologically aging yeast? By substantially decreasing ethanol concentration in non-CR yeast, *adh1Δ* accelerated not only the consumption of FFA but also the lipolysis of neutral lipids deposited in LBs (Figures 3.10D-3.10G). Moreover, by elevating ethanol level in non-CR yeast, *adh2Δ* decelerated both these processes (Figures 3.10D-3.10G). These findings
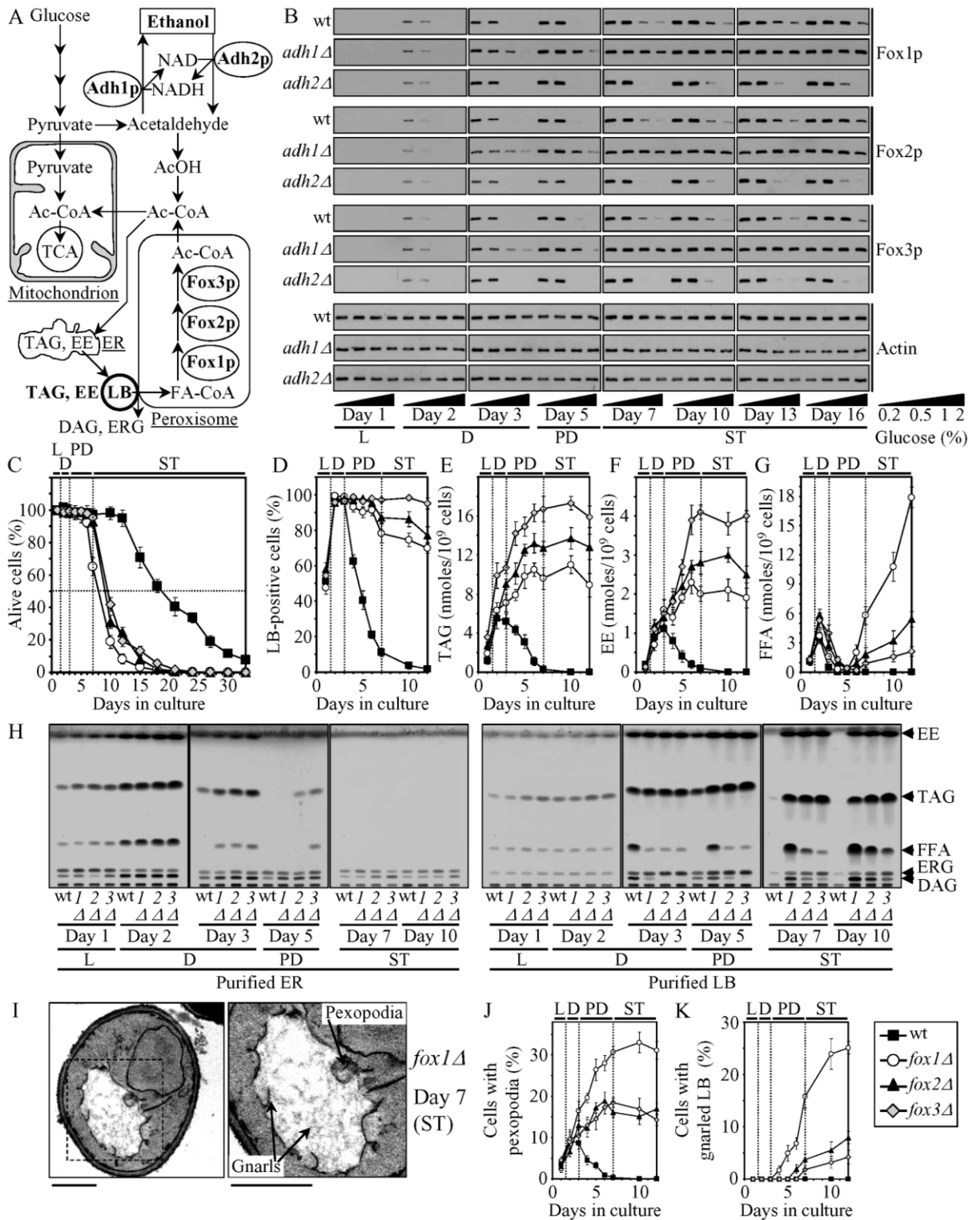
Figure 3.11. By suppressing fatty acid oxidation in peroxisomes that are associated with lipid bodies (LBs), ethanol and *fox1Δ*, *fox2Δ* and *fox3Δ* mutations decelerate the lipolytic consumption of neutral lipids

deposited in LBs. (A) Outline of metabolic pathways and interorganellar communications operating in chronologically aging yeast cells. (B) Western blot analysis of Fox1p, Fox2p, Fox3p and actin in aging WT, *adh1Δ* and *adh2Δ* cultured in YP medium initially containing 0.2%, 0.5%, 1% or 2% glucose. Protein recovered in total cell lysates were resolved by SDS-PAGE and detected by immunoblotting. (C) Survival of WT, *fox1Δ, fox2Δ* and *fox3Δ*. Data are presented as mean ± SEM (n = 4). (D) Percent of WT, *fox1Δ, fox2Δ* and *fox3Δ* cells that contain lipid bodies. Data are presented as mean ± SEM (n = 4). (E-G) TAG (E), EE (F) and FFA (G) levels in aging WT, *fox1Δ, fox2Δ* and *fox3Δ*. Data are presented as mean ± SEM (n = 5-6). (H) Spectra of lipids that were extracted from purified ER and lipid bodies of WT, *fox1Δ, fox2Δ* and *fox3Δ* cells. The equivalent of 200 μg of ER proteins and 20 μg of lipid body proteins was used for lipid extraction at each time point. Lipids were analyzed by TLC. A representative of 3 independent experiments is shown. (I) Transmission electron micrographs of aging *fox1Δ* cells recovered at day 7. Panels show two magnifications of the same micrograph. Bars, 1 μm. (J and K) Percent of cells that contain pexopodia (J) and/or gnarls (K). Images similar to the representative image shown in (I) were quantitated. Data are presented as mean ± SEM (n = 3). (C-K) Cells were cultured in YP medium initially containing 0.2% glucose.

strongly suggest that any diet or genetic manipulation that decelerates peroxisomal oxidation of FFA by Fox1p, Fox2p and/or Fox3p could also decelerate the lipolysis of neutral lipids in LBs, perhaps due to a feedback inhibition of the lipolysis by the concentrations of FFA or FA-CoA exceeding a critical level. This suggestion was further supported by my finding that lack of Fox1p, Fox2p or Fox3p abolishes the lipolysis of LB-deposited neutral lipids even in CR yeast (Figures 3.11D-3.11F). Importantly, I found that lack of Fox1p, Fox2p or Fox3p shortens the chronological life span of CR yeast (Figure 3.11C), implying that both the lipolysis of neutral lipids in LBs and the subsequent oxidation of FFA in peroxisomes are mandatory for the observed extension of life span by CR.

The proposed feedback inhibition of the lipolysis of neutral lipids by the concentrations of FFA or FA-CoA exceeding a critical level could be due to a recently described extensive physical contact existing between LBs and peroxisomes [239]. Such

tight contact has been shown to stimulate the lipolysis of neutral lipids within LBs, thereby initiating the import of the newly formed FFA into and their oxidation within peroxisomes [239]. The LBs-peroxisome association can lead to peroxisome invasion into the lipid core of LBs, thereby generating so-called pexopodia [239]. Importantly, pexopodia of the yeast mutants that are unable to oxidize FFA due to the absence of Fox1p, Fox2p or Fox3p cause the accumulation of electron-dense arrays of FFA (called gnarls) within LBs (Figure 3.11I; [239]). I found that, during D phase, all WT, *fox1Δ*, *fox2Δ* and *fox3Δ* grown on 0.2% glucose accumulate pexopodia (Figure 3.11J). Pexopodia in WT cells disappeared during the subsequent PD phase, concomitantly with the complete consumption of FFA within LBs of these cells (Figures 3.11G-3.11J). In contrast, pexopodia in prematurely aging *fox1Δ*, *fox2Δ* and *fox3Δ* continued to proliferate during PD phase, eventually becoming very abundant (Figure 3.11J). By the end of PD phase and in the beginning of ST phase, with the number of pexopodia in their cells reached a plateau (Figure 3.11J), *fox1Δ*, *fox2Δ* and *fox3Δ* began accumulating FFA (Figure 3.11G). These FFA were formed due to the lipolysis of limited amounts of ER-originated neutral lipids within LBs of the mutant strains (Figure 3.11H). I found that the accumulation of FFA within LBs of these *fox* mutants coincide with the build-up of gnarls (Figures 3.11I and 3.11K), which represent organized arrays of FFA [239]. Of note, the closer to the beginning of the peroxisomal β-oxidation pathway the reaction missing in a *fox* mutant was (Figure 3.11A), the more pexopodia and, eventually, gnarls accumulated within its LBs (Figures 3.11J and 3.11K). Altogether, my findings suggest that the build-up of gnarls within LBs of aging non-CR yeast initiates several negative feedback loops regulating the biosynthesis and degradation of TAG in the ER and LBs

(Figure 3.12). Due to the action of these negative feedback loops (Figure 3.12), aging non-CR yeast accumulate FFA and DAG (Figures 3.4F and 3.4G).
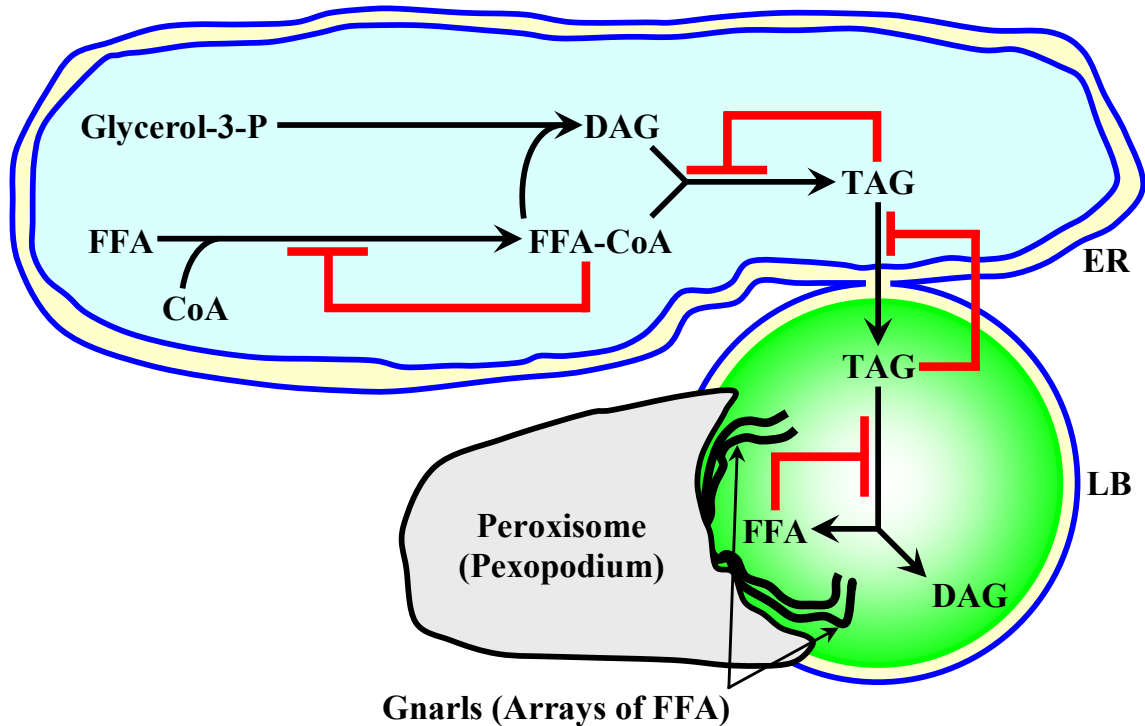
Figure 3.12. Several negative feedback loops regulate the biosynthesis and degradation of triacylglycerols (TAG) in the ER and lipid bodies (LBs). In chronologically aging yeast placed on a calorie-rich diet, the accumulation of electron-dense arrays of free fatty acids (called gnarls) within LBs initiates several negative feedback loops that regulate the biosynthesis and degradation of TAG in the ER and LBs. Due to the action of these negative feedback loops, yeast placed on a calorie-rich diet accumulate FFA and DAG. Abbreviations: DAG, diacylglycerols; ER, endoplasmic reticulum; FA-CoA, CoA esters of fatty acids; FFA, free fatty acids; LB, lipid bodies; TAG, triacylglycerols.

3.4.6. Peroxisomal fatty acid oxidation could regulate longevity via three different mechanisms

As I found, lack of Fox1p, Fox2p or Fox3p shortens the chronological life span of CR yeast (Figure 3.11C) but has no effect on longevity of non-CR yeast (Figure 3.14A). Hence, peroxisomal oxidation of FFA is mandatory for life-span extension by CR. At least three aspects of FFA oxidation in peroxisomes could influence longevity of WT

yeast under CR. First, the formation of hydrogen peroxide in the Fox1p-dependent reaction of fatty acid oxidation in peroxisomes (Figure 3.13A) could generate the bulk quantities of this ROS molecule, which is known for its essential role in regulating longevity [223, 240 - 244]. Second, the formation of acetyl-CoA via FFA oxidation in peroxisomes followed by its delivery to mitochondria for the oxidation via the TCA cycle (Figure 3.13A) could be responsible for the synthesis of the bulk quantities of ATP in mitochondria and could affect other longevity-related mitochondrial processes. Third, by regulating the biosynthesis and degradation of TAG in the ER and LBs via several negative feedback loops, fatty acid oxidation in peroxisomes controls the levels of FFA and DAG (Figures 3.11 and 3.12). Importantly, a short-term exposure to exogenously added FFA (*i.e.*, palmitoleic acid and oleic acid) and DAG induces necrotic cell death in chronologically aging yeast (Figure 3.15) [222]. Furthermore, DAG also modulates a signal transduction network affecting multiple longevity-related cellular targets [245, 246]. It is conceivable therefore that the accumulation of FFA and DAG in aging yeast that have low rate of peroxisomal fatty acid oxidation could trigger their necrotic cell death and, perhaps, other processes shortening their life span.

3.4.7. ROS produced in peroxisomes during fatty acid oxidation do not influence longevity

Although the bulk of ROS is produced in mitochondria, they are also formed during peroxisomal oxidation of FFA [223, 237, 240]. The only chemical reaction in yeast peroxisomes that generates hydrogen peroxide, the most abundant ROS molecule in the cell [241], is catalyzed by Fox1p (Figure 3.13A). Importantly, the peroxisomal isoform

Cta1p of catalase decomposes hydrogen peroxide inside the organelle (Figure 3.13A), thereby protecting yeast from oxidative damage by this ROS molecule [223, 237]. Hence, the steady-state level of hydrogen peroxide in the peroxisome depends on a balance of enzymatic activities of Fox1p and Cta1p. To elucidate the importance of peroxisome-produced ROS in the chronological aging of CR yeast, I compared the life spans of WT, *fox1Δ* and *cta1Δ* grown on 0.2% glucose. I reasoned that if peroxisomal ROS modulate longevity, the *fox1Δ* mutation would prolong life span by decreasing ROS level in the peroxisome, whereas the *cta1Δ* mutation would have an opposite effect on life span by raising the concentration of peroxisomal ROS. However, as I mentioned earlier, lack of ROS-generating Fox1p shortened life span (Figure 3.13C) for a reason discussed in the next section of this Chapter of my thesis. Furthermore, I found that lack of ROS-decomposing Cta1p has no effect on the life span of CR yeast (Figure 3.13C). I therefore concluded that ROS that are made during FFA oxidation in peroxisomes of chronologically aging yeast do not influence their longevity. Moreover, it appeared that FFA oxidation in peroxisomes does not produce a considerable fraction of ROS generated in yeast cell. In fact, I found that lack of ROS-decomposing Cta1p has no effect on the intracellular concentration of ROS formed in CR yeast (Figures 3.13D and 3.13E). Furthermore, the observed during D phase spike in the intracellular level of ROS in the *fox1Δ* mutant (Figures 3.13D and 3.136E), which lacks the only ROS-generating peroxisomal enzyme, further supports the notion that peroxisomes do not produce significant amounts of ROS in CR yeast. The sharp rise of ROS and its following rapid decline in CR cells of *fox1Δ*, a pattern that was also seen in *fox2Δ* and *fox3Δ*, was due to an important role that peroxisomal FFA oxidation plays in modulating essential processes

taking place in ROS-producing mitochondria (see next section of this Chapter of my thesis).

3.4.8. Fatty acid oxidation in peroxisomes controls longevity in part by modulating essential processes in mitochondria

As soon as CR cells of prematurely aging *fox1Δ, fox2Δ* and *fox3Δ* entered ST phase, a rapid decline in the percentage of viable cells occurred (Figure 3.11C). I found that such premature aging of the three *fox* mutants during ST phase precedes by a sharp decrease in oxygen consumption by their mitochondria (Figure 3.13F) and by an abrupt decline in the steady-state level of mitochondrially synthesized ATP during PD phase (Figure 3.13B). I therefore concluded that, during PD phase, CR yeast synthesize the bulk of their ATP in mitochondria by oxidizing the pool of acetyl-CoA that has been generated in peroxisomes via Fox1p-, Fox2p- and Fox3p-dependent FFA oxidation. In contrast, the pools of acetyl-CoA formed via oxidation of pyruvate in mitochondria or cytosol (Figure 3.13A) are not the major sources of NADH and $FADH_2$ for oxidative phosphorylation that takes place in mitochondria of aging CR yeast.

My conclusion that peroxisomal FFA oxidation in CR yeast controls longevity in part by modulating ATP synthesis in mitochondria prompted me to examine if the efficiency of acetyl-CoA formation in peroxisomes influences any other essential processes in mitochondria. I found that lack of Fox1p, Fox2p or Fox3p: 1) in CR yeast entering D phase, dramatically increases the amplitude of the observed spike in the rates of oxygen consumption and ROS generation by mitochondria (Figures 3.13D and 3.13F); and 2) in CR yeast entering PD phase, results in a sharp decrease of oxygen consumption
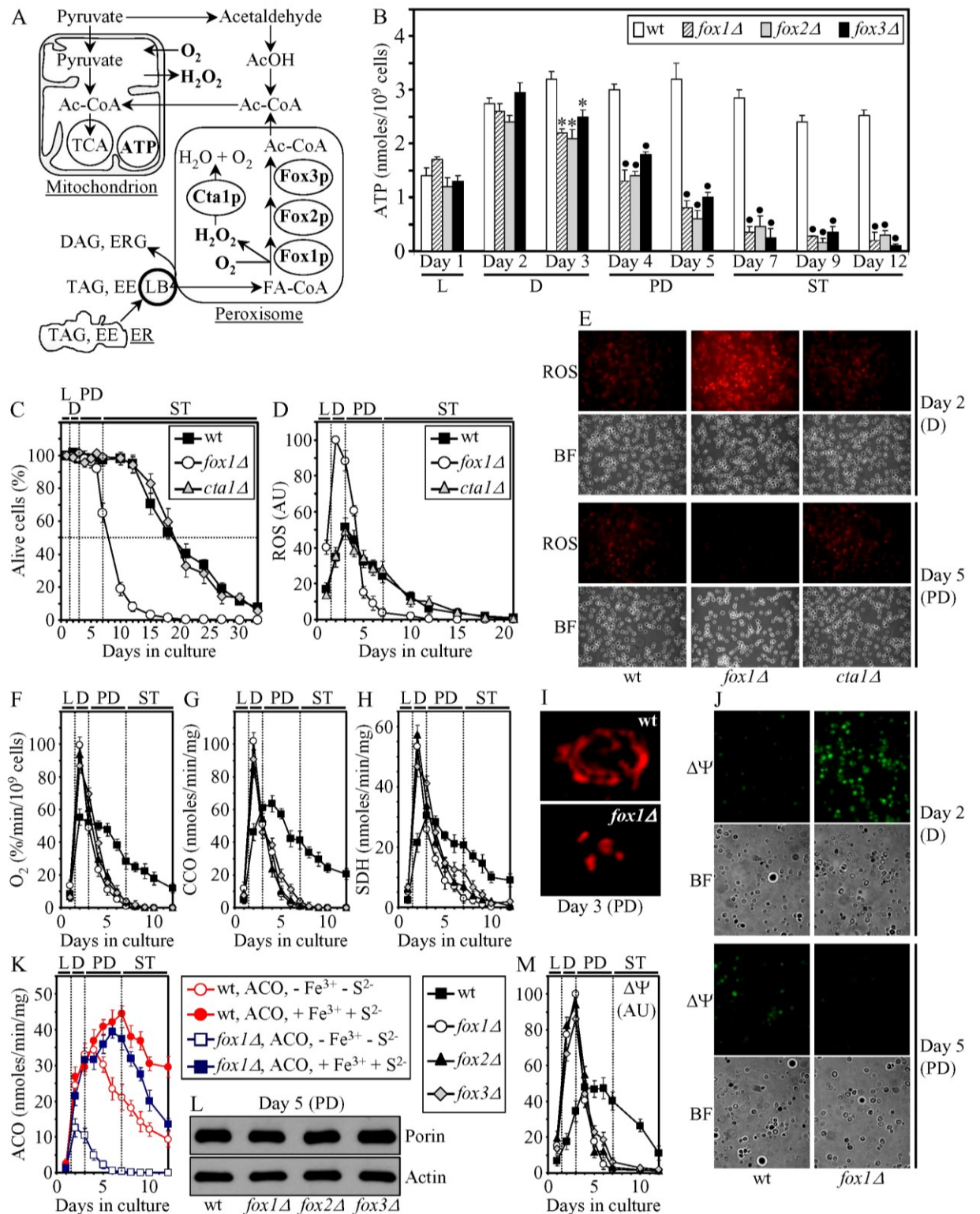
Figure 3.13. In CR yeast, the efficiency of fatty acid oxidation in peroxisomes modulates essential processes in mitochondria. (A) Outline of metabolic pathways and interorganellar communications

operating in chronologically aging yeast cells. (B) ATP levels in WT, *fox1Δ*, *fox2Δ* and *fox3Δ* cells. Data are presented as mean ± SEM (n = 3); *p < 0.05, •p < 0.005. (C) Survival of WT, *fox1Δ* and *cta1Δ*. Data are presented as mean ± SEM (n = 4). (D) ROS levels in aging WT, *fox1Δ* and *cta1Δ*. ROS were visualized using the fluorescent dye Dihydrorhodamine-123 (DHR). At least 800 cells were used for quantitation of DHR staining for each of 4 independent experiments. Data are presented as mean ± SEM (n = 4). (E) Representative images of WT, *fox1Δ* and *cta1Δ* cells stained with DHR. ROS were visualized using fluorescence microscopy. (F) Rates of oxygen consumption by aging WT, *fox1Δ*, *fox2Δ* and *fox3Δ* cells. Data are presented as mean ± SEM (n = 5). (G and H) Enzymatic activities of cytochrome c oxidase (CCO; G) and succinate dehydrogenase (H; SDH) in mitochondria purified from aging WT, *fox1Δ*, *fox2Δ* and *fox3Δ*. Data are presented as mean ± SEM (n = 3). (I) Morphology of mitochondria in WT and *fox1Δ* cells. Mitochondria were visualized by indirect immunofluorescence microscopy using monoclonal anti-porin primary antibodies and Alexa Fluor 568-conjugated goat anti-mouse IgG secondary antibodies. Representative images are shown. (J) Representative images of WT and *fox1Δ* and *cta1Δ* cells stained with rhodamine 123 (R123) for monitoring the mitochondrial membrane potential (ΔΨ) in living cells. ΔΨ was visualized using fluorescence microscopy. (K) Enzymatic activities of aconitase (ACO) in total cell lysates of aging WT and *fox1Δ*. The ACO activity was measured with or without the reactivation agents Fe^{3+} and Na_2S. Data are presented as mean ± SEM (n = 3). (L) Western blot analysis of porin and actin in aging WT, *fox1Δ*, *fox2Δ* and *fox3Δ*. Protein recovered in total cell lysates were resolved by SDS-PAGE and detected by immunoblotting. (M) ΔΨ values for aging WT, *fox1Δ*, *fox2Δ* and *fox3Δ*. ΔΨ was visualized using the fluorescent dye R123. At least 1000 cells were used for quantitation of R123 staining for each of 3 independent experiments. Data are presented as mean ± SEM (n = 3). (B-M) Cells were cultured in YP medium initially containing 0.2% glucose. Abbreviations: AU, arbitrary units; BF, bright field.

and ROS production by mitochondria (Figures 3.13D and 3.13F). Thus, the efficiency of acetyl-CoA formation via peroxisomal FFA oxidation modulates the efficiencies of electron flow through the mitochondrial electron transport chain (ETC) and of the ROS-generating transfer of a single electron to oxygen.

It seems that the observed early spike in ROS production by mitochondria of all three *fox* mutants irreversibly damaged some key mitochondrial proteins. In fact, I found that lack of any of the three Fox proteins resulted in rapid inactivation of cytochrome c oxidase (CCO), succinate dehydrogenase (SDH) and aconitase (ACO) in mitochondria of
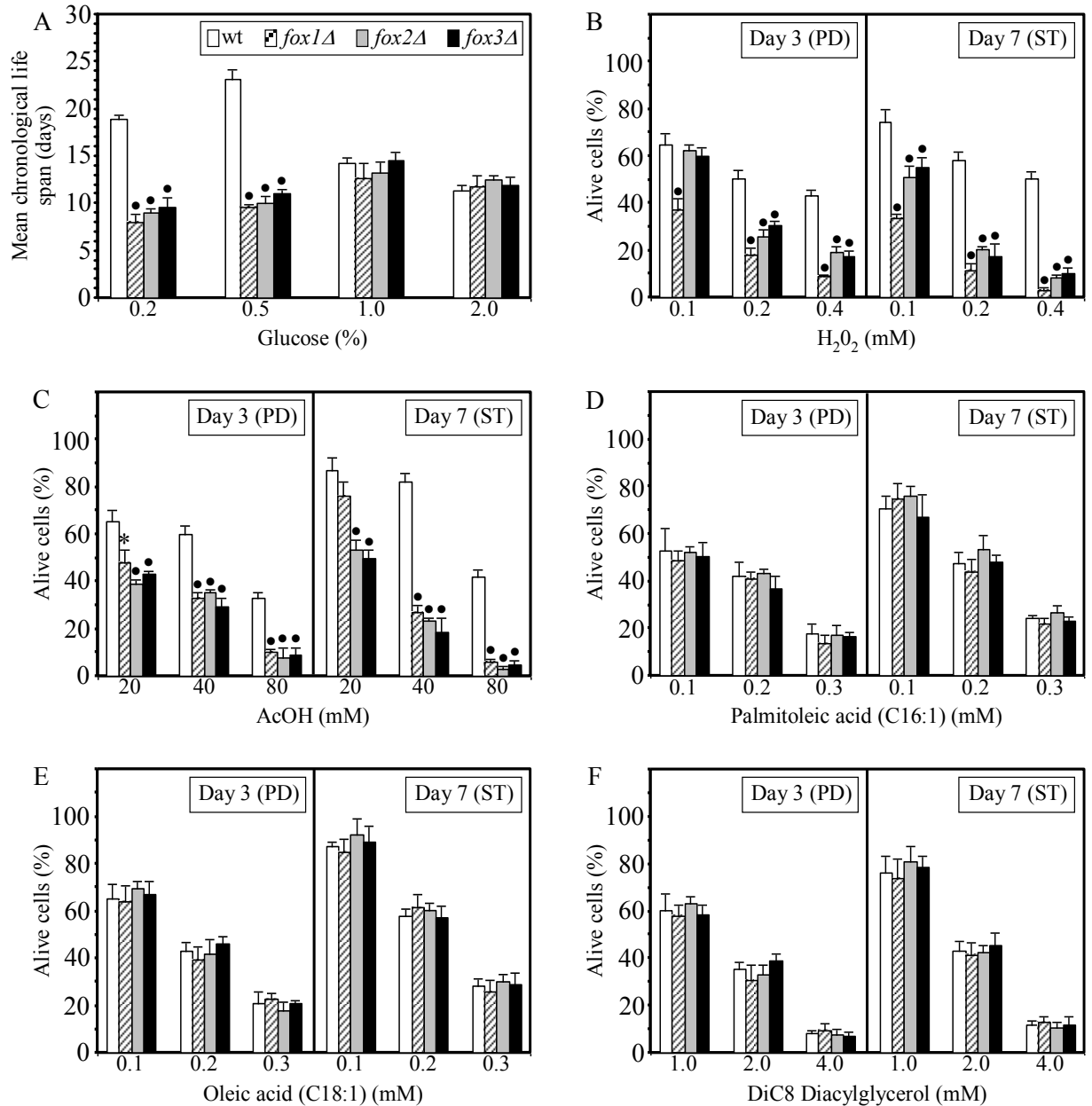
Figure 3.14. Lack of Fox1p, Fox2p or Fox3p shortens the chronological life span of yeast only under CR conditions, enhances their susceptibility to mitochondria-controlled cell death induced by exogenous hydrogen peroxide or acetic acid, but does not alter their susceptibility to cell death induced by exogenously added FFA or DAG. (A) The mean chronological life spans of WT, *fox1Δ*, *fox2Δ* and *fox3Δ*. Data are presented as mean ± SEM (n = 4-5); •p < 0.005. Cells were cultured in YP medium containing 0.2%, 0.5%, 1% or 2% glucose. (B - F) Viability of WT, *fox1Δ*, *fox2Δ* and *fox3Δ* cells treated with different concentrations of hydrogen peroxide (B), acetic acid (C), palmitoleic acid (D), oleic acid (E) or DiC8 diacylglycerol (F). Data are presented as mean ± SEM (n = 3-4); •p < 0.005. Cells were cultured in YP medium containing 0.2% glucose.

the prematurely aging *fox* mutants entering PD phase (Figures 3.13G, 3.13H and 3.13K). Each of these three mitochondrial proteins is a key target for the oxidative damage by ROS [18, 240, 247].

I next used fluorescence microscopy to monitor the mitochondrial membrane potential ($\Delta\Psi$) in living cells of WT and *fox* mutant strains, all placed on the CR diet. I found that lack of Fox1p, Fox2p or Fox3p: 1) in cells entering D phase, drastically increases $\Delta\Psi$, thereby leading to the hyper-polarization of the inner mitochondrial membrane (Figures 3.13J and 3.13M); and 2) in cells entering PD phase, results in an abrupt decline of $\Delta\Psi$ (Figures 3.13J and 3.13M), thereby rapidly abrogating the $\Delta\Psi$-dependent processes in mitochondria, including the transport of solutes and the synthesis of ATP.

It should be stressed that, although the inability of each of the three *fox* mutants to form acetyl-CoA via peroxisomal FFA oxidation caused the above age-related changes in essential mitochondrial processes, it did not affect the abundance of mitochondria in CR yeast. Indeed, the levels of porin, one of the most abundant mitochondrial proteins, were very similar in WT, *fox1Δ*, *fox2Δ* and *fox3Δ* cells (Figure 3.13L). However, the morphology of mitochondria in CR cells of the *fox* mutants was altered. Mitochondria in chronologically aging WT formed a tubular network (Figure 3.13I). In contrast, in each of the three *fox* mutants, this network was fragmented into individual mitochondria (Figure 3.13I). Thus, the efficiency with which peroxisomes supply acetyl-CoA for its
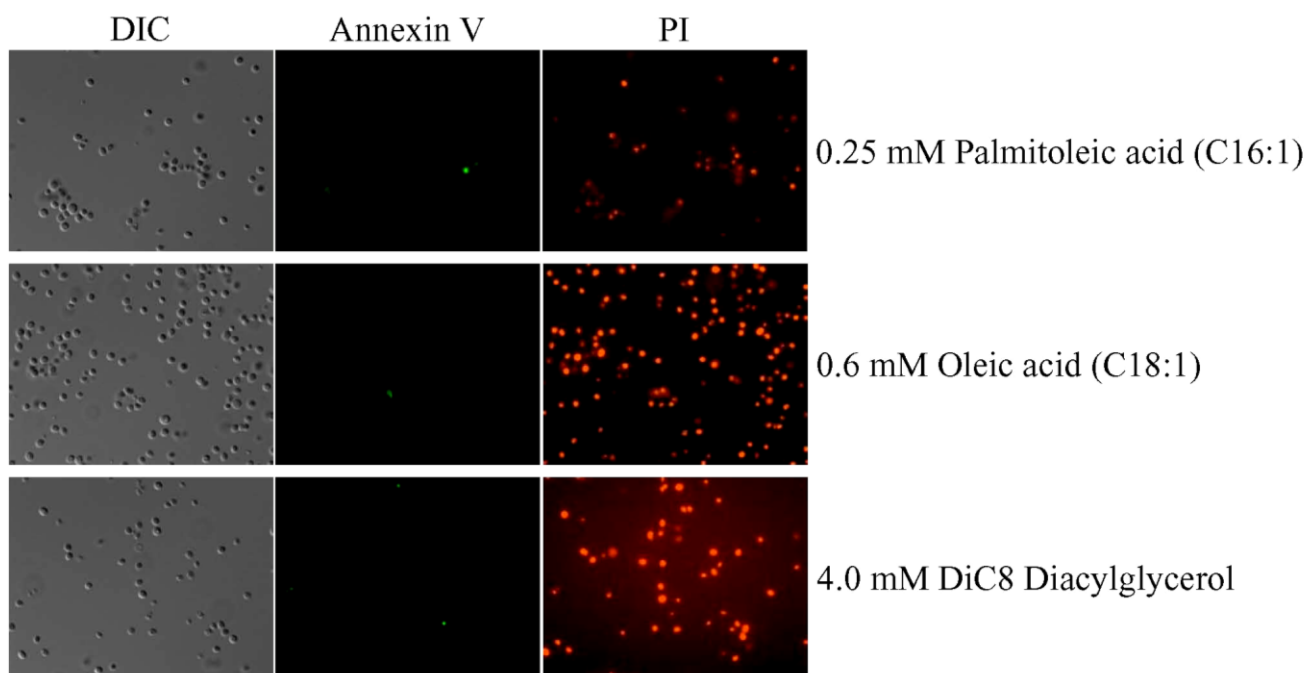
Figure 3.15. A short-term exposure to exogenously added FFA and DAG causes necrotic, not apoptotic, cell death. Fluorescence microscopy of WT yeast treated for 2 h with 0.25 mM palmitoleic acid, 0.6 mM oleic acid or 4.0 mM DiC8 diacylglycerol. Cells were co-stained with 1) Annexin V for visualizing the externalization of phosphatidylserine, a hallmark event of apoptosis; and 2) propidium iodide (PI) for visualizing the loss of plasma membrane integrity, a hallmark event of necrosis. Abbreviations: DIC, differential interference contrast.

oxidation via the TCA cycle in mitochondria modulates, by a yet-to-be established mechanism, the balance of fission and fusion of mitochondrial tubules. Such delicate balance plays a pivotal role in establishing and maintaining the shape of mitochondria [248, 249]. Notably, a balance between the opposing processes of mitochondrial fission and fusion modulates the ability of yeast to survive a short-term exposure to hydrogen peroxide or acetic acid, each of which induces a mitochondria-controlled, caspase-dependent pathway of apoptosis [250 - 252]. In fact, mitochondrial fragmentation due to excessive mitochondrial fission plays a casual role in this form of programmed cell death

132

[252 - 254]. Importantly, the observed fragmentation of the mitochondrial network in cells of each of the three prematurely aging *fox* mutants coincided with their increased susceptibility to mitochondria-controlled, hydrogen peroxide- and acetic acid-induced apoptosis (Figures 3.14B and 3.14C).

3.4.9. Free fatty acids (FFA) and diacylglycerol (DAG) regulate longevity by two different mechanisms that operate at two different stages of the aging process

As I found, a short-term exposure to exogenously added FFA (*i.e.*, palmitoleic acid and oleic acid) and DAG induces necrotic cell death in chronologically aging yeast (Figure 3.15) [222]. To test the validity of my hypothesis (see section 3.4.8 of this Chapter) that the accumulation of FFA and DAG in yeast shortens their chronological life span by triggering cell death (apoptotic and/or necrotic), I first compared the susceptibility of WT, *fox1Δ*, *fox2Δ* and *fox3Δ* to a short-term exposure to exogenous FFA and DAG. Under CR conditions, each of the three *fox* mutations caused the build-up of both these lipids in LBs as soon as cells entered ST phase (Figures 3.11G and 3.11H). The observed during ST phase rapid accumulation of FFA and DAG in LBs of the *fox* mutants coincided with a prompt decline in the percentage of their viable cells during this phase (Figure 3.11C). Importantly, despite the observed build-up of FFA and DAG in *fox* cells beginning of ST phase, none of the *fox* mutations had an effect on the susceptibility of yeast to necrotic cell death induced in response to their short-term exposure to exogenous FFA or DAG (Figures 3.14D-3.14F). In contrast, as I found (see section 3.4.8 of this Chapter), all three *fox* mutations increased the susceptibility of yeast to mitochondria-

controlled, hydrogen peroxide- and acetic acid-induced apoptosis (Figures 3.14B and 3.14C). Importantly, unlike CR cells of each of the three *fox* mutants that reached ST phase, CR cells of these mutants during PD phase did not accumulate FFA or DAG (Figures 3.11G and 3.11H) and were viable (Figure 3.11C), and did not differ from WT cells in their susceptibility to cell death induced by exogenous FFA or DAG (Figures 3.14D-3.146F, left panels). Altogether, these findings suggest that the observed during ST phase rapid build-up of FFA and DAG in LBs of the *fox* mutants causes their premature aging by promoting mitochondria-controlled apoptotic cell death, but not by activating FFA- and DAG-induced necrotic cell death pathway.

As a further test of the validity of my hypothesis (see section 3.4.8 of this Chapter) on the essential negative role of FFA and DAG in regulating longevity by promoting cell death, I then measured the chronological life spans of mutants impaired in the biosynthesis or degradation of TAG (Figure 3.16). Importantly, most of the enzymes involved in these metabolic pathways are redundant and all of these redundant enzymes are not essential proteins (Figure 3.16) [212, 255]. I reasoned that, in the absence of any of them, cells would still be able to produce FFA and DAG. However, lack of any of them would change the concentration of each of these two lipid species (Figure 3.16). I expected therefore that, if my hypothesis is correct, any mutation that reduces the concentration of a critical lipid (*i.e.*, FFA and/or DAG) by eliminating a redundant enzyme would extend the life span of CR yeast. Conversely, any mutation that increases the concentration of a critical lipid by eliminating a redundant enzyme would shorten the life span of CR yeast. Concomitantly with measuring the life spans of the mutants lacking individual redundant enzymes of the metabolic pathways depicted in Figure 3.16, I

monitored their FFA and DAG levels at different stages of the aging process and their
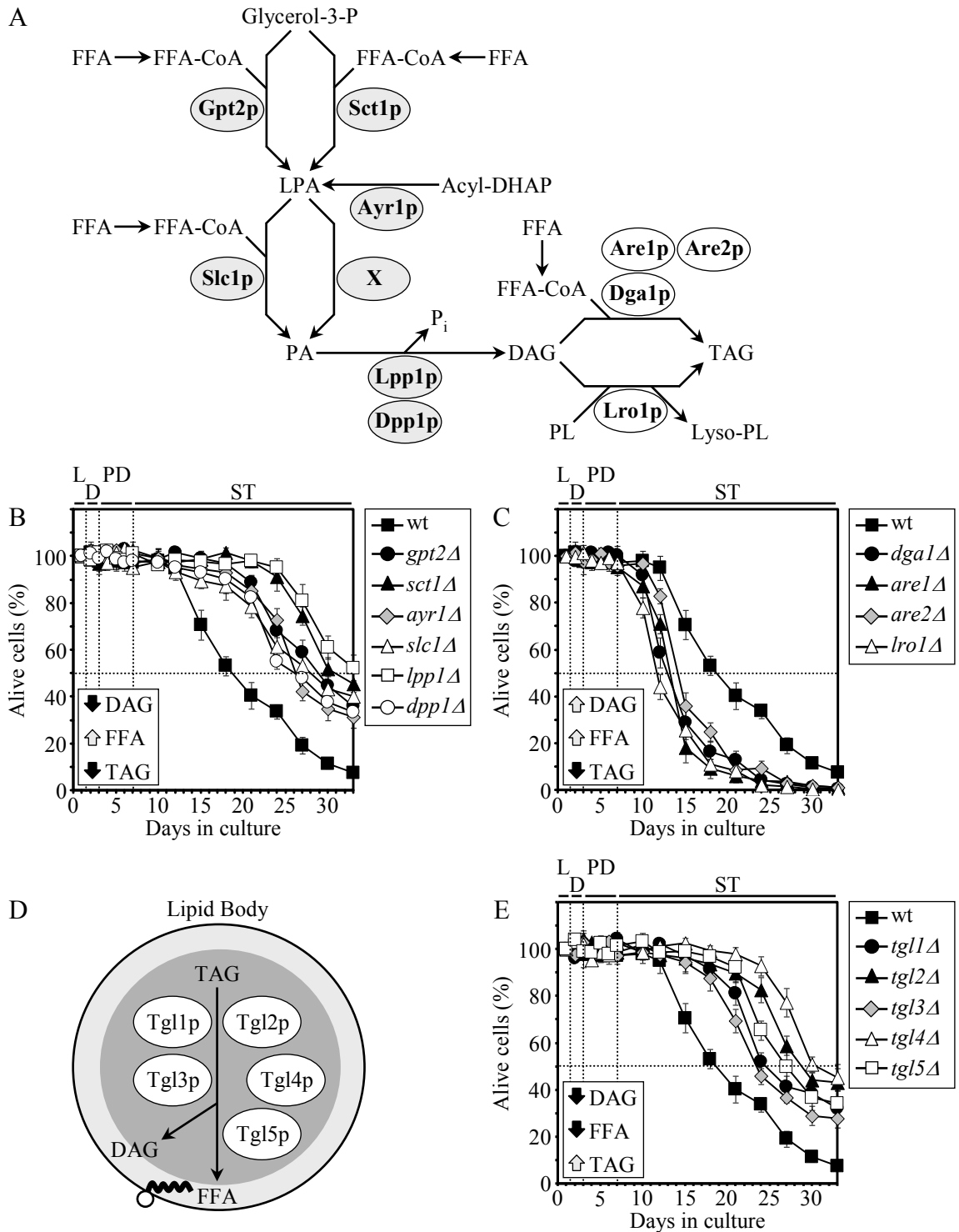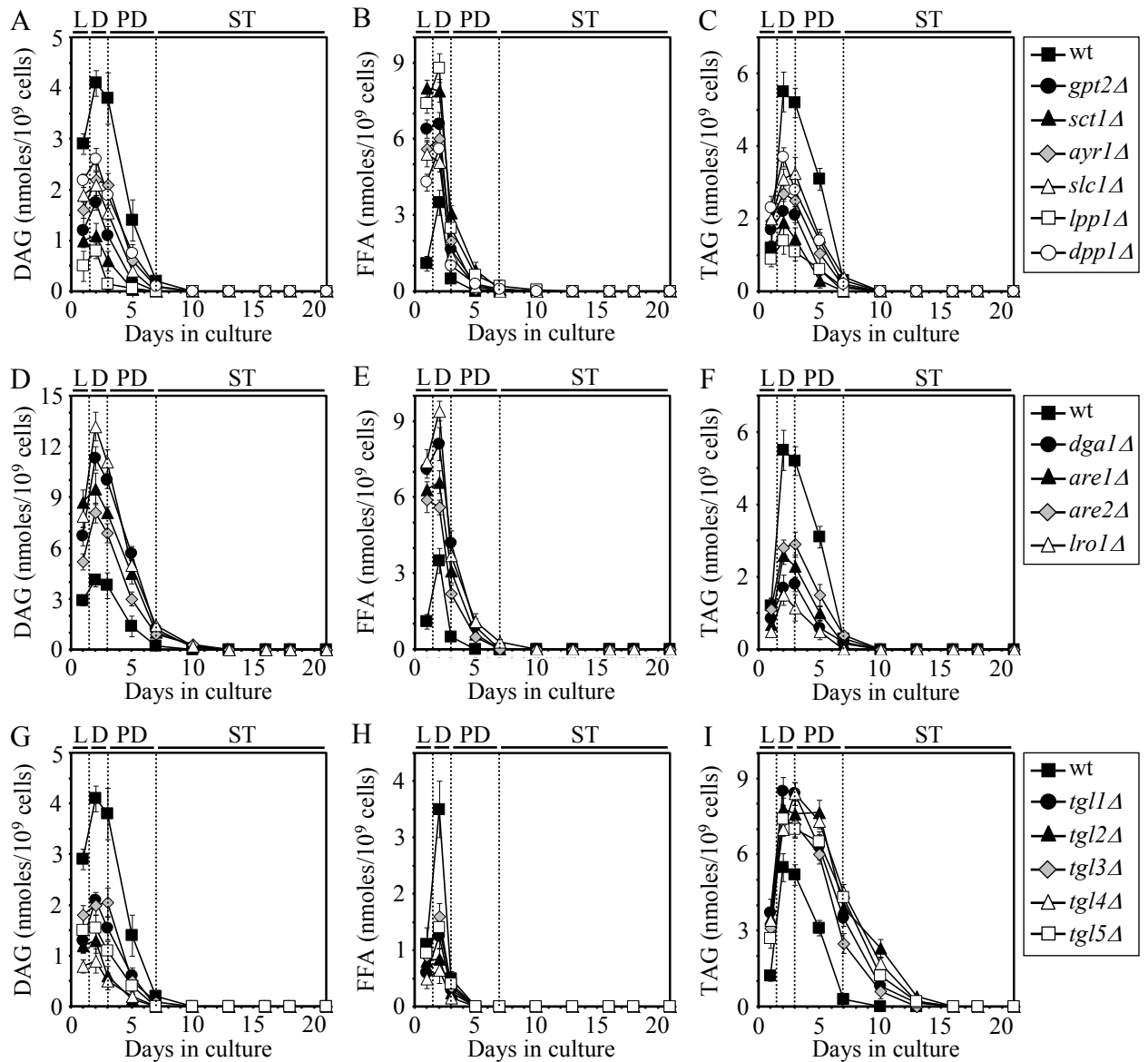

Figure 3.16. Any mutation that reduces the level of DAG by eliminating a redundant enzyme involved in the biosynthesis or degradation of triacylglycerols (TAG) extends the life span of CR yeast. (A and D) Outline of metabolic pathways for the biosynthesis (A) and degradation (D) of TAG. (B, C and E) Survival

of WT strain and single-gene-deletion mutant strains, each lacking a redundant enzyme involved in the biosynthesis (B and C) or degradation (E) of TAG. Data are presented as mean ± SEM (n = 3). Some of the mutations increase (⇧) the concentrations of diacylglycerol (DAG), free fatty acids (FFA) or TAG, whereas the other mutations decrease (⬇) them. Cells were cultured in YP medium initially containing 0.2% glucose.

susceptibility to FFA- and DAG-induced cell death.

I found that any mutation that reduces the level of DAG by eliminating a redundant enzyme extends the life span of CR yeast, regardless of its effect on the level of FFA (Figure 3.16). In fact, the ability of mutations eliminating individual redundant enzymes of DAG biosynthesis or TAG degradation to extend life span coincided with their ability to decrease DAG concentration but did not correlate with the specific changes in the concentration of FAA they caused (Figures 3.16B and 3.16E). Moreover, any mutation that increases the level of DAG by eliminating a redundant enzyme of TAG biosynthesis from DAG shortens the life span of CR yeast (Figure 3.16C). Noteworthy, the effect of all of these life-span shortening mutations on the level of FFA was very similar to that of the life-span extending mutations eliminating individual redundant enzymes of DAG biosynthesis (compare Figures 3.16B and 3.16C). It should be stressed that, although any mutation that eliminates a redundant enzyme involved in the biosynthesis or degradation of TAG extended or shortened life span by increasing or decreasing cell viability during ST phase (Figure 3.16), it altered the concentrations of FFA and DAG only during the preceding D and PD phases (Figure 3.17). Indeed, akin to WT cells, cells of the mutant strains carrying any of these mutations entirely consumed both FFA and DAG prior to entry into ST phase (Figure 3.17). I therefore concluded that the viability of yeast during ST phase could be programmed, in part, by the concentration of DAG that yeast are able

Figure 3.17. Any mutation that eliminates a redundant enzyme involved in the biosynthesis or degradation of triacylglycerols (TAG) alters the concentrations of FFA and DAG during growth phases preceding the non-proliferative ST phase. The dynamics of age-dependent changes in the levels of diacylglycerol (DAG) (A, D and G), free fatty acids (FFA) (B, E and H) and TAG (C, F and I) during chronological aging of WT strain and single-gene-deletion mutant strains, each lacking a redundant enzyme involved in the biosynthesis (A - F) or degradation (G - I) of TAG. Data are presented as mean ± SEM (n = 3). Cells were cultured in rich YP medium containing 0.2% glucose.

to maintain during D and PD phase in a diet- and genotype-dependent fashion. On the contrary, my findings imply that the concentration of FFA during D and PD phase does

not influence the viability of CR yeast during ST phase. Furthermore, the observed lack of correlation between the life spans of mutant strains missing individual redundant enzymes of DAG biosynthesis or TAG degradation and the levels of TAG maintained during D, PD and ST phases in their cells (Figures 3.16 and 3.17) implies that TAG species do not regulate longevity.

I then examined how the *lpp1Δ*, *lro1Δ* and *tgl4Δ* mutations, each having a different effect on the intracellular levels of FFA and DAG in CR yeast during D and PD phases by eliminating a different redundant enzyme involved in the biosynthesis or degradation of TAG, influences the susceptibility of CR yeast to 1) mitochondria-controlled apoptotic cell death caused by their short-term exposure to exogenous hydrogen peroxide or acetic acid; and 2) necrotic cell death caused by their short-term exposure to exogenous FFA or DAG. The results of this kind of analysis are outlined below.

The *lpp1Δ* mutation: 1) increases the chronological life span (Figure 3.16B) of CR yeast; 2) reduces the intracellular concentration of DAG during D and PD phases (Figure 3.17A): 3) increases the intracellular concentration of FFA during D and PD phases (Figure 3.17B); and 4) does not prevent the complete consumption of the intracellular pools of DAG and FFA prior to entry into ST phase (Figures 3.17A and 3.17B). I found that the *lpp1Δ* mutation: 1) does not alter the susceptibility of CR yeast to mitochondria-controlled apoptotic cell death caused by their short-term exposure to exogenous hydrogen peroxide or acetic acid (Figures 3.18A and 3.18B); but 2) increases the resistance of CR yeast to necrotic cell death caused by a short-term exposure to exogenous FFA or DAG (Figures 3.18C, 3.18D and 3.18E).
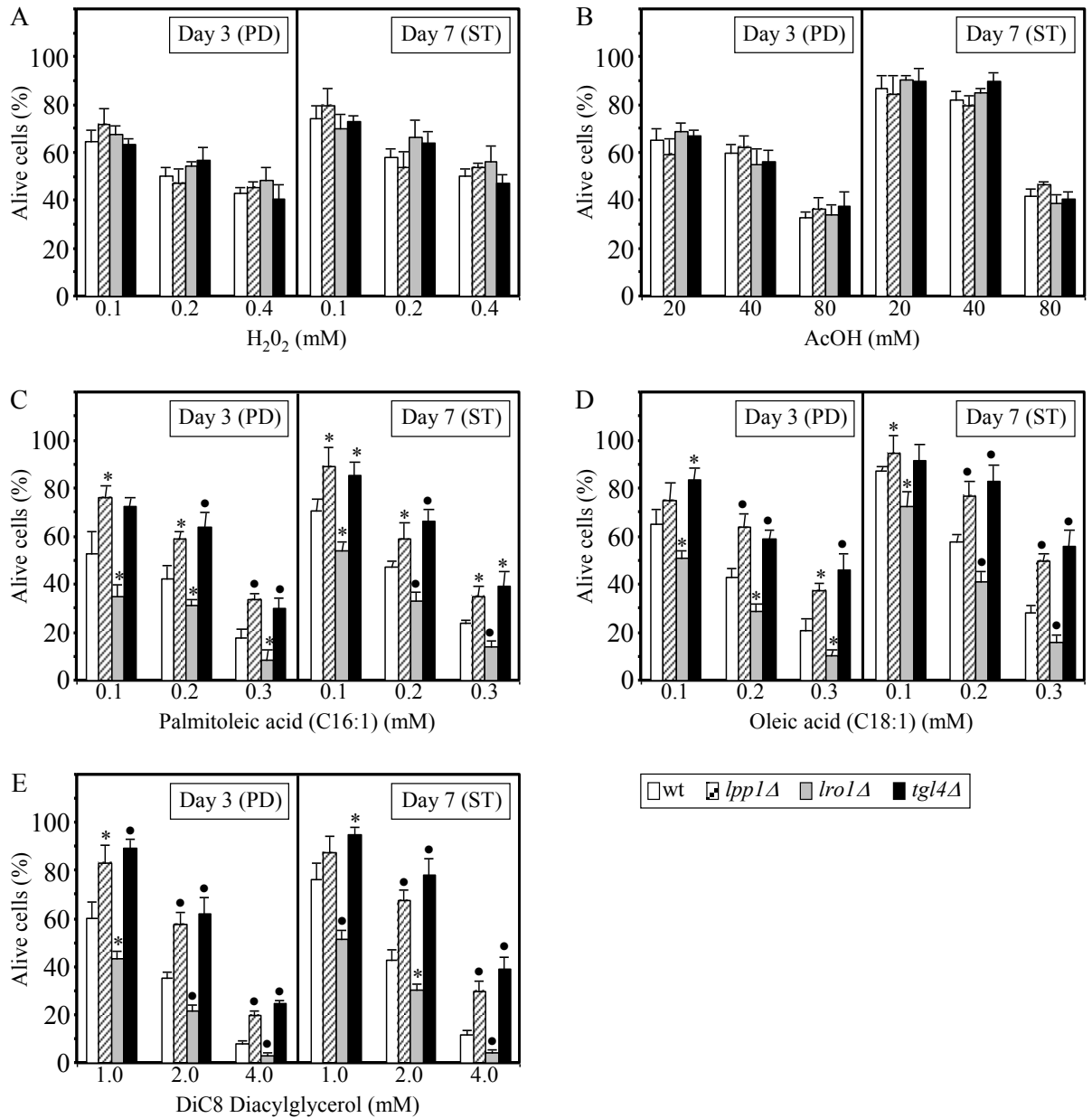
Figure 3.18. The single-gene-deletion mutations that alter DAG concentration prior to entry into ST phase have no effect on the mitochondrial pathway of programmed cell death, but alter the susceptibility of CR yeast to the programmed necrotic death. Viability of WT, *lpp1Δ*, *lro1Δ* and *tgl4Δ* cells treated with different concentrations of hydrogen peroxide (A), acetic acid (B), palmitoleic acid (C), oleic acid (D) or DiC8 diacylglycerol (E). Data are presented as mean ± SEM (n = 3). *p < 0.05, •p < 0.005. Cells were cultured in YP medium containing 0.2% glucose.

The *lro1Δ* mutation: 1) shortens the chronological life span (Figure 3.16C) of CR

yeast; 2) increases the intracellular concentration of DAG during D and PD phases (Figure 3.17D): 3) increases the intracellular concentration of FFA during D and PD phases (Figure 3.17E); and 4) does not prevent the complete consumption of the intracellular pools of DAG and FFA prior to entry into ST phase (Figures 3.17D and 3.17E). I found that the *lro1Δ* mutation: 1) does not alter the susceptibility of CR yeast to mitochondria-controlled apoptotic cell death caused by their short-term exposure to exogenous hydrogen peroxide or acetic acid (Figures 3.18A and 3.18B); but 2) reduces the resistance of CR yeast to necrotic cell death caused by a short-term exposure to exogenous FFA or DAG (Figures 3.18C, 3.18D and 3.18E).

The *tgl4Δ* mutation: 1) increases the chronological life span (Figure 3.16E) of CR yeast; 2) reduces the intracellular concentration of DAG during D and PD phases (Figure 3.17G): 3) reduces the intracellular concentration of FFA during D and PD phases (Figure 3.17H); and 4) does not prevent the complete consumption of the intracellular pools of DAG and FFA prior to entry into ST phase (Figures 3.17G and 3.17H). I found that the *tgl4Δ* mutation: 1) does not alter the susceptibility of CR yeast to mitochondria-controlled apoptotic cell death caused by their short-term exposure to exogenous hydrogen peroxide or acetic acid (Figures 3.18A and 3.18B); but 2) increases the resistance of CR yeast to necrotic cell death caused by a short-term exposure to exogenous FFA or DAG (Figures 3.18C, 3.18D and 3.18E).

Altogether, my findings imply that FFA and DAG regulate longevity by two different mechanisms that operate at two different stages of the aging process. One mechanism involves sensing the concentration of DAG maintained by cells (in a diet- and genotype-dependent fashion) during D and PD growth phases. DAG concentration during

D and PD phases programs cell viability during ST growth phase by modulating the FFA- and DAG-induced necrotic cell death pathway, but not by influencing the mitochondria-controlled apoptotic pathway of cell death. Another mechanism involves sensing the concentrations of FFA and DAG during ST phase. Any diet or genetic manipulation that causes the build-up of these two lipids during ST phase shortens the chronological life span of yeast in part by promoting rapid mitochondria-controlled apoptotic cell death, but not by activating FFA- and DAG-induced necrotic cell death pathway.

3.5. Discussion

Using a combination of functional genetic, cell biological, electron and fluorescence microscopical, proteomic, lipidomic, and metabolomic analyses, I established the molecular mechanism underlying the ability of CR to extend longevity of chronologically aging yeast by specifically remodelling lipid metabolism in the ER, LBs and peroxisomes. In this mechanism, LBs in yeast cells function as a hub in a regulatory network that modulates neutral lipids synthesis in the ER and fatty acid oxidation in peroxisomes. Ethanol accumulated in yeast placed on a calorie-rich diet represses the synthesis of Fox1p, Fox2p and Fox3p, thereby suppressing peroxisomal oxidation of FFA that originate from TAG synthesized in the ER and deposited within LBs. The resulting build-up of arrays of FFA (called gnarls) within LBs of non-CR yeast initiates several negative feedback loops regulating the metabolism of TAG. Due to the action of these negative feedback loops, chronologically aging non-CR yeast not only amass TAG in LBs but also accumulate FFA and DAG in the ER. FFA and DAG regulate longevity by two different mechanisms that operate at two different stages of the aging process. One

mechanism involves sensing the concentration of DAG maintained by cells (in a diet- and genotype-dependent fashion) during D and PD growth phases. DAG concentration during D and PD phases programs cell viability during the non-proliferative ST growth phase by modulating the FFA- and DAG-induced necrotic cell death pathway, but not by influencing the mitochondria-controlled apoptotic pathway of cell death. Another mechanism involves sensing the concentrations of FFA and DAG during ST phase. Any diet or genetic manipulation that causes the build-up of these two lipids during ST phase shortens the chronological life span of yeast in part by promoting rapid mitochondria-controlled apoptotic cell death, but not by activating FFA- and DAG-induced necrotic cell death pathway.

The proposed above mechanism can satisfactorily explain my data on the observed effects of various dietary and genetic interventions that I examined on age-related lipid dynamics and longevity. My explanations of these effects for each intervention I used are outlined below within the framework of the proposed here mechanism.

Chronologically aging WT cells placed on a calorie-rich diet generate the bulk of ATP via glycolytic oxidation of glycogen- and trehalose-derived glucose (Figure 3.19A). These cells accumulate ethanol, a product of glucose fermentation (Figure 3.19A). By repressing the synthesis of Fox1p, Fox2p and Fox3p, ethanol suppresses peroxisomal oxidation of FFA that originate from TAG synthesized in the ER and deposited within LBs. The low efficiency of peroxisomal oxidation of FFA causes the build-up of gnarls (the arrays of FFA) within LBs (Figure 3.19A). This, in turn, initiates several negative feedback loops that regulate the metabolism of TAG and ultimately result in the accumulation of TAG in LBs as well as FFA and DAG in the ER. Because DAG in WT
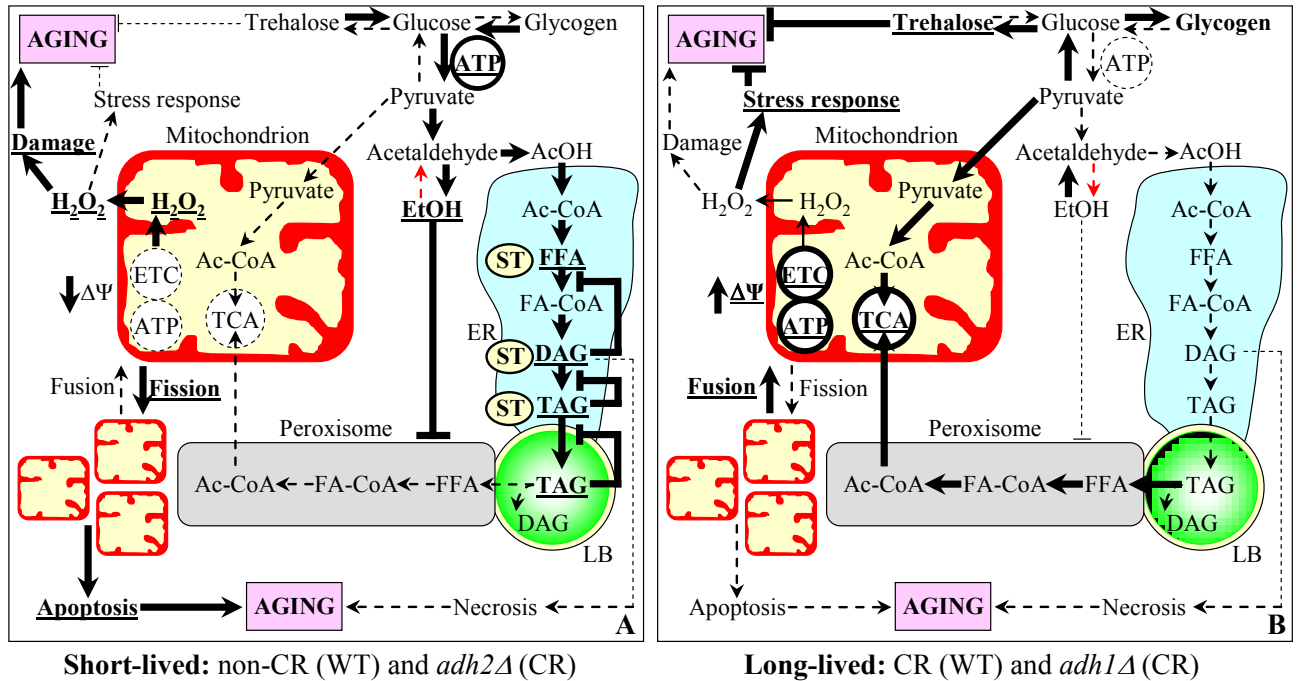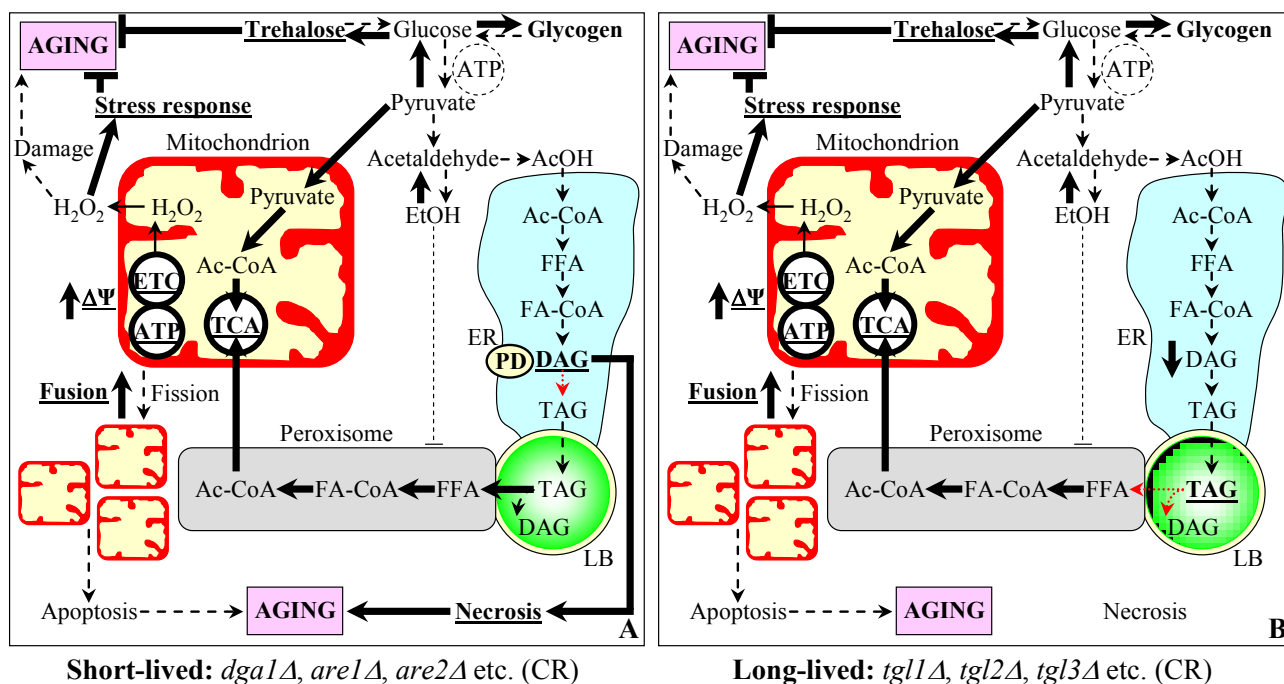
Figure 3.19. Outline of metabolic pathways and interorganellar communications operating in chronologically aging cells of WT and *adh* mutant strains grown under CR or non-CR conditions. The longevity-defining features of the diet- or mutation-driven metabolic design for each strain and growth condition are discussed in details in the Discussion section of this Chapter.

cells under non-CR conditions amasses only in the non-proliferative ST growth phase, it does not activate the age-related necrotic cell death pathway and, thus, does not play a role in shortening the chronological life span of these cells (Figure 3.19A). The reduced life span of WT cells placed on a calorie-rich diet is due to their rapid apoptotic death controlled by mitochondria and initiated upon their entry into ST phase. The primary reason for such activation of an age-related form of mitochondria-controlled apoptosis lies in the low levels of enzymes functioning in the formation of FA-CoA and in their uptake and subsequent oxidation by peroxisomes seen in non-CR WT cells. The diminished ability of these cells to oxidize FFA to acetyl-CoA via a peroxisome-confined pathway

143
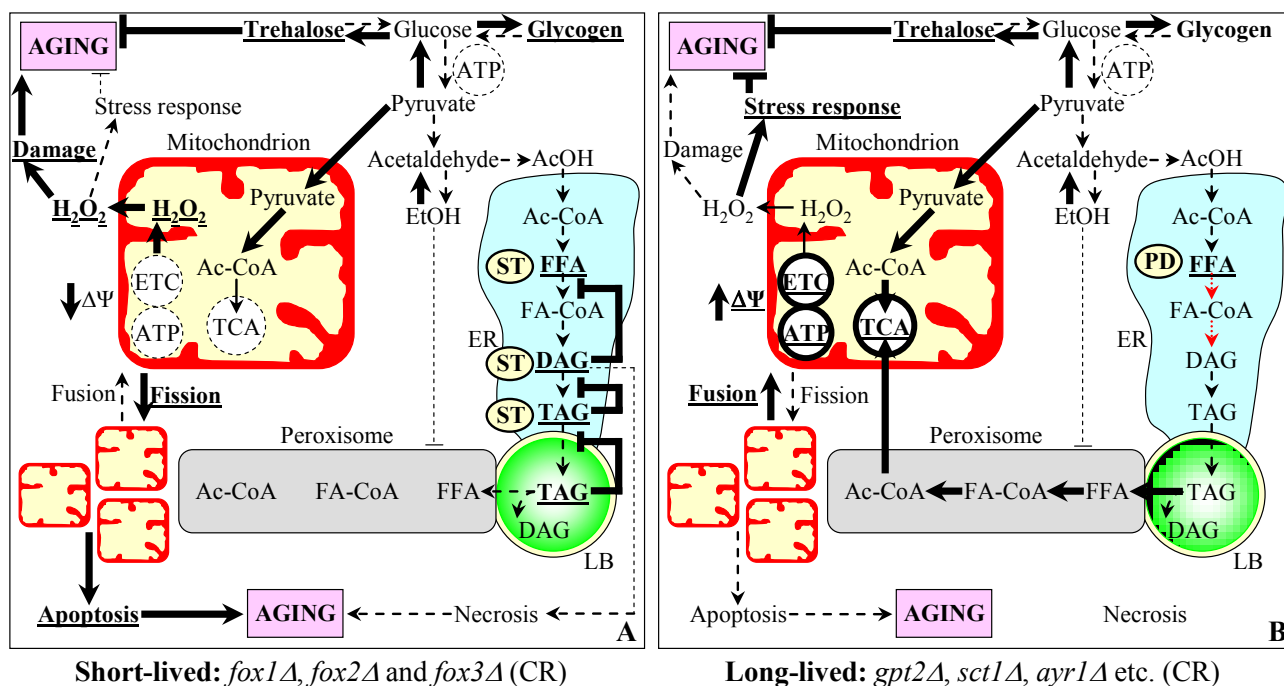
Figure 3.20. Outline of metabolic pathways and interorganellar communications operating in chronologically aging cells of *fox1Δ* and other mutant strains grown under CR conditions. The longevity-defining features of the mutation-driven metabolic design for each mutant strain and growth condition are discussed in details in the Discussion section of this Chapter.

during ST phase greatly impairs their ability to generate significant quantities of ATP by oxidizing peroxisome-derived acetyl-CoA in mitochondria. The resulting decline in oxidation-reduction processes within mitochondria 1) reduces the flow of electron pairs through the mitochondrial ETC, thereby intensifying the transfer of single electrons on molecular oxygen and the resulting production of excessive ROS, which accelerate aging by causing oxidative molecular damage; 2) decreases the electrochemical gradient across the inner mitochondrial membrane ($\Delta\Psi$); and 3) causes mitochondrial fragmentation by promoting fission of the mitochondrial tubular network (Figure 3.19A). The fragmentation of mitochondria in WT cells placed on a calorie-rich diet occurs upon their

Figure 3.21. Outline of metabolic pathways and interorganellar communications operating in chronologically aging cells of *dga1Δ* and other mutant strains grown under CR conditions. The longevity-defining features of the mutation-driven metabolic design for each mutant strain and growth condition are discussed in details in the Discussion section of this Chapter.

entry into ST phase and initiates the life-shortening process of age-related death, which is driven by the release of pro-apoptotic factors from fragmented mitochondria (Figure 3.19A). Of note, the low levels of trehalose in chronologically aging WT cells placed on a calorie-rich diet is another factor that could contribute to shortening their life span, as compared to WT cells grown under CR conditions (Figure 3.19A). Although trehalose has been long considered only as a reserve carbohydrate [256], it seems that the major function of this non-reducing disaccharide in yeast consists in enabling the survival of cells exposed to elevated temperature or ROS [257 - 259]. In fact, trehalose in yeast cells prevents aggregation of proteins denatured during and immediately after their exposure to these stresses [260]. I therefore propose that the reduced levels of trehalose seen in non-

CR cells of WT strain during PD phase are unable to protect from aggregation those proteins that have been denatured due to their exposure to ROS accumulated during this growth phase (Figure 3.19A). Lack of such protective effect of trehalose in WT cells grown under non-CR conditions, due to the low concentrations of this non-reducing disaccharide (as compared to CR cells of WT strain), could contribute to the reduced (as compared WT cells grown under CR conditions) survival of non-CR cells during the following ST phase.

Within the framework of the proposed here mechanism, WT cells grown under CR conditions have extended chronological life span (as compared to that of WT cells placed on a calorie-rich diet) due to the following features of their diet-driven metabolic design (Figure 3.19B): 1) the very low level of ethanol, which therefore is unable to repress the synthesis of Fox1p, Fox2p and Fox3p and to suppress peroxisomal oxidation of FFA that originate from TAG synthesized in the ER and deposited within LBs; 2) lack of gnarls, due to the rapid oxidation of FFA in peroxisomes, and the resulting inability to initiate several negative feedback loops that regulate the metabolism of TAG and would ultimately result in the accumulation of TAG in LBs as well as FFA and DAG in the ER; 3) the very low level of DAG in PD phase and the complete consumption of this lipid in ST phase (it should be stressed that, if DAG amasses in PD phase, it can initiate age-related necrotic cell death; see below); 4) the highly efficient ability to oxidize FFA to acetyl-CoA via a peroxisome-confined pathway during ST phase, which not only allows cells to generate the bulk of ATP by oxidizing peroxisome-derived acetyl-CoA in mitochondria but also activates oxidation-reduction processes in mitochondria, maintains high $\Delta\Psi$, and prevents the fragmentation of the mitochondrial tubular network - thereby

protecting cells from age-related form of apoptotic death controlled by mitochondria; and 5) the elevated level trehalose, which contributes to the life span extension seen in CR cells of WT strain by protecting from aggregation those proteins that have been denatured due to their exposure to mitochondrially produced ROS.

Within the framework of the proposed here mechanism, *adh2Δ* cells under CR conditions have shortened chronological life span (as compared to that of calorie-limited WT cells) due to the following features of their *adh2Δ* mutation-driven metabolic design (Figure 3.19A): 1) the elevated level of ethanol, which therefore is able to repress the synthesis of Fox1p, Fox2p and Fox3p and to suppress peroxisomal oxidation of FFA that originate from TAG synthesized in the ER and deposited within LBs; 2) the build-up of gnarls within LBs, due to suppressed oxidation of FFA in peroxisomes, and the resulting initiation of several negative feedback loops that regulate the metabolism of TAG and ultimately result in the accumulation of TAG in LBs as well as FFA and DAG in the ER; 3) the reduced efficiency of oxidizing FFA to acetyl-CoA via a peroxisome-confined pathway during ST phase, which not only impairs ATP synthesis in mitochondria but also leads to a decline in oxidation-reduction processes within mitochondria, enhances mitochondrial ROS production, decreases $\Delta\Psi$ and causes fragmentation of the mitochondrial tubular network - thereby promoting the age-related form of apoptotic cell death controlled by mitochondria and shortening life span.

Within the framework of the proposed here mechanism, *adh1Δ* cells under CR conditions have increased chronological life span (as compared to that of calorie-limited WT cells) due to the following features of their *adh1Δ* mutation-driven metabolic design (Figure 3.19B): 1) the greatly reduced level of ethanol, which therefore is unable to

repress the synthesis of Fox1p, Fox2p and Fox3p and to suppress peroxisomal oxidation of FFA that originate from TAG synthesized in the ER and deposited within LBs; 2) lack of gnarls, due to the accelerated oxidation of FFA in peroxisomes, and the resulting inability to initiate several negative feedback loops that regulate the metabolism of TAG and would ultimately result in the accumulation of TAG in LBs as well as FFA and DAG in the ER; 3) the very low level of DAG in PD phase and the complete consumption of this lipid in ST phase (it should be stressed that, if DAG amasses in PD phase, it can initiate age-related necrotic cell death; see below); 4) the enhanced ability to oxidize FFA to acetyl-CoA via a peroxisome-confined pathway during ST phase, which not only allows cells to generate the bulk of ATP by oxidizing peroxisome-derived acetyl-CoA in mitochondria but also activates oxidation-reduction processes in mitochondria, maintains high $\Delta\Psi$, and prevents the fragmentation of the mitochondrial tubular network - thereby protecting cells from age-related form of apoptotic death controlled by mitochondria; and 5) the greatly elevated level trehalose, which contributes to the life span extension seen in CR cells of *adh1Δ* strain by protecting from aggregation those proteins that have been denatured due to their exposure to mitochondrially produced ROS.

Within the framework of the proposed here mechanism, *fox1Δ* , *fox2Δ* and *fox3Δ* cells grown under CR conditions have shortened chronological life span (as compared to that of calorie-limited WT cells) due to the following features of their *fox* mutation-driven metabolic design (Figure 3.20A): 1) the complete inability to oxidize FFA that originate from TAG synthesized in the ER and deposited within LBs; 2) the build-up of gnarls within LBs, due to impaired oxidation of FFA in peroxisomes, and the resulting initiation of several negative feedback loops that regulate the metabolism of TAG and

ultimately result in the accumulation of TAG in LBs as well as FFA and DAG in the ER (it should be stressed that, although *fox1Δ* , *fox2Δ* and *fox3Δ* cells grown under CR conditions amass DAG, they do so only in ST phase; therefore, the shortened life spans of these cells is not due to accelerated age-related necrotic cell death, which can be initiated by DAG only if it accumulates in PD phase - see below); and 3) the inability to oxidize FFA to acetyl-CoA via a peroxisome-confined pathway during ST phase not only impairs ATP synthesis in mitochondria but also leads to a decline in oxidation-reduction processes within mitochondria, enhances mitochondrial ROS production, decreases $\Delta\Psi$ and causes fragmentation of the mitochondrial tubular network - thereby promoting the age-related form of apoptotic cell death controlled by mitochondria and shortening life span.

Within the framework of the proposed here mechanism, *gpt2Δ, sct1Δ, ayr1Δ, slc1Δ, lpp1Δ* and *dpp1Δ* cells grown under CR conditions have increased chronological life span (as compared to that of calorie-limited WT cells) due to the reduced level of DAG in D and PD phases (Figures 3.17A and 3.20B). As I found, DAG concentration during D and PD phases programs cell viability during ST growth phase by modulating the FFA- and DAG-induced necrotic cell death pathway, but not by influencing the mitochondria-controlled apoptotic pathway of cell death. Thus, the reduced (as compared to calorie-limited WT cells) level of DAG in D and PD phases extends the chronological life spans of *gpt2Δ, sct1Δ, ayr1Δ, slc1Δ, lpp1Δ* and *dpp1Δ* cells grown under CR by delaying their age-related, FFA- and DAG-induced necrotic cell death during ST phase (Figure 3.20B).

Within the framework of the proposed here mechanism, *dga1Δ, are1Δ, are2Δ* and

lro1Δ cells grown under CR conditions have reduced chronological life span (as compared to that of calorie-limited WT cells) due to the elevated level of DAG in D and PD phases (Figures 3.17D and 3.21A). As I found, DAG concentration during D and PD phases programs cell viability during ST growth phase by modulating the FFA- and DAG-induced necrotic cell death pathway, but not by influencing the mitochondria-controlled apoptotic pathway of cell death. Thus, the elevated (as compared to calorie-limited WT cells) level of DAG in D and PD phases shortens the chronological life spans of *dga1Δ*, *are1Δ*, *are2Δ* and *lro1Δ* cells grown under CR conditions by accelerating their age-related, FFA- and DAG-induced necrotic cell death during ST phase (Figure 3.21A).

Within the framework of the proposed here mechanism, *tgl1Δ*, *tgl2Δ*, *tgl3Δ*, *tgl4Δ* and *tgl5Δ* cells grown under CR conditions have increased chronological life span (as compared to that of calorie-limited WT cells) due to the reduced level of DAG in D and PD phases (Figures 3.17G and 3.21B). As I found, DAG concentration during D and PD phases programs cell viability during ST growth phase by modulating the FFA- and DAG-induced necrotic cell death pathway, but not by influencing the mitochondria-controlled apoptotic pathway of cell death. Thus, the reduced (as compared to calorie-limited WT cells) level of DAG in D and PD phases extends the chronological life spans of *tgl1Δ*, *tgl2Δ*, *tgl3Δ*, *tgl4Δ* and *tgl5Δ* cells grown under CR conditions by delaying their age-related, FFA- and DAG-induced necrotic cell death during ST phase (Figure 3.20B).

3.6. Conclusions

My functional genetic, cell biological, electron and fluorescence microscopical, proteomic, lipidomic, and metabolomic analyses resulted in defining the molecular

mechanism underlying the ability of CR to extend longevity of chronologically aging yeast by specifically remodelling lipid metabolism in the ER, LBs and peroxisomes. I expect that this knowledge will be instrumental for designing high-throughput screening of novel anti-aging drugs that can extend longevity by targeting different aspects of this mechanism.

4. A mechanism underlying the ability of a novel anti-aging drug to extend yeast life span by targeting the longevity-defining aspects of lipid metabolism confined to the ER, LBs and peroxisomes

4.1. Abstract

As described in Chapter 3 of this thesis, I established the molecular mechanism underlying the ability of caloric restriction (CR) to extend longevity of chronologically aging yeast by specifically remodelling lipid metabolism in the endoplasmic reticulum (ER), lipid bodies (LBs) and peroxisomes. This knowledge has been instrumental for choosing the single-gene-deletion mutant *pex5Δ* as a short-lived mutant strain for high-throughput screen of novel anti-aging drugs that can extend longevity by targeting such mechanism under CR conditions. In experiments described in this Chapter, I first elucidated how the *pex5Δ* mutation affects different aspects of the mechanism linking longevity and lipid metabolism in the ER, LBs and peroxisomes. I found that in yeast placed on a CR diet this mutation leads to: 1) increase in free fatty acids (FFA), diacylglycerols (DAG), triacylglycerols (TAG) and ergosteryl esters (EE) and their build-up in the ER and LBs; 2) excessive accumulation of the ER membranes and ER-originated LBs; and 3) enhanced susceptibility to necrotic cell death caused to a short-term exposure to exogenously added FFA and DAG. Using the short-lived *pex5Δ* mutant strain, Alexander Goldberg in Dr. Titorenko's laboratory conducted a high-throughput screen of novel anti-aging compounds that can extend the chronological life span (CLS) of yeast by targeting these longevity-defining aspects of lipid metabolism under CR conditions. One of the life-extending compounds identified in such screen was lithocholic

acid (LCA), a bile acid. Studies in Dr. Titorenko's laboratory revealed that LCA greatly extends the CLS of wild-type (WT) strain of yeast placed on a CR diet. By elucidating how LCA influences the metabolism of lipids as well as age-related forms of necrotic and apoptotic death in chronologically aging yeast and how it alters yeast proteome, in experiments described in this Chapter I established the molecular mechanism underlying the ability of LCA to extend yeast CLS by targeting these longevity-defining aspects of lipid metabolism confined to the ER, LBs and peroxisomes. In such mechanism, under CR conditions LCA accelerates the biosynthesis of TAG from FFA and DAG in the ER as well as decelerates the FFA- and DAG-generating lipolysis of TAG in LBs. The resulting reduction of the ER- and LB-confined levels of FFA and DAG during diauxic (D), post-diauxic (PD) and stationary (ST) growth phases affects both mechanisms (see Chapter 3 of this thesis) by which these two lipid species regulate longevity. First, by lowering the intracellular concentration of DAG during D and PD phases, LCA attenuates the FFA- and DAG-induced necrotic cell death pathway – thereby impairing the age-related form of necrotic cell death and ultimately extending longevity of chronologically aging yeast placed on a CR diet. Second, by reducing the intracellular concentrations of FFA and DAG during ST phase, LCA attenuates the mitochondria-controlled apoptotic cell death pathway – thereby impairing the age-related form of apoptotic cell death and ultimately extending longevity of chronologically aging yeast under CR conditions.

4.2. Introduction

As I described in Chapter 1 of this thesis, certain pharmacological interventions

can extend life span across phyla and, in some cases, improve overall health by beneficially influencing age-related pathologies (see Figure 4.1). Noteworthy, two anti-aging compounds known prior to my study have been shown to alter lipid levels in mammals and fruit flies under non-DR conditions. Specifically, resveratrol treatment reduces the levels of the neutral lipids TAG and increases FFA levels in mouse adipocytes [116]. Furthermore, feeding rapamycin to fruit flies results in elevated TAG levels [38].

Although it remains to be seen if such effects of resveratrol and rapamycin on lipid levels play a casual role in their anti-aging action under non-DR conditions, it should be stressed that lipid metabolism has been shown to be involved in longevity regulation in yeast [18, 153], worms [46, 63, 182, 190], fruit flies [183, 190] and mice [140, 141, 185, 187, 188, 190] (see Chapters 1 and 3 for a detailed discussion of this topic). In Chapter 3 of this thesis, I proposed a mechanism linking yeast longevity and lipid dynamics in the ER, LBs and peroxisomes. In this mechanism, a CR diet extends yeast CLS by activating FFA oxidation in peroxisomes [18, 153]. It is conceivable that the identification of small molecules targeting this mechanism could yield novel anti-aging compounds. Such compounds can be used as research tools for defining the roles for different longevity pathways in modulating lipid metabolism and in integrating lipid dynamics with other longevity-related processes. Furthermore, the availability of such compounds would enable a quest for housekeeping longevity assurance pathways that do not overlap (or only partially overlap) with the adaptable TOR and cAMP/PKA pathways (see Chapter 1 of this thesis for a detailed discussion of this topic). Moreover, such compounds would have a potential to be used as pharmaceutical agents for increasing life span and

promoting healthy aging by delaying the onset of age-related diseases caused by various defects in lipid metabolism and signaling, regardless of an organism's dietary regimen.

A performed by Alexander Goldberg in Dr. Titorenko's laboratory high-throughput screen of novel anti-aging compounds that can extend yeast longevity under CR conditions by altering lipid metabolism identified LCA as one of these compounds. In studies described in this Chapter, I established the molecular mechanism underlying the ability of LCA to extend yeast CLS by targeting the essential longevity-defining aspects of lipid metabolism confined to the ER, LBs and peroxisomes.

4.3. Materials and Methods

Strains and media

The wild-type strain *Saccharomyces cerevisiae* BY4742 (*MATα his3Δ1 leu2Δ0 lys2Δ0 ura3Δ0*) and mutant strains *pex5Δ* (*MATα his3Δ1 leu2Δ0 lys2Δ0 ura3Δ0 pex5Δ::kanMX4*), *tor1Δ* (*MATα his3Δ1 leu2Δ0 lys2Δ0 ura3Δ0 tor1Δ::kanMX4*), *ras2Δ* (*MATα his3Δ1 leu2Δ0 lys2Δ0 ura3Δ0 ras2Δ::kanMX4*) and *rim15Δ* (*MATα his3Δ1 leu2Δ0 lys2Δ0 ura3Δ0 rim15Δ::kanMX4*) were used in this study. Media components were as follows: 1) YEPD (0.2% Glucose), 1% yeast extract, 2% peptone, 0.2% glucose; 2) YEPD (0.5% Glucose), 1% yeast extract, 2% peptone, 0.5% glucose; 3) YEPD (1% Glucose), 1% yeast extract, 2% peptone, 1% glucose; and 4) YEPD (2% Glucose), 1% yeast extract, 2% peptone, 2% glucose.

A plating assay for the analysis of chronological life span

Cells were grown in YEPD medium initially containing 0.2%, 0.5%, 1% or 2% glucose as carbon source at 30°C with rotational shaking at 200 rpm in Erlenmeyer flasks at a flask volume/medium volume ratio of 5:1. A sample of cells was removed from each culture at various time points. A fraction of the cell sample was diluted in order to determine the total number of cells per ml of culture using a hemacytometer. 10 μl of serial dilutions (1:10 to $1:10^{3}$) of cells were applied to the hemacytometer, where each large square is calibrated to hold 0.1 μl. The number of cells in 4 large squares was then counted and an average was taken in order to ensure greater accuracy. The concentration of cells was calculated as follows: number of cells per large square x dilution factor $\times$ 10 $\times$ 1,000 = total number of cells per ml of culture. A second fraction of the cell sample was diluted and serial dilutions ($1:10^{2}$ to $1:10^{5}$) of cells were plated onto YEPD (2% Glucose) plates in triplicate in order to count the number of viable cells per ml of each culture. 100 μl of diluted culture was plated onto each plate. After a 48-h incubation at 30°C, the number of colonies per plate was counted. The number of colony forming units (CFU) equals to the number of viable cells in a sample. Therefore, the number of viable cells was calculated as follows: number of colonies $\times$ dilution factor $\times$ 10 = number of viable cells per ml. For each culture assayed, % viability of the cells was calculated as follows: number of viable cells per ml / total number of cells per ml $\times$ 100%. The % viability of cells in mid-logarithmic phase was set at 100% viability for that particular culture.

Visualization of intracellular lipid bodies (LBs)

Wild-type and mutant cells grown in YEPD medium initially containing 0.2%, 0.5%, 1% or 2% glucose as carbon source were tested microscopically for the presence of intracellular LBs by incubation with BODIPY 493/503. Cells were also probed with a fluorescent counterstain CW in order to visualize all cells in the population. BODIPY 493/503 was stored in the dark at –20°C as 100 μl aliquots of a 1 mM solution in ethanol. CW was stored in the dark at –20°C as the 5 mM stock solution in anhydrous DMSO.

The concurrent staining of cells with BODIPY 493/503 and CW was carried out as follows. The required amounts of the 100 μl BODIPY 493/503 aliquots (1 mM) and of the 5 mM stock solution of CW were taken out of the freezer and warmed to room temperature. The solutions of DHR and CW were then centrifuged at 21,000 × g for 5 min in order to clear them of any aggregates of fluorophores. For cell cultures with a titre of ~ 10^7 cells/ml, 100 μl was taken out of the culture to be treated. If the cell titre was lower, proportionally larger volumes were used. The samples were then centrifuged at 21,000 × g for 1 min, and pelleted cells were resuspended in 100 μl of TNT buffer (25 mM Tris/HCl (pH 7.5), 150 mM NaCl and 0.2 % Triton X-100). After a 10-min incubation at room temperature, the samples were centrifuged at 21,000 × g for 1 min. Pellets were then resuspended in 100 μl of TN buffer (25 mM Tris/HCl (pH 7.5), 150 mM NaCl), and the samples were subjected to centrifugation at 21,000 × g for 1 min. Pelleted cells were finally resuspended in 100 μl of TN buffer. Each 100 μl aliquot of cells was then supplemented with 1 μl of the 1 mM BODIPY 493/503 and 1 μl of the 5 mM CW solutions. After a 15-min incubation in the dark at room temperature, the samples were centrifuged at 21,000 × g for 5 min. Pellets were resuspended in 100 μl of TN buffer. The samples were centrifuged again at 21,000 × g for 5 min, and pellets were

resuspended in 100 µl of TN buffer. 10 µl of the BODIPY 493/503- and CW-treated cell suspension was then added to a microscope slide and covered with a coverslip. The slides were then sealed using nail polish. Once the slides were prepared, they were visualized under the Zeiss Axioplan fluorescence microscope mounted with a SPOT Insight 2 megapixel color mosaic digital camera. Several pictures of the cells on each slide were taken, with two pictures taken of each frame. One of the two pictures was of the cells seen through a fluorescein filter in order to detect cells dyed with BODIPY 493/503. The second picture was of the cells seen through a DAPI filter in order to visualize CW, and therefore all the cells present in the frame. For evaluating the percentage of BODIPY 493/503-positive cells, the UTHSCSA Image Tool (Version 3.0) software was used to calculate both the total number of cells and the number of stained cells.

Electron microscopy and morphometric analysis

Cells were fixed in 1.5% $KMnO_4$ for 20 min at room temperature, dehydrated by successive incubations in increasing concentrations of ethanol, and embedded in Poly/Bed 812 epoxy resin (Polysciences). Ultrathin sections were cut using an Ultra-Cut E Microtome (Reichert-Jung). Silver/gold thin sections from the embedded blocks were examined in a JEOL JEM-2000FX transmission electron microscope. For morphometric analysis of random electron microscopic sections of cells, digitized images were analyzed using the UTHSCSA Image Tool (Version 3.0) software. In each of 2 independent experiments, the percentage of cells that contain pexopodia and/or accumulate gnarled LBs was calculated by analyzing at least 300 cells that were collected at each time point.

The values of the percentage of cells containing pexopodia and/or accumulating gnarled LBs were plotted as a function of the number of days cells were cultured.

Preparation of total cell lysates

An aliquot containing 1×10^9 cells was centrifuged for 7 min at 3,000 rpm at room temperature. Pelleted cells were washed twice with distilled water and further centrifuged for 3 min at $16,000 \times$ g at room temperature. The recovered cell pellet was then resuspended in 500 μl of 4% CHAPS in 25 mM Tris/HCl buffer (pH 8.5) and centrifuged for 15 sec at $16,000 \times$ g at room temperature. The cells were then washed again, first by resuspending them in 500 μl of 4% CHAPS in 25 mM Tris/HCl buffer (pH 8.5) and then by centrifuging for 15 sec at $16,000 \times$ g at room temperature. The pellet of washed cells was then resuspended in 1 ml of ice-cold 4% CHAPS in 25 mM Tris/HCl buffer (pH 8.5), divided into 5 equal aliquots of 200 μl each and placed in Eppendorf tubes kept on ice. Each 200 μl aliquot was supplemented with ~100 μl of glass beads and vortexed three times for 1 minute. Apart from the vortexing steps, the samples were kept on ice at all times. Glass beads and cell debris were then pelleted by 5 min centrifugation at $16,000 \times$ g at 4°C. The resulting supernatant of the glass bead lysate was immediately transferred into a pre-chilled Eppendorf tube and stored at -20°C for further analysis.

Purification of the ER

Reagents and solutions

1. TSD reduction buffer: 0.1 M Tris/Sulfate (pH 9.4), 10 mM DTT

2. HEPES lysis buffer: 20 mM HEPES/KOH, pH 6.8, 50 mM KCl, 200 mM sorbitol, 2 mM EDTA, 1 mM DTT

3. Spheroplast medium A (pH 7.5): 0.67% yeast nitrogen base (w/o) amino acids, 2 % (w/v) glucose, 1 M sorbitol, 20 mM Tris/HCl (pH 7.5)

4. Spheroplast medium B: 0.67% yeast nitrogen base (w/o) amino acids, 2 % (w/v) glucose, 1 M sorbitol

5. 1.2 M sucrose/ HEPES, 36% (w/w): 7.2 g sucrose + 12.8 ml HEPES lysis buffer

6. 1.5 M sucrose/ HEPES, 43% (w/w): 8.6 g sucrose + 11.4 ml HEPES lysis buffer

7. MES buffer 1 (MES breaking buffer): 10 mM MES/Tris (pH 6.9), 12 % (w/w) Ficoll 400, 0.2 mM EDTA

8. MES buffer 2: 10 mM MES/Tris (pH 6.9), 8 % (w/w) Ficoll 400, 0.2 mM EDTA

9. MES buffer 3: 10 mM MES/Tris (pH 6.9), 0.6 M sorbitol, 8 % (w/w) Ficoll 400, 0.2 mM EDTA

10. MES buffer 4: 10 mM MES/Tris (pH 6.9), 0.25 M sorbitol, 0.2 mM EDTA

11. KPi buffer (pH 7.4): 20 mM KH_2PO_4/KOH (pH 7.4), 1.2 M sorbitol

Procedure

Wild-type and mutant cells were grown in YEPD medium initially containing 0.2%, 0.5%, 1% or 2% glucose as carbon source. Cultures were harvested at mid-exponential and diauxic phases, checked for contamination by bright-field microscopy and used to measure cell density at OD_{600}. The non-contaminated wild-type and mutant cells were pelleted at 4,000 × g for 5 min at room temperature. Cells were then resuspended at 10 OD_{600} units/ml in TSD reduction buffer, incubated for 10 min at room temperature and

160

centrifuged for 5 min at 4,000 × g at room temperature. Pelleted cells were then resuspended at 20 OD_{600} units/ml in Spheroplast medium A and supplemented with Zymolyase 100T at a concentration of 7.5 µg per OD_{600} units of cells. 10 µl of each cell suspension was then removed, diluted in 990 µl of H_2O and used to measure the OD_{600}. The remaining cell suspensions were incubated at 30°C for 30 min and the efficiency of cell wall removal was monitored by measuring the OD_{600}. Cell wall digestion was allowed to proceed until the OD_{600} measurement of the diluted cell suspension became 5% of the original value, with the total digestion time not exceeding 1 hour. Spheroplasts were then harvested by centrifugation at 1,500 × g for 5 min at room temperature, followed by resuspending at 1 to 5 OD_{600} units/ml in Spheroplast medium B by gentle swirling of the tube or gentle stirring with a glass rod. Spheroplasts were then harvested by centrifugation at 1,500 × g for 5 min at 4°C and then resuspended at a concentration of 1,000 OD_{600} units/ml of ice-cold HEPES lysis buffer with freshly-added DTT. Spheroplasts were then homogenized using 20 strokes and resulting lysates were centrifuged at 1, 000 × g for 10 min at 4°C. The supernatants (S_{1000}) were subjected to another round of centrifugation at 1, 000 × g for 10 min at 4°C, and resulting supernatants were further centrifuged at 27,000 × g for 10 min at 4°C. The pelleted membranes ($P_{27,000}$) were resuspended in 1.0 ml of HEPES lysis buffer (5,000 OD_{600} equivalents per ml) using a trimmed 1-ml pipette tip and carefully layered on top of a sucrose gradient prepared in advance (2.1 ml of 1.5 M sucrose/HEPES solution was deposited to the bottom of a Beckman Ultra-Clear centrifuge tube for the Beckman MLS-50 rotor, and then overlaid with 2.1 ml of 1.2 M sucrose/HEPES solution). The gradient tubes were then placed in the pre-chilled swinging bucket Beckman MLS-50 rotor and

centrifuged at 100,000 × g (36,000 rpm) for 1 hr at 4°C using the slow acceleration and deceleration setting to minimize disruption of gradients. 18 gradient fractions of 227 μl each were then collected starting from the top of the sucrose gradient and stored at -20°C for further analyses.

Purification of LBs

Reagents and solutions

1. TSD reduction buffer: 0.1 M Tris/Sulfate (pH 9.4), 10 mM DTT

2. HEPES lysis buffer: 20 mM HEPES/KOH, pH 6.8, 50 mM KCl, 200 mM sorbitol, 2 mM EDTA, 1 mM DTT

3. Spheroplast medium A (pH 7.5): 0.67% yeast nitrogen base (w/o) amino acids, 2 % (w/v) glucose, 1 M sorbitol, 20 mM Tris/HCl (pH 7.5)

4. Spheroplast medium B: 0.67% yeast nitrogen base (w/o) amino acids, 2 % (w/v) glucose, 1 M sorbitol

5. 1.2 M sucrose/ HEPES, 36% (w/w): 7.2 g sucrose + 12.8 ml HEPES lysis buffer

6. 1.5 M sucrose/ HEPES, 43% (w/w): 8.6 g sucrose + 11.4 ml HEPES lysis buffer

7. MES buffer 1 (MES breaking buffer): 10 mM MES/Tris (pH 6.9), 12 % (w/w) Ficoll 400, 0.2 mM EDTA

8. MES buffer 2: 10 mM MES/Tris (pH 6.9), 8 % (w/w) Ficoll 400, 0.2 mM EDTA

9. MES buffer 3: 10 mM MES/Tris (pH 6.9), 0.6 M sorbitol, 8 % (w/w) Ficoll 400, 0.2 mM EDTA

10. MES buffer 4: 10 mM MES/Tris (pH 6.9), 0.25 M sorbitol, 0.2 mM EDTA

11. KPi buffer (pH 7.4): 20 mM KH_2PO_4/KOH (pH 7.4), 1.2 M sorbitol

Procedure

Wild-type and mutant cells were grown in YEPD medium initially containing 0.2%, 0.5%, 1% or 2% glucose as carbon source. Cultures were harvested at mid-exponential and diauxic phases, checked for contamination by bright-field microscopy and used to measure cell density at OD_{600}. The non-contaminated wild-type and mutant cells were pelleted at $4,000 \times g$ for 5 min at room temperature. The cells were then washed once with distilled water and resuspended in the TSD reduction buffer at 10 x OD_{600} units/ml. Following a 10-min incubation at room temperature, the cells were pelleted by centrifugation at $4,000 \times g$ for 5min at room temperature and then washed once in Spheroplasts medium A. The cells were then resuspended in Spheroplasts medium A at $20 \times OD_{600}$ units/ml, supplemented with Zymolyase 100T at a concentration of 2.5 μg per OD_{600} units of cells, and incubated at 30°C for 45 min on a shaker set at 75 rpm. Spheroplasts were then pelleted by 5min centrifugation at $1,500 \times g$ at room temperature, resuspended in the ice-cold Spheroplasts medium B at $5 \times OD_{600}$ units/ml using pipettes with cut tips, and centrifuged for 5 min at $1,500 \times g$ at $4^{o}C$. Spheroplasts were then washed twice by resuspending the pellets in ice-cold KPi buffer at a concentration of 5 OD_{600} units/ml followed by centrifugation for 5 min at $1,500 \times g$ at $4^{o}C$. After the second wash and centrifugation step, clean spheroplasts were resuspended in ice-cold MES Buffer 1 at a concentration of 1,000 OD_{600} units/ml using pipettes with non-cut tips. Spheroplasts were then lysed in a homogenizer using 20 strokes at 4°C. Lysates were centrifuged for 5 min at $5,000 \times g$ at 4°C and the resulting supernatants ($S_{5,000}$) were transferred to pre-chilled centrifuge tubes kept on ice. LBs were then purified by subjecting the spheroplast lysates to a series of flotation gradient centrifugations using a

MLS 50 swinging bucket rotor (Beckman). The first flotation gradient was prepared by placing 2.5 ml of the $S_{5,000}$ fraction to the bottom of a centrifuge tube (Ultra-Clear Beckman tubes for MLS 50 rotor) and overlaying it with 2.5 ml of ice-cold MES Buffer 1. Following 1 hour centrifugation at 100,000 × g (36,000 rpm) at 4°C, the floating layer from the top portions of the gradients was collected with a cut tip and transferred to the bottom of a new centrifuge tube, which was then supplemented with MES buffer 2 to a total volume of 2.5 ml and gently mixed by pipetting. Resulting suspension was overlaid with 2.5 ml of ice-cold MES buffer 2 and then centrifuged for 1 hr at 100,000 × g (36,000 rpm) at 4°C. The floating layer from the top portions of the gradients was again collected with a cut tip and transferred to the bottom of a new centrifuge tube, which was then supplemented with MES buffer 3 to a total volume of 2.5 ml and gently mixed by pipetting. Resulting suspension was overlaid with 2.5 ml of ice-cold MES buffer 4 and then centrifuged for 1 hr at 100,000 × g (36,000 rpm) at 4°C. The floating layer from the top portions of the gradients was collected with a cut tip and purified lipid bodies were stored -20°C for further analyses.

Protein precipitation, SDS-PAGE and silver staining of gels

Protein concentration was determined using the RC DC protein assay kit (Bio-Rad) according to the manufacturer's instructions. Proteins were precipitated by adding trichloroacetic acid (TCA) to the final concentration of 10%, incubated on ice for 30 min, pelleted by centrifugation, and then washed with ice-cold 80% acetone. Dried protein pellets were then resuspended in the SDS-PAGE sample buffer and the pH was adjusted to neutral using 2 M Tris/HCl (pH 8.8). The samples were boiled for 5 min at 63°C,

centrifuged for 30 sec at 16,000 x g, loaded onto a 7.5%, 10%, 12.5% or 16% gel and resolved by SDS-PAGE. Following an overnight incubation of the gels in 50% methanol, proteins were visualized by silver staining using the mass spectrometry-compatible silver staining kit (Bio-Rad Silver Staining Plus) according to the manufacturer's instructions. The Bio-Rad unstained molecular marker and a 0.1 mg/ml solution of BSA in the SDS-PAGE sample buffer were also subjected to SDS-PAGE. The proteins were then visualized by silver staining.

Analysis of proteins by mass spectrometry

Proteins were resolved by SDS-PAGE and visualized by silver staining [226]. Protein bands were excised from the gel, reduced, alkylated and in-gel digested with trypsin [226]. The proteins were identified by matrix-assisted laser desorption/ionization mass spectrometric (MALDI MS) peptide mapping [227], using a Micromass M@LDI time-of-flight (TOF) mass spectrometer (Waters). Database searching using peptide masses was performed with the Mascot web-based search engine. For evaluating relative levels of individual proteins recovered in total cell lysates or purified mitochondria, a selected protein band was excised from the silver-stained gel and placed into an Eppendorf tube. A band of BSA containing 2 μg of this protein, which was also excised from the silver-stained gel, was added to each of the protein bands to be analyzed. Protein bands were reduced, alkylated and in-gel digested with trypsin [226]. The desalted peptide mixture was added to the surface of a MALDI target plate and allowed to air dry. The sample spot was then overlaid with MALDI matrix solution containing the Angiotensin I peptide standard (1:1 ratio). The presence of Angiotensin I in the sample carrying the analyzed

mixture of peptides provided an additional estimate of the mass measurement accuracy after calibration, giving an opportunity to calculate the value of peptide mass tolerance for each individual mass spectrum. After the desalted peptide mixture was analyzed by MALDI-TOF, the monoisotopic masses of recovered BSA peptides and the intensities of their monoisotopic peaks were grouped separately from the masses and intensities of peptides originated from the protein of interest. These data provided an additional estimate of the mass measurement accuracy and were used for the quantitation of relative levels of the same protein recovered in different samples. For evaluating relative levels of the protein of interest found in the samples to be compared, a ratio "the intensity of the monoisotopic peak of a peptide originated from the protein of interest/the intensity of the monoisotopic peak of a BSA peptide with the monoisotopic mass closest to the mass of the peptide of interest" was calculated for each peptide originated from the protein of interest. Based on these data, the average value for relative levels of the protein of interest found in the two compared samples was calculated. The method for evaluating relative levels of the protein of interest recovered in different samples was validated by calculating relative levels of several standard proteins in the samples supplemented with different quantities of each of these proteins.

Analysis of lipids by mass spectrometry

1×10^{10} cells were harvested by centrifugation and washed three times with cold water. The lipids were extracted by resuspending the cells in 3.8 ml of chloroform - methanol - water (1:2:0.8) and by vortexing the cell suspension with glass beads two times for 1 min. 1 ml of chloroform was then added, and the extract was incubated for 5 min with

occasional mixing. 1 ml of water was then added, and the extract was incubated for 5 min with occasional mixing. The extract was centrifuged and the entire supernatant was collected. The pellet was resuspended in 1.6 ml of chloroform, and the lipids were extracted by vortexing the suspension with glass beads two times for 1 min. The extract was then centrifuged and the entire supernatant was collected. The pooled supernatants were centrifuged and the organic phase was collected. The lipid extract was dried under nitrogen. The lipid film was dissolved in 400 μl of chloroform - methanol (1:1) containing either 3 mM ammonium hydroxide for positive-ion analyses or no additive for negative-ion measurements. Mass spectrometric analyses were performed with a Micromass Q-TOF 2 mass spectrometer equipped with a nano-electrospray source operating at a flow rate of 1 μl/min. The instrument was used in the single-stage mass spectrometry mode for positive- or negative-ion analyses as described in Chapter 2 of this thesis. For quantification of individual lipid molecular species, the commercially available lipids (Avanti Polar Lipids, Larodan AB and Sigma) with non-natural fatty acid compositions were used as internal standards that do not occur in a significant amount in the sample to be analyzed. Lipid quantification was performed as described in Chapter 2 of this thesis.

Miscellaneous procedures

Protocols for lipid extraction, separation by TLC, visualization by 5% phosphomolybdic acid in ethanol, and quantitation by densitometric analysis of TLC plates have been described elsewhere [232]. Preparation of cellular extracts and microanalytic biochemical

assays for measuring ATP, glucose, trehalose and glycogen concentrations was performed as previously described [233].

4.4. Results

4.4.1. A rationale for choosing a short-lived mutant strain to conduct a high-throughput screen of novel anti-aging compounds that can extend longevity by altering lipid metabolism in chronologically aging yeast

My pilot experiments on elucidating the metabolism of lipids in various yeast mutants were aimed at finding a short-lived mutant strain most suitable for conducting a high-throughput screen of novel anti-aging compounds that can extend longevity by altering lipid metabolism under CR conditions. Based on my findings, I proposed to use *pex5Δ* as such mutant strain. Because *pex5Δ* lacks a cytosolic shuttling receptor for peroxisomal import of Fox1p and Fox2p, these two enzymes of the β-oxidation of FFA reside in the cytosol of *pex5Δ* cells [261] (Figure 4.1). In contrast, the Pex5p-independent peroxisomal
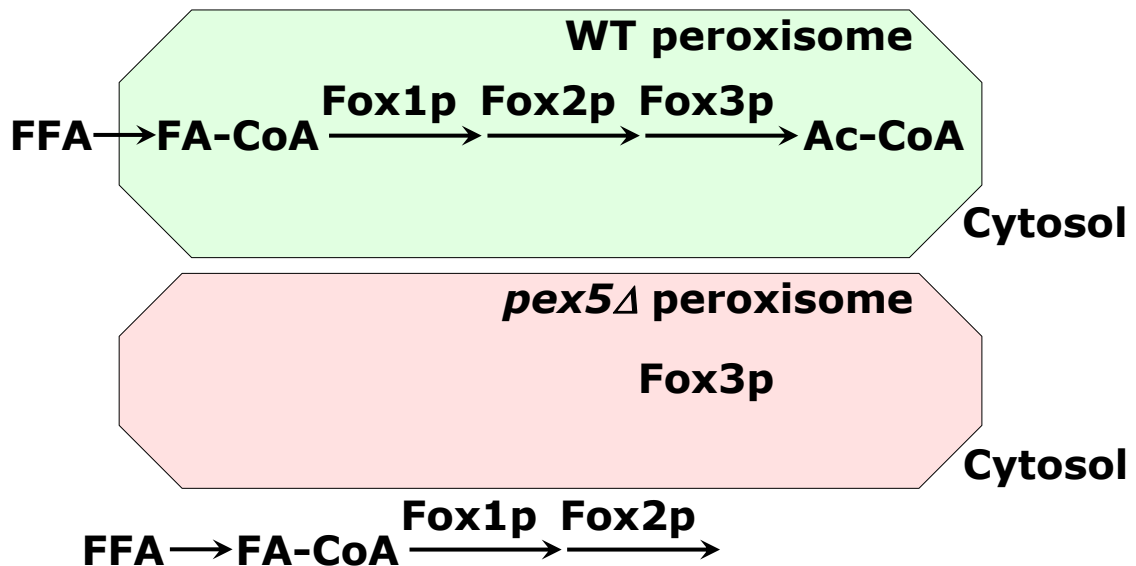
Figure 4.1. By spatially separating Fox1p and Fox2p from Fox3p within a cell, the *pex5Δ* mutation impairs

oxidation of free fatty acids (FFA) in the peroxisome. Outline of subcellular localization of the Fox1p, Fox2p and Fox3p enzymes of FFA oxidation in β-oxidation in WT and *pex5Δ* cells.

import of Fox3p, the third enzyme of the FFA β-oxidation pathway, sorts it to the peroxisome in *pex5Δ* cells [261]. By spatially separating Fox1p and Fox2p from Fox3p within a cell, the *pex5Δ* mutation impairs FFA oxidation (Figure 4.1). In chronologically aging yeast grown under CR conditions on 0.2% or 0.5% glucose, peroxisomal FFA oxidation regulates longevity by 1) efficiently generating acetyl-CoA to synthesize the bulk of ATP in mitochondria; and 2) acting as a rheostat that modulates the age-related dynamics of FFA and DAG, two regulatory lipids that, as I found (see Chapter 3 of this thesis), promote longevity-shortening necrotic cell death. Unlike CR yeast, chronologically aging non-CR yeast grown on 1% or 2% glucose are unable to generate significant quantities of ATP by oxidizing peroxisome-derived acetyl-CoA in mitochondria and, instead, produce the bulk of ATP via glycolytic oxidation of glycogen- and trehalose-derived glucose (see Chapters 1 and 3 of this thesis for a detailed discussion of this topic). As Alexander Goldberg in Dr. Titorenko's laboratory found, consistent with the essential role of peroxisomal FFA oxidation as a longevity assurance process only under CR conditions, the *pex5Δ* mutation substantially shortens the CLS of CR yeast but causes a significantly lower reduction of longevity in non-CR yeast, especially in yeast grown on 2% glucose [18].

4.4.2. The *pex5Δ*-dependent remodelling of lipid metabolism makes the short-lived *pex5Δ* mutant most suitable for conducting a high-throughput screen of anti-aging compounds that extend longevity by

altering the metabolism of lipids

As described in Chapter 3 of this thesis, I found that in chronologically aging CR yeast peroxisomal FFA oxidation modulates, perhaps via several negative feedback loops, the following three processes: 1) the ER-confined biosynthesis of TAG from FFA and DAG; 2) the subsequent deposition of TAG, the major neutral lipid reserves, in LBs; and 3) the consequent lipolysis of deposited TAG and the resulting formation of FFA and DAG. As I found, by impairing the ability of peroxisomal FFA oxidation to act as a rheostat that regulates cellular aging by modulating the age-related dynamics of FFA, DAG and TAG in the ER and LBs, the *pex5Δ* mutation causes the accumulation of the closely apposed ER membranes and ER-originated LBs in CR yeast (Figure 4.2). Of note, these morphological features of *pex5Δ* yeast under CR conditions were similar to those observed in a mouse model for the peroxisome biogenesis disorder Zellweger syndrome with hepatocyte-specific elimination of the *PEX5* gene [262].
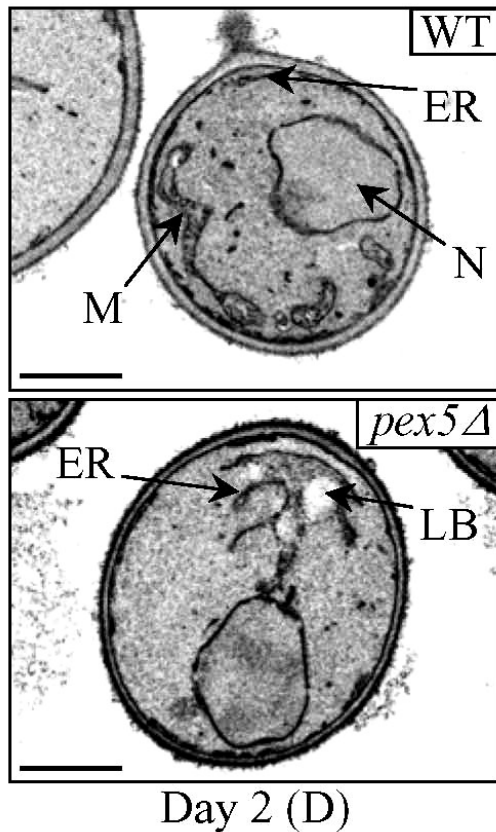
Figure 4.2. The *pex5Δ* mutation alters cell morphology by causing the accumulation of the closely apposed ER membranes and ER-originated lipid bodies in CR yeast. Transmission electron micrographs of WT and *pex5* yeast grown on 0.2% glucose for 2 days. Abbreviations: D, diauxic growth phase; M, mitochondrion; N, nucleus.

Furthermore, I found that the *pex5Δ* mutation also increases the concentrations of FFA, DAG and TAG in CR yeast (Figure 4.3), promoting their build-up in the ER and LBs (Figure 4.4). In addition, CR yeast carrying the *pex5Δ* mutation accumulate the ER-derived and LBs-deposited EE neutral lipid species (Figure 4.4).
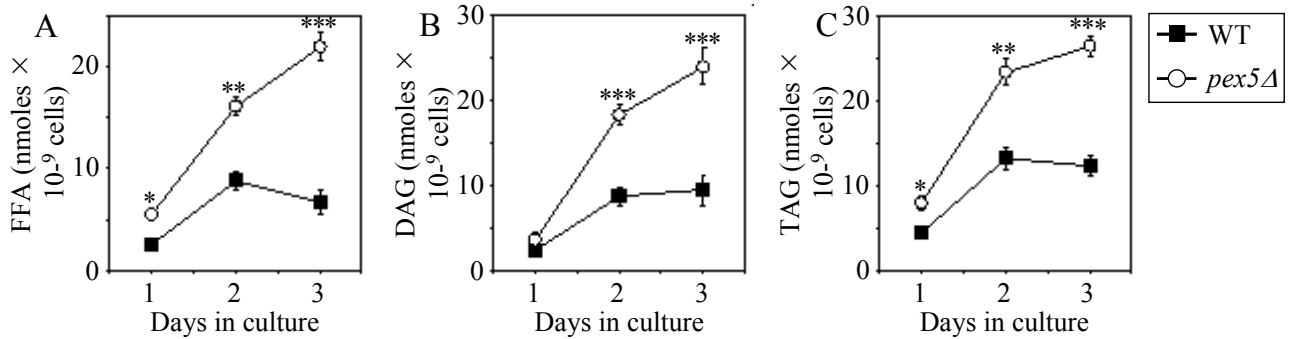
Figure 4.3. The *pex5Δ* mutation increases the concentrations of free fatty acids (FFA), diacylglycerols (DAG) and triacylglycerols (TAG) in CR yeast. Levels of FFA (A), DAG (B) and TAG (C) in WT and *pex5* yeast grown on 0.2% glucose and taken for analyses at the indicated time-points are shown. FFA and TAG were measured by quantitative mass spectrometry. The levels of DAG were quantitated by densitometric analysis of TLC plates. Data are presented as means ± SEM (n = 3-8; ***p < 0.001; **p < 0.01; *p < 0.05).

Moreover, I found that, following a short-term exposure to exogenous FFA (palmitoleic acid or oleic acid) or DAG, WT cells grown under CR conditions die (Figure 4.5A). The vast majority of these WT cells displayed propidium iodide (PI) positive staining characteristic of the loss of plasma membrane integrity, a hallmark event of necrotic cell death (Figures 4.5B and 4.5C). In contrast, only a minor portion of these WT cells displayed Annexin V positive staining used to visualize the externalization of phosphatidylserine, a hallmark event of apoptotic cell death (Figures 4.5B and 4.5C). Thus, a brief exposure of WT cells grown under CR conditions to exogenous FFA or DAG causes their necrotic, not apoptotic, death. Importantly, I found that the *pex5Δ* mutation enhances the susceptibility of CR yeast to necrotic death caused by a short-term exposure to exogenous FFA or DAG (Figures 4.5A and 4.5C), perhaps due to the increased concentrations of endogenous FFA and DAG seen in *pex5Δ* cells under CR (Figures 4.3A and 4.3B).
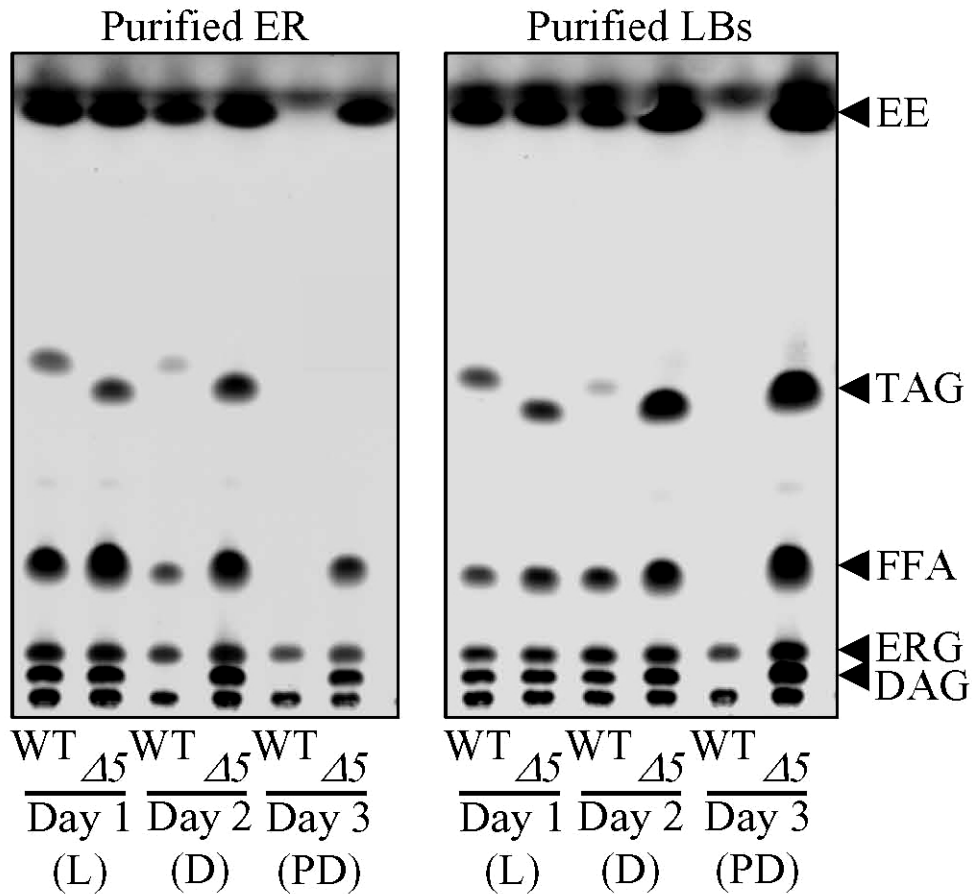
Figure 4.4. Spectra of lipids extracted from purified endoplasmic reticulum (ER) and lipid bodies (LBs) and analyzed by TLC for WT and *pex5Δ* (*Δ5*) yeast grown on 0.2% glucose and taken for analyses at the indicated time-points. Abbreviations: D, diauxic growth phase; EE, ethyl esters; ERG, ergosterol; L, logarithmic growth phase; M, mitochondrion; N, nucleus; PD, post-diauxic growth phase; ST, stationary growth phase.
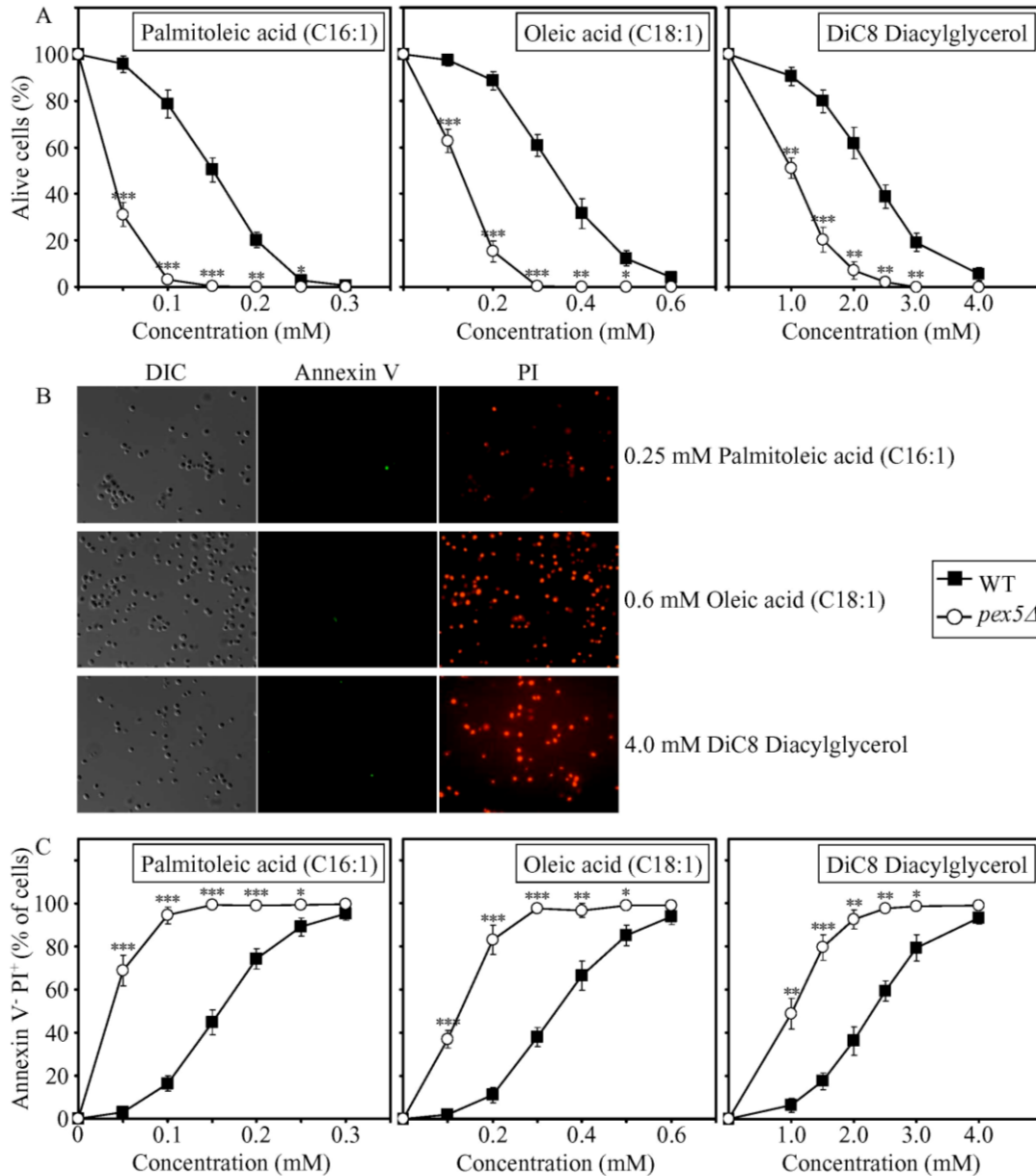
Figure 4.5. The *pex5Δ* mutation enhances the susceptibility of CR yeast to necrotic death caused by a short-term exposure to exogenous lipids. (A) Viability of WT and *pex5Δ* cells treated for 2 h with palmitoleic acid, oleic acid or DiC8 diacylglycerol. (B) Fluorescence microscopy of WT yeast treated for 2 h with 0.25 mM palmitoleic acid, 0.6 mM oleic acid or 4.0 mM DiC8 diacylglycerol. Cells were co-stained with 1) Annexin V for visualizing the externalization of phosphatidylserine, a hallmark event of apoptosis; and 2) propidium iodide (PI) for visualizing the loss of plasma membrane integrity, a hallmark event of necrosis. (C) Percent of WT and *pex5Δ* cells that following their treatment with palmitoleic acid, oleic acid or DiC8 diacylglycerol displayed Annexin V negative and PI positive (Annexin V- and PI+) staining characteristic of necrotic cell death. Data in A and C are presented as means ± SEM (n = 3-5; ***p < 0.001;

174

**p < 0.01; *p < 0.05). Prior to their exposure to exogenous lipids, CR yeast were grown for 2 days on 0.2% glucose. Abbreviations: DIC, differential interference contrast.

Altogether, my findings imply that, by impairing peroxisomal FFA oxidation and affecting lipid metabolism in the ER and LBs, the *pex5Δ* mutation affects the longevity-defined aspects of the mechanism linking longevity and lipid metabolism confined to the ER, LBs and peroxisomes. Noteworthy, Tatiana Boukh-viner and Alexander Goldberg in Dr. Titorenko's laboratory found that this mutation also alters the levels of numerous pro- and anti-aging proteins and impacts many longevity-related processes, thereby shortening the CLS of yeast when calorie supply is limited. Therefore, a decision was made to use the short-lived *pex5Δ* strain to carry out a chemical genetic screen for anti-aging compounds that target lipid metabolism to extend CLS in yeast placed on a CR diet.

4.4.3. A mechanism underlying the ability of a novel anti-aging compound to extend yeast life span by targeting the longevity-defining aspects of lipid metabolism confined to the ER, LBs and peroxisomes

Using the short-lived *pex5Δ* mutant strain, Alexander Goldberg in Dr. Titorenko's laboratory conducted a high-throughput screen of novel anti-aging compounds that can extend the CLS of yeast by targeting the longevity-defining aspects of lipid metabolism under CR conditions. One of the life-extending compounds identified in such screen was lithocholic acid (LCA), a bile acid. Studies in Dr. Titorenko's laboratory revealed that LCA greatly extends the CLS of WT strain of yeast placed on a CR diet.

To establish the molecular mechanism underlying the ability of LCA to extend yeast CLS by targeting the longevity-defining aspects of lipid metabolism confined to the

ER, LBs and peroxisomes, I first used the mass spectrometry (MS)-based identification and quantitation of proteins recovered in total cell lysates to elucidate how this bile acid influences the age-related dynamics of changes in the proteome of chronologically aging yeast under CR conditions. I found that the exposure of chronologically aging CR yeast to LCA elevated during PD and ST phases the levels of proteins that function in the following metabolic pathways and stress-response processes: 1) glycogen degradation; 2) glycolysis; 3) acetyl-CoA synthesis in the cytosol; 4) pyruvate oxidation, the tricarboxylic cycle (TCA) and ATP synthesis in mitochondria; 5) biosynthesis of TAG from FFA and DAG in the ER; 6) stress response in the cytosol; 7) reactive oxygen species (ROS) scavenging in the cytosol; and 8) stress response in mitochondria (Figure 4.6). My MS-based proteomic analysis also revealed that the exposure of chronologically aging CR yeast to LCA reduced during PD and ST phases the levels of proteins that function in the following metabolic pathways and mitochondria biogenesis processes: 1) glyoxylate cycle in the cytosol; 2) glyoxylate cycle in mitochondria; 3) lipolysis of TAG to FFA and DAG in LBs; 4) mitochondrial division (Figure 4.6). Many of these proteins have been implicated in longevity regulation (see Chapter 1 for a detailed discussion of this topic) - including proteins involved in lipid metabolism (whose essential role in longevity regulation I revealed in experiments described in Chapter 3). Thus, during PD and ST growth phases LCA alters the levels of numerous pro- and anti-aging proteins and impacts lipid metabolism along with several other longevity-related processes, thereby extending the CLS of yeast placed on a CR diet.
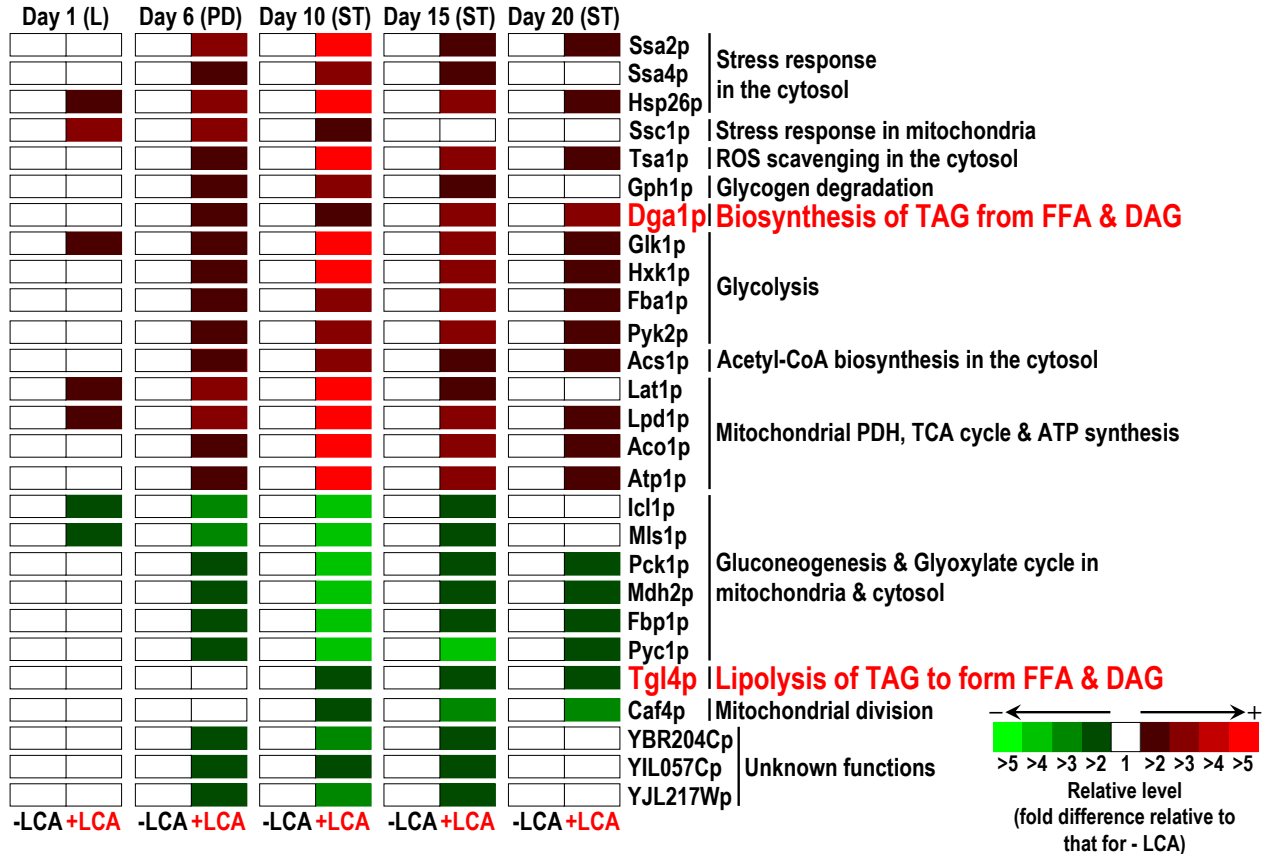
Figure 4.6. LCA alters the age-related dynamics of changes in the proteome of chronologically aging yeast under CR conditions. Relative levels (fold difference relative to that in yeast not exposed to LCA) of proteins recovered in total lysates of yeast cells grown under CR conditions on 0.2% glucose in the presence of LCA.

I then used MS-assisted quantitative lipidomics and thin layer chromatography (TLC)-based lipid quantitation to assess how LCA influences the dynamics of age-dependent changes in levels of TAG, EE, FFA and DAG during chronological aging of CR yeast. I found that during PD phase LCA elevates the levels of TAG and EE (Figure 4.7) and greatly reduces the levels of FFA and DAG (Figure 4.8). I therefore concluded that during PD phase, LCA accelerates the ER-confined biosynthesis of TAG from FFA
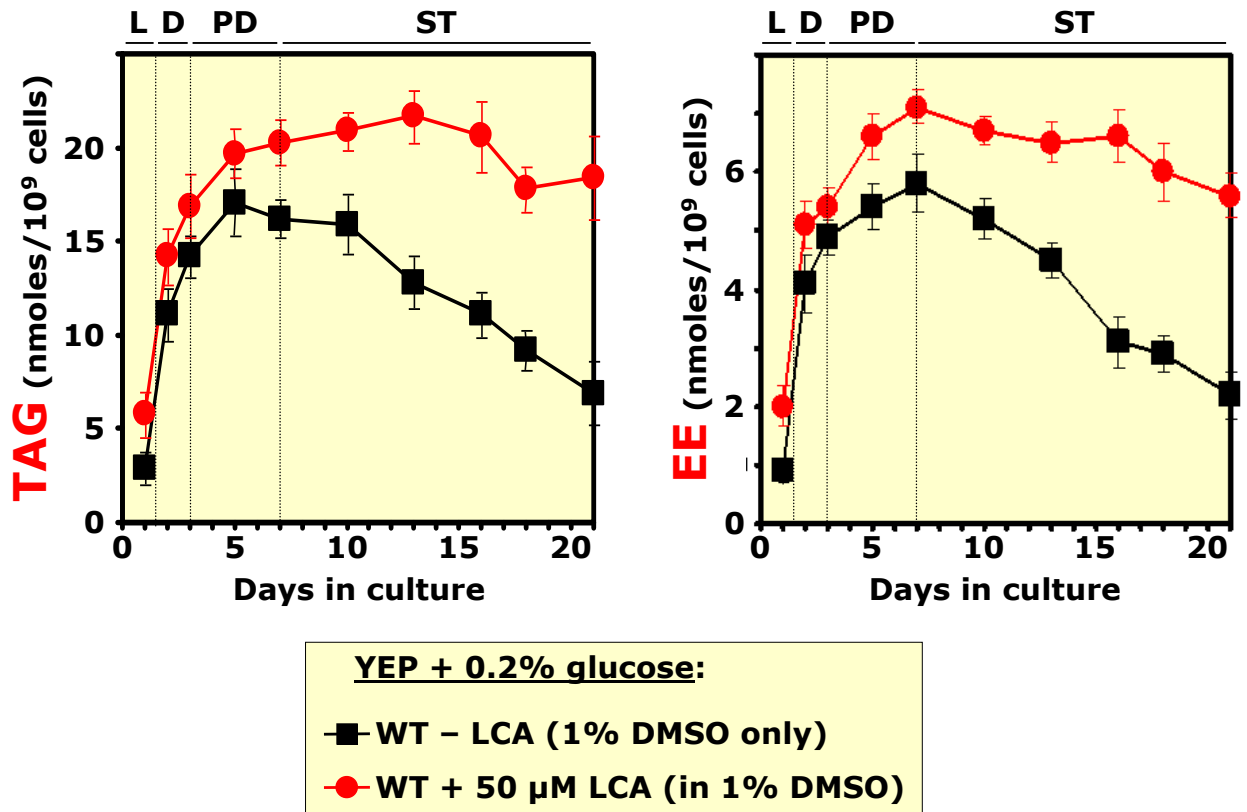
Figure 4.7. LCA alters the dynamics of age-dependent changes in levels of neutral lipids during chronological aging of yeast grown under CR conditions on 0.2% glucose with or without LCA. During PD phase, LCA elevates the levels of TAG and EE. During ST phase, LCA greatly decelerates the age-related decline in the levels of both these neutral lipids.

and DAG as well as of EE from FFA and ergosterol (ERG). My MS- and TLC-based lipidomic analysis also revealed that during ST phase LCA greatly decelerates the age-related decline in the levels of neutral lipids (TAG and EE; Figure 4.7) as well as of FFA and DAG (Figure 4.8). I therefore concluded that during ST phase, LCA decelerates the LB-confined lipolysis of TAG and EE – thereby slowing down both the consumption of neutral lipids and the resulting formation of FFA and DAG.
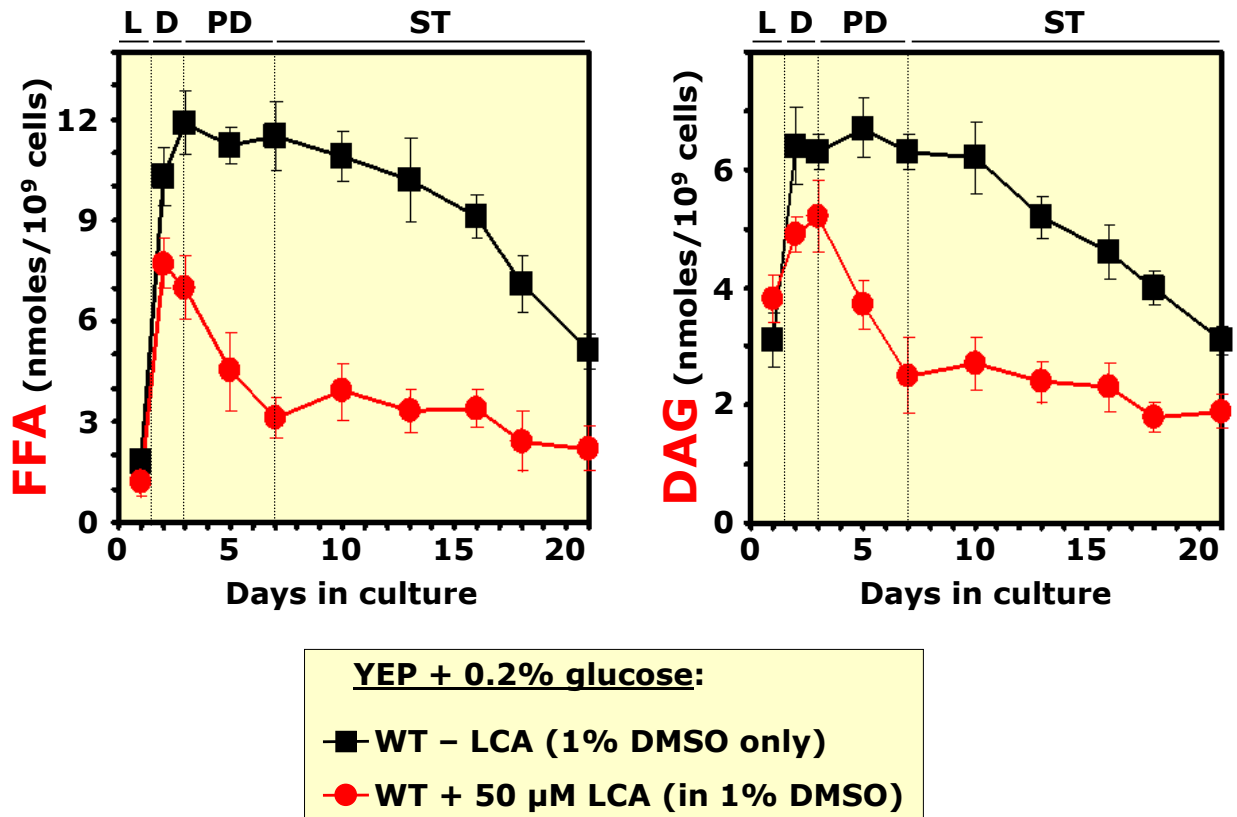
Figure 4.8. LCA alters the dynamics of age-dependent changes in levels of FFA and DAG during chronological aging of yeast grown under CR conditions on 0.2% glucose with or without LCA. During PD phase, LCA greatly reduces the levels of FFA and DAG. During ST phase, LCA greatly decelerates the age-related decline in the levels of these two lipid species.

As I described in Chapter 3, my studies revealed that FFA and DAG regulate longevity by two different mechanisms that operate at two different stages of the aging process. One mechanism involves sensing the concentration of DAG maintained by cells (in a diet- and genotype-dependent fashion) during D and PD growth phases. DAG concentration during D and PD phases programs cell viability during ST growth phase by modulating the FFA- and DAG-induced necrotic cell death pathway, but not by
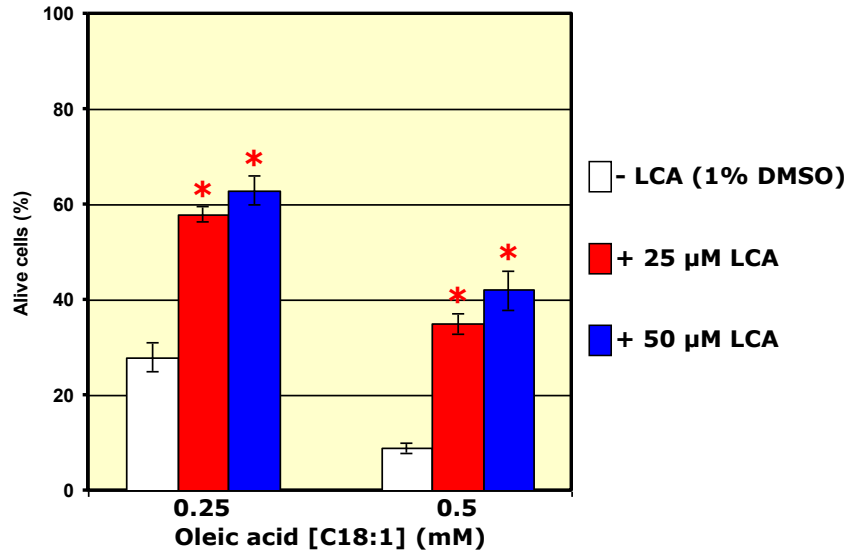
Figure 4.9. LCA reduces the susceptibility of CR yeast recovered from the beginning of PD growth phase (at day 3) to necrotic death caused by a short-term exposure to exogenous oleic acid. WT cells grown under CR conditions on 0.2% glucose and recovered from the beginning of PD growth phase (at day 3) were treated for 2 h with 0.25 mM or 0.5 mM oleic acid. Data on cell viability are presented as means ± SEM (n = 3-4; *p < 0.01).
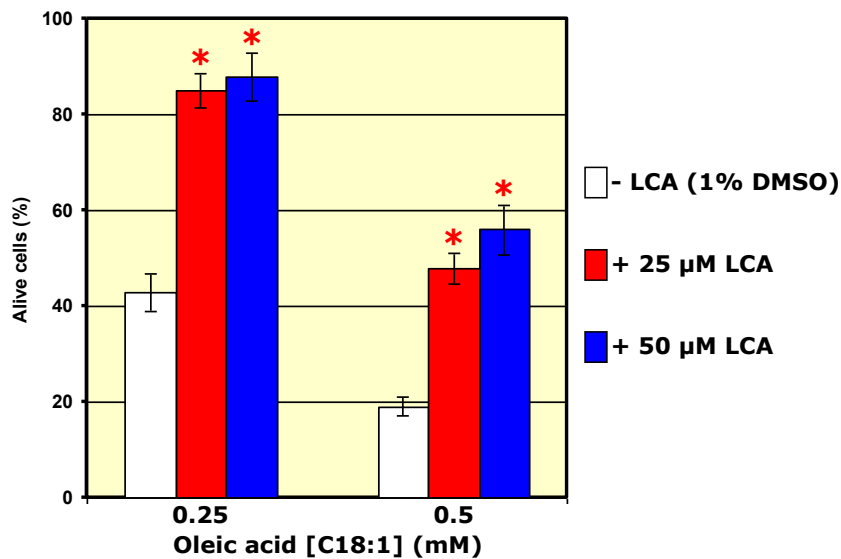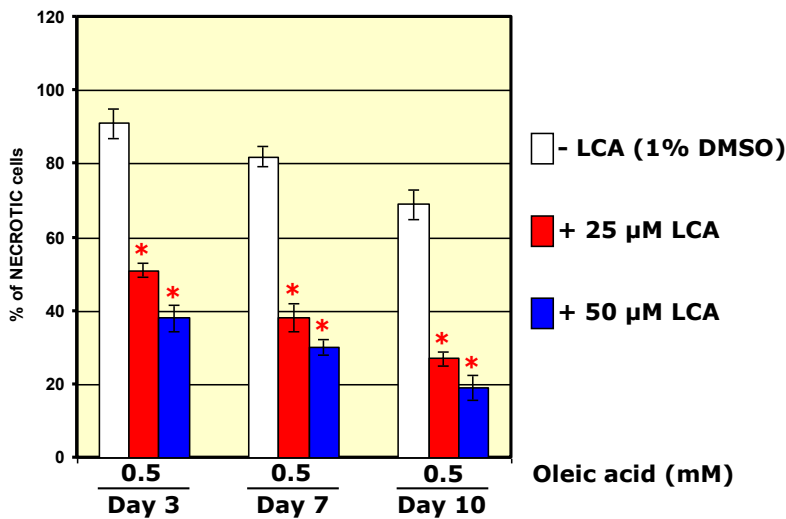

Figure 4.10. LCA reduces the susceptibility of CR yeast recovered from the beginning of ST phase (at day 7) to necrotic death caused by a short-term exposure to exogenous oleic acid. WT cells grown under CR conditions on 0.2% glucose and recovered from the beginning of ST phase (at day 7) were treated for 2 h with 0.25 mM or 0.5 mM oleic acid. Data on cell viability are presented as means ± SEM (n = 3-4; *p < 0.01).

influencing the mitochondria-controlled apoptotic pathway of cell death. Another mechanism that I revealed involves sensing the concentrations of FFA and DAG during ST phase. Any diet or genetic manipulation that causes the build-up of these two lipids during ST phase shortens the chronological life span of yeast in part by promoting rapid mitochondria-controlled apoptotic cell death, but not by activating FFA- and DAG-induced necrotic cell death pathway. Because LCA alters the dynamics of age-dependent changes in levels of FFA and DAG during chronological aging of yeast grown under CR conditions (see data in Figures 4.7 and 4.8 and their discussion above), I next elucidated how this life-extending bile acid influences the susceptibility of CR yeast to necrotic and apoptotic forms of cell death.

I found that LCA reduces the susceptibility of CR yeast recovered from the beginning of PD phase (at day 3), beginning of ST phase (at day 7) and early ST phase (at day 10) to necrotic cell death caused by a short-term exposure to: 1) exogenous oleic acid (Figures 4.9 - 4.12); 2) exogenous palmitoleic acid (Figures 4.13 - 4.16); or 3) exogenous DAG (Figures 4.17 - 4.19). Such necrotic cell death was defined by Annexin V$^-$/PI (propidium iodide)$^+$ staining (Figures 4.12 and 4.16) due to compromised integrity of the plasma membrane, a hallmark event of necrosis (see Chapters 1 and 3 for a detailed discussion of this characteristic event of necrotic cell death). Furthermore, I also found that LCA reduces the susceptibility of CR yeast recovered from the beginning of PD phase (at day 3), beginning of ST phase (at day 7) and early ST phase (at day 10) to mitochondria-controlled apoptotic cell death caused by a short-term exposure to: 1) exogenous hydrogen peroxide (Figures 4.20 - 4.24); or 2) exogenous acetic acid (Figures 4.25 - 4.29). Such mitochondria-controlled apoptotic cell death was defined by nuclear
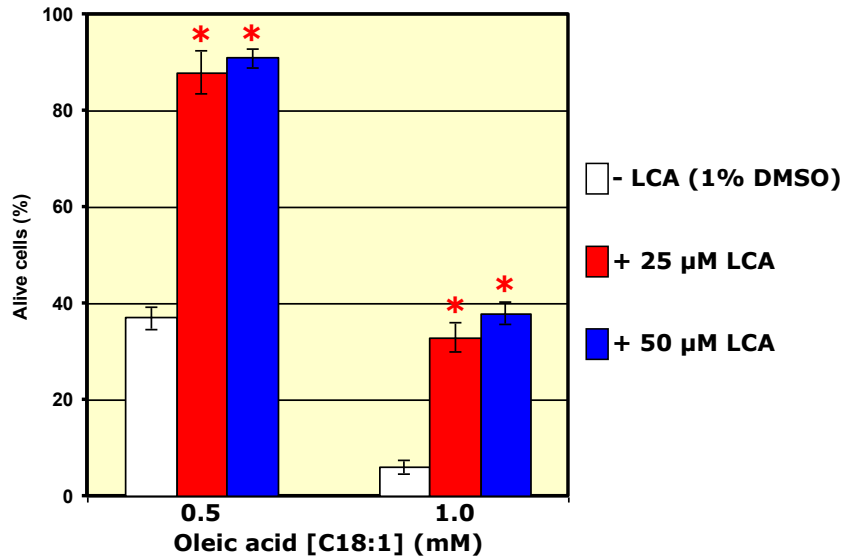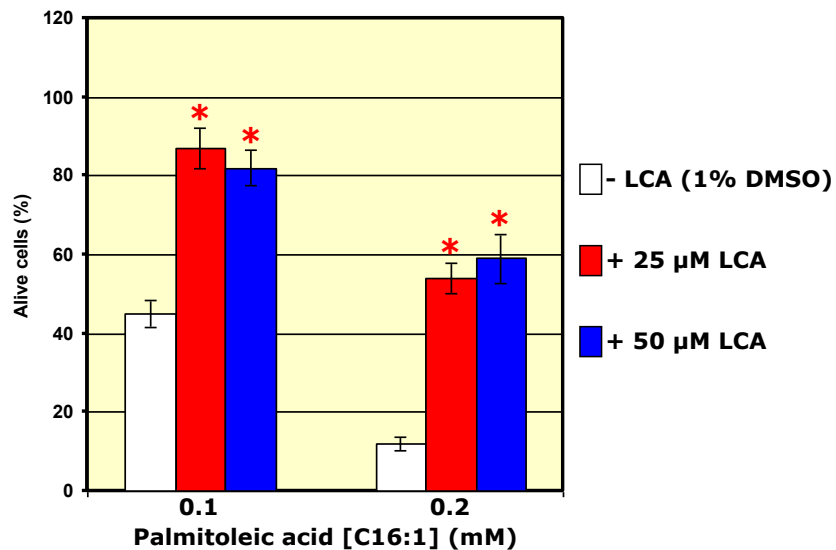
Figure 4.11. LCA reduces the susceptibility of CR yeast recovered from early ST phase (at day 10) to necrotic death caused by a short-term exposure to exogenous oleic acid. WT cells grown under CR conditions on 0.2% glucose and recovered from early ST phase (at day 10) were treated for 2 h with 0.5 mM or 1.0 mM oleic acid. Data on cell viability are presented as means ± SEM (n = 3-4; *p < 0.01).
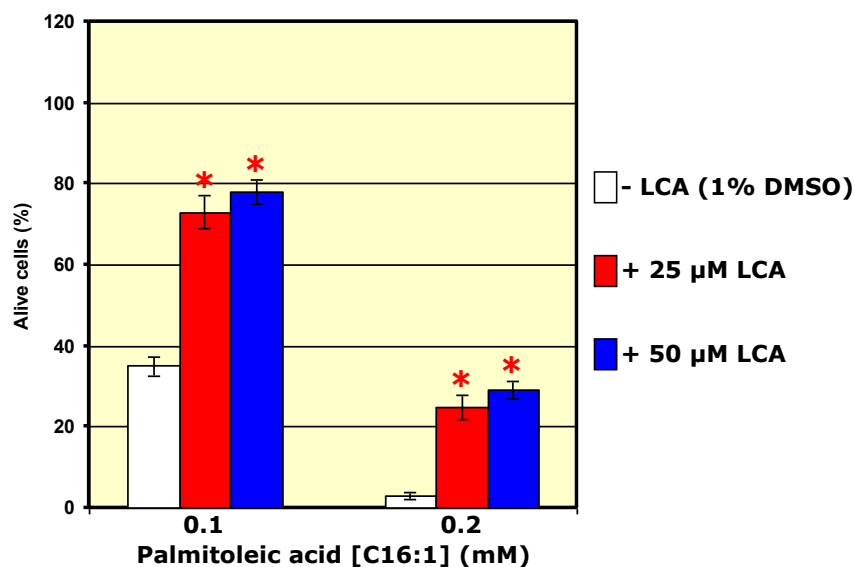

Figure 4.12. LCA reduces the susceptibility of CR yeast to necrotic death caused by a short-term exposure to exogenous oleic acid. WT cells grown under CR conditions on 0.2% glucose and recovered from the beginning of PD phase (at day 3), beginning of ST phase (at day 7) or early ST phase (at day 10) were treated for 2 h with 0.5 mM oleic acid. Data on the percentage of cells displaying propidium iodide staining, a hallmark event of necrotic death, are presented as means ± SEM (n = 3; *p < 0.01).
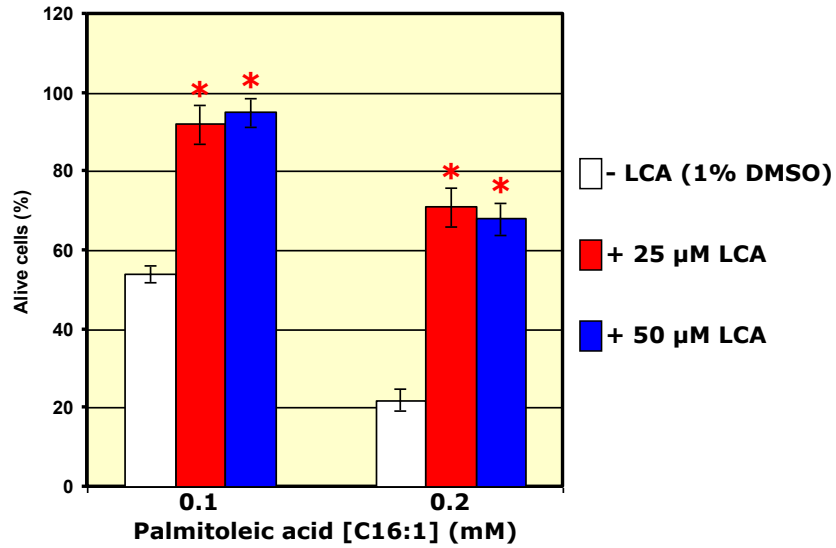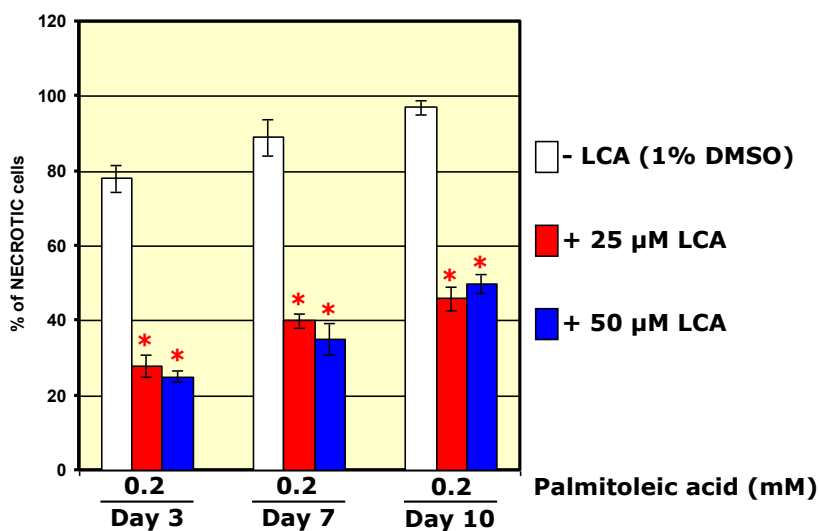
Figure 4.13. LCA reduces the susceptibility of CR yeast recovered from the beginning of PD growth phase (at day 3) to necrotic death caused by a short-term exposure to exogenous palmitoleic acid. WT cells grown under CR conditions on 0.2% glucose and recovered from the beginning of PD growth phase (at day 3) were treated for 2 h with 0.1 mM or 0.2 mM palmitoleic acid. Data on cell viability are presented as means ± SEM (n = 3-4; *p < 0.01).
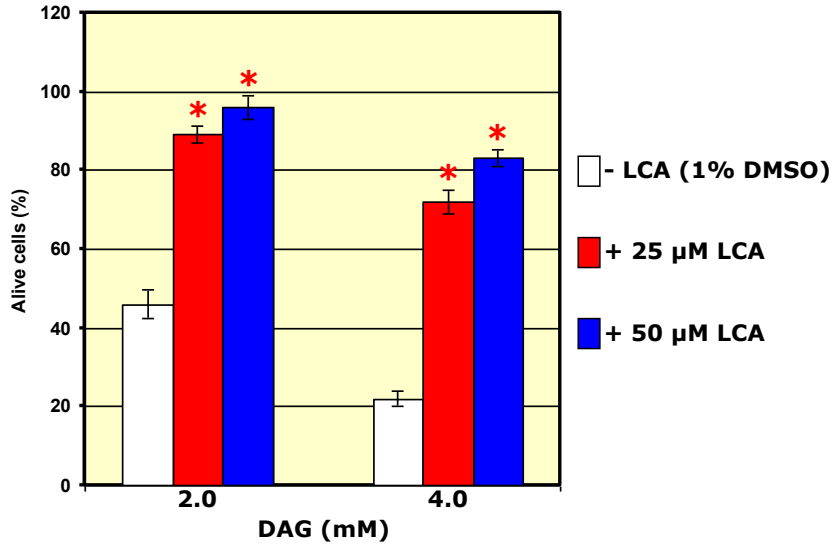

Figure 4.14. LCA reduces the susceptibility of CR yeast recovered from the beginning of ST phase (at day 7) to necrotic death caused by a short-term exposure to exogenous palmitoleic acid. WT cells grown under CR conditions on 0.2% glucose and recovered from the beginning of ST phase (at day 7) were treated for 2 h with 0.1 mM or 0.2 mM palmitoleic acid. Data on cell viability are presented as means ± SEM (n = 3-4; *p < 0.01).
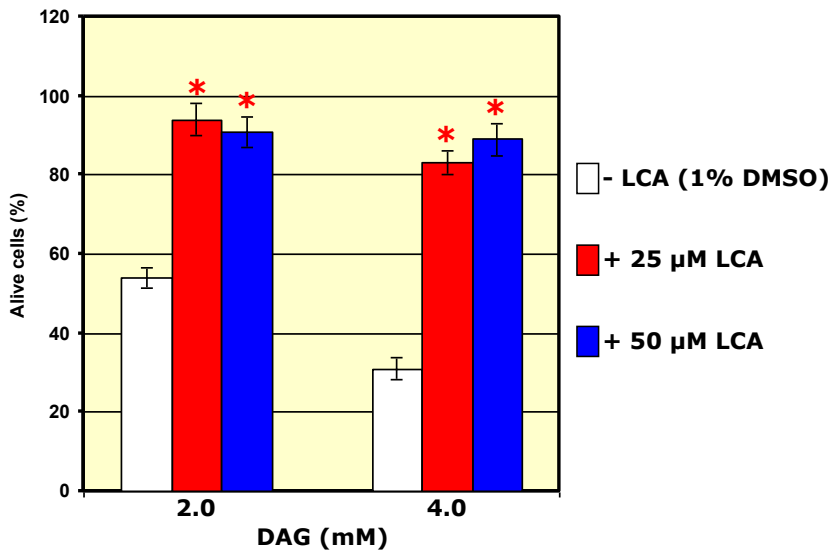
Figure 4.15. LCA reduces the susceptibility of CR yeast recovered from early ST phase (at day 10) to necrotic death caused by a short-term exposure to exogenous palmitoleic acid. WT cells grown under CR conditions on 0.2% glucose and recovered from early ST phase (at day 10) were treated for 2 h with 0.1 mM or 0.2 mM palmitoleic acid. Data on cell viability are presented as means ± SEM (n = 3-4; *p < 0.01).
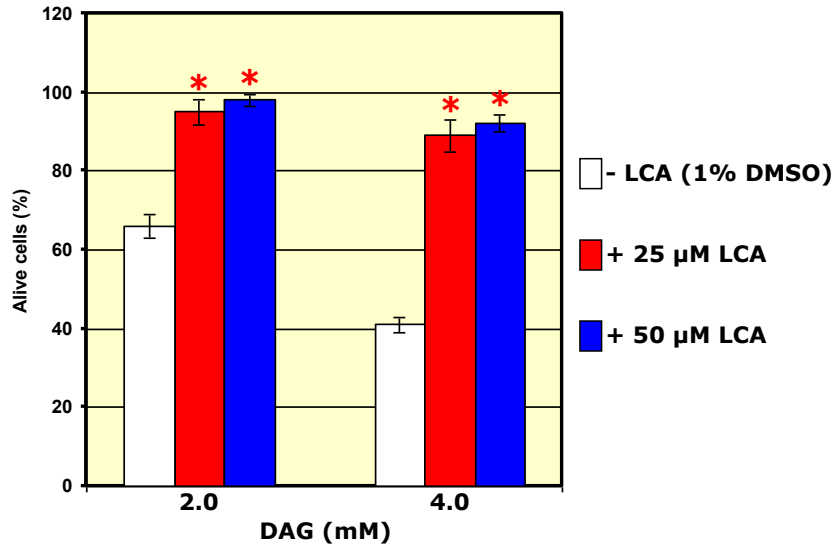

Figure 4.16. LCA reduces the susceptibility of CR yeast to necrotic death caused by a short-term exposure to exogenous palmitoleic acid. WT cells grown under CR conditions on 0.2% glucose and recovered from the beginning of PD phase (at day 3), beginning of ST phase (at day 7) or early ST phase (at day 10) were treated for 2 h with 0.2 mM palmitoleic acid. Data on the percentage of cells displaying propidium iodide staining, a hallmark event of necrotic death, are presented as means ± SEM (n = 3; *p < 0.01).
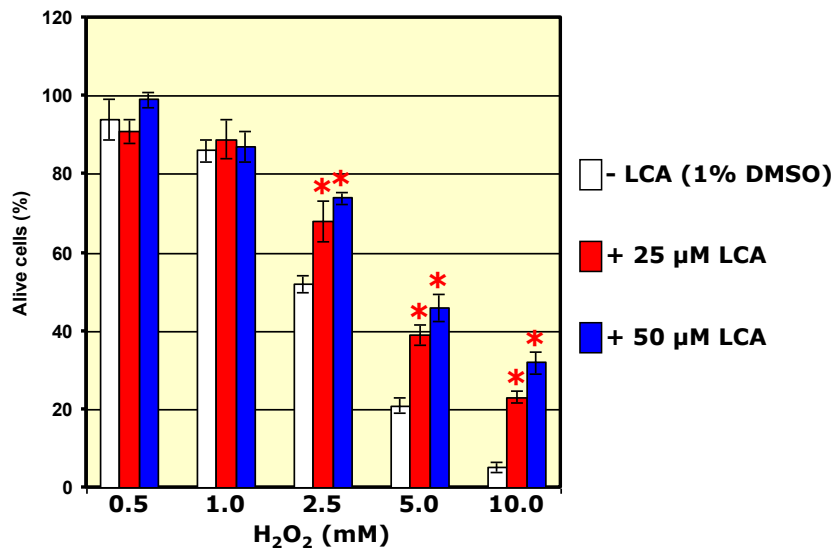
184

Figure 4.17. LCA reduces the susceptibility of CR yeast recovered from the beginning of PD growth phase (at day 3) to necrotic death caused by a short-term exposure to exogenous DAG. WT cells grown under CR conditions on 0.2% glucose and recovered from the beginning of PD growth phase (at day 3) were treated for 2 h with 2.0 mM or 4.0 mM DiC8 DAG. Data on cell viability are presented as means ± SEM (n = 3-4; *p < 0.01).
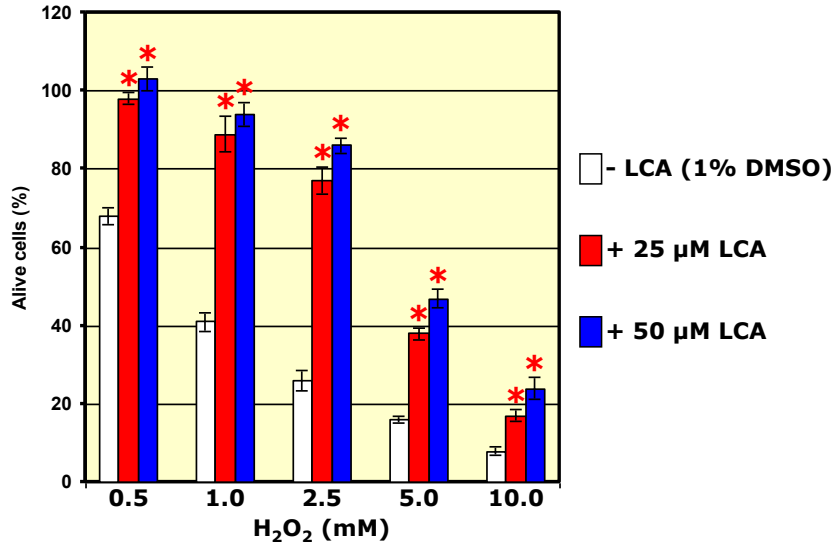

Figure 4.18. LCA reduces the susceptibility of CR yeast recovered from the beginning of ST phase (at day 7) to necrotic death caused by a short-term exposure to exogenous DAG. WT cells grown under CR conditions on 0.2% glucose and recovered from the beginning of ST phase (at day 7) were treated for 2 h with 2.0 mM or 4.0 mM DiC8 DAG. Data on cell viability are presented as means ± SEM (n = 3-4; *p < 0.01).
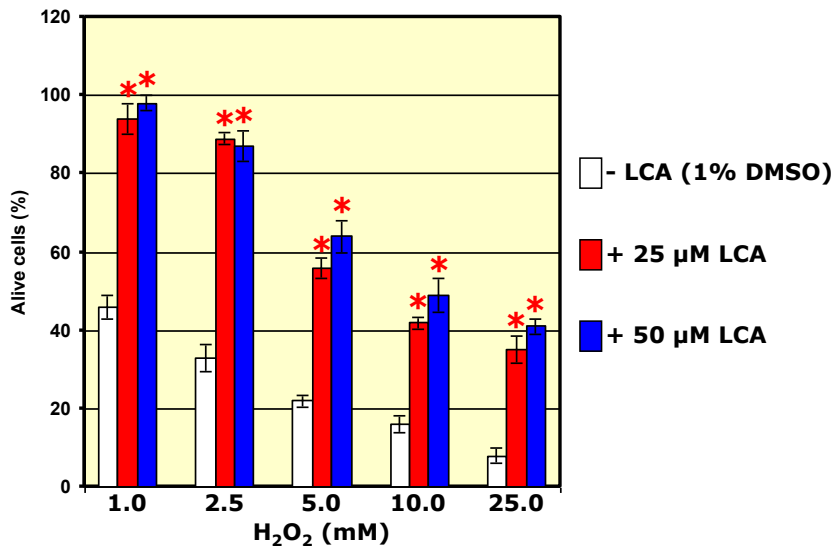
Figure 4.19. LCA reduces the susceptibility of CR yeast recovered from early ST phase (at day 10) to necrotic death caused by a short-term exposure to exogenous DAG. WT cells grown under CR conditions on 0.2% glucose and recovered from early ST phase (at day 10) were treated for 2 h with 2.0 mM or 4.0 mM DiC8 DAG. Data on cell viability are presented as means ± SEM (n = 3-4; *p < 0.01).
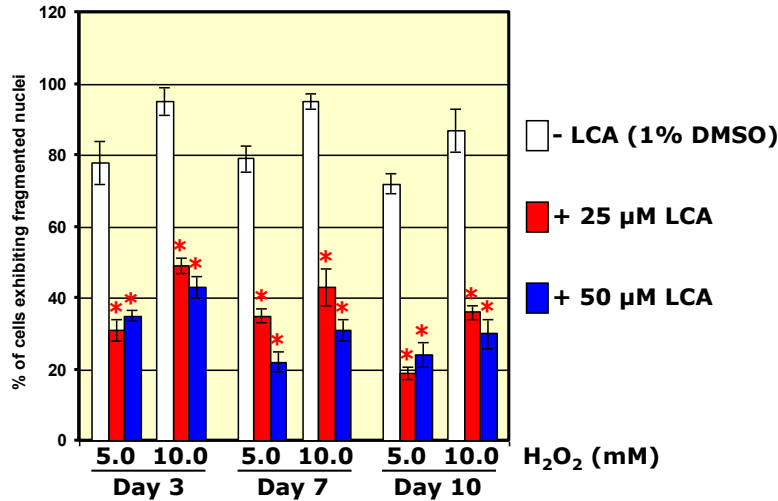

Figure 4.20. LCA reduces the susceptibility of CR yeast recovered from the beginning of PD growth phase (at day 3) to apoptotic death caused by a short-term exposure to exogenous hydrogen peroxide. WT cells grown under CR conditions on 0.2% glucose and recovered from the beginning of PD growth phase (at day 3) were treated for 2 h with various concentrations of hydrogen peroxide. Data on cell viability are presented as means ± SEM (n = 4-6; *p < 0.01).
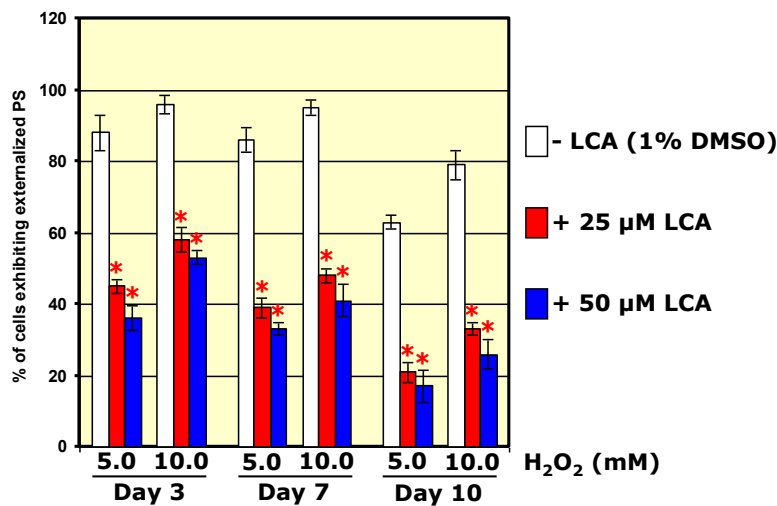
186

Figure 4.21. LCA reduces the susceptibility of CR yeast recovered from the beginning of ST phase (at day 7) to apoptotic death caused by a short-term exposure to exogenous hydrogen peroxide. WT cells grown under CR conditions on 0.2% glucose and recovered from the beginning of ST phase (at day 7) were treated for 2 h with various concentrations of hydrogen peroxide. Data on cell viability are presented as means ± SEM (n = 4-6; *p < 0.01).

Figure 4.22. LCA reduces the susceptibility of CR yeast recovered from early ST phase (at day 10) to apoptotic death caused by a short-term exposure to exogenous hydrogen peroxide. WT cells grown under CR conditions on 0.2% glucose and recovered from early ST phase (at day 10) were treated for 2 h with various concentrations of hydrogen peroxide. Data on cell viability are presented as means ± SEM (n = 4-6; *p < 0.01).

187

Figure 4.23. LCA reduces the susceptibility of CR yeast to apoptotic death caused by a short-term exposure to exogenous hydrogen peroxide. WT cells grown under CR conditions on 0.2% glucose and recovered from the beginning of PD phase (at day 3), beginning of ST phase (at day 7) or early ST phase (at day 10) were treated for 2 h with 5.0 mM or 10.0 mM hydrogen peroxide. Data on the percentage of cells exhibiting fragmented nuclei, a hallmark event of apoptotic death, are presented as means ± SEM (n = 5; *p < 0.01).
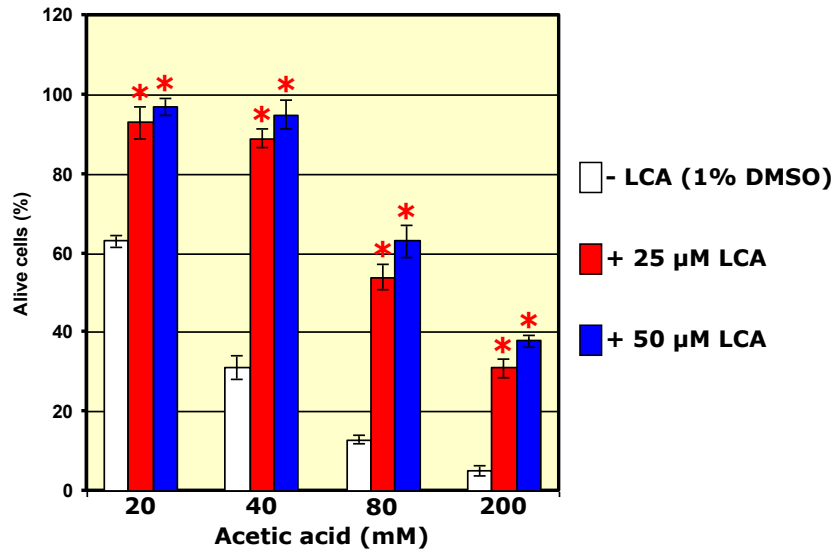

Figure 4.24. LCA reduces the susceptibility of CR yeast to apoptotic death caused by a short-term exposure to exogenous hydrogen peroxide. WT cells grown under CR conditions on 0.2% glucose and recovered from the beginning of PD phase (at day 3), beginning of ST phase (at day 7) or early ST phase (at day 10) were treated for 2 h with 5.0 mM or 10.0 mM hydrogen peroxide. Data on the percentage of cells exhibiting phosphatidylserine (PS) translocation from the inner to the outer leaflet of the plasma membrane, a hallmark event of apoptotic death, are presented as means ± SEM (n = 5; *p < 0.01).

Figure 4.25. LCA reduces the susceptibility of CR yeast recovered from the beginning of PD growth phase (at day 3) to apoptotic death caused by a short-term exposure to exogenous acetic acid. WT cells grown under CR conditions on 0.2% glucose and recovered from the beginning of PD growth phase (at day 3) were treated for 2 h with various concentrations of acetic acid. Data on cell viability are presented as means ± SEM (n = 3-5; *p < 0.01).
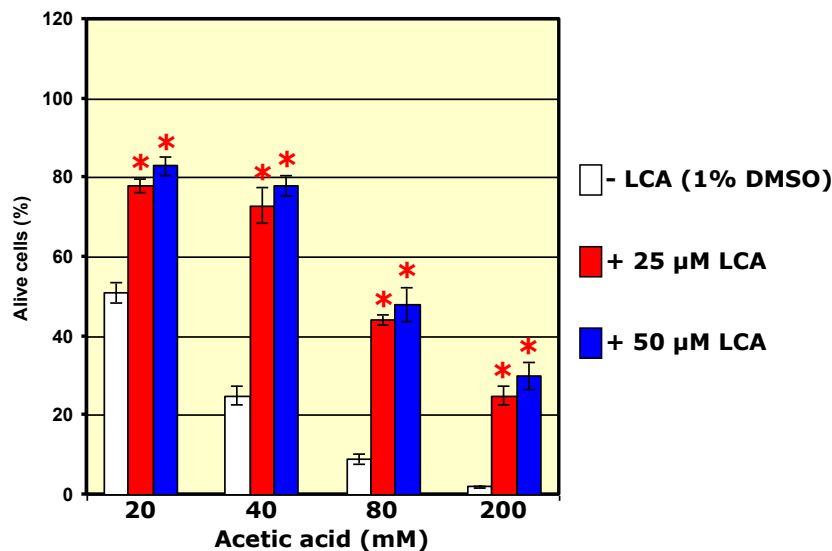
Figure 4.26. LCA reduces the susceptibility of CR yeast recovered from the beginning of ST phase (at day 7) to apoptotic death caused by a short-term exposure to exogenous acetic acid. WT cells grown under CR conditions on 0.2% glucose and recovered from the beginning of ST phase (at day 7) were treated for 2 h with various concentrations of acetic acid. Data on cell viability are presented as means ± SEM (n = 3-5; *p < 0.01).
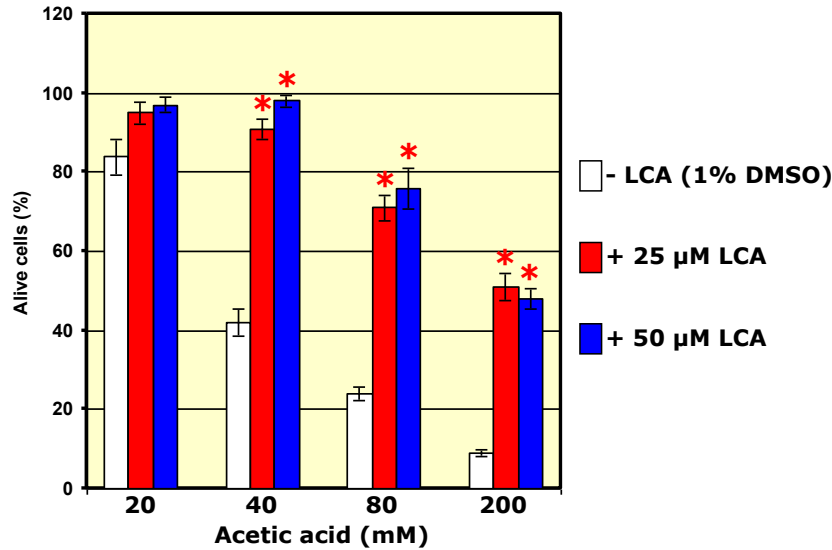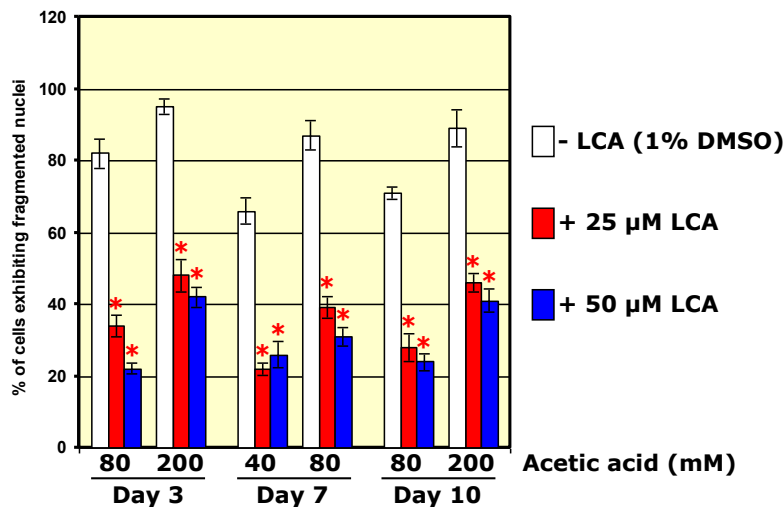
Figure 4.27. LCA reduces the susceptibility of CR yeast recovered from early ST phase (at day 10) to apoptotic death caused by a short-term exposure to exogenous acetic acid. WT cells grown under CR conditions on 0.2% glucose and recovered from early ST phase (at day 10) were treated for 2 h with various concentrations of acetic acid. Data on cell viability are presented as means ± SEM (n = 3-5; *p < 0.01).
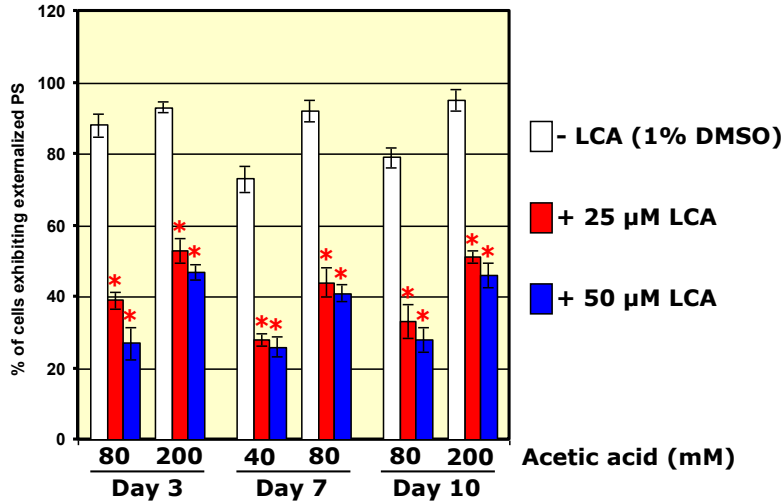

Figure 4.28. LCA reduces the susceptibility of CR yeast to apoptotic death caused by a short-term exposure to exogenous acetic acid. WT cells grown under CR conditions on 0.2% glucose and recovered from the beginning of PD phase (at day 3), beginning of ST phase (at day 7) or early ST phase (at day 10) were treated for 2 h with 80 mM or 200 mM acetic acid. Data on the percentage of cells exhibiting fragmented nuclei, a hallmark event of apoptotic death, are presented as means ± SEM (n = 4; *p < 0.01).

Figure 4.29. LCA reduces the susceptibility of CR yeast to apoptotic death caused by a short-term exposure to exogenous acetic acid. WT cells grown under CR conditions on 0.2% glucose and recovered from the beginning of PD phase (at day 3), beginning of ST phase (at day 7) or early ST phase (at day 10) were treated for 2 h with 80 mM or 200 mM acetic acid. Data on the percentage of cells exhibiting phosphatidylserine (PS) translocation from the inner to the outer leaflet of the plasma membrane, a hallmark event of apoptotic death, are presented as means ± SEM (n = 4; *p < 0.01).

fragmentation (Figures 4.23 and 4.28) and phosphatidylserine (PS) translocation from the inner to the outer leaflet of the plasma membrane (Figures 4.24 and 4.29), the two hallmark events of apoptosis (see Chapters 1 and 3 for a detailed discussion of these characteristic events of apoptotic cell death).

4.5. Discussion

Altogether, my findings described in Chapter 4 of this thesis revealed the molecular mechanism underlying the ability of LCA to extend yeast CLS by targeting the longevity-defining aspects of lipid metabolism confined to the ER, LBs and peroxisomes (Figure 4.30C). In such mechanism, under CR conditions LCA accelerates the biosynthesis of TAG from FFA and DAG in the ER as well as decelerates the FFA- and DAG-generating
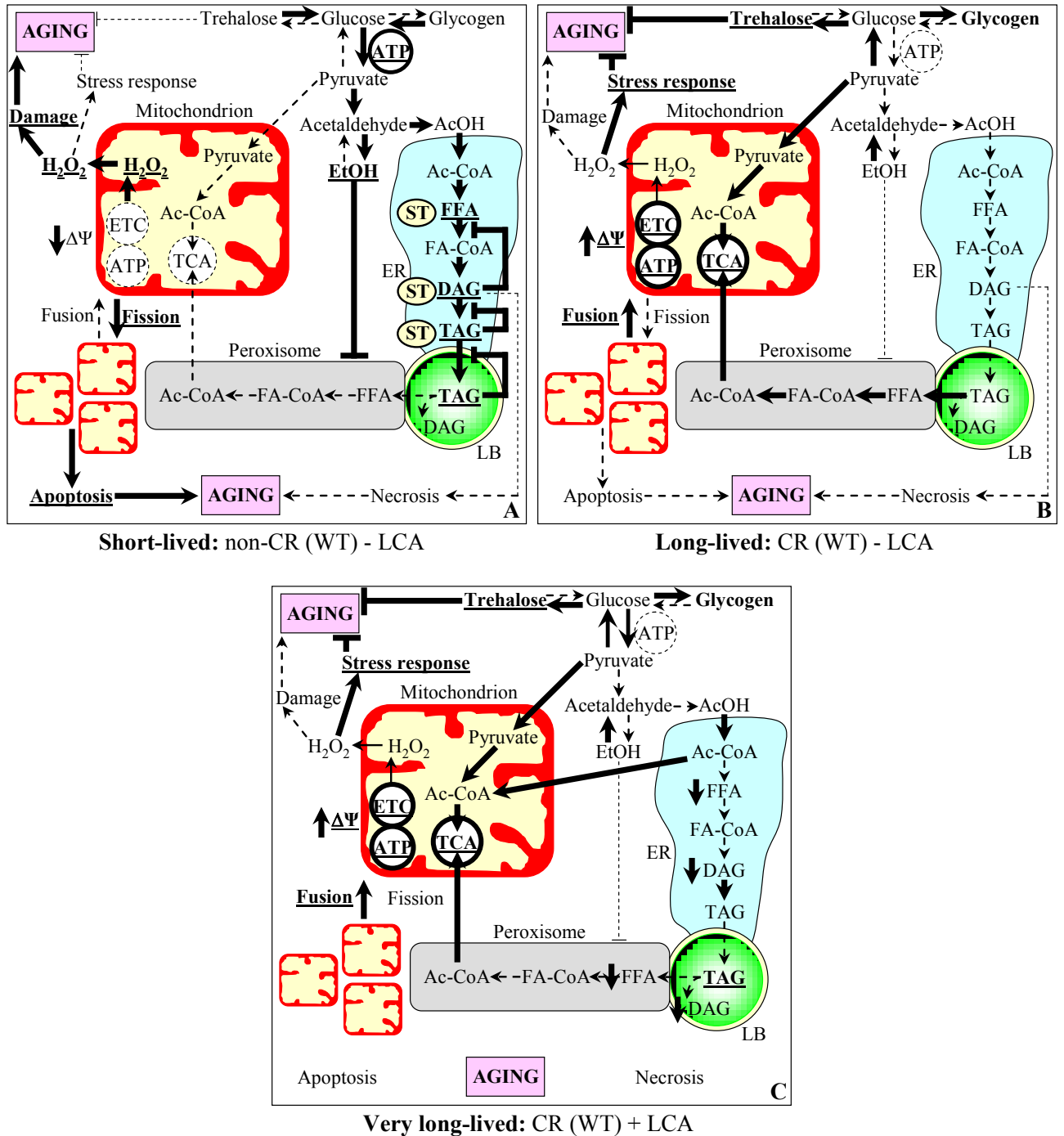
Figure 4.30. Outline of metabolic pathways and interorganellar communications operating in chronologically aging cells of WT strain grown under CR or non-CR conditions with or without LCA. The longevity-defining features of the diet- or LCA-driven metabolic design for each type of growth conditions are discussed in details in the Discussion section of this Chapter.

lipolysis of TAG in LBs. The resulting reduction of the ER- and LB-confined levels of FFA and DAG during PD and ST growth phases affects both mechanisms (Figure 4.30B; see Chapter 3 for a detailed discussion of this topic) by which these two lipid species regulate longevity. First, by lowering the intracellular concentration of DAG during D and PD phases, LCA attenuates the FFA- and DAG-induced necrotic cell death pathway – thereby impairing the age-related form of necrotic cell death and ultimately extending longevity of chronologically aging yeast placed on a CR diet (Figure 4.30C). Second, by reducing the intracellular concentrations of FFA and DAG during ST phase, LCA attenuates the mitochondria-controlled apoptotic cell death pathway – thereby impairing the age-related form of apoptotic cell death and ultimately further extending longevity of chronologically aging yeast under CR conditions (Figure 4.30C).

My findings described and discussed in Chapters 3 and 4 of this thesis imply that there are two different ways of delaying chronological aging of yeast by targeting the longevity-defining aspects of lipid metabolism confined to the ER, LBs and peroxisomes. One way is by placing yeast on a CR diet in the absence of LCA, thereby making them "lean" by accelerating both the lipolysis of neutral lipids in LBs and the oxidation of FFA in peroxisomes (compare Figures 4.30A and Figure 4.30B). The resulting reduction of FFA and DAG levels during PD and ST phases slows down both the necrotic and apoptotic forms of cell death, thereby extending longevity of chronologically aging CR yeast - as compared to longevity of non-CR yeast (compare Figures 4.30A and Figure 4.30B). The other way is by placing yeast on a CR diet in the presence of LCA, thereby making them "fat" by: 1) accelerating the synthesis of TAG from FFA and DAG; and 2) decelerating the FFA- and DAG-producing lipolysis of TAG in LBs (compare Figures

4.30B and Figure 4.30C). The resulting further reduction of FFA and DAG levels during PD and ST phases (as compared to CR yeast grown without LCA) causes additional attenuation of the necrotic and apoptotic forms of cell death, thereby further extending longevity of chronologically aging CR yeast exposed to LCA - as compared to longevity of CR yeast not exposed to this bile acid (compare Figures 4.30B and Figure 4.30C).

4.6. Conclusions

By elucidating how a novel anti-aging compound LCA influences the metabolism of lipids as well as age-related forms of necrotic and apoptotic death in chronologically aging yeast and how it alters yeast proteome, I established the molecular mechanism underlying the ability of LCA to extend yeast CLS by targeting these longevity-defining aspects of lipid metabolism confined to the ER, LBs and peroxisomes.

5. A mechanism underlying the ability of a novel anti-aging drug to extend yeast life span by altering the composition of mitochondrial membrane lipids

5.1. Abstract

As described in Chapters 3 and 4 of this thesis, I established the molecular mechanisms underlying the ability of caloric restriction (CR) and lithocholic acid (LCA) to extend yeast chronological life span by targeting the longevity-defining aspects of lipid metabolism confined to the endoplasmic reticulum (ER), lipid bodies (LBs) and peroxisomes. Recent studies by other graduate students in Dr. Titorenko's laboratory have revealed that in chronologically aging yeast LCA has a pleiotropic effect on the mitochondrial protein machines involved in mitochondrial respiration, maintenance of the electrochemical potential across the inner mitochondrial membrane, reactive oxygen species (ROS) production in mitochondria, mitochondrial fusion and mitochondria-controlled apoptosis. These findings prompted me to elucidate how LCA influences the composition of mitochondrial membrane lipids and their metabolism in yeast. Cardiolipin (CL) is a mitochondria-specific dimeric glycerophospholipid, which is synthesized and almost exclusively localized in the mitochondrial inner membrane [193, 195, 196, 198 - 200]. Phosphatidylethanolamine (PE) is a glycerophospholipid, which is almost exclusively synthesized in the mitochondrial inner membrane – from which it is then distributed to various other cellular membranes [198, 200]. In experiments described in this Chapter, I first elucidated how mutations eliminating nucleus-encoded mitochondrial proteins involved in the synthesis of CL and PE within the mitochondrial inner membrane influence the life-extending efficacy of LCA in chronologically aging yeast

grown under CR conditions. I found that the synthesis of both these membrane lipids in mitochondria plays a pivotal role in the ability of LCA to extend yeast longevity under CR conditions. To establish the molecular mechanism underlying the essential role of CL and PE dynamics in longevity-extending effect of LCA, I then used mass spectrometry (MS)-based lipidomics to elucidate how LCA influences the composition and quantities of membrane lipids in mitochondria that were purified from wild-type (WT) strain and from various long- and short-lived mutant strains impaired in different aspects of CL and PE metabolism. By correlating the effects of LCA on the age-related dynamics of changes in the repertoire of membrane lipids in mitochondria of these strains to the effects of this bile acid on their chronological life span (CLS), I concluded that under CR conditions LCA extends yeast longevity by remodeling the composition of mitochondrial membrane lipids and thereby modulating longevity-defining processes confined to and/or governed by mitochondria. My findings imply that LCA extends the CLS of WT yeast by: 1) increasing the level of phosphatidylserine (PS; a precursor for the synthesis of PE in mitochondria) in the mitochondrial membrane, thereby enhancing its positive effect on longevity-defining processes in this membrane; 2) decreasing the level of PE in the mitochondrial membrane, thereby weakening its negative effect on longevity-defining processes in this membrane; and 3) proportionally decreasing the levels of PE and CL in the mitochondrial membrane, thereby increasing PS/CL and PS/PE ratios but maintaining PE/CL ratio of mitochondrial membrane lipids and causing some longevity-extending changes in this membrane. My analysis of the biological implications of these specific changes in mitochondrial membrane lipids revealed that, by altering the levels of PS, CL and PE, LCA: 1) changes the curvature of the inner mitochondrial membrane; and 2)

enhances the positive effect of PS and weakens the negative effect of PE on membrane proteins whose activity depends on these two lipid species - thereby enhancing the ability of the inner mitochondrial membrane to form cristae and activating protein machines involved in mitochondrial respiration, the maintenance of mitochondrial membrane potential and ROS production in mitochondria.

5.2. Introduction

CL is a unique class of membrane lipids whose various molecular species can be found only in mitochondria – mostly in the mitochondrial inner membrane, but also (up to 20% of the total CL pool) in the mitochondrial outer membrane [195, 198 - 200]. Because of the ability to interact with a number of functionally distinct proteins in the mitochondrial inner membrane and to serve as a precursor for the synthesis of the potent signaling molecule phosphatidic acid (PA), CL has been shown to govern a number of vital processes taking place in and/or orchestrated from this membrane, including 1) the assembly and functional state of all five complexes of the mitochondrial respiratory chain and their organization into supercomplexes; 2) the retention in the mitochondrial inner membrane of cytochrome c, a heme-containing mobile component of the mitochondrial respiratory chain also known for its essential role in mitochondria-controlled apoptosis; 3) the functional state of the adenine nucleotide translocator in the mitochondrial membrane; 4) the maintenance of the electrochemical gradient across the mitochondrial inner membrane; 5) the fluidity and stability of the inner membrane of mitochondria; 6) the susceptibility of mitochondrial membrane proteins and lipids to an ROS-inflicted oxidative damage; 7) the import of various proteins into mitochondria; 8) the fusion of

individual mitochondria into a tubular network; and 9) the fission (division) of mitochondria leading to fragmentation of this tubular mitochondrial network [194 - 203]. Due to the essential role of CL in a plethora of basic biological processes, certain changes in its content and/or species composition have been have been shown to cause pathological states characteristic of various disorders. Among these disorders are: 1) a Barth Syndrome spectrum of X-linked recessive disorders, which includes cardioskeletal myopathy, neutropenia and abnormal growth [193, 195, 198]; 2) Tangier disease [195, 198]; 3) diabetic cardiomyopathy [195, 198]; 4) dilated cardiomyopathy with ataxia [195, 198]; and 5) non-alcoholic fatty liver disease [195, 198].

Importantly, reduced levels of CL and the resulting accumulation of dysfunctional mitochondria are characteristic of the early stages of aging in rodents and humans [194, 195, 198]. Moreover, I found that a longevity-extending CR diet reduces the level of CL in the mitochondrial membrane of chronologically aging yeast [18]. It is conceivable therefore that CL plays a pivotal role in regulating various mitochondria-governed processes whose dysfunction underlies aging and age-related pathologies. However, the molecular basis of such essential role for CL in modulating longevity-defining processes confined to and/or governed by mitochondria remains elusive. In studies described in this Chapter, I used a combination of functional genetic, cell biological, electron and fluorescence microscopical, and lipidomic experimental approaches to decipher the molecular mechanism underlying the ability of LCA to extend longevity of chronologically aging yeast by altering the concentrations of CL and other mitochondrial membrane lipids and by modifying the spectra of their various molecular species.

5.3. Materials and Methods

Strains and media

The wild-type strain *Saccharomyces cerevisiae* BY4742 (*MATα his3Δ1 leu2Δ0 lys2Δ0 ura3Δ0*) and mutant strains *ups1Δ* (*MATα his3Δ1 leu2Δ0 lys2Δ0 ura3Δ0 ups1Δ::kanMX4*), *taz1Δ* (*MATα his3Δ1 leu2Δ0 lys2Δ0 ura3Δ0 taz1Δ::kanMX4*), *gep1Δ* (*MATα his3Δ1 leu2Δ0 lys2Δ0 ura3Δ0 gep1Δ::kanMX4*), *psd1Δ* (*MATα his3Δ1 leu2Δ0 lys2Δ0 ura3Δ0 psd1Δ::kanMX4*) and *crd1Δ* (*MATα his3Δ1 leu2Δ0 lys2Δ0 ura3Δ0 crd1Δ::kanMX4*) were used in this study. Yeast were grown in YEPD medium initially containing 0.2% glucose as carbon source at 30°C with rotational shaking at 200 rpm in Erlenmeyer flasks at a flask volume/medium volume ratio of 5:1.

A plating assay for the analysis of chronological life span

A sample of cells was removed from each culture at various time points. A fraction of the cell sample was diluted in order to determine the total number of cells per ml of culture using a hemacytometer. 10 μl of serial dilutions (1:10 to 1:10^3) of cells were applied to the hemacytometer, where each large square is calibrated to hold 0.1 μl. The number of cells in 4 large squares was then counted and an average was taken in order to ensure greater accuracy. The concentration of cells was calculated as follows: number of cells per large square x dilution factor × 10 × 1,000 = total number of cells per ml of culture. A second fraction of the cell sample was diluted and serial dilutions (1:10^2 to 1:10^5) of cells were plated onto YEPD (2% Glucose) plates in triplicate in order to count the number of viable cells per ml of each culture. 100 μl of diluted culture was plated onto each plate. After a 48-h incubation at 30°C, the number of colonies per plate was counted. The

number of colony forming units (CFU) equals to the number of viable cells in a sample. Therefore, the number of viable cells was calculated as follows: number of colonies × dilution factor × 10 = number of viable cells per ml. For each culture assayed, % viability of the cells was calculated as follows: number of viable cells per ml / total number of cells per ml × 100%. The % viability of cells in mid-logarithmic phase was set at 100% viability for that particular culture.

Electron microscopy and morphometric analysis

Cells were fixed in 1.5% $KMnO_4$ for 20 min at room temperature, dehydrated by successive incubations in increasing concentrations of ethanol, and embedded in Poly/Bed 812 epoxy resin (Polysciences). Ultrathin sections were cut using an Ultra-Cut E Microtome (Reichert-Jung). Silver/gold thin sections from the embedded blocks were examined in a JEOL JEM-2000FX transmission electron microscope. For morphometric analysis of random electron microscopic sections of cells, digitized images were analyzed using the UTHSCSA Image Tool (Version 3.0) software. In each of 2 independent experiments, the percentage of cells that contain pexopodia and/or accumulate gnarled LBs was calculated by analyzing at least 300 cells that were collected at each time point. The values of the percentage of cells containing pexopodia and/or accumulating gnarled LBs were plotted as a function of the number of days cells were cultured.

Analysis of lipids by mass spectrometry

1×10^{10} cells were harvested by centrifugation and washed three times with cold water. The lipids were extracted by resuspending the cells in 3.8 ml of chloroform - methanol -

water (1:2:0.8) and by vortexing the cell suspension with glass beads two times for 1 min. 1 ml of chloroform was then added, and the extract was incubated for 5 min with occasional mixing. 1 ml of water was then added, and the extract was incubated for 5 min with occasional mixing. The extract was centrifuged and the entire supernatant was collected. The pellet was resuspended in 1.6 ml of chloroform, and the lipids were extracted by vortexing the suspension with glass beads two times for 1 min. The extract was then centrifuged and the entire supernatant was collected. The pooled supernatants were centrifuged and the organic phase was collected. The lipid extract was dried under nitrogen. The lipid film was dissolved in 400 μl of chloroform - methanol (1:1) containing either 3 mM ammonium hydroxide for positive-ion analyses or no additive for negative-ion measurements. Mass spectrometric analyses were performed with a Micromass Q-TOF 2 mass spectrometer equipped with a nano-electrospray source operating at a flow rate of 1 μl/min. The instrument was used in the single-stage mass spectrometry mode for positive- or negative-ion analyses as described in Chapter 2 of this thesis. For quantification of individual lipid molecular species, the commercially available lipids (Avanti Polar Lipids, Larodan AB and Sigma) with non-natural fatty acid compositions were used as internal standards that do not occur in a significant amount in the sample to be analyzed. Lipid quantification was performed as described in Chapter 2 of this thesis.

5.4. Results

5.4.1. The synthesis of CL and PE within the mitochondrial inner membrane defines the life-extending efficacy of LCA in chronologically

As a first step towards probing a role of CL and other mitochondrial membrane lipids in the longevity-extending ability of LCA, I tested if LCA can increase the CLS of various single-gene-deletion mutants lacking nuclear genes that encode different mitochondrial proteins involved in the synthesis of CL and PE within the mitochondrial inner membrane. The individual steps of the partially overlapping biosynthetic pathways for CL and PE in yeast mitochondria, as well as mitochondrial proteins catalyzing or regulating each of these steps, are well established (Figure 5.1) [197, 198, 200, 205 – 207].
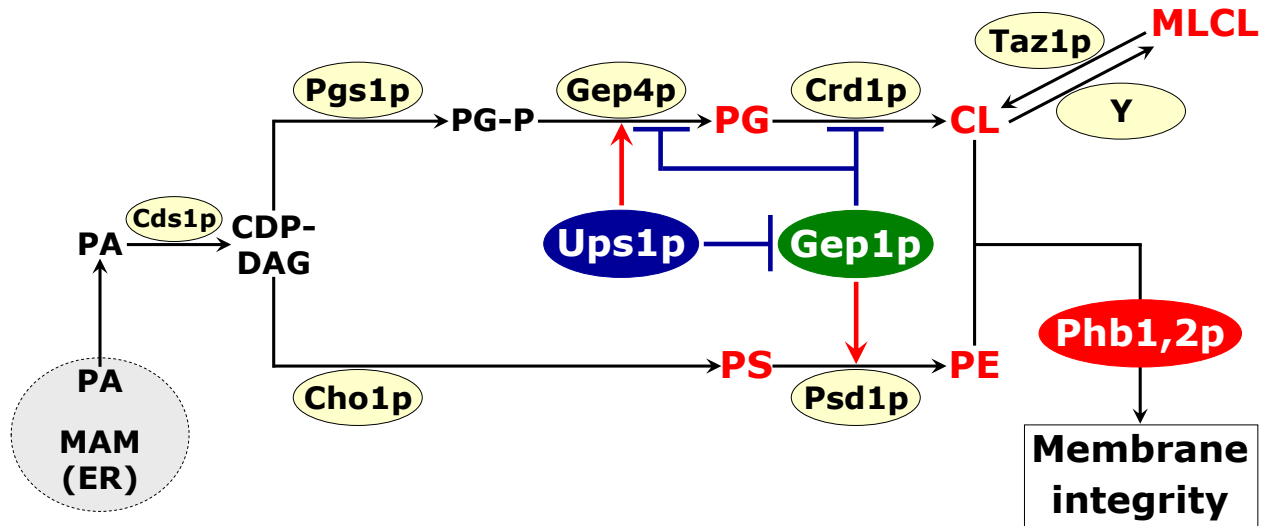
Figure 5.1. Outline of the biosynthesis of cardiolipin (CL), phosphatidylglycerol (PG), phosphatidylethanolamine (PE) and phosphatidylserine (PS) from phosphatidic acid (PA) in the mitochondrial inner membrane. PA is delivered top the mitochondrial inner membrane from the mitochondria-associated membrane (MAM) domain of the endoplasmic reticulum (ER), where it is synthesized. PA is then converted to cytidine diphosphodiacylglycerol (CDP-DAG), which serves as a precursor for synthesis of both CL and PE in the mitochondrial inner membrane. It has been proposed that both CL and PE modulate the ability of prohibitins Phb1p and Phb2p - two evolutionarily conserved proteins that form large complexes with each other in the mitochondrial inner membrane - to maintain the organization and functional integrity of this membrane [197, 200, 204 - 207]. Other abbreviations: PG-P, phosphatidylglycerol phosphate; MLCL, monolysocardiolipin.

I found that mutations eliminating the Crd1p, Taz1p, Psd1p, Ups1p or Gep1p mitochondrial proteins involved in the synthesis of CL and PE within the mitochondrial inner membrane differentially alter the ability of LCA to extend the CLS of yeast grown under CR conditions on 0.2% glucose. Specifically, LCA is unable to extend the CLS of

the *ups1Δ* mutant (Figure 5.2) lacking a protein that regulates the biosynthesis of PG, CL and PE (Figure 5.1). Furthermore, LCA is unable to extend the CLS of the *taz1Δ* mutant (Figure 5.3) - which lacks an enzyme catalyzing the conversion of MLCL to CL (Figure 5.1). Moreover, the *gep1Δ* mutation - which eliminates a protein regulating the biosynthesis of CL and PE (Figure 5.1) - enhances the ability of LCA to extend the CLS of yeast under CR conditions (Figure 5.4). In addition, the *psd1Δ* mutation - which
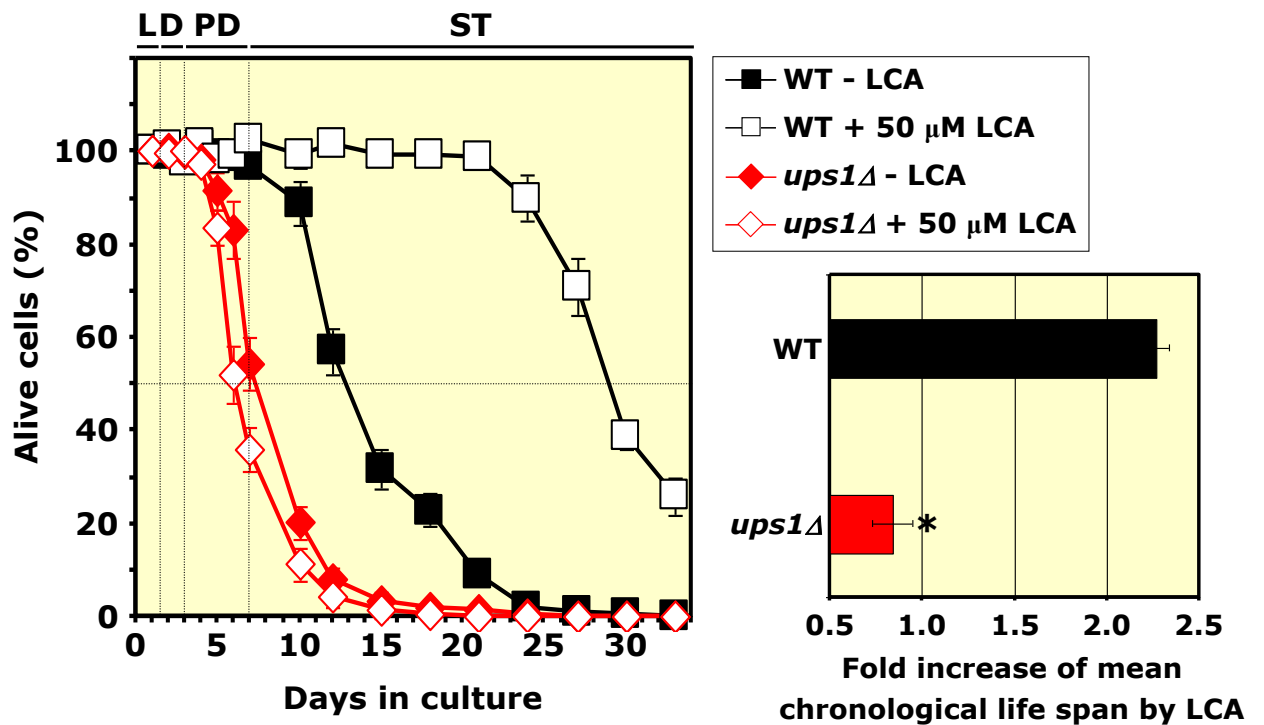
Figure 5.2. LCA is unable to extend the CLS of the *ups1Δ* mutant lacking a protein that regulates the biosynthesis of PG, CL and PE.
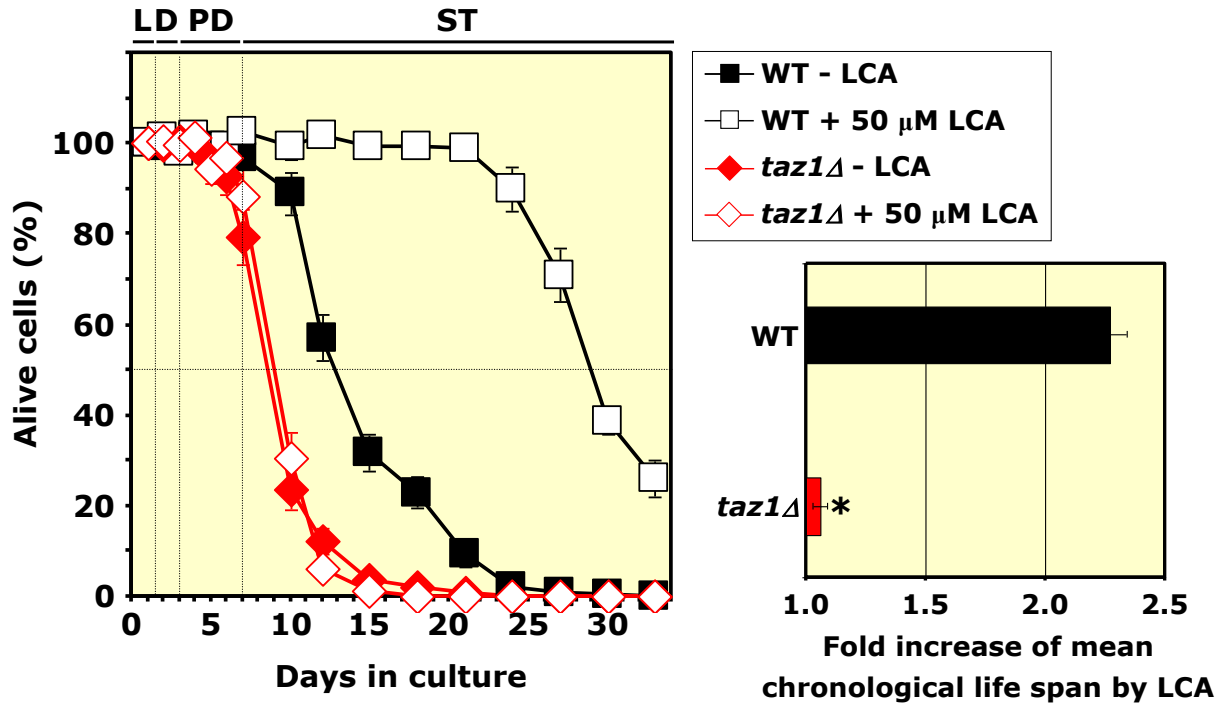
Figure 5.3. LCA is unable to extend the CLS of the *taz1Δ* mutant, which lacks an enzyme catalyzing the conversion of MLCL to CL.
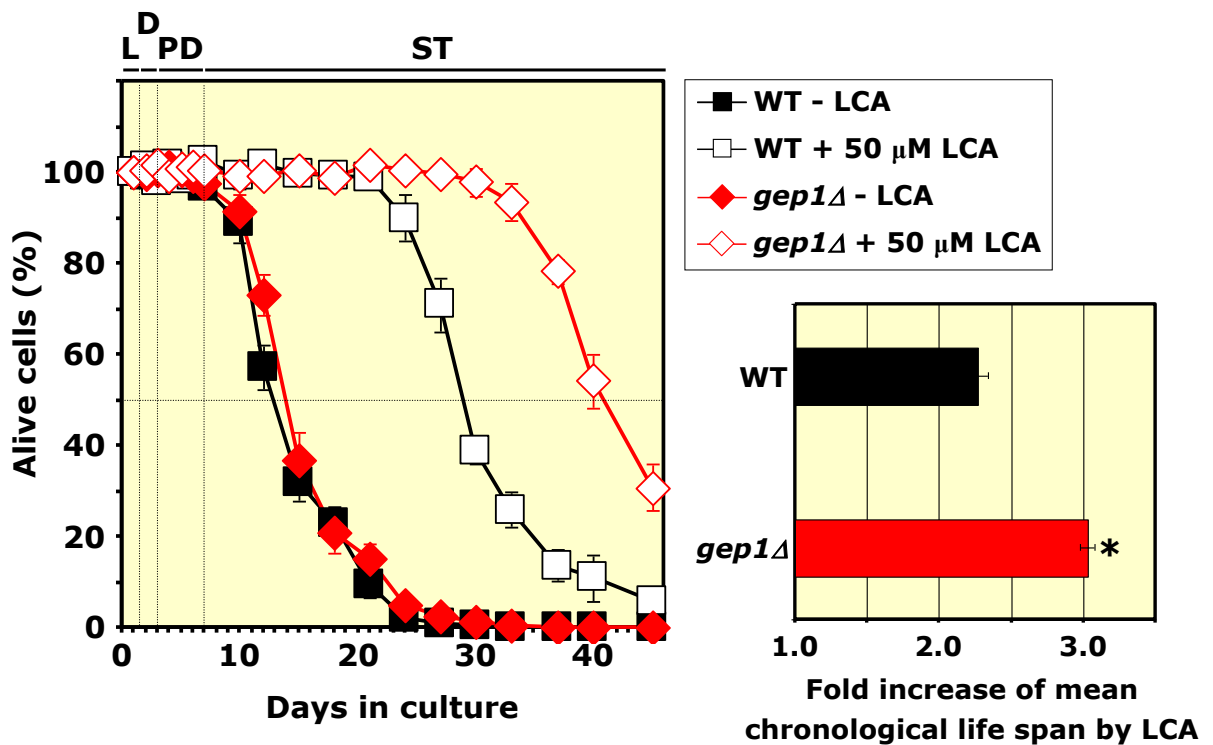
Figure 5.4. The *gep1Δ* mutation - which eliminates a protein regulating the biosynthesis of CL and PE - enhances the ability of LCA to extend the CLS of yeast under CR conditions.
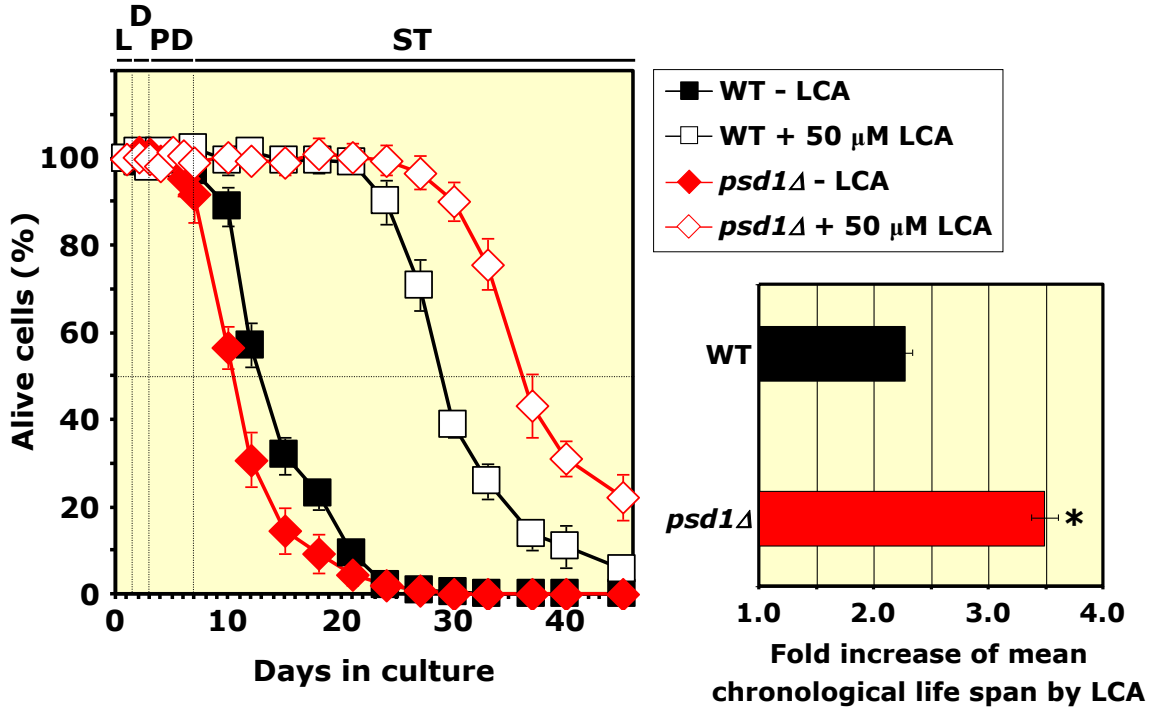
Figure 5.5. The *psd1Δ* mutation – which eliminates an enzyme catalyzing the biosynthesis of PE - enhances the ability of LCA to extend longevity of chronologically aging yeast grown under CR conditions.

Figure 5.6. The *crd1Δ* mutation – which eliminates an enzyme catalyzing the biosynthesis of CL - enhances the ability of LCA to extend the CLS of yeast grown under CR conditions.

eliminates an enzyme catalyzing the biosynthesis of PE (Figure 5.1) - enhances the ability of LCA to extend longevity of chronologically aging yeast grown under CR conditions (Figure 5.5). Finally, the *crd1Δ* mutation − which eliminates an enzyme catalyzing the biosynthesis of CL (Figure 5.1) - enhances the ability of LCA to extend the CLS of yeast grown under CR conditions (Figure 5.6).

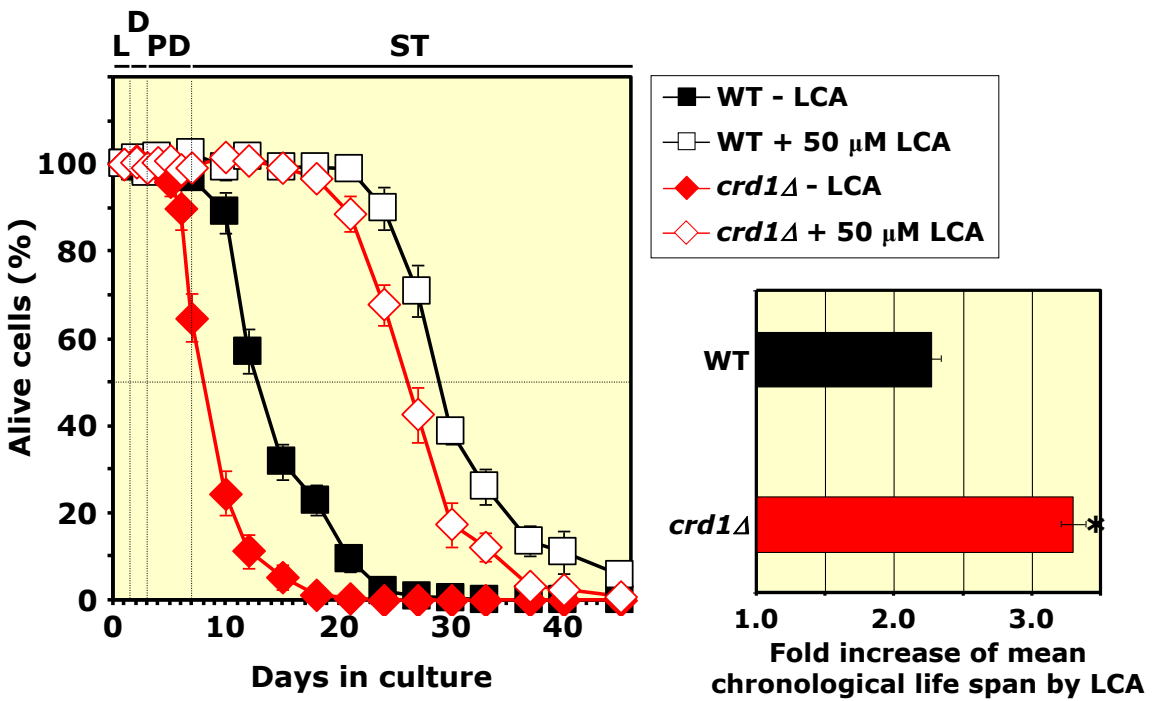Altogether, these data imply that the rates of synthesis of CL and PE from their precursors PG and PS (respectively), as well as the rate of remodeling of acyl chains of CL by the sequential action of a phospholipase A (converting CL to MLCL) and a transacylation reaction catalyzed by Taz1p (Figure 5.1), within the mitochondrial inner membrane define the longevity-extending efficacy of LCA. I therefore hypothesized that one of the mechanisms underlying the ability of LCA to extend yeast longevity consists in the LCA-driven remodeling of the mitochondrial membrane by altering the concentrations of CL, PE, PG, PS and/or MLCL and, perhaps, by changing the relative abundance of certain molecular species of these membrane lipids. In my hypothesis, such LCA-driven remodeling of the composition of mitochondrial membrane lipids extends the CLS of CR yeast by modulating longevity-defining processes confined to and/or governed by mitochondria.

5.4.2. LCA alters the concentrations of membrane lipids and their relative abundance in mitochondria of WT cells

In my hypothesis, LCA remodels the mitochondrial membrane by altering the concentrations of CL, PE, PG, PS and/or MLCL and, perhaps, by changing their relative abundance. To test the validity of my hypothesis, I used MS-based lipidomics to monitor
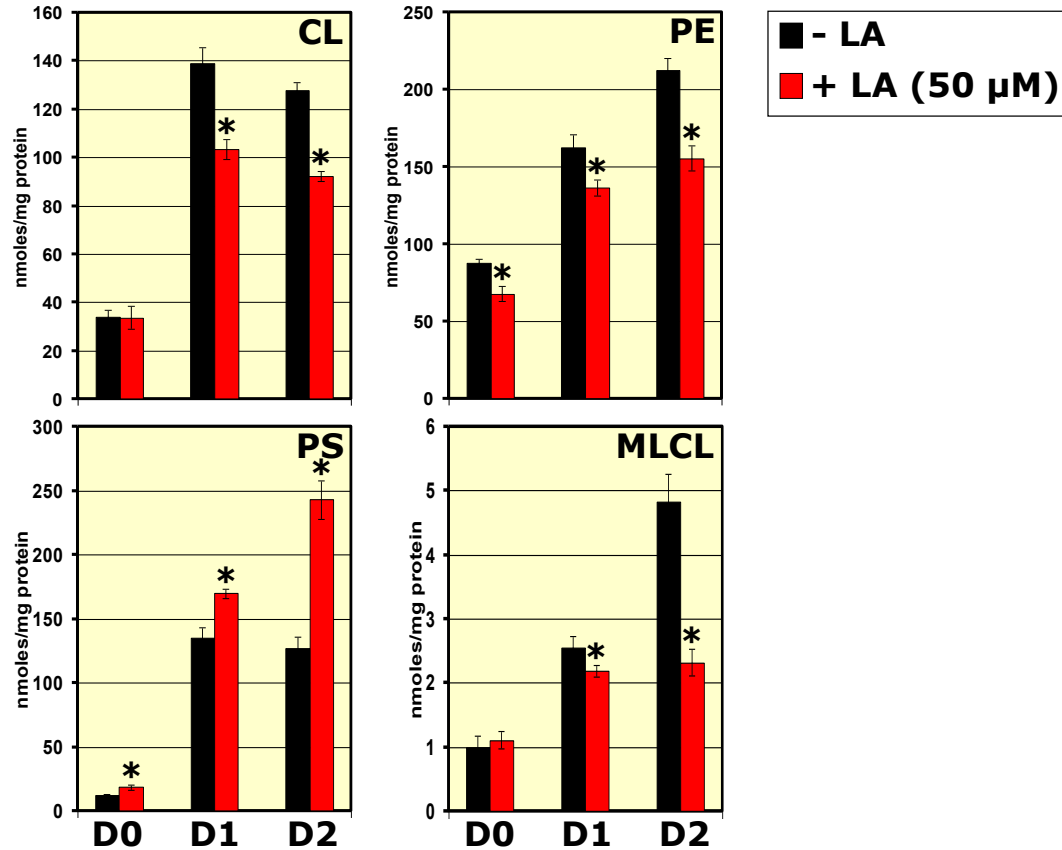
Figure 5.7. Effect of LCA on the age-related dynamics of changes in the total levels of CL, PE, PS and MLCL in the membranes of mitochondria purified from WT cells. Yeast were grown in YEPD medium initially containing 0.2% glucose as carbon source, without LCA or with this bile acid (used in the concentration of 50 μM), and collected for the purification of mitochondria at days 0, 1 or 2. Mitochondrial membrane lipids were identified and quantitated by MS as described in Materials and Methods. *$p < 0.05$.

how LCA influences the age-related dynamics of changes in the levels of CL, PE, PS and MLCL in the membrane of mitochondria purified from WT cells (Of note, because CDP-DAG, PG-P and PG do not accumulate in significant amounts in mitochondrial membranes under normal conditions [198, 200], these important intermediates for the synthesis of CL, PE, PS and MLCL within the mitochondrial inner membrane (Figure 5.1) were not detectable even by MS in mitochondria purified from WT cells; I was able to detect PG accumulation by MS only in mitochondria purified from the *crd1Δ* mutant,
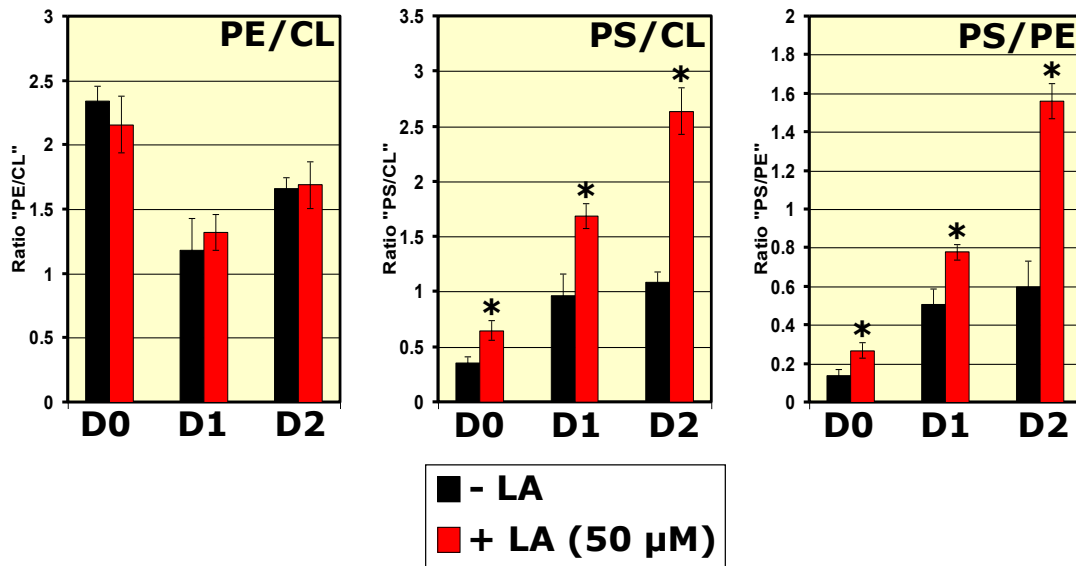
Figure 5.8. Effect of LCA on the age-related dynamics of changes in PE/CL, PS/CL and PS/PE ratios in the membranes of mitochondria purified from WT cells. Yeast were grown in YEPD medium initially containing 0.2% glucose as carbon source, without LCA or with this bile acid (used in the concentration of 50 μM), and collected for the purification of mitochondria at days 0, 1 or 2. Mitochondrial membrane lipids were identified and quantitated by MS as described in Materials and Methods. *$p < 0.05$.

which lacks an enzyme catalyzing the synthesis of CL from PG and CDP-DAG). I found that LCA reduces the total levels of CL, PE and MLCL but significantly elevates the total level of PE (Figure 5.7). The observed effect of LCA on the quantities of CL, PE and PS enables to maintain PE/CL ratio in the mitochondrial membrane (Figure 5.8). On the other hand, by elevating the total level of PS, LCA greatly increases PS/CL and PS/PE ratios in the membrane of WT mitochondria (Figure 5.8). Taken together, my findings suggest that LCA inhibits the Crd1p- and Psd1p-driven reactions of the biosynthesis of CL and PE (respectively) in the mitochondrial inner membrane - thereby reducing the quantities of these two lipid classes and increasing the quantity of PS, a precursor of PE (Figure 5.9).
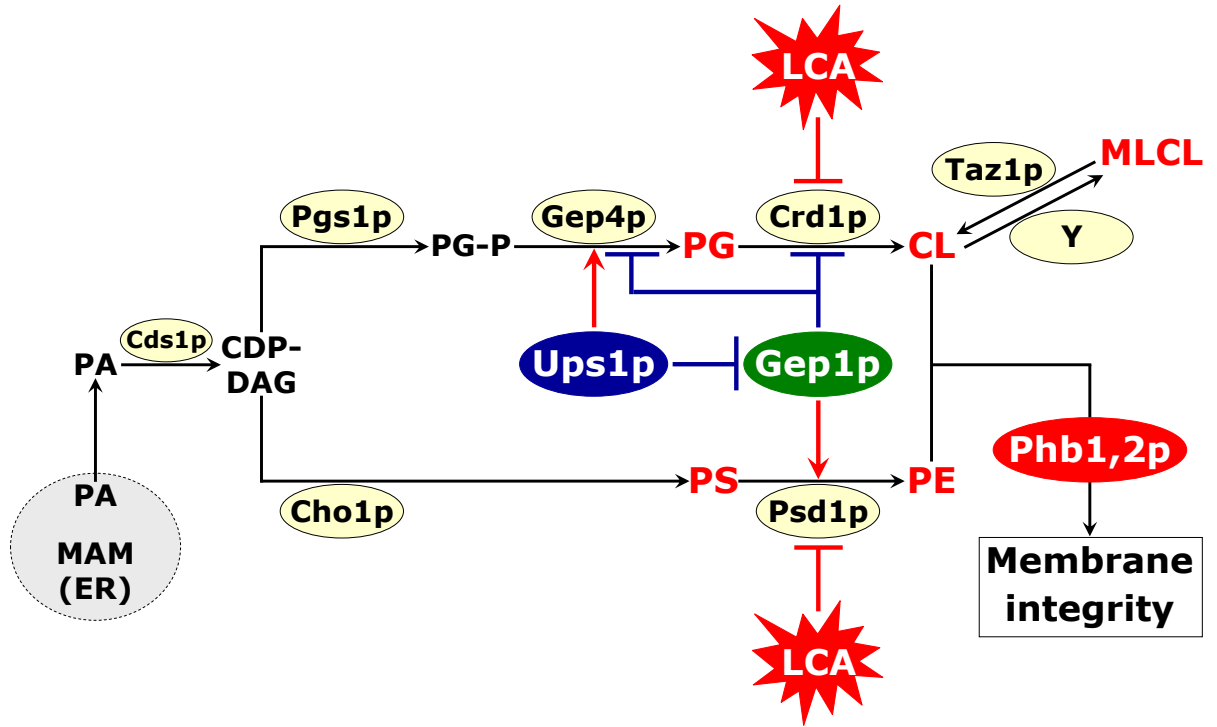
Figure 5.9. Based on my findings, I propose that LCA inhibits the Crd1p- and Psd1p-driven reactions of the biosynthesis of CL and PE (respectively) in the mitochondrial inner membrane - thereby reducing the quantities of these two lipid classes and increasing the quantity of PS, a precursor of PE.

5.4.3. The LCA-driven remodeling of the mitochondrial membrane by altering the concentrations and relative abundancies of CL, PE and PS is essential for the longevity-extending ability of LCA and defines its efficacy

In my hypothesis, the observed LCA-driven remodeling of the mitochondrial membrane by altering the concentrations and relative abundancies of CL, PE and PS is essential for the longevity-extending ability of LCA and defines its efficacy. To test the validity of such hypothesis, I used MS-based lipidomics for the identification and quantitation of various species of CL, PE and PS extracted from purified mitochondria of *ups1Δ, taz1Δ,*

psd1Δ or *gep1Δ* mutant cells grown in medium without LCA or with LCA (used in the concentration of 25 μM or 50 μM) and collected at days 0, 1 or 2. My comparative MS-
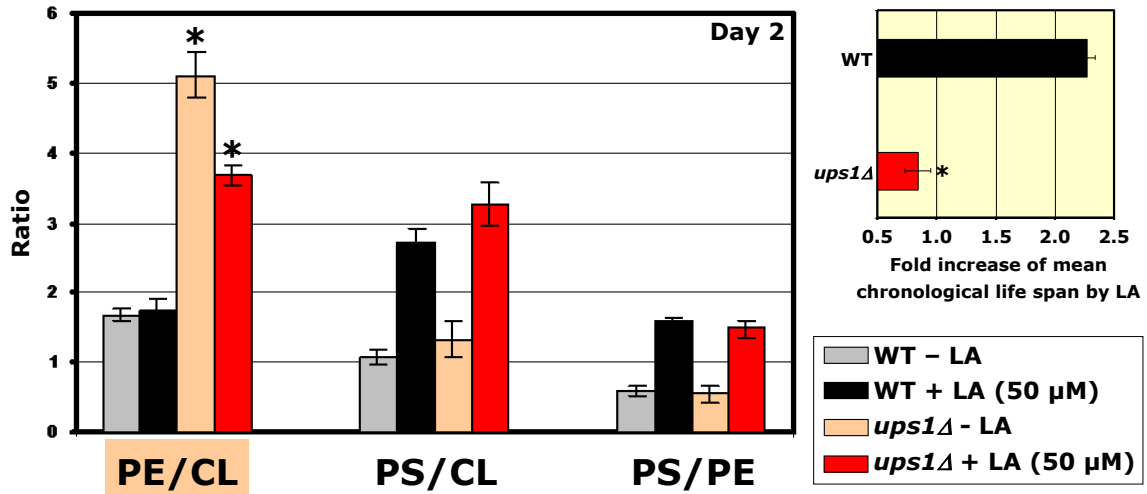
Figure 5.10. LCA cannot extend the life span of the *ups1Δ* mutant which has greatly elevated (as compared to WT strain) PE/CL ratio, in spite of the ability of LCA to reduce this ratio in the mitochondrial membranes of *ups1Δ*. Yeast were grown in YEPD medium initially containing 0.2% glucose as carbon source, without LCA or with this bile acid (used in the concentration of 50 μM), and collected for the purification of mitochondria at day 2. Mitochondrial membrane lipids were identified and quantitated by MS as described in Materials and Methods. *p < 0.05.
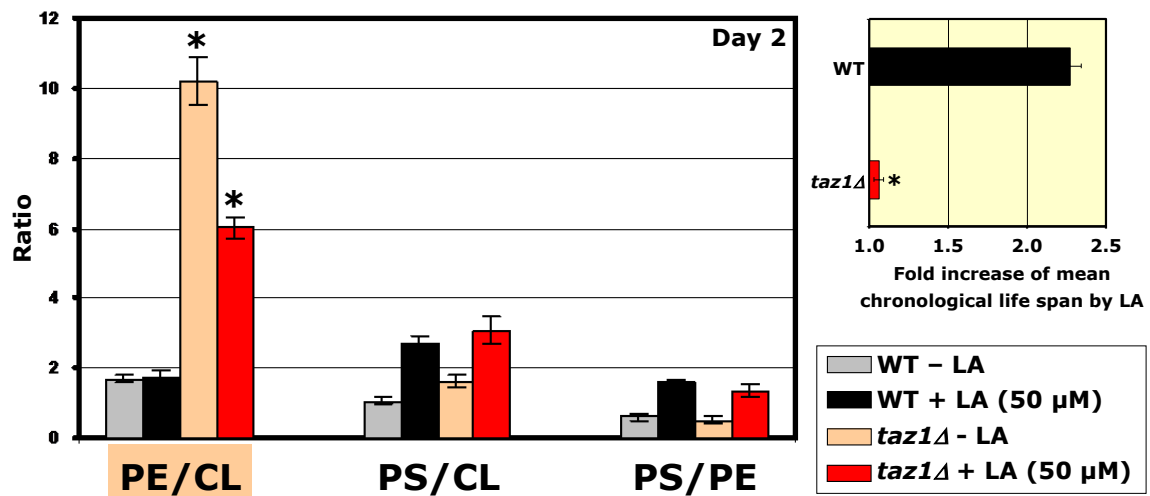
Figure 5.11. LCA cannot extend the life span of the *taz1Δ* mutant which has greatly elevated (as compared to WT strain) PE/CL ratio, in spite of the ability of LA to reduce this ratio in the mitochondrial membranes of *taz1Δ*. Yeast were grown in YEPD medium initially containing 0.2% glucose as carbon source, without LCA or with this bile acid (used in the concentration of 50 μM), and collected for the purification of

210

mitochondria at day 2. Mitochondrial membrane lipids were identified and quantitated by MS as described in Materials and Methods. *p < 0.05.
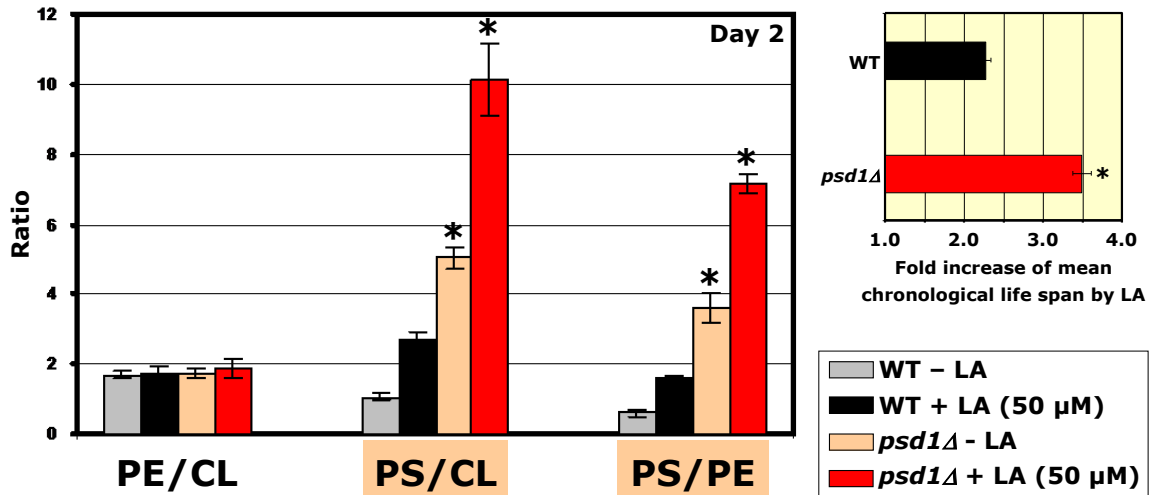
Figure 5.12. The ability of LCA to extend life span is enhanced in the *psd1Δ* mutant strain which maintains PE/CL ratio at the same level as WT strain and has greatly elevated (as compared to WT strain) PS/CL and PS/PE ratios, both of which are further increased by LCA. Yeast were grown in YEPD medium initially containing 0.2% glucose as carbon source, without LCA or with this bile acid (used in the concentration of 50 μM), and collected for the purification of mitochondria at day 2. Mitochondrial membrane lipids were identified and quantitated by MS as described in Materials and Methods. *p < 0.05.

Figure 5.13. The ability of LCA to extend life span is enhanced in the *gep1Δ* mutant strain which maintains PE/CL ratio at the same level as WT strain and has greatly elevated (as compared to WT strain) PS/CL and PS/PE ratios, both of which are further increased by LCA. Yeast were grown in YEPD medium

211

initially containing 0.2% glucose as carbon source, without LCA or with this bile acid (used in the concentration of 50 μM), and collected for the purification of mitochondria at day 2. Mitochondrial membrane lipids were identified and quantitated by MS as described in Materials and Methods. *p < 0.05.

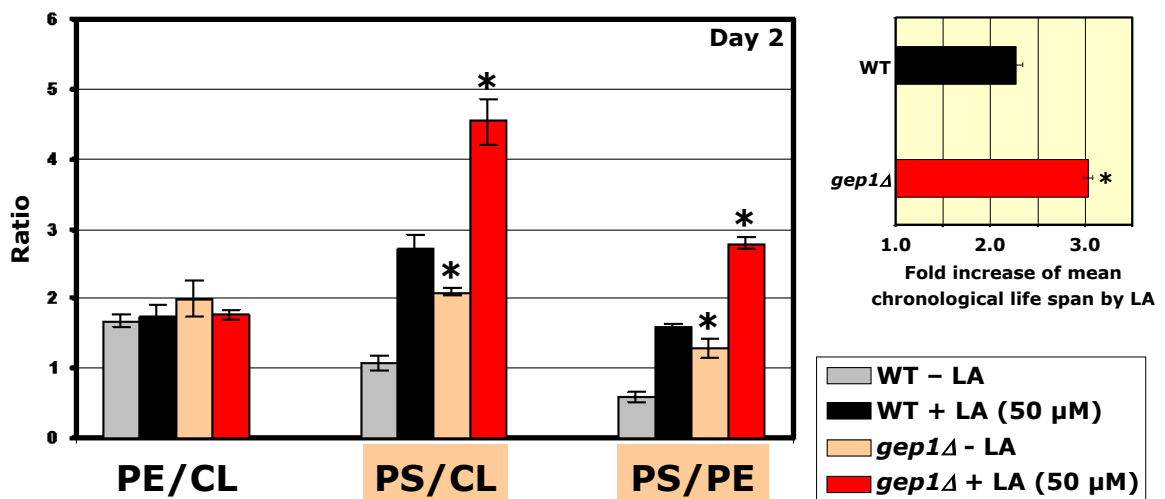assisted lipidomic analysis leads to the following conclusions. First, LCA cannot extend the life span of the *ups1Δ* mutant which has greatly elevated (as compared to WT strain) PE/CL ratio, in spite of the ability of LCA to reduce this ratio in the mitochondrial membranes of *ups1Δ* (Figure 5.10). Second, LCA cannot extend the life span of the *taz1Δ* mutant which has greatly elevated (as compared to WT strain) PE/CL ratio, in spite of the ability of LA to reduce this ratio in the mitochondrial membranes of *taz1Δ* (Figure 5.11). Third, the ability of LCA to extend life span is enhanced in the *psd1Δ* mutant strain which maintains PE/CL ratio at the same level as WT strain and has greatly elevated (as compared to WT strain) PS/CL and PS/PE ratios, both of which are further increased by LCA (Figure 5.12). Finally, the ability of LCA to extend life span is enhanced in the *gep1Δ* mutant strain which maintains PE/CL ratio at the same level as WT strain and has greatly elevated (as compared to WT strain) PS/CL and PS/PE ratios, both of which are further increased by LCA (Figure 5.13).

Altogether, my findings imply that under CR conditions LCA extends longevity of chronologically aging yeast by: 1) increasing the level of phosphatidylserine (PS; a precursor for the synthesis of PE in mitochondria) in the mitochondrial membrane, thereby enhancing its positive effect on longevity-defining processes in this membrane; 2) decreasing the level of PE in the mitochondrial membrane, thereby weakening its negative effect on longevity-defining processes in this membrane; and 3) proportionally decreasing the levels of PE and CL in the mitochondrial membrane, thereby increasing

PS/CL and PS/PE ratios but maintaining PE/CL ratio of mitochondrial membrane lipids and causing some longevity-extending changes in this membrane.

5.4.4.   The known ability of prohibitins to preserve the organization and functional integrity of the mitochondrial inner membrane by sensing the relative abundancies of PE and CL is not essential for the longevity-extending ability of LCA

It has been proposed that in yeast both PE and CL modulate the ability of prohibitins Phb1p and Phb2p - two evolutionarily conserved proteins that form large complexes with each other in the mitochondrial inner membrane - to maintain the organization and functional integrity of this membrane [197, 200, 204 - 207]. I therefore hypothesized that, by maintaining PE/CL ratio, LCA supports this essential function of prohibitins – which they are believed [200, 205 - 207] to perform by sensing the relative levels of PE and CL enriched in the mitochondrial inner membrane domains delimited by the Phb1p-Phb2p supercomplexes. However, my functional genetic analysis did not validate such hypothesis. Indeed, I found that the *phb1Δ* mutation does not reduce the longevity-extending efficacy of LCA under CR conditions (Figure 5.14).

5.4.5.   By altering the concentrations and relative abundancies of different molecular species of PS, CL and PE, LCA causes profound changes in mitochondrial size, number, morphology and longevity-related function

I then put forward a hypothesized that, by altering the levels of PS, CL and PE, LCA may: 1) change the curvature of the inner mitochondrial membrane; and/or 2) enhance

the positive effect of PS and weaken the negative effect of PE on membrane proteins whose activity depends on these two lipids. I thought that, by causing such remodeling of lipids in the mitochondrial membrane, LCA may activate protein machines involved in
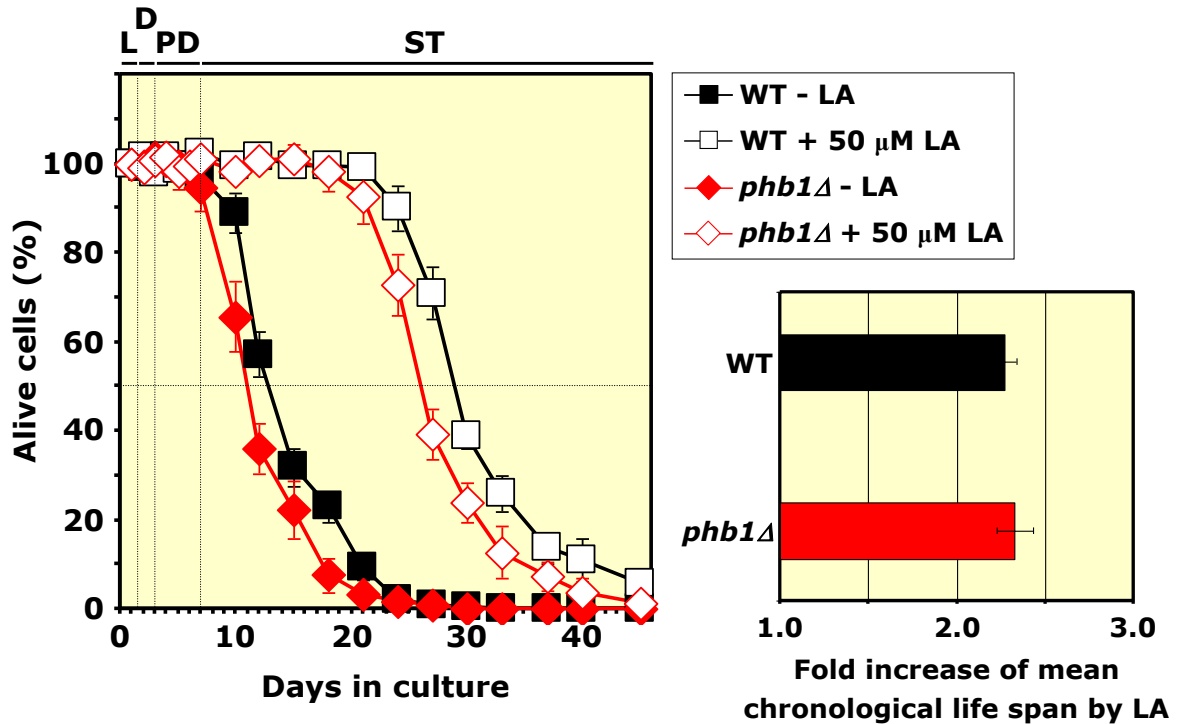
Figure 5.14. The *phb1Δ* mutation does not reduce the longevity-extending efficacy of LCA under CR conditions. Yeast were grown in YEPD medium initially containing 0.2% glucose as carbon source, without LCA or with this bile acid (used in the concentration of 50 μM).

mitochondrial respiration, the maintenance of mitochondrial membrane potential and ROS production in mitochondria as well as may enhance the ability of the inner mitochondrial membrane to form cristae. All these processes have recently been shown by Dr. Titorenko's laboratory to define longevity of chronologically aging yeast (Michelle T. Burstein *et al*., manuscript in preparation). But how exactly PS, CL and PE can influence the curvature of the inner mitochondrial membrane, thereby altering its ability to form cristae, contact sites or remain flat - as well as, perhaps, specifically

modulating the longevity-defining morphology and functional state of mitochondria? My

analysis of the effect of LCA on the levels of various molecular forms of PS, CL and PE

– that differ from each other by the extent of saturation of the hydrophobic tails and their
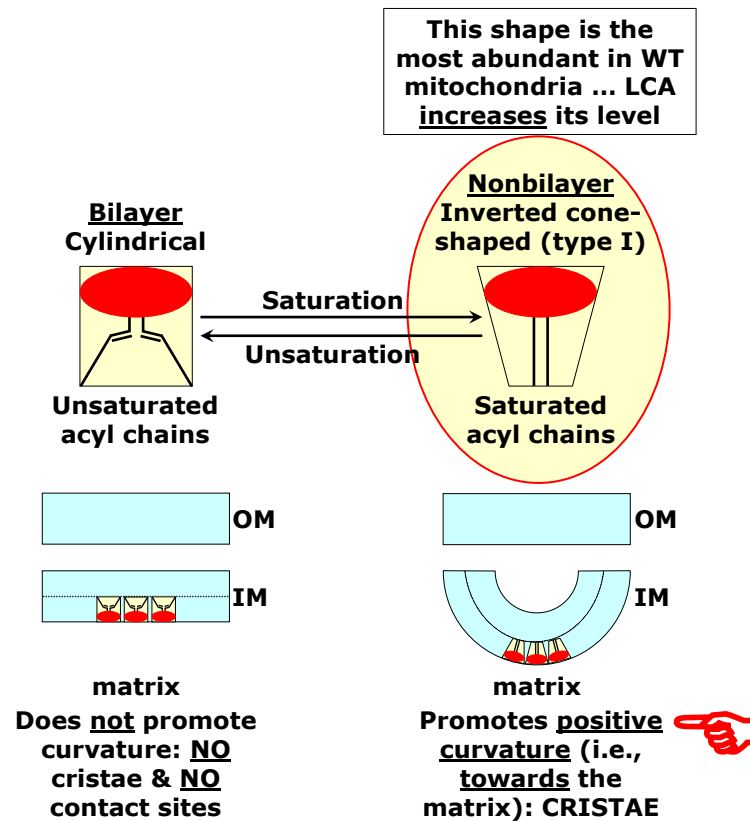
Figure 5.15. LCA increases the level of the inverted cone-shaped species of PS enriched in saturated fatty acids, and thus is expected to enhance cristae formation by promoting positive curvature of the inner mitochondrial membrane.

length – implies that: 1) LCA increases the level of the inverted cone-shaped species of

PS enriched in saturated fatty acids, and thus is expected to enhance cristae formation by

promoting positive curvature of the inner mitochondrial membrane (Figure 5.15); 2) LCA

decreases the level of the cone-shaped species of CL enriched in unsaturated fatty acids,

and thus is expected to decrease the number of contact sites by reducing negative

curvature of the inner mitochondrial membrane; perhaps by causing such effect, LCA

may shift the equilibrium of membrane curvature towards the enhancement of cristae formation by promoting positive curvature of the inner mitochondrial membrane (Figure
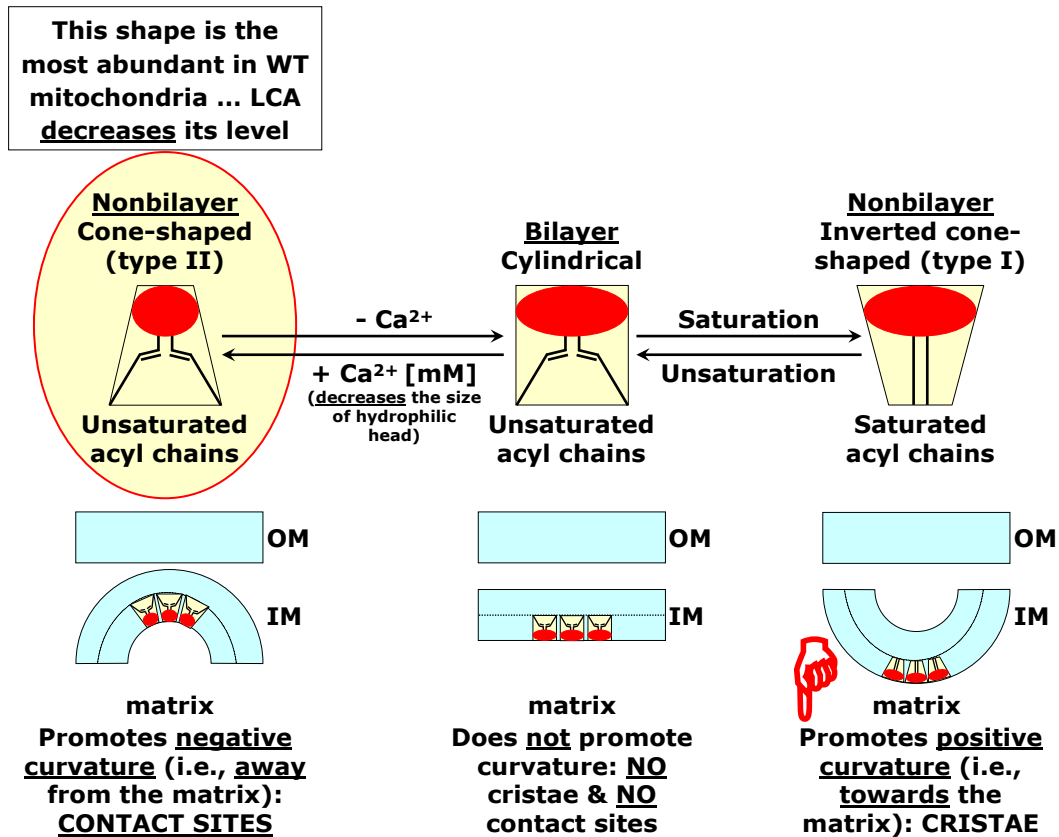
Figure 5.16. LCA decreases the level of the cone-shaped species of CL enriched in unsaturated fatty acids, and thus is expected to decrease the number of contact sites by reducing negative curvature of the inner mitochondrial membrane; perhaps by causing such effect, LCA may shift the equilibrium of membrane curvature towards the enhancement of cristae formation by promoting positive curvature of the inner mitochondrial membrane.

5.16); and 3) LCA decreases the level of the cone-shaped species of PE enriched in unsaturated fatty acids, and thus is expected to decrease the number of contact sites by reducing negative curvature of the inner mitochondrial membrane (Figure 5.17).

Based on these findings, I hypothesized that, by enhancing the ability of the inner mitochondrial membrane to form cristae, LA alters the dynamics of mitochondrial

216

respiration, electrochemical membrane potential maintenance, ROS production - ultimately increasing life span. In support of my hypothesis, I found that LCA causes
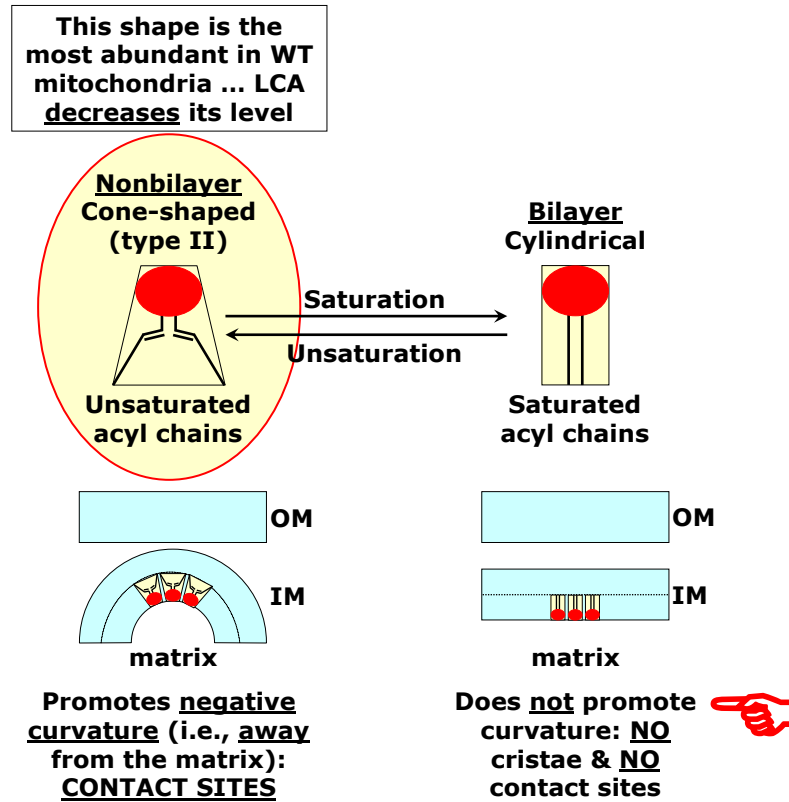
Figure 5.17. LCA decreases the level of the cone-shaped species of PE enriched in unsaturated fatty acids, and thus is expected to decrease the number of contact sites by reducing negative curvature of the inner mitochondrial membrane.

profound changes in the size and number of mitochondria as well as in the length and morphology of mitochondrial cristae in WT cells (Figures 5.18 and 5.19) and in *gep1Δ*, *psd1Δ* and *crd1Δ* cells (Figures 5.20, 5.21 and 5.22, respectively) - in which LCA is even more potent anti-aging compound (see Figures 5.4, 5.5 and 5.6). As a further validation of my hypothesis, I revealed that LCA not only changes mitochondrial morphology, but also alters the age-related dynamics of several longevity-defining processes confined to

mitochondria, including respiration (Figure 5.23), electrochemical potential across the mitochondrial inner membrane (Figure 5.24) and ROS generation (Figure 5.25).
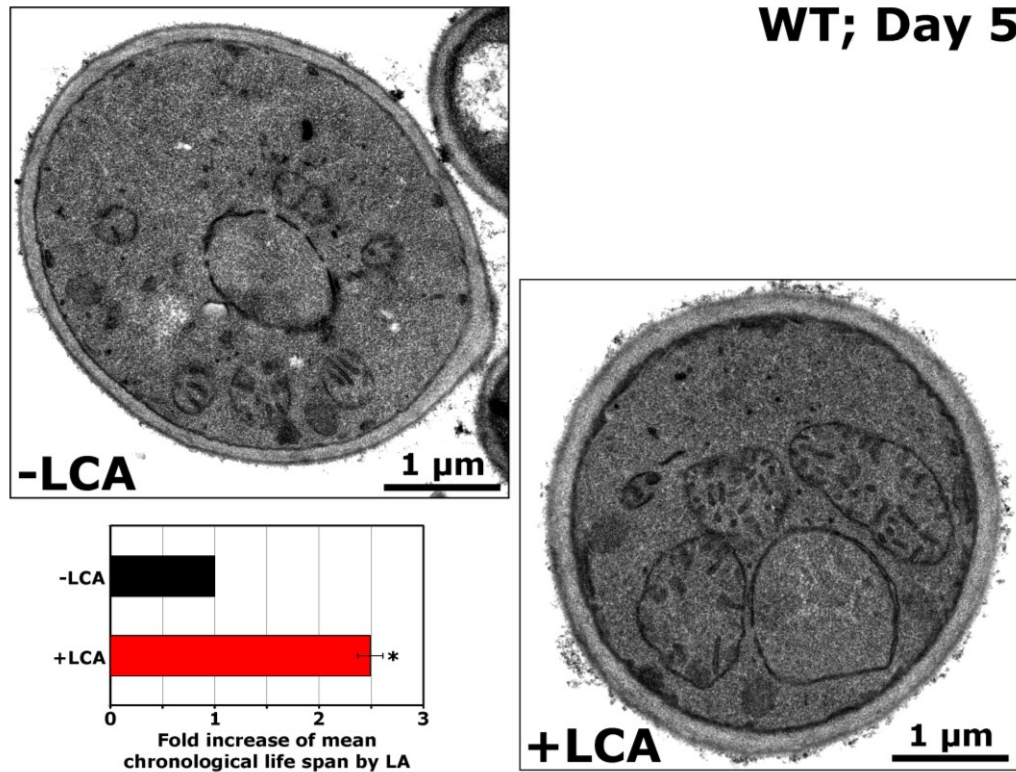
Figure 5.18. LCA causes profound changes in the size and number of mitochondria as well as in the length and morphology of mitochondrial cristae in WT cells. Yeast were grown in YEPD medium initially containing 0.2% glucose as carbon source, without LCA or with this bile acid (used in the concentration of 50 μM), collected at day 5, and processed for electron microscopy as described in Materials and Methods.
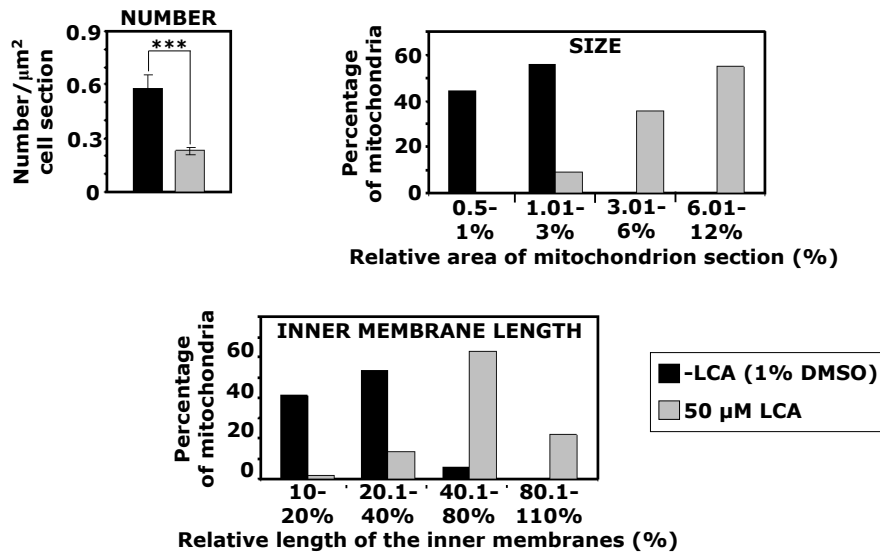
Figure 5.19. LCA greatly reduces the number of mitochondria, increasing their size and expanding their inner membrane in WT cells. Yeast were grown in YEPD medium initially containing 0.2% glucose as carbon source, without LCA or with this bile acid (used in the concentration of 50 μM), collected at day 5, and then processed for electron microscopy and morphometric analysis as described in Materials and Methods.
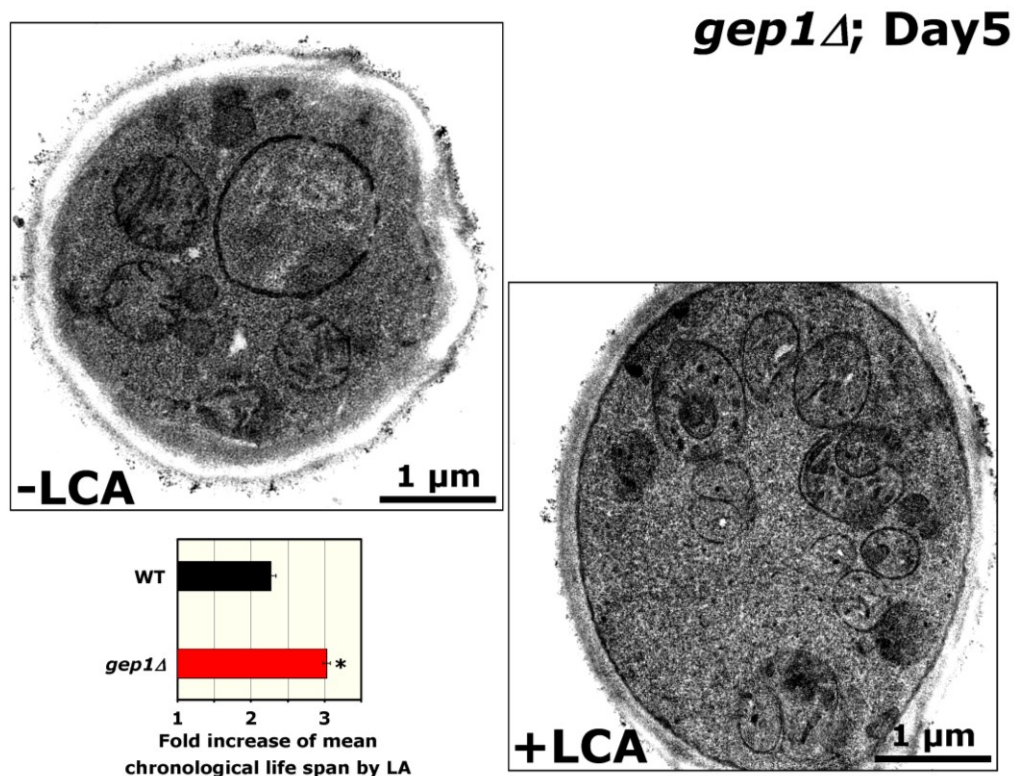
Figure 5.20. LCA alters the length and morphology of mitochondrial cristae in *gep1Δ* cells, in which LCA is even more potent anti-aging compound than it is in WT cells. Yeast were grown in YEPD medium initially containing 0.2% glucose as carbon source, without LCA or with this bile acid (used in the concentration of 50 μM), collected at day 5, and processed for electron microscopy as described in Materials and Methods.

5.5. Discussion

Altogether, my findings described in Chapter 5 of this thesis provide evidence that LCA extends longevity of chronologically aging yeast in part by altering the composition of mitochondrial membrane lipids. Indeed, LCA causes the remodeling of the mitochondrial membrane by proportionally reducing the quantities of PE and CL and simultaneously increasing the quantity of PS, a precursor of PE. I hypothesize that such LCA-driven
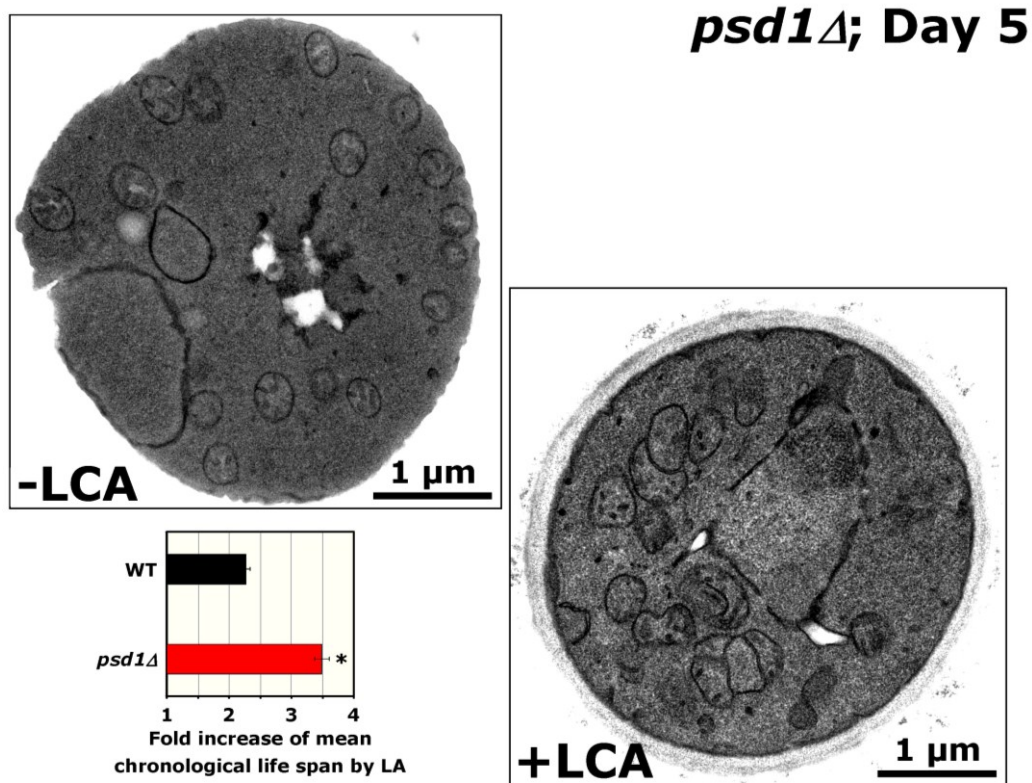
Figure 5.21. LCA alters the length and morphology of mitochondrial cristae in *psd1Δ* cells, in which LCA is even more potent anti-aging compound than it is in WT cells. Yeast were grown in YEPD medium initially containing 0.2% glucose as carbon source, without LCA or with this bile acid (used in the

concentration of 50 µM), collected at day 5, and processed for electron microscopy as described in Materials and Methods.

specific remodeling of the repertoire of mitochondrial membrane lipids is due to an inhibiting effect of LCA on the Crd1p- and Psd1p-driven reactions of the biosynthesis of CL and PE (respectively) in the mitochondrial inner membrane. LCA not only alters the total levels of PS, PE and CL in the mitochondrial membrane, but also has a specific effect in the relative abundance of their various molecular forms that differ from each other by the extent of saturation of the hydrophobic tails and their length. In fact, LCA: 1) elevates the concentration of the inverted cone-shaped species of PS enriched in saturated fatty acids, thereby enhancing cristae formation by promoting positive curvature of the

Figure 5.22. LCA alters the shape and number of mitochondria as well as the length and morphology of mitochondrial cristae in *crd1Δ* cells, in which LCA is even more potent anti-aging compound than it is in WT cells. Yeast were grown in YEPD medium initially containing 0.2% glucose as carbon source, without

LCA or with this bile acid (used in the concentration of 50 µM), collected at day 5, and processed for electron microscopy as described in Materials and Methods.

inner mitochondrial membrane; and 2) reduces the concentrations of the cone-shaped species of CL and PE enriched in unsaturated fatty acids, thereby shifting the equilibrium of membrane curvature towards the enhancement of cristae formation by promoting positive curvature of the inner mitochondrial membrane. Such LCA-driven remodeling of differently shaped molecular forms of PS, CL and PE reduces the number of mitochondria and increases their size. I hypothesized that the observed effect of LCA on the abundance of mitochondria is caused by the ability of this bile acid to shift a balance between the opposing processes of mitochondrial fission and fusion towards fusion,
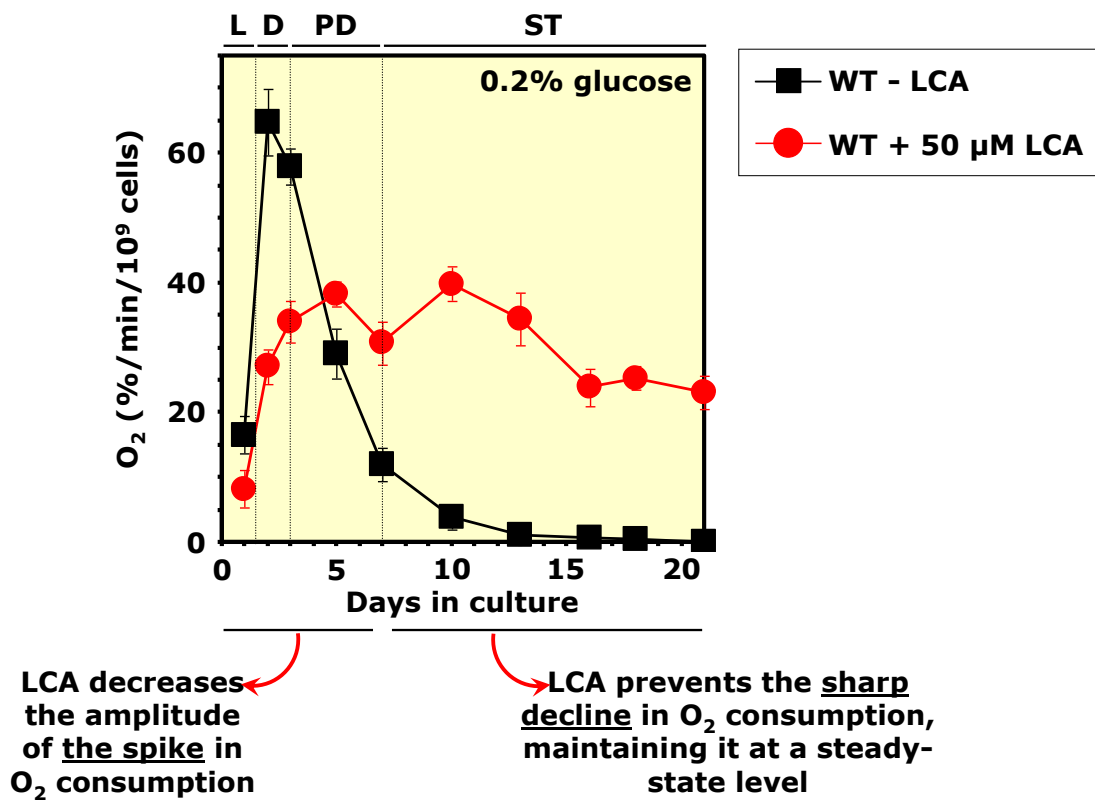
Figure 5.23. LCA alters the age-dependent dynamics of cellular respiration by modulating mitochondrial oxygen consumption in WT cells. Yeast were grown in YEPD medium initially containing 0.2% glucose as carbon source, without LCA or with this bile acid (used in the concentration of 50 µM). Oxygen

consumption in aliquots of cells taken at different time-points was measured as described in Materials and Methods.

thereby preventing the fragmentation of mitochondria and the resulting efflux of cytochrome c and several other pro-apoptotic proteins from the mitochondrial intermembrane space. Ultimately, such effect of LCA on mitochondrial morphology results in the observed delay of the age-related form of mitochondria-controlled apoptosis and longevity extension (see Chapter 4 for a detailed discussion of this topic). Another outcome of the observed LCA-driven remodeling of differently shaped molecular forms of PS, CL and PE consists in significant expansion of the mitochondrial inner membrane,
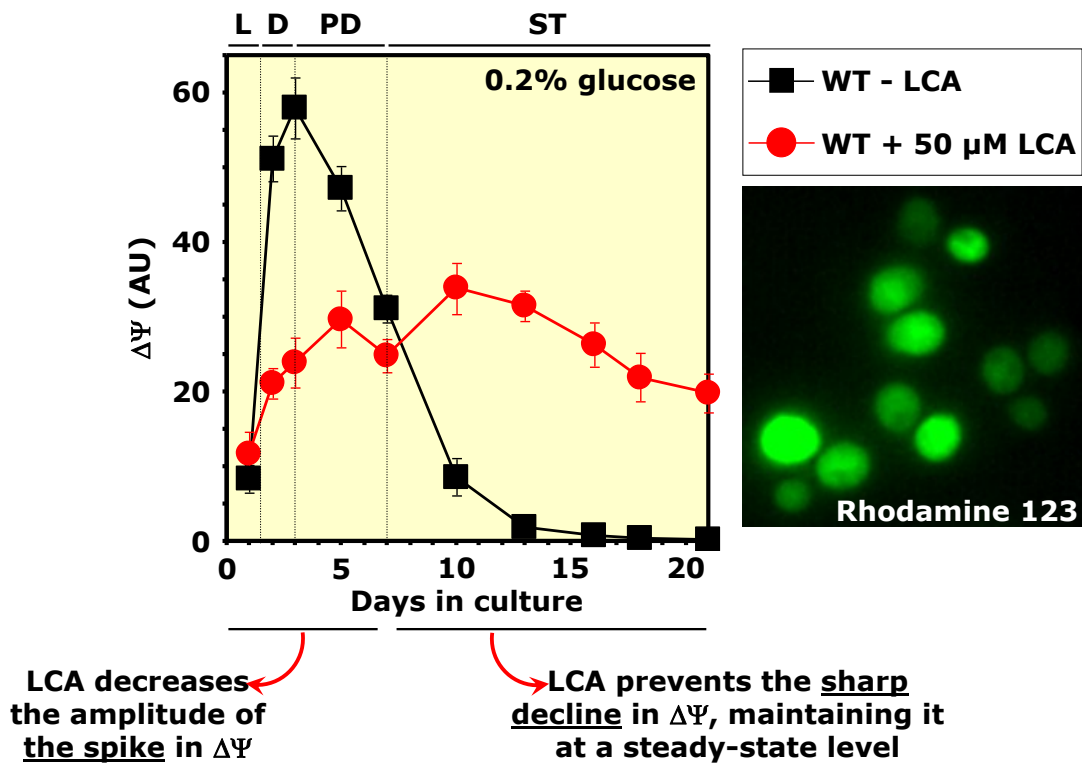
Figure 5.24. LCA alters the age-dependent dynamics of the electrochemical potential across the inner mitochondrial membrane (ΔΨ) in WT cells. Yeast were grown in YEPD medium initially containing 0.2% glucose as carbon source, without LCA or with this bile acid (used in the concentration of 50 μM). ΔΨ in aliquots of cells taken at different time-points was monitored using fluorescence microscopy followed by quantitative analysis as described in Materials and Methods.

which is manifested in a great increase of the length of mitochondrial cristae and in a change of their morphology. It is conceivable that such LCA-driven enhancement of the ability of the mitochondrial inner membrane to form cristae is responsible for the observed ability of LCA to alter the age-related dynamics of several longevity-defining processes confined to mitochondria, including respiration, electrochemical potential across the mitochondrial inner membrane and ROS generation.
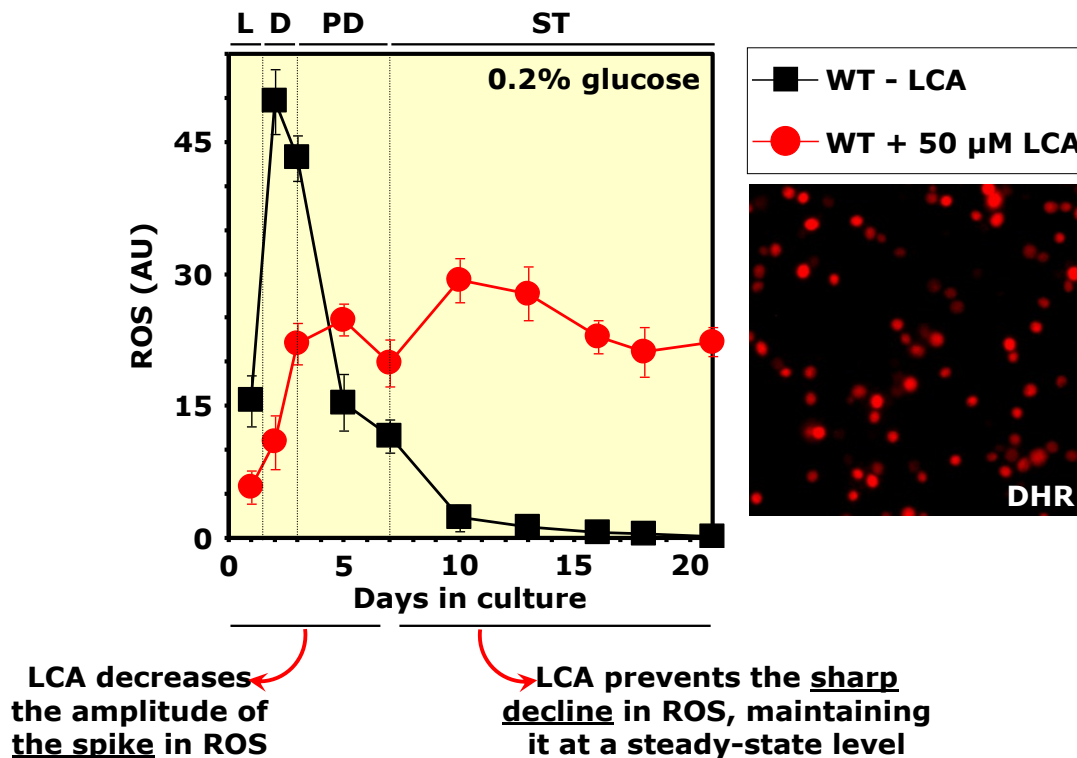
Figure 5.25. LCA alters the age-dependent dynamics of ROS generation in mitochondria of WT cells. Yeast were grown in YEPD medium initially containing 0.2% glucose as carbon source, without LCA or with this bile acid (used in the concentration of 50 μM). ROS in aliquots of cells taken at different time-points was monitored using fluorescence microscopy followed by quantitative analysis as described in Materials and Methods.

5.6. Conclusions

By elucidating how a novel anti-aging compound LCA changes the composition of mitochondrial membrane lipids and how genetic interventions affecting its ability to cause such changes influence its longevity-extending efficacy, I established the molecular mechanism underlying the ability of LCA to extend yeast CLS under CR conditions by altering the repertoire of membrane lipids in mitochondria.

6. Conclusions and suggestions for future work

6.1. General conclusions

6.1.1. A method that I developed for quantitative assessment of the lipidomes of yeast and cultured human cells using survey-scan electrospray ionization mass spectrometry (ESI/MS)

Altogether, my findings reported in Chapter 2 imply that I was able to solve the inherent limitations of the currently used methods for lipidomic analysis (including the limitations characteristic of the ESI/MS-MS-based analysis) by developing a survey-scan method for quantitative assessment of the the entire complement of lipids in yeast cells and cultured human cells using ESI/MS.

Using this method of MS-based lipidomic analysis I demonstrated that: 1) yeast has a relatively simple lipidome with 7 major lipid classes, namely PA, PE, PS, PI, CL, PC and TAG; 2) the majority of individual molecular forms within each of these different lipid classes have chain length of 16 or 18 carbon atoms; and 3) the fatty acyl moieties of all of lipid species composing yeast lipidome are either mono-unsaturated or saturated, perhaps due to the presence of a single acyl desaturase enzyme in yeast [212 - 215].

It should be stressed that the method that I developed is highly sensitive. In fact, it is: 1) sensitive to the low µM range (0.6 to 2 µM depending on lipid class) for all lipid species tested; and 2) linear to the hundreds of µM range, with the concentration linearity spreading over 2 to 3 orders of magnitude. Moreover, the method that I developed enables very accurate quantitation of different lipid species within a wide range of lipid concentrations.

Importantly, if compared to the currently used ESI/MS-MS-based method of lipidomic analysis [213 - 220], my method has the following important advantages: 1) unlike the ESI/MS-MS-based method, it can be carried out within a very limited period of time; 2) unlike the ESI/MS-MS-based method, it does not require to maintain stable spray conditions at the ESI source for long periods of time; 3) unlike the ESI/MS-MS-based method, it does not have a bias towards certain lipid species, thereby being sufficiently sensitive to unexpected changes in lipid spectra of analyzed cells; 4) it is more sensitive than the ESI/MS-MS-based method and, thus, does not require abundant quantities of cells for lipid extraction and analysis; and 5) it has lower than the ESI/MS-MS-based method limits of detection and quantitation for all yeast lipid species.

In sum, my findings reported in Chapter 2 support the notion that the survey-scan ESI/MS method of lipidomic analysis that I developed enables within a very limited period of time and using a very low number of cells to resolve, unequivocally identify and accurately quantitate all molecular forms of lipid species composing yeast lipidome and the majority of molecular forms of lipid species composing the lipidome of cultured human microglial cells.

6.1.2. A mechanism underlying the ability of CR to extend longevity of chronologically aging yeast by specifically remodelling lipid metabolism in the ER, LBs and peroxisomes

The results of my functional genetic, cell biological, electron and fluorescence microscopical, proteomic, lipidomic, and metabolomic analyses described in Chapter 3 revealed the molecular mechanism underlying the ability of CR to extend longevity of

chronologically aging yeast by specifically remodelling lipid metabolism in the ER, LBs and peroxisomes.

In this mechanism, LBs in yeast cells function as a hub in a regulatory network that modulates neutral lipids synthesis in the ER and fatty acid oxidation in peroxisomes. Ethanol accumulated in yeast placed on a calorie-rich diet represses the synthesis of Fox1p, Fox2p and Fox3p, thereby suppressing peroxisomal oxidation of FFA that originate from TAG synthesized in the ER and deposited within LBs. The resulting build-up of arrays of FFA (called gnarls) within LBs of non-CR yeast initiates several negative feedback loops regulating the metabolism of TAG. Due to the action of these negative feedback loops, chronologically aging non-CR yeast not only amass TAG in LBs but also accumulate FFA and DAG in the ER. FFA and DAG regulate longevity by two different mechanisms that operate at two different stages of the aging process. One mechanism involves sensing the concentration of DAG maintained by cells (in a diet- and genotype-dependent fashion) during D and PD growth phases. DAG concentration during D and PD phases programs cell viability during the non-proliferative ST growth phase by modulating the FFA- and DAG-induced necrotic cell death pathway, but not by influencing the mitochondria-controlled apoptotic pathway of cell death. Another mechanism involves sensing the concentrations of FFA and DAG during ST phase. Any diet or genetic manipulation that causes the build-up of these two lipids during ST phase shortens the chronological life span of yeast in part by promoting rapid mitochondria-controlled apoptotic cell death, but not by activating FFA- and DAG-induced necrotic cell death pathway.

6.1.3. A mechanism underlying the ability of a novel anti-aging compound to extend yeast life span by targeting the longevity-defining aspects of lipid metabolism confined to the ER, LBs and peroxisomes

My findings described in Chapter 4 revealed the molecular mechanism underlying the ability of LCA, a novel anti-aging compound, to extend yeast chronological life span by targeting the longevity-defining aspects of lipid metabolism confined to the ER, LBs and peroxisomes. In such mechanism, under CR conditions LCA accelerates the biosynthesis of TAG from FFA and DAG in the ER as well as decelerates the FFA- and DAG-generating lipolysis of TAG in LBs. The resulting reduction of the ER- and LB-confined levels of FFA and DAG during PD and ST growth phases affects both mechanisms by which these two lipid species regulate longevity. First, by lowering the intracellular concentration of DAG during D and PD phases, LCA attenuates the FFA- and DAG-induced necrotic cell death pathway – thereby impairing the age-related form of necrotic cell death and ultimately extending longevity of chronologically aging yeast placed on a CR diet. Second, by reducing the intracellular concentrations of FFA and DAG during ST phase, LCA attenuates the mitochondria-controlled apoptotic cell death pathway – thereby impairing the age-related form of apoptotic cell death and ultimately further extending longevity of chronologically aging yeast under CR conditions.

My findings described and discussed in Chapters 3 and 4 of this thesis imply that there are two different ways of delaying chronological aging of yeast by targeting the longevity-defining aspects of lipid metabolism confined to the ER, LBs and peroxisomes. One way is by placing yeast on a CR diet in the absence of LCA, thereby making them "lean" by accelerating both the lipolysis of neutral lipids in LBs and the oxidation of FFA

in peroxisomes. The resulting reduction of FFA and DAG levels during PD and ST phases slows down both the necrotic and apoptotic forms of cell death, thereby extending longevity of chronologically aging CR yeast - as compared to longevity of non-CR yeast. The other way is by placing yeast on a CR diet in the presence of LCA, thereby making them "fat" by: 1) accelerating the synthesis of TAG from FFA and DAG; and 2) decelerating the FFA- and DAG-producing lipolysis of TAG in LBs. The resulting further reduction of FFA and DAG levels during PD and ST phases (as compared to CR yeast grown without LCA) causes additional attenuation of the necrotic and apoptotic forms of cell death, thereby further extending longevity of chronologically aging CR yeast exposed to LCA - as compared to longevity of CR yeast not exposed to this bile acid.

6.1.4. A mechanism underlying the ability of a novel anti-aging compound to extend yeast life span by altering the composition of mitochondrial membrane lipids

By elucidating how a novel anti-aging compound LCA changes the composition of mitochondrial membrane lipids and how genetic interventions affecting its ability to cause such changes influence its longevity-extending efficacy, I established the molecular mechanism underlying the ability of LCA to extend yeast life span under CR conditions by altering the repertoire of membrane lipids in mitochondria. In this mechanism, which is described in Chapter 5, LCA causes the remodeling of the mitochondrial membrane by proportionally reducing the quantities of PE and CL and simultaneously increasing the quantity of PS, a precursor of PE. It is plausible that such LCA-driven specific

remodeling of the repertoire of mitochondrial membrane lipids is due to an inhibiting effect of LCA on the Crd1p- and Psd1p-driven reactions of the biosynthesis of CL and PE (respectively) in the mitochondrial inner membrane. LCA not only alters the total levels of PS, PE and CL in the mitochondrial membrane, but also has a specific effect in the relative abundance of their various molecular forms that differ from each other by the extent of saturation of the hydrophobic tails and their length. In fact, LCA: 1) elevates the concentration of the inverted cone-shaped species of PS enriched in saturated fatty acids, thereby enhancing cristae formation by promoting positive curvature of the inner mitochondrial membrane; and 2) reduces the concentrations of the cone-shaped species of CL and PE enriched in unsaturated fatty acids, thereby shifting the equilibrium of membrane curvature towards the enhancement of cristae formation by promoting positive curvature of the inner mitochondrial membrane. Such LCA-driven remodeling of differently shaped molecular forms of PS, CL and PE reduces the number of mitochondria and increases their size. It seems likely that the observed effect of LCA on the abundance of mitochondria is caused by the ability of this bile acid to shift a balance between the opposing processes of mitochondrial fission and fusion towards fusion, thereby preventing the fragmentation of mitochondria and the resulting efflux of cytochrome c and several other pro-apoptotic proteins from the mitochondrial intermembrane space. Ultimately, such effect of LCA on mitochondrial morphology results in the delay of the age-related form of mitochondria-controlled apoptosis and longevity extension. Another outcome of the observed LCA-driven remodeling of differently shaped molecular forms of PS, CL and PE consists in significant expansion of the mitochondrial inner membrane, which is manifested in a great increase of the length

of mitochondrial cristae and in a change of their morphology. It is conceivable that such LCA-driven enhancement of the ability of the mitochondrial inner membrane to form cristae is responsible for the observed ability of LCA to alter the age-related dynamics of several longevity-defining processes confined to mitochondria, including respiration, electrochemical potential across the mitochondrial inner membrane and ROS generation.

6.2. Suggestions for future work

In the established by me mechanism underlying the essential role of lipid metabolism in modulating programmed by calorie availability chronological aging in yeast, LBs in yeast cells function as a hub in a regulatory network that modulates neutral lipids synthesis in the ER and fatty acid oxidation in peroxisomes. Ethanol accumulated in yeast placed on a calorie-rich diet represses the synthesis of Fox1p, Fox2p and Fox3p, thereby suppressing peroxisomal oxidation of FFA that originate from TAG synthesized in the ER and deposited within LBs. The resulting build-up of arrays of free fatty acids (gnarls) within LBs of non-CR yeast initiates several negative feedback loops regulating the metabolism of TAG. Due to the action of these negative feedback loops, chronologically aging non-CR yeast not only amass TAG in LBs but also accumulate FFA and DAG in the ER. FFA and DAG regulate longevity by two different mechanisms that operate at two different stages of the aging process. One mechanism involves sensing the concentration of DAG maintained by cells (in a diet- and genotype-dependent fashion) during D and PD growth phases. DAG concentration during D and PD phases programs cell viability during ST growth phase by modulating the FFA- and DAG-induced necrotic cell death pathway, but not by influencing the mitochondria-controlled apoptotic pathway of cell death. Another

mechanism involves sensing the concentrations of FFA and DAG during ST phase. Any diet or genetic manipulation that causes the build-up of these two lipids during ST phase shortens the chronological life span of yeast in part by promoting rapid mitochondria-controlled apoptotic cell death, but not by activating FFA- and DAG-induced necrotic cell death pathway.

The two most outstanding questions for the future research aimed at providing further insight into a cascade of molecular events underlying the above mechanism are: 1) what upstream regulators govern the observed under CR conditions longevity-extending remodeling of lipid and carbohydrate metabolism, stress response pathways, oxidation-reduction processes in mitochondria, mitochondrial biogenesis, and mitochondria-controlled apoptotic cell death? and 2) what are the downstream sensors of FFA and DAG that govern the age-related forms of apoptotic and necrotic cell death pathways by sensing the CR-triggered changes in the intracellular concentrations of these two lipid species? My analysis of the observed global changes in the proteomes of yeast placed on a CR diet has revealed a limited set of transcriptional regulators that, according to my database search, have been shown to regulate transcription of their encoding genes. These global transcriptional regulators include Rtg2p, Sfp1p, Yap1p, Msn2p and Msn4p. I propose that, by sensing calorie availability, these transcriptional regulators modulate expression of several global clusters of genes encoding proteins identified in my proteomic analysis as the ones whose levels are significantly altered in yeast placed on a CR diet. To test the validity of my hypothesis, one could evaluate how mutations eliminating Rtg2p, Sfp1p, Yap1p, Msn2p or Msn4p influence the life-extending efficacy of CR as well as the cellular and mitochondrial proteomes of chronologically aging CR

and non-CR yeast, their cellular and organellar (*i.e.*, the ER and LBs) lipidomes, their susceptibility to apoptotic and necrotic death caused by a short-term exposure to exogenously added pro-apoptotic and pro-necrotic stimuli, the chronology of the events characteristic of their apoptotic and/or necrotic death during ST growth phase, and the age-related dynamics of changes in the abundance and morphology of the ER, LBs and mitochondria in their chronologically aging cells.

To answer the second of the above two most outstanding questions consisting in establishing the identity of the downstream sensors of FFA and DAG that govern the age-related forms of apoptotic and necrotic cell death pathways by sensing the CR-triggered changes in the intracellular concentrations of these two lipid species, one could assess how mutations eliminating the well-known protein regulators of these death pathways (including Yca1p, Ndi1p, Rny1p, Bir1p, Nma11p, Aif1p, Nuc1p and Dnm1p) influence the life-extending efficacy of CR as well as the susceptibility of chronologically aging CR and non-CR yeast to apoptotic and necrotic death caused by a short-term exposure to exogenously added pro-apoptotic and pro-necrotic stimuli, and the chronology of the events characteristic of their apoptotic and/or necrotic death during ST growth phase.

In the future, one could use a similar to the above experimental strategy to define 1) the upstream regulators of the longevity-extending remodeling of lipid and carbohydrate metabolism, stress response pathways, oxidation-reduction processes in mitochondria, mitochondrial biogenesis, and mitochondria-controlled apoptotic cell death that I observed in chronologically aging CR yeast exposed to LCA; and 2) the downstream sensors of FFA and DAG that ultimately execute an anti-aging program triggered in response to exposure of chronologically aging CR yeast to LCA.

In the established by me mitochondria-centered mechanism underlying the anti-aging effect of LCA, this bile acid extends yeast longevity under CR conditions by remodeling the composition of mitochondrial membrane lipids and thereby affecting longevity-defining processes confined to and/or governed by mitochondria. In this mechanism, LCA extends yeast longevity by: 1) increasing the level of PS, a precursor for the synthesis of PE in the mitochondrial membrane, thereby enhancing its positive effect on longevity-defining processes in this membrane; 2) decreasing the level of PE in the mitochondrial membrane, thereby weakening its negative effect on longevity-defining processes in this membrane; and 3) proportionally decreasing the levels of PE and CL in the mitochondrial membrane, thereby increasing PS/CL and PS/PE ratios but maintaining PE/CL ratio of mitochondrial membrane lipids and causing some longevity-extending changes in this membrane. By altering the levels of PS, CL and PE in the mitochondrial membrane, LCA: 1) changes the curvature of the inner mitochondrial membrane; and 2) enhances the positive effect of PS and weakens the negative effect of PE on membrane proteins whose activity depends on these two lipid species - thereby enhancing the ability of the inner mitochondrial membrane to form cristae and activating protein machines involved in mitochondrial respiration, the maintenance of mitochondrial membrane potential and ROS production in mitochondria. To provide further insight into a cascade of molecular events underlying this mitochondria-centered mechanism, one could consider performing the following set of experiments: 1) to examine how LCA influences the stoichiometry, composition and functional state of respiratory supercomplexes ("respirasomes") in the inner mitochondrial membrane; and 2) to test my hypothesis

(which has been indirectly supported by some of the recent findings in Dr. Titorenko's laboratory) that LCA prevents the fragmentation of the mitochondrial network during late ST phase and thereby inhibits an age-related, mitochondria-controlled form of apoptosis by activating the Fzo1p and Ugo1p protein components of the mitochondrial outer membrane fusion machine.

7. References

1. Kirkwood, T.B.L. (2005). Understanding the odd science of aging. *Cell* 120:437-447.

2. Guarente, L.P., Partridge, L. and Wallace, D.C. (Editors) (2008). *Molecular Biology of Aging*. Cold Spring Harbor Laboratory Press, Cold Spring Harbor, New York, 610 pages.

3. Fontana, L., Partridge, L. and Longo, V.D. (2010). Extending healthy life span - from yeast to humans. *Science* 328:321-326.

4. Masoro, E.J. and Austad, S.N. (Editors) (2011). *Handbook of the Biology of Aging*. 7th Edition. Academic Press (an imrint of Elsevier), Amsterdam, 572 pages.

5. Kirkwood, T.B.L. (2008). Understanding ageing from an evolutionary perspective. *J. Intern. Med.* 263:117-127.

6. Kirkwood, T.B.L., Boys, R.J., Gillespie, C.S., Proctor, C.J., Shanley, D.P. and Wilkinson, D.J. (2003). Towards an e-biology of ageing: integrating theory and data. *Nat. Rev. Mol. Cell Biol.* 4:243-249.

7. Greer, E.L. and Brunet, A. (2008). Signaling networks in aging. *J. Cell Sci.* 121:407-412.

8. Lin, S.-J. and Sinclair, D. (2008). Molecular mechanisms of aging: insights from budding yeast. In: Guarente, L.P., Partridge, L., Wallace, D.C. (Eds.), *Molecular Biology of Aging*. Cold Spring Harbor Laboratory Press, Cold Spring Harbor, New York, pp. 483-516.

9. Mair, W. and Dillin, A. (2008). Aging and survival: the genetics of life span

extension by dietary restriction. *Annu. Rev. Biochem.* 77:727-754.

10. Puigserver, P. and Kahn, C.R. (2008). Mammalian metabolism in aging. In: Guarente, L.P., Partridge, L., Wallace, D.C. (Eds.), *Molecular Biology of Aging*. Cold Spring Harbor Laboratory Press, Cold Spring Harbor, New York, pp. 545-574.

11. Tavernarkis, N. (Editor) (2010). *Protein Metabolism and Homeostasis in Aging*. Landes Bioscience and Springer Science+Business Media, New York, 249 pages.

12. Antebi, A. (2005). Physiology. The tick-tock of aging? *Science* 310:1911-1913.

13. Blagosklonny, M.V. (2007). Paradoxes of aging. *Cell Cycle* 6:2997-3003.

14. Blagosklonny, M.V. (2007). Program-like aging and mitochondria: instead of random damage by free radicals. *J. Cell. Biochem.* 102:1389-1399.

15. Budovskaya, Y.V., Wu, K., Southworth, L.K., Jiang, M., Tedesco, P., Johnson, T.E. and Kim, S.K. (2008). An elt-3/elt-5/elt-6 GATA transcription circuit guides aging in *C. elegans*. *Cell* 134:291-303.

16. Longo, V.D., Mitteldorf, J. and Skulachev, V.P. (2005). Programmed and altruistic ageing. *Nat. Rev. Genet.* 6:866-872.

17. Skulachev, V.P. and Longo, V.D. (2005). Aging as a mitochondria-mediated atavistic program: can aging be switched off? *Ann. N. Y. Acad. Sci.* 1057:145-164.

18. Goldberg, A.A., Bourque, S.D., Kyryakov, P., Gregg, C., Boukh-Viner, T., Beach, A., Burstein, M.T., Machkalyan, G., Richard, V., Rampersad, S., Cyr, D., Milijevic, S. and Titorenko, V.I. Effect of calorie restriction on the metabolic history of chronologically aging yeast. (2009) *Exp. Gerontol*. 44:555-571.

19. Lithgow, G.J. (2006). Why aging isn't regulated: a lamentation on the use of language in aging literature. *Exp. Gerontol.* 41:890-893.

20. Kenyon, C. (2001). A conserved regulatory system for aging. *Cell* 105:165-168.

21. Longo, V.D. and Finch, C.E. (2003). Evolutionary medicine: from dwarf model systems to healthy centenarians? *Science* 299:1342-1346.

22. Bitterman, K.J., Medvedik, O. and Sinclair, D.A. (2003). Longevity regulation in *Saccharomyces cerevisiae*: linking metabolism, genome stability, and heterochromatin. *Microbiol. Mol. Biol. Rev.* 67:376-399.

23. Kenyon, C. (2005). The plasticity of aging: insights from long-lived mutants. *Cell* 120:449-460.

24. Guarente, L. (2006). Sirtuins as potential targets for metabolic syndrome. *Nature* 444:868-874.

25. Kaeberlein, M., Burtner, C.R. and Kennedy, B.K. (2007). Recent developments in yeast aging. *PLoS Genet.* 3:e84.

26. Wei, M., Fabrizio, P., Hu, J., Ge, H., Cheng, C., Li, L. and Longo, V.D. (2008). Life span extension by calorie restriction depends on Rim15 and transcription factors downstream of Ras/PKA, Tor, and Sch9. *PLoS Genet*. 4:e13.

27. Narasimhan, S.D., Yen, K. and Tissenbaum, H.A. (2009). Converging pathways in lifespan regulation. *Curr. Biol*. 19:R657-R666.

28. Piper, M.D., Selman, C., McElwee, J.J. and Partridge, L. (2008). Separating cause from effect: how does insulin/IGF signalling control lifespan in worms, flies and mice? *J. Intern. Med*. 263:179-191.

29. Puigserver, P. and Kahn, C.R. (2008). Mammalian metabolism in aging. In: *Molecular Biology of Aging* (Guarente LP, Partridge L, Wallace DC, eds). Cold Spring Harbor Laboratory Press, Cold Spring Harbor, New York, pp. 545-574.

30. Salih, D.A. and Brunet, A. (2008). FoxO transcription factors in the maintenance of cellular homeostasis during aging. *Curr. Opin. Cell Biol*. 20:126-136.

31. Wolff, S. and Dillin, A. (2006). The trifecta of aging in *Caenorhabditis elegans*. *Exp. Gerontol*. 41:894-903.

32. Murphy, C.T. (2006). The search for DAF-16/FOXO transcriptional targets: approaches and discoveries. *Exp. Gerontol*. 41:910-921.

33. Oh, S.W., Mukhopadhyay, A., Dixit, B.L., Raha, T., Green, M.R. and Tissenbaum, H.A. (2006). Identification of direct DAF-16 targets controlling longevity, metabolism and diapause by chromatin immunoprecipitation. *Nat. Genet*. 38:251-257.

34. Laplante, M. and Sabatini, D.M. (2009). mTOR signaling at a glance. *J. Cell Sci*. 122:3589-3594.

35. Shaw, R.J. (2009). LKB1 and AMP-activated protein kinase control of mTOR signalling and growth. *Acta Physiol*. 196:65-80.

36. Harrison, D.E., Strong, R., Sharp, Z.D., Nelson, J.F., Astle, C.M., Flurkey, K., Nadon, N.L., Wilkinson, J.E., Frenkel, K., Carter, C.S., Pahor, M., Javors, M.A., Fernandez, E. and Miller, R.A. (2009). Rapamycin fed late in life extends lifespan in genetically heterogeneous mice. *Nature* 460:392-395.

37. Selman, C., Tullet, J.M., Wieser, D., Irvine, E., Lingard, S.J., Choudhury, A.I., Claretm, M., Al-Qassab, H., Carmignac, D., Ramadani, F., Woods, A., Robinson, I.C., Schuster, E., Batterham, R.L., Kozma, S.C., Thomas, G., Carling, D., Okkenhaug, K., Thornton, J.M., Partridge, L., Gems, D. and Withers, D.J. (2009). Ribosomal protein S6 kinase 1 signaling regulates mammalian life span. *Science*

326:140-144.

38. Bjedov, I., Toivonen, J.M., Kerr, F., Slack, C., Jacobson, J., Foley, A. and Partridge, L. (2010). Mechanisms of life span extension by rapamycin in the fruit fly *Drosophila melanogaster*. *Cell Metab*. 11:35-46.

39. Díaz-Troya, S., Pérez-Pérez, M.E., Florencio, F.J. and Crespo, J.L. (2008). The role of TOR in autophagy regulation from yeast to plants and mammals. *Autophagy* 4:851-865.

40. Huber, A., Bodenmiller, B., Uotila, A., Stahl, M., Wanka, S., Gerrits, B., Aebersold, R. and Loewith, R. (2009). Characterization of the rapamycin-sensitive phosphoproteome reveals that Sch9 is a central coordinator of protein synthesis. *Genes Dev*. 23:1929-1943.

41. Pan, Y. and Shadel, G.S. (2009). Extension of chronological life span by reduced TOR signaling requires down-regulation of Sch9p and involves increased mitochondrial OXPHOS complex density. *Aging* 1:131-145.

42. Kim, E., Goraksha-Hicks, P., Li, L., Neufeld, T.P. and Guan, K.L. (2008). Regulation of TORC1 by Rag GTPases in nutrient response. *Nat. Cell Biol*. 10:935-945.

43. Sancak, Y., Peterson, T.R., Shaul, Y.D., Lindquist, R.A., Thoreen, C.C., Bar-Peled, L. and Sabatini, D.M. (2008). The Rag GTPases bind raptor and mediate amino acid signaling to mTORC1. *Science* 320:1496-1501.

44. Avruch, J., Long, X., Ortiz-Vega, S., Rapley, J., Papageorgiou, A. and Dai, N. (2009). Amino acid regulation of TOR complex 1. *Am. J. Physiol. Endocrinol. Metab*. 296:E592-E602.

45. Binda, M., Péli-Gulli, M.P., Bonfils, G., Panchaud, N., Urban, J., Sturgill, T.W., Loewith, R. and De Virgilio, C. (2009). The Vam6 GEF controls TORC1 by activating the EGO complex. *Mol. Cell* 35:563-573.

46. Narbonne, P. and Roy, R. (2009). *Caenorhabditis elegans* dauers need LKB1/AMPK to ration lipid reserves and ensure long-term survival. *Nature* 457:210-214.

47. Santangelo, G.M. (2006). Glucose signaling in *Saccharomyces cerevisiae*. *Microbiol. Mol. Biol. Rev*. 70:253-282.

48. Gancedo, J.M. (2008). The early steps of glucose signalling in yeast. *FEMS Microbiol. Rev*. 32:673-704.

49. Medvedik, O., Lamming, D.W., Kim, K.D. and Sinclair, D.A. (2007). MSN2 and MSN4 link calorie restriction and TOR to sirtuin-mediated lifespan extension in *Saccharomyces cerevisiae*. *PLoS Biol*. 5:e261.

50. Lee, P., Cho, B.R., Joo, H.S. and Hahn, J.S. (2008). Yeast Yak1 kinase, a bridge between PKA and stress-responsive transcription factors, Hsf1 and Msn2/Msn4. *Mol. Microbiol*. 70:882-895.

51. Smets, B., Ghillebert, R., De Snijder, P., Binda, M., Swinnen, E., De Virgilio, C. and Winderickx, J. (2010). Life in the midst of scarcity: adaptations to nutrient availability in *Saccharomyces cerevisiae*. *Curr. Genet*. 56:1-32.

52. Roosen, J., Engelen, K., Marchal, K., Mathys, J., Griffioen, G., Cameroni, E., Thevelein, J.M., De Virgilio, C., De Moor, B. and Winderickx, J. (2005). PKA and Sch9 control a molecular switch important for the proper adaptation to nutrient availability. *Mol. Microbiol*. 55:862-880.

53. Cheng, C., Fabrizio, P., Ge, H., Longo, V.D. and Li, L.M. (2007). Inference of transcription modification in long-live yeast strains from their expression profiles. *BMC Genomics* 8:219.

54. Cheng, C., Fabrizio, P., Ge, H., Wei, M., Longo, V.D. and Li, L.M. (2007). Significant and systematic expression differentiation in long-lived yeast strains. *PLoS One* 2:e1095.

55. Slattery, M.G., Liko, D. and Heideman, W. (2008). Protein kinase A, TOR, and glucose transport control the response to nutrient repletion in *Saccharomyces cerevisiae*. *Eukaryot. Cell* 7:358-367.

56. Fabrizio, P. and Longo, V.D. (2003). The chronological life span of *Saccharomyces cerevisiae*. *Aging Cell* 2:73-81.

57. Anderson, R.M., Bitterman, K.J., Wood, J.G., Medvedik, O. and Sinclair, D.A. (2003). Nicotinamide and *PNC1* govern lifespan extension by calorie restriction in *Saccharomyces cerevisiae*. *Nature* 423:181-185.

58. Yan, L., Vatner, D.E., O'Connor, J.P., Ivessa, A., Ge, H., Chen, W., Hirotani, S., Ishikawa, Y., Sadoshima, J. and Vatner, S.F. (2007). Type 5 adenylyl cyclase disruption increases longevity and protects against stress. *Cell* 130:247-258.

59. Enns, L.C., Morton, J.F., Mangalindan, R.S., McKnight, G.S., Schwartz, M.W., Kaeberlein, M.R., Kennedy, B.K., Rabinovitch, P.S. and Ladiges, W.C. (2009). Attenuation of age-related metabolic dysfunction in mice with a targeted disruption of the Cβ subunit of protein kinase A. *J. Gerontol. A Biol. Sci. Med. Sci*. 64:1221-1231.

60. Enns, L.C., Morton, J.F., Treuting, P.R., Emond, M.J., Wolf, N.S., McKnight, G.S., Rabinovitch, P.S. and Ladiges, W.C. (2009). Disruption of protein kinase A in mice enhances healthy aging. *PLoS One* 4:e5963.

61. Finkel, T., Deng, C.X. and Mostoslavsky, R. (2009). Recent progress in the biology and physiology of sirtuins. *Nature* 460:587-591.

62. Finley, L.W. and Haigis, M.C. (2009). The coordination of nuclear and mitochondrial communication during aging and calorie restriction. *Ageing Res. Rev.* 8:173-188.

63. Soukas, A.A., Kane, E.A., Carr, C.E., Melo, J.A. and Ruvkun, G. (2009). Rictor/TORC2 regulates fat metabolism, feeding, growth, and life span in *Caenorhabditis elegans*. *Genes Dev.* 23:496-511.

64. Giorgio, M., Trinei, M., Migliaccio, E. and Pelicci, P.G. (2007). Hydrogen peroxide: a metabolic by-product or a common mediator of ageing signals? *Nat. Rev. Mol. Cell Biol.* 8:722-728.

65. Weindruch, R. and Walford, R.L. (1988). *The Retardation of Aging and Disease by Dietary Restriction*. Thomas, Springfield.

66. Masoro, E.J. (2002). *Caloric Restriction: A Key to Understanding and Modulating Aging*. Elsevier, Amsterdam.

67. Colman, R.J., Anderson, R.M., Johnson, S.C., Kastman, E.K., Kosmatka, K.J., Beasley, T.M., Allison, D.B., Cruzen, C., Simmons, H.A., Kemnitz, J.W. and Weindruch, R. (2009). Caloric restriction delays disease onset and mortality in rhesus monkeys. *Science* 325:201-204.

68. Sinclair, D.A. (2005). Toward a unified theory of caloric restriction and longevity regulation. *Mech. Ageing Dev*. 126:987-1002.

69. Min, K.J., Flatt, T., Kulaots, I. and Tatar, M. (2007). Counting calories in *Drosophila* diet restriction. *Exp. Gerontol*. 42:247-251.

70. Zimmerman, J.A., Malloy, V., Krajcik, R. and Orentreich, N. (2003). Nutritional control of aging. *Exp. Gerontol*. 38:47-52.

71. Mair, W., Piper, M.D. and Partridge, L. (2005). Calories do not explain extension of life span by dietary restriction in *Drosophila*. *PLoS Biol*. 3:e223.

72. Piper, M.D., Mair, W. and Partridge, L. (2005). Counting the calories: the role of specific nutrients in extension of life span by food restriction. *J. Gerontol. A Biol. Sci. Med. Sci*. 60:549-555.

73. Blagosklonny, M.V. (2006). Aging and immortality: quasi-programmed senescence and its pharmacologic inhibition. *Cell Cycle* 5:2087-2102.

74. Blagosklonny, M.V. (2008). Aging: ROS or TOR. *Cell Cycle* 7:3344-3354.

75. Blagosklonny, M.V. (2009). TOR-driven aging: speeding car without brakes. *Cell Cycle* 8:4055-4059.

76. Kaeberlein, M., Powers, R.W., 3rd, Steffen, K.K., Westman, E.A., Hu, D., Dang, N., Kerr, E.O., Kirkland, K.T., Fields, S. and Kennedy, B.K. (2005). Regulation of yeast replicative life span by TOR and Sch9 in response to nutrients. *Science* 310:1193-1196.

77. Meissner, B., Boll, M., Daniel, H. and Baumeister, R. (2004). Deletion of the intestinal peptide transporter affects insulin and TOR signaling in *Caenorhabditis elegans*. *J. Biol. Chem*. 279:36739-36745.

78. Hansen, M., Taubert, S., Crawford, D., Libina, N., Lee, S.J. and Kenyon, C. (2007). Lifespan extension by conditions that inhibit translation in *Caenorhabditis elegans*. *Aging Cell* 6:95-110.

79. Chen, D. and Guarente, L. (2007). SIR2: a potential target for calorie restriction mimetics. *Trends Mol. Med*. 13:64-71.

80. Kaeberlein, M. and Powers, R.W., 3rd. (2007). Sir2 and calorie restriction in yeast: a skeptical perspective. *Ageing Res. Rev*. 6:128-140.

81. Kaeberlein, M., Kirkland, K.T., Fields, S. and Kennedy, B.K. (2004). Sir2-independent life span extension by calorie restriction in yeast. *PLoS Biol*. 2:E296.

82. Lin, S.J., Defossez, P.A. and Guarente, L. (2000). Requirement of NAD and SIR2 for life-span extension by calorie restriction in *Saccharomyces cerevisiae*. *Science* 289:2126-2128.

83. Lin, S.J., Kaeberlein, M., Andalis, A.A., Sturtz, L.A., Defossez, P.A., Culotta, V.C., Fink, G.R. and Guarente, L. (2002). Calorie restriction extends *Saccharomyces cerevisiae* lifespan by increasing respiration. *Nature* 418:344-348.

84. Clancy, D.J., Gems, D., Hafen, E., Leevers, S.J. and Partridge, L. (2002). Dietary restriction in long-lived dwarf flies. *Science* 296:319.

85. Bartke, A., Masternak, M.M., Al-Regaiey, K.A. and Bonkowski, M.S. (2007). Effects of dietary restriction on the expression of insulin-signaling-related genes in long-lived mutant mice. *Interdiscip. Top. Gerontol*. 35:69-82.

86. Greer, E.L., Dowlatshahi, D., Banko, M.R., Villen, J., Hoang, K., Blanchard, D., Gygi, S.P. and Brunet, A. (2007). An AMPK-FOXO pathway mediates longevity

induced by a novel method of dietary restriction in *C. elegans*. *Curr. Biol*. 17:1646-1656.

87. Iser, W.B. and Wolkow, C.A. (2007). DAF-2/insulin-like signaling in *C. elegans* modifies effects of dietary restriction and nutrient stress on aging, stress and growth. *PLoS One* 2:e1240.

88. Lakowski, B. and Hekimi, S. (1998). The genetics of caloric restriction in *Caenorhabditis elegans*. *Proc. Natl. Acad. Sci. USA* 95:13091-13096.

89. Bartke, A., Wright, J.C., Mattison, J.A., Ingram, D.K., Miller, R.A. and Roth, G.S. (2001). Extending the lifespan of long-lived mice. *Nature* 414:412.

90. Kaeberlein, T.L., Smith, E.D., Tsuchiya, M., Welton, K.L., Thomas, J.H., Fields, S., Kennedy, B.K. and Kaeberlein, M. (2006). Lifespan extension in *Caenorhabditis elegans* by complete removal of food. *Aging Cell* 5:487-494.

91. Bishop, N.A. and Guarente, L. (2007). Two neurons mediate diet-restriction-induced longevity in *C. elegans*. *Nature* 447:545-549.

92. Houthoofd, K., Gems, D., Johnson, T.E. and Vanfleteren, J.R. (2007). Dietary restriction in the nematode *Caenorhabditis elegans*. *Interdiscip. Top. Gerontol*. 35:98-114.

93. Min, K.J., Yamamoto, R., Buch, S., Pankratz, M. and Tatar, M. (2008). Drosophila lifespan control by dietary restriction independent of insulin-like signaling. *Aging Cell* 7:199-206.

94. Greer, E.L. and Brunet, A. (2009). Different dietary restriction regimens extend lifespan by both independent and overlapping genetic pathways in *C. elegans*. *Aging Cell* 8:113-127.

95. Onken, B. and Driscoll, M. (2010). Metformin induces a dietary restriction-like state and the oxidative stress response to extend *C. elegans* healthspan via AMPK, LKB1, and SKN-1. *PLoS ONE* 5:e8758.

96. Anisimov, V.N., Berstein, L.M., Egormin, P.A., Piskunova, T.S., Popovich, I.G., Zabezhinski, M.A., Tyndyk, M.L., Yurova, M.V., Kovalenko, I.G., Poroshina, T.E., Semenchenko, A.V., Anisimov, V.N., Berstein, L.M., Egormin, P.A., Piskunova, T.S., Popovich, I.G., Zabezhinski, M.A., Tyndyk, M.L., Yurova, M.V., Kovalenko, I.G., Poroshina, T.E. and Semenchenko, A.V. (2008). Metformin slows down aging and extends life span of female SHR mice. *Cell Cycle* 7:2769-2773.

97. Crespo, J.L., Powers, T., Fowler, B. and Hall, M.N. (2002). The TOR-controlled transcription activators GLN3, RTG1, and RTG3 are regulated in response to intracellular levels of glutamine. *Proc. Natl. Acad. Sci. USA* 99:6784-6789.

98. Powers, R.W. 3rd, Kaeberlein, M., Caldwell, S.D., Kennedy, B.K. and Fields, S. (2006). Extension of chronological life span in yeast by decreased TOR pathway signaling. *Genes Dev*. 20:174-184.

99. Demidenko, Z.N., Shtutman, M. and Blagosklonny, M.V. (2009). Pharmacologic inhibition of MEK and PI-3K converges on the mTOR/S6 pathway to decelerate cellular senescence. *Cell Cycle* 8:1896-1900.

100. Bonawitz, N.D., Chatenay-Lapointe, M., Pan, Y. and Shadel, G.S. (2007). Reduced TOR signaling extends chronological life span via increased respiration and upregulation of mitochondrial gene expression. *Cell Metab*. 5:265-277.

101. Demidenko, Z.N., Zubova, S.G., Bukreeva, E.I., Pospelov, V.A., Pospelova, T.V. and Blagosklonny, M.V. (2009). Rapamycin decelerates cellular senescence. *Cell Cycle* 8:1888-1895.

102. Wanke, V., Cameroni, E., Uotila, A., Piccolis, M., Urban, J., Loewith, R. and De Virgilio, C. (2008). Caffeine extends yeast lifespan by targeting TORC1. *Mol. Microbiol.* 69:277-285.

103. Petrascheck, M., Ye, X. and Buck, L.B. (2007). An antidepressant that extends lifespan in adult *Caenorhabditis elegans*. *Nature* 450:553-556.

104. Evason, K., Collins, J.J., Huang, C., Hughes, S. and Kornfeld, K. (2008). Valproic acid extends *Caenorhabditis elegans* lifespan. *Aging Cell* 7:305-317.

105. Morselli, E., Galluzzi, L., Kepp, O., Criollo, A., Maiuri, M.C., Tavernarakis, N., Madeo, F. and Kroemer, G. (2009). Autophagy mediates pharmacological lifespan extension by spermidine and resveratrol. *Aging* 1:961-970.

106. Kaeberlein, M. and Kennedy, B.K. (2007). Does resveratrol activate yeast Sir2 in vivo? *Aging Cell* 6:415-416.

107. Pacholec, M., Chrunyk, B., Cunningham, D., Flynn, D., Griffith, D., Griffor, M., Loulakis, P., Pabst, B., Qiu, X., Stockman, B., Thanabal, V., Varghese, A., Ward, J., Withka, J. and Ahn, K. (2010). SRT1720, SRT2183, SRT1460, and resveratrol are not direct activators of SIRT1. *J. Biol. Chem.* 285:8340-8351.

108. Harikumar, K.B. and Aggarwal, B.B. (2008). Resveratrol: a multitargeted agent for age-associated chronic diseases. *Cell Cycle* 7:1020-1035.

109. Shakibaei, M., Harikumar, K.B. and Aggarwal, B.B. (2009). Resveratrol addiction: to die or not to die. *Mol. Nutr. Food Res.* 53:115-128.

110. Howitz, K.T., Bitterman, K.J., Cohen, H.Y., Lamming, D.W., Lavu, S., Wood, J.G., Zipkin, R.E., Chung, P., Kisielewski, A., Zhang, L.L., Scherer, B. and Sinclair, D.A. (2003). Small molecule activators of sirtuins extend *Saccharomyces cerevisiae* lifespan. *Nature* 425:191-196.

111. Demidenko, Z.N. and Blagosklonny, M.V. (2009). At concentrations that inhibit mTOR, resveratrol suppresses cellular senescence. *Cell Cycle* 8:1901-1904.

112. Wood, J.G., Rogina, B., Lavu, S., Howitz, K., Helfand, S.L., Tatar, M. and Sinclair, D. (2004). Sirtuin activators mimic caloric restriction and delay ageing in metazoans. *Nature* 430:686-689.

113. Baur, J.A., Pearson, K.J., Price, N.L., Jamieson, H.A., Lerin, C., Kalra, A., Prabhu, V.V., Allard, J.S., Lopez-Lluch, G., Lewis, K., Pistell, P.J., Poosala, S., Becker, K.G., Boss, O., Gwinn, D., Wang, M., Ramaswamy, S., Fishbein, K.W., Spencer, R.G., Lakatta, E.G., Le Couteur, D., Shaw, R.J., Navas, P., Puigserver, P., Ingram, D.K., de Cabo, R. and Sinclair, D.A. (2006). Resveratrol improves health and survival of mice on a high-calorie diet. *Nature* 444:337-342.

114. Valenzano, D.R., Terzibasi, E., Genade, T., Cattaneo, A., Domenici, L. and Cellerino, A. (2006). Resveratrol prolongs lifespan and retards the onset of age-related markers in a short-lived vertebrate. *Curr. Biol*. 16:296-300.

115. Pearson, K.J., Baur, J.A., Lewis, K.N., Peshkin, L., Price, N.L., Labinskyy, N., Swindell, W.R., Kamara, D., Minor, R.K., Perez, E., Jamieson, H.A., Zhang, Y., Dunn, S.R., Sharma, K., Pleshko, N., Woollett, L.A., Csiszar, A., Ikeno, Y., Le Couteur, D., Elliott, P.J., Becker, K.G., Navas, P., Ingram, D.K., Wolf, N.S., Ungvari, Z., Sinclair, D.A. and de Cabo, R. (2008). Resveratrol delays age-related

deterioration and mimics transcriptional aspects of dietary restriction without extending life span. *Cell Metab*. 8:157-168.

116. Picard, F., Kurtev, M., Chung, N., Topark-Ngarm, A., Senawong, T., Machado De Oliveira, R., Leid, M., McBurney, M.W. and Guarente, L. (2004). Sirt1 promotes fat mobilization in white adipocytes by repressing PPAR-γ. *Nature* 429:771-776.

117. Viswanathan, M., Kim, S.K., Berdichevsky, A. and Guarente, L. (2005). A role for SIR-2.1 regulation of ER stress response genes in determining *C. elegans* life span. *Dev. Cell* 9:605-615.

118. Lagouge, M., Argmann, C., Gerhart-Hines, Z., Meziane, H., Lerin, C., Daussin, F., Messadeq, N., Milne, J., Lambert, P., Elliott, P., Geny, B., Laakso, M., Puigserver, P. and Auwerx, J. (2006). Resveratrol improves mitochondrial function and protects against metabolic disease by activating SIRT1 and PGC-1α. *Cell* 127:1109-1122.

119. Morselli, E., Maiuri, M.C., Markaki, M., Megalou, E., Pasparaki, A., Palikaras, K., Criollo, A., Galluzzi, L., Malik, S.A., Vitale, I., Michaud, M., Madeo, F., Tavernarakis, N. and Kroemer, G. (2010). Caloric restriction and resveratrol promote longevity through the Sirtuin-1-dependent induction of autophagy. *Cell Death Dis*. 1:e10.

120. Engel, N. and Mahlknecht, U. (2008). Aging and anti-aging: unexpected side effects of everyday medication through sirtuin1 modulation. *Int. J. Mol. Med*. 21:223-232.

121. Eisenberg, T., Knauer, H., Schauer, A., Büttner, S., Ruckenstuhl, C., Carmona-Gutierrez, D., Ring, J., Schroeder, S., Magnes, C., Antonacci, L., Fussi, H., Deszcz, L., Hartl, R., Schraml, E., Criollo, A., Megalou, E., Weiskopf, D., Laun, P., Heeren, G., Breitenbach, M., Grubeck-Loebenstein, B., Herker, E., Fahrenkrog, B., Fröhlich,

K.U., Sinner, F., Tavernarakis, N., Minois, N., Kroemer, G. and Madeo, F. (2009). Induction of autophagy by spermidine promotes longevity. *Nat. Cell Biol*. 11:1305-1314.

122. McColl, G., Killilea, D.W., Hubbard, A.E., Vantipalli, M.C., Melov, S. and Lithgow, G.J. (2008). Pharmacogenetic analysis of lithium-induced delayed aging in *Caenorhabditis elegans*. *J. Biol. Chem*. 283:350-357.

123. Skulachev, V.P., Anisimov, V.N., Antonenko, Y.N., Bakeeva, L.E., Chernyak, B.V., Erichev, V.P., Filenko, O.F., Kalinina, N.I., Kapelko, V.I., Kolosova, N.G., Kopnin, B.P., Korshunova, G.A., Lichinitser, M.R., Obukhova, L.A., Pasyukova, E.G., Pisarenko, O.I., Roginsky, V.A., Ruuge, E.K., Senin, I.I., Severina, I.I., Skulachev, M.V., Spivak, I.M., Tashlitsky, V.N., Tkachuk, V.A., Vyssokikh, M.Y., Yaguzhinsky, L.S. and Zorov, D.B. (2009). An attempt to prevent senescence: a mitochondrial approach. *Biochim. Biophys. Acta* 1787:437-461.

124. Lapointe, J. and Hekimi, S. (2010). When a theory of aging ages badly. *Cell Mol. Life Sci*. 67:1-8.

125. Bauer, J.H., Goupil, S., Garber, G.B. and Helfand, S.L. (2004). An accelerated assay for the identification of lifespan-extending interventions in *Drosophila melanogaster*. *Proc. Natl. Acad. Sci. USA* 101:12980-12985.

126. Benedetti, M.G., Foster, A.L., Vantipalli, M.C., White, M.P., Sampayo, J.N., Gill, M.S., Olsen, A. and Lithgow, G.J. (2008). Compounds that confer thermal stress resistance and extended lifespan. *Exp. Gerontol*. 43:882-891.

127. Ingram, D.K., Roth, G.S., Lane, M.A., Ottinger, M.A., Zou, S., de Cabo, R. and Mattison, J.A. (2006). The potential for dietary restriction to increase longevity in humans: extrapolation from monkey studies. *Biogerontology* 7:143-148.

128. Ingram, D.K., Zhu, M., Mamczarz, J., Zou, S., Lane, M.A., Roth, G.S. and de Cabo, R. (2006). Calorie restriction mimetics: an emerging research field. *Aging Cell* 5:97-108.

129. Lane, M.A., Roth, G.S. and Ingram, D.K. (2007). Caloric restriction mimetics: a novel approach for biogerontology. *Methods Mol. Biol*. 371:143-149.

130. Kaeberlein, M., Burtner, C.R. and Kennedy, B.K. (2007). Recent developments in yeast aging. *PLoS Genet*. 3:e84.

131. Lin, S.J. and Sinclair, D. (2008). Molecular mechanisms of aging: insights from budding yeast. In: Guarente, L.P., Partridge, L., Wallace, D.C. (Eds.), *Molecular Biology of Aging*. Cold Spring Harbor Laboratory Press, Cold Spring Harbor, New York, pp. 483-516.

132. Longo, V.D. and Kennedy, B.K. (2006). Sirtuins in aging and age-related disease. *Cell* 126:257-268.

133. Bitterman, K.J., Medvedik, O. and Sinclair, D.A. (2003). Longevity regulation in *Saccharomyces cerevisiae*: linking metabolism, genome stability, and heterochromatin. *Microbiol. Mol. Biol. Rev*. 67:376-399.

134. Mair, W. and Dillin, A. (2008). Aging and survival: the genetics of life span extension by dietary restriction. *Annu. Rev. Biochem*. 77:727-754.

135. Masoro, E.J. (2005). Overview of caloric restriction and ageing. *Mech. Ageing Dev*. 126:913-922.

136. Sinclair, D.A. (2005). Toward a unified theory of caloric restriction and longevity regulation. *Mech. Ageing Dev*. 126:987-1002.

137. Kaeberlein, M. (2010). Lessons on longevity from budding yeast. *Nature* 464:513-519.

138. Bordone, L. and Guarente, L. (2005). Calorie restriction, SIRT1 and metabolism: understanding longevity. *Nat. Rev. Mol. Cell Biol.* 6:298-305.

139. Picard, F., Kurtev, M., Chung, N., Topark-Ngarm, A., Senawong, T., Machado De Oliveira, R., Leid M., McBurney, M.W. and Guarente, L. (2004). Sirt1 promotes fat mobilization in white adipocytes by repressing PPAR-γ. *Nature* 429:771-776.

140. Gerhart-Hines, Z., Rodgers, J.T., Bare, O., Lerin, C., Kim, S.H., Mostoslavsky, R., Alt, F.W., Wu, Z. and Puigserver, P. (2007). Metabolic control of muscle mitochondrial function and fatty acid oxidation through SIRT1/PGC-1α. *EMBO J.* 26:1913-1923.

141. Haemmerle, G., Lass, A., Zimmermann, R., Gorkiewicz, G., Meyer, C., Rozman, J., Heldmaier, G., Maier, R., Theussl, C., Eder S., Kratky, D., Wagner, E.F,. Klingenspor, M., Hoefler, G. and Zechner, R. (2006). Defective lipolysis and altered energy metabolism in mice lacking adipose triglyceride lipase. *Science* 312:734-737.

142. Schneiter, R., Brügger, B., Sandhoff, R., Zellnig, G., Leber, A., Lampl, M., Athenstaedt, K., Hrastnik, C., Eder, S., Daum, G., Paltauf, F., Wieland, F.T. and Kohlwein, S.D. (1999) Electrospray ionization tandem mass spectrometry (ESI-MS/MS) analysis of the lipid molecular species composition of yeast subcellular membranes reveals acyl chain-based sorting/remodeling of distinct molecular species en route to the plasma membrane. *J. Cell Biol.* 146:741-754.

143. Wagner, A. and Daum, G. (2005). Formation and mobilization of neutral lipids in the yeast Saccharomyces cerevisiae. *Biochem. Soc. Trans*. 33:1174-1177.

144. Kurat, C.F., Natter, K., Petschnigg, J., Wolinski, H., Scheuringer, K., Scholz, H., Zimmermann, R., Leber, R., Zechner, R. and Kohlwein, S.D. (2006) Obese yeast: Triglyceride lipolysis is functionally conserved from mammals to yeast. *J. Biol. Chem.* 281:491-500.

145. Feng, H., Ren, M., Chen, L. and Rubin, C.S. (2007) Properties, regulation and *in vivo* functions of a novel protein kinase D: *C. elegans* DKF-2 links diacylglycerol second messenger to the regulation of stress responses and lifespan. *J. Biol. Chem*. 282:31273-31288.

146. Spitaler, M. and Cantrell, D.A. (2004). Protein kinase C and beyond. *Nat. Immunol.* 5:785-790.

147. Czabany, T., Athenstaedt, K. and Daum, G. (2007). Synthesis, storage and degradation of neutral lipids in yeast. *Biochim. Biophys. Acta* 1771:299-309.

148. Low, C.P., Liew, L.P., Pervaiz, S. and Yang, H. (2005). Apoptosis and lipoapoptosis in the fission yeast *Schizosaccharomyces pombe. FEMS Yeast Res*. 5:1199-1206.

149. Guarente, L. (2006). Sirtuins as potential targets for metabolic syndrome. *Nature* 444:868-874.

150. Longo, V.D. and Kennedy, B.K. (2006). Sirtuins in aging and age-related disease. *Cell* 126:257-268.

151. Merry, B.J. (2002). Molecular mechanisms linking calorie restriction and longevity. *Int. J. Biochem. Cell Biol.* 34:1340-1354.

152. Mullner, H. and Daum, G. (2004). Dynamics of neutral lipid storage in yeast. *Acta Biochim. Pol.* 51:323-347.

153. Goldberg, A.A., Bourque, S.D., Kyryakov, P., Boukh-Viner, T., Gregg, C., Beach, A., Burstein, M.T., Machkalyan, G., Richard, V., Rampersad, S. and Titorenko, V.I. (2009). A novel function of lipid droplets in regulating longevity. *Biochem. Soc. Trans.* 37:1050-1055.

154. Murphy, D.J. (2001). The biogenesis and functions of lipid bodies in animals, plants and microorganisms. *Prog. Lipid Res*. 40:325-438.

155. Wältermann, M. and Steinbüchel, A. (2005). Neutral lipid bodies in prokaryotes: recent insights into structure, formation, and relationship to eukaryotic lipid depots. *J. Bacteriol.* 187:3607-3619.

156. Martin, S. and Parton, R.G. (2005). Caveolin, cholesterol, and lipid bodies. *Semin. Cell Dev. Biol*. 16:163-174.

157. Fujimoto, T. and Ohsaki, Y. (2006). Cytoplasmic lipid droplets: rediscovery of an old structure as a unique platform. Ann. N. Y. Acad. Sci. 1086:104-115.

158. Martin, S. and Parton, R.G. (2006). Lipid droplets: a unified view of a dynamic organelle. *Nat. Rev. Mol. Cell Biol*. 7:373-378.

159. Olofsson, S.O., Boström, P., Andersson, L., Rutberg, M., Perman, J. and Borén, J. (2009). Lipid droplets as dynamic organelles connecting storage and efflux of lipids. *Biochim. Biophys. Acta* 1791:448-458.

160. Czabany, T., Athenstaedt, K. and Daum, G. (2007). Synthesis, storage and degradation of neutral lipids in yeast. *Biochim. Biophys. Acta* 1771:299-309.

161. Thiele, C. and Spandl, J. (2008). Cell biology of lipid droplets. *Curr. Opin. Cell Biol.* 20:378-385.

162. Binns, D., Januszewski, T., Chen, Y., Hill, J., Markin, V.S., Zhao, Y., Gilpin, C., Chapman, K.D., Anderson, R.G. and Goodman, J.M. (2006). An intimate collaboration between peroxisomes and lipid bodies. *J. Cell Biol*. 173:719-731.

163. Boström, P., Andersson, L., Rutberg, M., Perman, J., Lidberg, U., Johansson, B.R., Fernandez-Rodriguez, J., Ericson, J., Nilsson, T., Borén, J. and Olofsson, S.O. (2007). SNARE proteins mediate fusion between cytosolic lipid droplets and are implicated in insulin sensitivity. *Nat. Cell Biol*. 9:1286-1293.

164. Ducharme, N.A. and Bickel, P.E. (2008). Lipid droplets in lipogenesis and lipolysis. Endocrinology 149:942-949.

165. Dugail, I. and Hajduch, E. (2007). A new look at adipocyte lipid droplets: towards a role in the sensing of triacylglycerol stores? *Cell. Mol. Life Sci*. 64:2452-2458.

166. Goodman, J.M. (2008). The gregarious lipid droplet. *J. Biol. Chem*. 283:28005-28009.

167. Guo, Y., Cordes, K.R., Farese, R.V. and Walther, T.C. (2009). Lipid droplets at a glance. *J. Cell Sci*. 122:749-752.

168. Guo, Y., Walther, T.C., Rao, M., Stuurman, N., Goshima, G., Terayama, K., Wong, J.S., Vale, R.D., Walter, P. and Farese, R.V. (2008). Functional genomic screen reveals genes involved in lipid-droplet formation and utilization. *Nature* 453, 657-661.

169. Kuerschner, L., Moessinger, C. and Thiele, C. (2008). Imaging of lipid biosynthesis: how a neutral lipid enters lipid droplets. *Traffic* 9:338-352.

170. Robenek, H., Hofnagel, O., Buers, I., Robenek, M.J., Troyer, D. and Severs, N.J. (2006) Adipophilin-enriched domains in the ER membrane are sites of lipid droplet biogenesis. *J. Cell Sci*. 119:4215-4224.

171. Welte, M.A. (2007). Proteins under new management: lipid droplets deliver. *Trends Cell Biol*. 17:363-369.

172. Zechner, R., Kienesberger, P.C., Haemmerle, G., Zimmermann, R. and Lass, A. (2009). Adipose triglyceride lipase and the lipolytic catabolism of cellular fat stores. *J. Lipid Res*. 50:3-21.

173. Kurat, C.F., Wolinski, H., Petschnigg, J., Kaluarachchi, S., Andrews, B., Natter, K. and Kohlwein, S.D. (2009). Cdk1/Cdc28-dependent activation of the major triacylglycerol lipase Tgl4 in yeast links lipolysis to cell-cycle progression. *Mol. Cell* 33:53-63.

174. Bordone, L. and Guarente, L. (2005). Calorie restriction, SIRT1 and metabolism: understanding longevity. *Nat. Rev. Mol. Cell Biol*. 6:298-305.

175. Rosen, E.D. and Spiegelman, B.M. (2006). Adipocytes as regulators of energy balance and glucose homeostasis. *Nature* 444:847-853.

176. Guilherme, A., Virbasius, J.V., Puri, V. and Czech, M.P. (2008) Adipocyte dysfunctions linking obesity to insulin resistance and type 2 diabetes. *Nat. Rev. Mol. Cell Biol*. 9:367-377.

177. Cao, H., Gerhold, K., Mayers, J.R., Wiest, M.M., Watkins, S.M. and Hotamisligil, G.S. (2008). Identification of a lipokine, a lipid hormone linking adipose tissue to systemic metabolism. *Cell* 134:933-944.

178. Palanker, L., Tennessen, J.M., Lam, G. and Thummel, C.S. (2009) Drosophila HNF4 regulates lipid mobilization and β-oxidation. *Cell Metab*. 9:228-239.

179. Ohsaki, Y., Cheng, J., Fujita, A., Tokumoto, T. and Fujimoto, T. (2006). Cytoplasmic lipid droplets are sites of convergence of proteasomal and autophagic degradation of apolipoprotein B. *Mol. Biol. Cell* 17:2674-2683.

180. Jiang, H., He, J., Pu, S., Tang, C. and Xu, G. (2007). Heat shock protein 70 is translocated to lipid droplets in rat adipocytes upon heat stimulation. *Biochim. Biophys. Acta* 1771:66-74.

181. Cermelli, S., Guo, Y., Gross, S.P. and Welte, M.A. (2006). The lipid-droplet proteome reveals that droplets are a protein-storage depot. *Curr. Biol*. 16:1783-1795.

182. Wang, M.C., O'Rourke, E.J. and Ruvkun, G. (2008). Fat metabolism links germline stem cells and longevity in *C. elegans*. *Science* 322:957-960.

183. Grönke, S., Mildner, A., Fellert, S., Tennagels, N., Petry, S., Müller, G., Jäckle, H. and Kühnlein, R.P. (2005). Brummer lipase is an evolutionary conserved fat storage regulator in *Drosophila*. *Cell Metab*. 1:323-330.

184. Haemmerle, G., Lass, A., Zimmermann, R., Gorkiewicz, G., Meyer, C., Rozman, J., Heldmaier, G., Maier, R., Theussl, C., Eder, S., Kratky, D., Wagner, E.F., Klingenspor, M., Hoefler, G. and Zechner, R. (2006). Defective lipolysis and altered energy metabolism in mice lacking adipose triglyceride lipase. *Science* 312:734-737.

185. Blüher, M., Kahn, B.B. and Kahn, C.R. (2003). Extended longevity in mice lacking the insulin receptor in adipose tissue. *Science* 299:572-574.

186. Puigserver, P. and Kahn, C.R. (2008). Mammalian metabolism in aging. In: *Molecular Biology of Aging* (Guarente, L.P., Partridge, L. and Wallace, D.C., eds.), pp. 545-574, Cold Spring Harbor Laboratory Press, Cold Spring Harbor, New York.

187. Chiu, C.H., Lin, W.D., Huang, S.Y. and Lee, Y.H. (2004). Effect of a C/EBP gene replacement on mitochondrial biogenesis in fat cells. *Genes Dev*. 18:1970-1975.

188. Picard, F., Kurtev, M., Chung, N., Topark-Ngarm, A., Senawong, T., Machado De Oliveira, R., Leid, M., McBurney, M.W. and Guarente, L. (2004). Sirt1 promotes fat mobilization in white adipocytes by repressing PPAR-γ. *Nature* 429:771-776.

189. Gregor, M.F. and Hotamisligil, G.S. (2007). Adipocyte stress: the endoplasmic reticulum and metabolic disease. *J. Lipid Res*. 48:1905-1914.

190. Russell, S.J. and Kahn, C.R. (2007). Endocrine regulation of ageing. *Nat. Rev. Mol. Cell Biol*. 8:681-691.

191. Rodgers, J.T., Lerin, C., Gerhart-Hines, Z. and Puigserver, P. (2008). Metabolic adaptations through the PGC-1α and SIRT1 pathways. *FEBS Lett*. 582:46-53.

192. Olefsky, J.M. (2008). Fat talks, liver and muscle listen. *Cell* 134:914-916.

193. Hauff, K.D. and Hatch, G.M. (2006). Cardiolipin metabolism and Barth Syndrome. *Prog. Lipid Res*. 45:91-101.

194. Ott, M., Zhivotovsky, B., and Orrenius, S. (2007). Role of cardiolipin in cytochrome c release from mitochondria. *Cell Death Differ*. 14:1243-1247.

195. Houtkooper, R.H. and Vaz, F.M. (2008). Cardiolipin, the heart of mitochondrial metabolism. *Cell. Mol. Life Sci*. 65:2493-2506.

196. Schlame, M. (2008). Cardiolipin synthesis for the assembly of bacterial and mitochondrial membranes. *J. Lipid Res*. 49:1607-1620.

197. Gohil, V.M. and Greenberg, M.L. (2009). Mitochondrial membrane biogenesis: phospholipids and proteins go hand in hand. *J. Biol. Chem.*184:469-472.

198. Joshi, A.S., Zhou, J., Gohil, V.M., Chen, S. and Greenberg, M.L. (2009). Cellular functions of cardiolipin in yeast. *Biochim. Biophys. Acta* 1793:212-218.

199. Schlame, M. and Ren, M. (2009). The role of cardiolipin in the structural organization of mitochondrial membranes. *Biochim. Biophys. Acta* 1788:2080-2083.

200. Osman, C., Voelker, D.R. and Langer, T. (2011). Making heads or tails of phospholipids in mitochondria. *J. Cell Biol*. 192:7-16.

201. Karbowski, M., Jeong, S.Y., and Youle, R.J. (2004). Endophilin B1 is required for the maintenance of mitochondrial morphology. *J. Cell Biol.* 166:1027-1039.

202. Choi, S.Y., Huang, P., Jenkins, G.M., Chan, D.C., Schiller, J., and Frohman, M.A. (2006). A common lipid links Mfn-mediated mitochondrial fusion and SNARE-regulated exocytosis. *Nat. Cell Biol.* 8:1255-1262.

203. Jensen, R.E., and Sesaki, H. (2006). Ahead of the curve: mitochondrial fusion and phospholipase D. *Nat. Cell Biol.* 8:1215-1217.

204. Merkwirth, C., Dargazanli, S., Tatsuta, T., Geimer, S., Löwer, B., Wunderlich, F.T., von Kleist-Retzow, J.C., Waisman, A., Westermann, B. and Langer, T. (2008). Prohibitins control cell proliferation and apoptosis by regulating OPA1-dependent cristae morphogenesis in mitochondria. *Genes Dev*. 22:476-488.

205. Osman, C., Haag, M., Potting, C., Rodenfels, J., Dip, P.V., Wieland, F.T., Brügger, B., Westermann, B. and Langer, T. (2009). The genetic interactome of prohibitins: coordinated control of cardiolipin and phosphatidylethanolamine by conserved regulators in mitochondria. *J. Cell Biol*. 184:583-596.

206. Osman, C., Merkwirth, C. and Langer, T. (2009). Prohibitins and the functional compartmentalization of mitochondrial membranes. *J. Cell Sci*. 122:3823-3830.

207. Merkwirth, C. and Langer, T. (2009). Prohibitin function within mitochondria: essential roles for cell proliferation and cristae morphogenesis. *Biochim. Biophys. Acta* 1793:27-32.

208. Guo, T., Gregg, C., Boukh-Viner, T., Kyryakov, P., Goldberg, A., Bourque, S., Banu, F., Haile, S., Milijevic, S., San, K.H., Solomon, J., Wong, V. and Titorenko, V.I. (2007). A signal from inside the peroxisome initiates its division by promoting the remodeling of the peroxisomal membrane. *J. Cell Biol*. 177:289-303.

209. Russell, S.J. and Kahn, C.R. (2007). Endocrine regulation of ageing. *Nat. Rev. Mol. Cell Biol.* 8:681-691.

210. Cao, H., Gerhold, K., Mayers, J.R., Wiest, M.M., Watkins, S.M. and Hotamisligil, G.S. (2008). Identification of a lipokine, a lipid hormone linking adipose tissue to systemic metabolism. *Cell* 134:933-944.

211. Claypool, S.M., Oktay, Y., Boontheung, P., Loo, J.A. and Koehler, C.M. (2008). Cardiolipin defines the interactome of the major ADP/ATP carrier protein of the mitochondrial inner membrane. *J. Cell Biol*. 182:937-950.

212. Czabany, T., Athenstaedt, K. and Daum, G. (2007). Synthesis, storage and degradation of neutral lipids in yeast. *Biochim. Biophys. Acta* 1771:299-309.

213. Brügger, B., Erben, G., Sandhoff, R., Wieland, F.T. and Lehmann, W.D. (1997). Quantitative analysis of biological membrane lipids at the low picomole level by nano-electrospray ionization tandem mass spectroscopy. *Proc. Natl. Acad. Sci. USA* 94:2339-2344.

214. Schneiter, R., Brügger, B., Sandhoff, R., Zellnig, G., Leber, A., Lampl, M., Athenstaedt, K., Hrastnik, C., Eder, S., Daum, G., Paltauf, F., Wieland, F.T. and Kohlwein, S.D. (1999). Electrospray ionization tandem mass spectrometry (ESI-MS/MS) analysis of the lipid molecular species composition of yeast subcellular membranes reveals acyl chain-based sorting/remodeling of distinct molecular species en route to the plasma membrane. *J. Cell Biol*. 146:741-754.

215. Ejsing, C.S., Sampaio, J.L., Surendranath, V., Duchoslav, E., Ekroos, K., Klemm, R.W., Simons, K. and Shevchenko, A. (2009). Global analysis of the yeast lipidome by quantitative shotgun mass spectrometry. *Proc. Natl. Acad. Sci. USA* 106:2136-2141.

216. Athenstaedt, K., Zweytick, D., Jandrositz, a, Kohlwein, S. D. and Daum, G. (1999). Identification and characterization of major lipid particle proteins of the yeast *Saccharomyces cerevisiae*. *J. Bacteriol*. 181:6441-6448.

217. Pulfer, M. and Murphy, R.C. (2003). Electrospray mass spectrometry of phospholipids. *Mass Spec. Rev*. 22:332-364.

218. Koivusalo, M., Haimi, P., Heikinheimo, L., Kostiainen, R. and Somerharju, P. (2001). Quantitative determination of phospholipid compositions by ESI-MS: effects of acyl chain length, unsaturation, and lipid concentration on instrument response. *J. Lipid Res*. 42:663-672.

219. Schwudke, D., Hannich, J.T., Surendranath, V., Grimard, V., Moehring, T., Burton, L., Kurzchalia, T. and Shevchenko, A. (2007). Top-down lipidomic screens by multivariate analysis of high-resolution survey mass spectra. *Anal. Chem*. 79:4083-4093.

220. Bourque, S.D. and Titorenko, V.I. (2009). A quantitative assessment of the yeast lipidome using electrospray ionization mass spectrometry. *J. Vis. Exp.* 30:1-3, doi: 10.3791/1513.

221. Bligh, E.G. and Dyer, W.J. (1959). A rapid method of total lipid extraction and purification. *Can. J. Biochem. Physiol.* 37:911-917.

222. Goldberg, A.A., Richard, V.R., Kyryakov, P., Bourque, S.D., Beach, A., Burstein, M.T., Glebov, A., Koupaki, O., Boukh-Viner, T., Gregg, C., Juneau, M., English, A.M., Thomas, D.Y. and Titorenko, V.I. (2010). Chemical genetic screen identifies lithocholic acid as an anti-aging compound that extends yeast chronological life span in a TOR-independent manner, by modulating housekeeping longevity assurance processes. *Aging* 2:393-414.

223. Titorenko, V.I. and Terlecky, S.R. (2011). Peroxisome metabolism and cellular aging. *Traffic* 12:252-259.

224. Kirkwood, T.B.L., Boys, R.J., Gillespie, C.S., Proctor, C.J., Shanley, D.P. and Wilkinson, D.J. (2003). Towards an e-biology of ageing: integrating theory and data. *Nat. Rev. Mol. Cell Biol.* 4:243-249.

225. Murphy, M.P. and Partridge, L. (2008). Toward a control theory analysis of aging. *Annu. Rev. Biochem.* 77:777-798.

226. Shevchenko, A., Jensen, O.N., Podtelejnikov, A.V., Sagliocco, F., Mortensen, P., Shevchenko, A., Boucherie, H. and Mann, M. (1996). Linking genome and proteome by mass spectrometry: large-scale identification of yeast proteins from two dimensional gels. *Proc. Natl. Acad. Sci. USA* 93:14440-14445.

227. Jiménez, C.R., Huang, L., Qiu, Y. and Burlingame, A.L. (1998). Searching sequence databases over the Internet: protein identification using MS-Fit. In: *Current Protocols in Protein Science*, Coligan, J.E., Dunn, B.M., Ploegh, H.L., Speicher, D.W., Wigfield, P.T. (Eds.). John Wiley & Sons, Inc., pp. 16.5.1-16.5.6.

228. Titorenko, V.I., Smith, J.J., Szilard, R.K. and Rachubinski, R.A. (1998). Pex20p of the yeast *Yarrowia lipolytica* is required for the oligomerization of thiolase in the cytosol and for its targeting to the peroxisome. *J. Cell Biol*. 142:403-420.

229. Szilard, R.K., Titorenko, V.I., Veenhuis, M. and Rachubinski, R.A. (1995). Pay32p of the yeast *Yarrowia lipolytica* is an intraperoxisomal component of the matrix protein translocation machinery. *J. Cell Biol*. 131:1453-1469.

230. Graham, J.M. (1999). Purification of a crude mitochondrial fraction by density-gradient centrifugation. In: *Current Protocols in Cell Biology*. Bonifacino, J.S., Dasso, M., Harford, J.B., Lippincott-Schwartz, J., Yamada, K.M. (Eds.). John Wiley & Sons, Inc., pp. 3.4.1-3.4.22.

231. Fabrizio, P., Liou, L.L., Moy, V.N., Diaspro, A., Valentine, J.S., Gralla, E.B. and Longo, V.D. (2003). SOD2 functions downstream of Sch9 to extend longevity in yeast. *Genetics* 163:35-46.

232. Guo, T., Gregg, C., Boukh-Viner, T., Kyryakov, P., Goldberg, A., Bourque, S., Banu, F., Haile, S., Milijevic, S., San, K.H., Solomon, J., Wong, V. and Titorenko, V.I. (2007). A signal from inside the peroxisome initiates its division by promoting the remodeling of the peroxisomal membrane. *J. Cell Biol*. 177:289-303.

233. Lin, S.S., Manchester, J.K. and Gordon, J.I. (2001). Enhanced gluconeogenesis and increased energy storage as hallmarks of aging in *Saccharomyces cerevisiae*. *J. Biol. Chem*. 276: 36000-36007.

234. Murakami, C.J., Burtner, C.R., Kennedy, B.K. and Kaeberlein, M. (2008). A method for high-throughput quantitative analysis of yeast chronological life span. *J. Gerontol. A Biol. Sci. Med. Sci*. 63:113-121.

235. Smith, D.L. Jr., McClure, J.M., Matecic, M. and Smith, J.S. (2007). Calorie restriction extends the chronological lifespan of *Saccharomyces cerevisiae* independently of the Sirtuins. *Aging Cell* 6:649-662.

236. Burtner, C.R., Murakami, C.J., Kennedy, B.K. and Kaeberlein, M. (2009). A molecular mechanism of chronological aging in yeast. *Cell Cycle* 8:1256-1270.

237. Hiltunen, J.K., Mursula, A.M., Rottensteiner, H., Wierenga, R.K., Kastaniotis, A.J. and Gurvitz, A. (2003). The biochemistry of peroxisomal β-oxidation in the yeast *Saccharomyces cerevisiae*. *FEMS Microbiol. Rev*. 27:35-64.

238. van der Klei, I.J., Yurimoto, H., Sakai, Y. and Veenhuis, M. (2006). The significance of peroxisomes in methanol metabolism in methylotrophic yeast. *Biochim. Biophys. Acta* 1763:1453-1462.

239. Binns, D., Januszewski, T., Chen, Y., Hill, J., Markin, V.S., Zhao, Y., Gilpin, C., Chapman, K.D., Anderson, R.G. and Goodman, J.M. (2006). An intimate collaboration between peroxisomes and lipid bodies. *J. Cell Biol*. 173:719-731.

240. Balaban, R.S., Nemoto, S. and Finkel, T. (2005). Mitochondria, oxidants, and aging. *Cell* 120:483-495.

241. Giorgio, M., Trinei, M., Migliaccio, E. and Pelicci, P.G. (2007). Hydrogen peroxide: a metabolic by-product or a common mediator of ageing signals? *Nat. Rev. Mol. Cell Biol*. 8:722-728.

242. Guarente, L. (2008). Mitochondria - a nexus for aging, calorie restriction, and sirtuins? *Cell* 132:171-176.

243. Rea, S.L., Ventura, N. and Johnson, T.E. (2007). Relationship between mitochondrial electron transport chain dysfunction, development, and life extension in *Caenorhabditis elegans*. *PLoS Biol*. 5:2312-2329.

244. Schulz, T.J., Zarse, K., Voigt, A., Urban, N., Birringer, M. and Ristow, M. (2007). Glucose restriction extends *Caenorhabditis elegans* life span by inducing mitochondrial respiration and increasing oxidative stress. *Cell Metab*. 6:280-293.

245. Spitaler, M. and Cantrell, D.A. (2004). Protein kinase C and beyond. *Nat. Immunol*. 5:785-790.

246. Feng, H., Ren, M., Chen, L. and Rubin, C.S. (2007). Properties, regulation and *in vivo* functions of a novel protein kinase D: *C. elegans* DKF-2 links diacylglycerol second messenger to the regulation of stress responses and lifespan. *J. Biol. Chem*. 282:31273-31288.

247. Lin, M.T. and Beal, M.F. (2006). Mitochondrial dysfunction and oxidative stress in neurodegenerative diseases. *Nature* 443:787-795.

248. Okamoto, K. and Shaw, J.M. (2005). Mitochondrial morphology and dynamics in yeast and multicellular eukaryotes. *Annu. Rev. Genet.* 39:503-536.

249. Hoppins, S., Lackner, L. and Nunnari, J. (2007). The machines that divide and fuse mitochondria. *Annu. Rev. Biochem.* 76:751-780.

250. Madeo, F., Fröhlich, E., Ligr, M., Grey, M., Sigrist, S.J., Wolf, D.H. and Fröhlich, K.U. (1999). Oxygen stress: a regulator of apoptosis in yeast. *J. Cell Biol*. 145:757-767.

251. Ludovico, P., Rodrigues, F., Almeida, A., Silva, M.T., Barrientos, A. and Côrte-Real, M. (2002). Cytochrome c release and mitochondria involvement in programmed cell death induced by acetic acid in *Saccharomyces cerevisiae*. *Mol. Biol. Cell* 13:2598-2606.

252. Eisenberg, T., Büttner, S., Kroemer, G. and Madeo, F. (2007). The mitochondrial pathway in yeast apoptosis. *Apoptosis* 12:1011-1023.

253. Fannjiang, Y., Cheng, W.C., Lee, S.J., Qi, B., Pevsner, J., McCaffery, J.M., Hill, R.B., Basañez, G. and Hardwick, J.M. (2004). Mitochondrial fission proteins regulate programmed cell death in yeast. *Genes Dev*. 18:2785-2797.

254. Hardwick, J.M. and Cheng, W.C. (2004). Mitochondrial programmed cell death pathways in yeast. *Dev. Cell* 7:630-632.

255. The *Saccharomyces* Genome Database [http://www. yeastgenome.org/].

256. François J. And Parrou, J.L. (2001). Reserve carbohydrates metabolism in the yeast *Saccharomyces cerevisiae*. *FEMS Microbiol. Rev*. 25:125-145.

257. Benaroudj, N., Lee, D.H. and Goldberg, A.L. (2001). Trehalose accumulation during cellular stress protects cells and cellular proteins from damage by oxygen radicals. *J. Biol. Chem*. 276:24261-24267.

258. Simola, M., Hänninen, A.L., Stranius, S.M. and Makarow, M. (2000). Trehalose is required for conformational repair of heat-denatured proteins in the yeast

endoplasmic reticulum but not for maintenance of membrane traffic functions after severe heat stress. *Mol. Microbiol*. 37:42-53.

259. Singer, M.A. and Lindquist, S. (1998). Multiple effects of trehalose on protein folding *in vitro* and *in vivo*. *Mol. Cell* 1:639-648.

260. Singer, M.A. and Lindquist, S. (1998). Thermotolerance in *Saccharomyces cerevisiae*: the Yin and Yang of trehalose. *Trends Biotechnol*. 16:460-468.

261. Léon, S., Goodman, J.M. and Subramani, S. (2006). Uniqueness of the mechanism of protein import into the peroxisome matrix: transport of folded, co-factor-bound and oligomeric proteins by shuttling receptors. *Biochim. Biophys. Acta* 1763:1552-1264.

262. Dirkx, R., Vanhorebeek, I., Martens, K., Schad, A., Grabenbauer, M., Fahimi, D., Declercq, P., Van Veldhoven, P.P. and Baes, M. (2005). Absence of peroxisomes in mouse hepatocytes causes mitochondrial and ER abnormalities. *Hepatology* 41:868-878.

8. List of my publications and manuscripts in preparation (published papers are attached below)

Published papers

1. Guo, T., Gregg, C., Boukh-Viner, T., Kyryakov, P., Goldberg, A., **Bourque, S.**, Banu, F., Haile, S., Milijevic, S., Hung Yeung San, K., Solomon, J., Wong, V. and Titorenko, V.I. A signal from inside the peroxisome initiates its division by promoting the remodeling of the peroxisomal membrane. *J. Cell Biol.* (2007) 177:289-303.
    This article was an Editors' Choice article in *Science* (2007) 316:801.

2. Goldberg, A.A.*, **Bourque, S.D.***, Kyryakov, P.*, Boukh-Viner, T., Gregg, C., Beach, A., Burstein, M.T., Machkalyan, G., Richard, V., Rampersad, S. and Titorenko, V.I. A novel function of lipid droplets in regulating longevity. *Biochem. Soc. Trans.* (2009) 37:1050-1055.
    * Equally contributed first co-authors.

3. Goldberg, A.A.*, **Bourque, S.D.***, Kyryakov, P.*, Gregg, C., Boukh-Viner, T., Beach, A., Burstein, M.T., Machkalyan, G., Richard, V., Rampersad, S., Cyr, D., Milijevic, S. and Titorenko, V.I. Effect of calorie restriction on the metabolic history of chronologically aging yeast. *Exp. Gerontol.* (2009) **44**:555-571.
    * Equally contributed first co-authors.

4. **Bourque, S.D.** and Titorenko, V.I. A quantitative assessment of the yeast lipidome using electrospray ionization mass spectrometry. *J. Vis. Exp.* (2009) 30:1-3.

5. Goldberg, A.A.*, Richard, V.R.*, Kyryakov, P.*, **Bourque, S.D.***, Beach, A., Burstein, M.T., Glebov, A., Koupaki, O., Boukh-Viner, T., Gregg, C., Juneau, M.,

English, A.M., Thomas, D.Y. and Titorenko, V.I. Chemical genetic screen identifies lithocholic acid as an anti-aging compound that extends yeast chronological life span in a TOR-independent manner, by modulating housekeeping longevity assurance processes. *Aging* (2010) 2:393-414.

 * Equally contributed first co-authors.

This article was highlighted in the news media, including Radio-Canada (http: //www.radio-canada.ca/nouvelles/science/2010/09/16/002-longevite-bile.shtml); **TFI News France** (http://lci.tf1.fr/science/sante/2010-09/la-bile-un-espoir-contre-le-vieillissement-6071272.html); **The McGill Daily** (http://hotink. theorem.ca/system/ mcgilldaily/issues/000/004/689/ vol100iss7_screen_quality. pdf?1285709690); **Science Daily** (http://www.sciencedaily.com/releases/2010/09/ 100915100935.htm); **EurekAlert!** (http://www.eurekalert.org/pub_releases/2010-09/cu-foy091510.php); **Now Concordia** (http://now.concordia.ca/what-we-do/ research/20100921/fountain-of-youth-in-bile-longevity-molecule-identified.php); **Media Relations Concordia** (http://mediarelations. concordia.ca/pressreleases/ archives/2010/09/fountain_of_youth_in_bile_long.php?&print=1); **Bio Ethics Hawaii** (http://www.bioethicshawaii.org/s-science/the-key-to-human-longevity-in-yeast-could-be/); **Fight Aging!** (http://www.fightaging.org/archives/2010/ 09/bile-acids-and-yeast-longevity.php); **Xenophilia** (https://xenophilius. wordpress.com/2010/09/16/fountain-of-youth-in-bile-longevity-molecule-identified/); **Thaindian** (http:// www.thaindian.com/newsportal/health/bile-may-harbour-human-fountain-of-youth_ 100429315.html); **DNA India** (http://www.dnaindia.com/scitech/report_bile-may-harbour-human-fountain-of-youth_1438869); **India Vision** (http://www.indiavision.com/news/article/scitech/ 103189/); **REVLET** (http://www.revleft.com/vb/fountain-youth-bilei-t141779/ index.html?s=1294a5663f51df1055ad3ff2b53db082&p=1865643); **Stop Aging Solutions** (http://stopagingsolutions.com/?p=704); **Longevity Medicine** (http://www.longevitymedicine.tv/longevity-as-housekeeping-and-a-role-for-bile-acids/); **News Guide US** (http://newsguide.us/education/science/Fountain-of-youth-in-bile-Longevity-molecule-identified/?date=2010-03-26); **Dallas News** (http://topics. dallasnews.com/quote/06AP1cA3HLa9j?q=Diabetes); **e! Science News** (http:// esciencenews.com/articles/2010/09/15/fountain.youth.bile. longevity.molecule.identified);**TENDENCIAS CIENTIFICAS** (http://www. tendencias21.net/La-clave-de-la-longevidad-humana-podria-estar-en-la-levadura_ a4848.html?utm_source= feedburner& utm_medium=feed); **Canadian Health Reference Guide** (http://www.chrgonline.com/ news_detail. asp?ID=140067); **Techno-Science** (http://www.chrgonline.com/news_ detail.asp?ID=140067); **METRO** (http://www.journalmetro.com/plus/article/672613--la-bile-fontaine-de-jouvence) **and others.**

6. Goldberg, A.A.*, Kyryakov, P.*, **Bourque, S.D*.** and Titorenko, V.I. Xenohormetic, hormetic and cytostatic selective forces driving longevity at the ecosystemic level. *Aging* (2010) 2:361-370.

* Equally contributed first co-authors.

Manuscripts in preparation

1. Khatchadourian, A., Bourque, S.D., Richard, V.R., Titorenko, V.I. and Maysinger, D.*corresponding author. LPS induces lipid droplet accumulation and perilipin-2 expression in microglia. *FASEB J.*

2. Bourque, S.D., Richard, V.R., Beach, A. and Titorenko, V.I. Analysis of the *Saccharomyces cerevisiae* lipidome using survey-scan electrospray-ionization mass spectroscopy. *J. Lipid Res*.

3. Bourque, S.D., Richard, V.R., Beach, A., Burstein, M.T., Goldberg, A.A., Kyryakov, P. and Titorenko, V.I. A mechanism linking lipid metabolism and longevity in chronologically aging yeast. *Cell Metab*.

4. Bourque, S.D., Richard, V.R., Beach, A., Burstein, M.T., Goldberg, A.A., Kyryakov, P. and Titorenko, V.I. Lithocholic acid extends yeast longevity in part by targeting the longevity-defining aspects of lipid metabolism confined to the endoplasmic reticulum, lipid bodies and peroxisomes. *Dev. Cell*.

5. Bourque, S.D., Richard, V.R., Beach, A., Burstein, M.T., Koupaki, O., Goldberg, A.A., Kyryakov, P. and Titorenko, V.I. Lithocholic acid extends yeast longevity in part by altering the composition of mitochondrial membrane lipids. *J. Cell Biol*.